JPL PUBLICATION 86-29

Shuttle Imaging Radar-C Science Plan

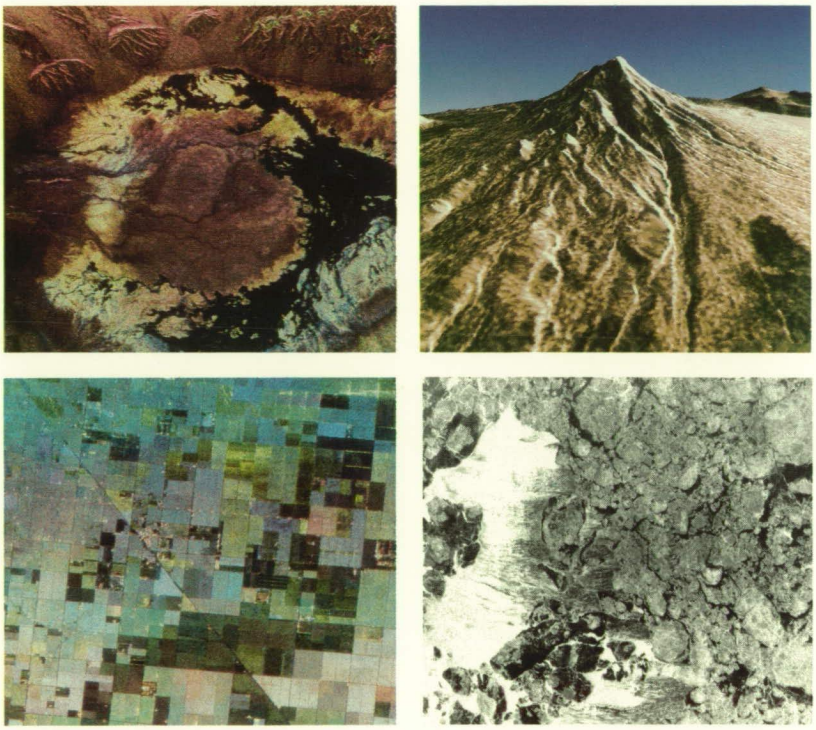

September 1, 1986

NASA
National Aeronautics and
Space Administration

Jet Propulsion Laboratory
California Institute of Technology
Pasadena, California

JPL PUBLICATION 86-29

Shuttle Imaging Radar-C Science Plan

September 1, 1986

NASA
National Aeronautics and
Space Administration

Jet Propulsion Laboratory
California Institute of Technology
Pasadena, California

The research described in this publication was carried out by the Jet Propulsion Laboratory, California Institute of Technology, under a contract with the National Aeronautics and Space Administration.

Abstract

The Shuttle Imaging Radar-C (SIR-C) mission will yield new and advanced scientific studies of the earth. SIR-C will be the first instrument to simultaneously acquire images at L-band and C-band with HH, VV, HV, or VH polarizations, as well as images of the phase difference between HH and VV polarizations. These data will be digitally encoded and recorded using onboard high-density digital tape recorders and will later be digitally processed into images using the JPL Advanced Digital SAR Processor.

There are a large number of potential SIR-C experiments. Geologic studies include cold-region geomorphology, fluvial geomorphology, rock weathering and erosional processes, tectonics and geologic boundaries, geobotany, and radar stereogrammetry. Hydrology investigations cover arid, humid, wetland, snow-covered, and high-latitude regions. Additionally, SIR-C will provide the data to identify and map vegetation types, interpret landscape patterns and processes, assess the biophysical properties of plant canopies, and determine the degree of radar penetration of plant canopies.

In the field of oceanography, SIR-C will provide the information necessary to: forecast ocean directional wave spectra; better understand internal wave-current interactions; study the relationship of ocean-bottom features to surface expressions and the correlation of wind signatures to radar backscatter; and detect current-system boundaries, oceanic fronts, and mesoscale eddies. And, as the first spaceborne SAR with multifrequency, multipolarization imaging capabilities, whole new areas of glaciology will be opened for study when SIR-C is flown in a polar orbit.

Preface

This Science Plan was written before the Shuttle Challenger accident in January, 1986. In addition to the tragic loss of lives, the accident has resulted in many changes in the Shuttle schedule. In particular, the resulting delay of launches from Vandenberg Air Force Base will preclude any U.S.-launched, polar-orbiting missions until its reopening. Any flights prior to that time will be restricted to 57° inclination orbits. In spite of these changes, the objectives and requirements presented in this report are still valid and serve as guidelines for the continuing National Aeronautics and Space Administration (NASA) Spaceborne Imaging Radar (SIR) program.

The SIR program consists of an evolutionary approach in which more sophisticated technology may be incorporated into a basic sensor as the scientific requirements become increasingly stringent. The first phases of the program, consisting of Seasat and SIR-A, have shown that, while single parameter synthetic aperture radar sensors provide the capability to observe global patterns on the earth's surface, more detailed surface information is required to relate these patterns to processes that are ongoing throughout the earth system. The multi-incidence angle radar data acquired by SIR-B in the second phase of the SIR program provided some insight into what kind of capabilities are required to better characterize the earth's surface and model its short-term and long-term evolutionary history. Clearly, global coverage and multitemporal coverage are two key requirements. In addition, sensor versatility is essential since different investigations may require very different scales, resolutions, or accuracies of observations.

The SIR-C sensor is designed to be versatile enough to meet a variety of observational requirements and will therefore require very little modification in terms of scientific data products before it is installed on a permanently orbiting polar platform as part of the Earth Observing System (EOS). However, the data handling and data analysis tools that will be required to utilize a continuous stream of multiparameter spaceborne radar data from EOS are seriously deficient; scientists need further experience with radar data to develop the capability to analyze it efficiently under high data-rate conditions. The SIR-C Science Working Group therefore recommends that NASA fly the SIR-C sensor in two different seasons as soon as possible to provide scientists with multitemporal data, even if the coverage is restricted to a 57° orbit. The Group further recommends that the basic SIR-C sensor be flown in a polar orbit as soon as the launch capability exists.

Executive Summary

The Shuttle Imaging Radar-C (SIR-C) mission will provide a powerful new tool for scientific studies of the earth, and will be a significant step forward in the evolution of an advanced spaceborne imaging radar. It will provide

(1) The first opportunity for *simultaneous multifrequency* radar imagery from space for geoscientific studies of the earth
(2) The first spaceborne high-resolution imaging sensor with *simultaneous multipolarization* capability
(3) The first *multiparameter* imaging radar, which will supply coverage during *two different seasons*

The SIR-C mission will include two Shuttle launches, thereby permitting two 8-day observing periods during different seasons. One-day repeat coverage would be provided during an 8-day mission.

SIR-C will allow the simultaneous acquisition of images at L-band and C-band with HH, VV, HV, or VH polarizations, as well as images of the phase difference between HH and VV polarizations. It will also be possible to electronically steer the antenna beam so that images may be acquired from 15°–55° angles of incidence. Plans also include the addition of a German-developed X-band SAR (X-SAR), which would then allow simultaneous imaging of selected sites at 23-cm, 6-cm, and 3-cm wavelengths. SIR-C swath widths will vary from 15 km to 90 km (depending on the number of simultaneous frequencies an polarizations selected) and the resolution will be approximately 30 m in the low-resolution mode and 15 m in the high-resolution mode.

SIR-C data will be digitally encoded and recorded using onboard high-density digital tape recorders. These raw data will later be digitally processed into images using the JPL Advanced Digital SAR Processor. The radiometric calibration goals include relative radiometric stability (during a mission and at a given frequency) of ± 1 dB, absolute accuracy (for comparison between missions) of ± 3 dB, and calibration of ± 1.5 dB of the L-band channel relative to the C-band channel for multiwavelength comparisons). The geometric calibration goals include absolute location accuracy to at least 1 km.

This science plan provides a detailed discussion of potential SIR-C experiments that could be performed in the areas of geology, hydrology, vegetation science, glaciology, and oceanography. It is envisioned that many of these experiments will make use of carefully selected test sites, i.e., "supersites," with enhanced ground truth instrumentation. In addition to these geoscientific experiments, a number of radar-technique related experiments are discussed.

Geology experiments include investigations of cold-region geomorphology, fluvial geomorphology, rock weathering and erosional processes, tectonics and geologic boundaries, geobotany, and radar stereogrammetry. Potential cold region geomorphology studies possible with SIR-C in a high inclination orbit include the determination of optimum frequencies and polarizations for glacial landform mapping, the optimum illumination angles and frequencies for the perception of permafrost and thermokarst boundaries, the analysis of Antarctic dry-valley surface properties and penetration depths, and the observation of ice-sheet pressure ridges, fractures, etc. SIR-C data should be especially valuable in fluvial geomorphology investigations, principally because of the sensitivity of radar to open bodies of water (including rivers) in contrast

to surrounding terrain. The multipolarization capability of SIR-C may make it possible to separate rock lithologies within dendritic stream patterns, and the L-band channel may allow additional studies of penetration to buried drainage networks within hyperarid zones. The multipolarization, multifrequency capabilities of SIR-C should allow the discrimination of sedimentary lithologies as well as relative age dating of some arid-zone Quaternary geomorphic surfaces. SIR-C may allow the determination of recent fault offsets and other tectonic expressions by noting the contrast in radar backscatter in units of different lithology and age separated by fault offsets; it is expected that these different lithologies will have distinctive polarization- and wavelength-dependent signatures. A polar orbit of SIR-C would allow studies of Precambrian shields in all continents, and improved structural mapping, both normal and parallel to selected fronts. Geobotanical investigations will also be possible, based on the dependence of plant morphology on underlying lithologies and on vegetation-substrate physiological interactions. Here, the images from both SIR-C flights would be compared to reveal seasonal differences as well as the effects of underlying lithologies. Finally, radar stereogrammetry techniques using SIR-C should allow the acquisition of high spatial resolution topographic data, using either interferometric techniques or two data takes with at least a 20° variation in incidence angle.

A wide variety of *hydrologic investigations* will become possible using SIR-C data, covering hydrologic regimes including arid, humid, wetland, snow-covered, and high-latitude regions. In hyperarid regimes, SIR-C will permit further investigations of surface penetration capability by ratioing L-band to C-band images as well as like- to cross-polarized. In semiarid regions, as well as humid regions, SIR-C will enable studies of temporal and spatial variability of soil moisture. Temporal studies would be made of sites where observations of a rain event early in the mission could be followed by one-day repeat coverage, thereby permitting up to 8 days of observation leading to the establishment of dry-down rates, etc. Spatial variability and scale in hydrologic systems would also be investigated using SIR-C data. Experiments could be conducted leading to estimates of SAR sensitivity to precipitation as well as hydrologic characteristics. SIR-C imagery would also be useful in both semiarid and humid regimes for identifying groundwater recharge and discharge areas. In wetland regimes, the use of multifrequency, multipolarization images could lead to the identification of understory land–water boundaries, an important parameter in studying the trace-gas fluxes and other processes of these valuable ecosystems. In snow-covered regimes, it will be possible to use the C-band and X-band channels to measure snowpack liquid water content, snow wetness, and areal extent. In northern latitudes, SIR-C images could lead to improved discrimination of glaciers, particularly the distribution of morainal material, crevasse patterns and ice surface roughness. It may also be possible to use SAR image texture for the delineation of permafrost boundaries.

SIR-C will provide unique data for *vegetation science studies*, including the identification and mapping of vegetation types, the interpretation of landscape patterns and processes, the assessment of the biophysical properties of plant canopies, and the determination of the degree of radar penetration of plant canopies. Multifrequency, multipolarization data acquired on both single dates (one flight) or in seasonal pairs (two flights) could be used to evaluate vegetation types by crop groups, forest types, physioagronomic regions, weather conditions, etc. It is expected that the shorter wavelengths, higher incidence angles, and full polarization data sets (including phase) will be most useful for these purposes. SIR-C will permit quantitative studies of the dependence of radar backscattering coefficients on canopy biophysical properties, including productivity and phytomass or leaf area index (LAI), canopy structure,

stress, etc. It is expected that such SIR-C experiments will lead to an evaluation of optimal wavelengths, polarizations, and incidence angles for these purposes. By using the ratios of images at L-, C-, and X- band, SIR-C will lead to a much improved understanding of the degree of attenuation introduced by plant canopies.

SIR-C *oceanography objectives* include the forecasting of ocean directional wave spectra, an improved understanding of internal wave–current interactions, the detection of current-system boundaries, oceanic fronts and mesoscale eddies, the relationship of ocean-bottom features to surface expressions and the correlation of wind signatures to radar backscatter. SIR-C, with its variable range-to-velocity ratio (via angle of incidence) and multiple frequencies, represents a valuable opportunity for designing experiments to distinguish among the various models for SAR imaging of the ocean surface, and to establish the degree of uniqueness between SAR-measured directional wave spectra and the actual ocean directional spectra. Dual-frequency SAR imagery of internal waves using SIR-C will present the first opportunity to acquire spaceborne images of both L-band Bragg waves (45 to 15 cm) and C-band Bragg waves ranging from short gravity waves (11 cm) to near-capillary waves (4 cm). This will lead to an improved understanding of the hydrodynamics of wave–current interactions over a wide range of the spectrum. SIR-C will also provide the means for detection of current-system boundaries, oceanic fronts, and mesoscale eddies via their influence on gravity waves as described above. It is expected that images of both cold-core and warm-core rings acquired at both L-band and C-band will shed additional light on the SAR imaging mechanism for these phenomena. The effect of bottom topography on SAR images of the ocean surface may be explained both by linear wave refraction models and by the flow of oceanic currents over bottom features. SIR-C, by virtue of its sensitivity to a wider range of Bragg waves, will offer the opportunity to study and quantify these phenomena further. The dependence of wind signatures on SAR wavelength, polarization, and incidence angle should lead to an improved understanding of the mechanism of SAR response to local wind stresses.

The SIR-C mission is especially exciting for *glaciological investigations,* because it will be the first spaceborne SAR with multifrequency, multipolarization imaging capabilities. This will allow valuable quantitative investigations of sea ice, lake ice, ice shelves, ice sheets and glaciers, and snowpacks. It will be possible to use the SIR-C multifrequency data with different polarizations and angles to significantly improve our understanding of sea-ice features and scattering mechanisms, and to study spatial variations in pack ice and ice-margin eddies. SIR-C should also allow much improved sea-ice type discrimination, because of wavelength and polarization sensitivity to ice geometry and chemical structure in the ice surface layers. SIR-C observations of lake ice are likewise possible, although complicated by significant returns from the lower ice-water interface. However, this may lead to a means for SIR-C bathymetry for Arctic coastal-plain lakes, using detailed studies of strong-return, weak-return pairs as a measure of ice thickness. As pointed out in the above paragraph on hydrology, SIR-C will also be useful for ice sheet and glacier boundaries as well as snowpack properties. It is very desirable to have X-band data for these snow studies.

In addition to the geoscientific experiments described in the above paragraphs, it is expected that a number of worthwhile radar-technique related experiments will be possible. These include calibration experiments (the use of passive corner reflectors, active radar calibrators, and ground receivers), squint experiments (e.g., for oceanographic investigations of the azimuth dependence of radar backscatter), bistatic obser-

vations of backscatter in connection with an underflying aircraft radar, SCANSAR (a technique for doubling or tripling the swath by electronically scanning the antenna beam between bursts), the observation of scattering statistics, and interferometric topography (by measuring the phase of the echo as received by two or more spatially separated locations of the SIR-C sensor). It may also be possible, under the proper conditions, to map the location, altitude and intensity of rain cells using the C-band channel. The SIR-C system, operated in the proper spatial orientation and pulse repetition frequency (PRF), may be able to measure rainfall rates in excess of about 1 mm/second.

The degree to which all these experiments can be successfully conducted depends critically on the actual SIR-C performance, particularly its radiometric and geometric calibration, its dynamic range, and the timing of the mission flights. Although this Science Plan summarizes certain performance goals (e.g., the required degree of calibration, dynamic range, and timing), it is recognized that fiscal constraints may prevent the achievement of all of these goals. Therefore, some of these experiments may be difficult and a few may even be impossible. However, it is expected that the majority of those discussed here are achievable with SIR-C.

The SIR-C Science Working Group

The SIR-C Science Working Group (SWG) was cochaired by Keith Carver (University of Massachusetts) and Charles Elachi of the Jet Propulsion Laboratory (JPL). Diane Evans (JPL) served as Executive Secretary. Six discipline teams were formed:

Radar Techniques Team	Leader: Gordon Pettengill, Massachusetts Institute of Technology
Geology Team	Leader: Catherine Kitcho,* NASA Headquarters
Hydrology Team	Leader: Richard Newton, Texas A&M University
Oceanography Team	Leader: Robert Beal, The Johns Hopkins University Applied Physics Laboratory
Vegetation Team	Leader: Fawwaz Ulaby, University of Michigan
Ice Team	Leader: Wilford Weeks, Cold Regions Research and Engineering Laboratory (CRREL)

Two meetings of the SWG were held:

April 4–5, 1984	Reston, Virginia
February 6–7, 1985	JPL, Pasadena, California

The first meeting was used to develop a candidate series of SIR-C experiments, and the second to refine the resulting draft of the SIR-C Science Plan.

SIR-C SWG Team Members and Observers who actively participated are listed below:

SIR-C Science Working Group

Team Members

Miriam Baltuck*	NASA Headquarters
Robert Beal	The Johns Hopkins University Applied Physics Laboratory
Andrew Blanchard	University of Texas, Arlington
Carol Breed	U.S. Geological Survey
Frank Carsey	Jet Propulsion Laboratory
Keith Carver	University of Massachusetts
Richard Craig	Kent State University
Charles Elachi	Jet Propulsion Laboratory
Ted Engman	USDA ARS Hydrology Laboratory
Diane Evans	Jet Propulsion Laboratory
Thomas Farr	Jet Propulsion Laboratory
John Ford	Jet Propulsion Laboratory
Mike Freilich	Jet Propulsion Laboratory
Richard Gasparovic	The Johns Hopkins University Applied Physics Laboratory
Richard Goldstein	Jet Propulsion Laboratory
Forrest Hall	Johnson Space Center
Robert Harger	University of Maryland
Daniel Held	Jet Propulsion Laboratory
Roger Hoffer	Purdue University
Ray Jackson	U.S. Department of Agriculture
Ed Kanemasu	Kansas State University
Catherine Kitcho*	NASA Headquarters
Paul Lowman	Goddard Space Flight Center
Chuck Luther	Office of Naval Research
David Lyzenga	Environmental Research Institute of Michigan
Marshall McFarland	Texas A&M University
David McGinnis	U.S. Department of Commerce
Peter Molnar	Massachusetts Institute of Technology
Richard Moore	University of Kansas
Peter Mouginis-Mark*	University of Hawaii
Richard Newton	Texas A&M University
Gordon Pettengill	Massachusetts Institute of Technology
Robert Ragan	University of Maryland
Rene Ramseier	Atmospheric Environment Service
Barry Rock	Jet Propulsion Laboratory
Gerald Schaber	U.S. Geological Survey
Mark Settle	ARCO Oil and Gas Company
Robert Shuchman	Environmental Research Institute of Michigan
Calvin Swift	University of Massachusetts
Robert Thomas	NASA Headquarters
Fawwaz Ulaby	University of Michigan
Jim Wang	Goddard Space Flight Center
Wilford Weeks	Cold Regions Research and Engineering Laboratory
Robert Winokur	Office of Naval Research

*Catherine Kitcho left NASA HQ in March, 1985. Peter Mouginis-Mark (University of Hawaii) subsequently became Geology Team Leader; and upon his departure from NASA in July, 1986 Miriam Baltuck (Tulane University) became Geology Team Leader.

Observers/Reviewers

Evert Attema	ESA–ESTEC
Arthur Benton, Jr.	Texas A&M University
Bruce Blanchard	Goddard Space Flight Center
Josef Cihlar	Canada Centre for Remote Sensing
John Curlander	Jet Propulsion Laboratory
Anthony England	Johnson Space Center
Ron Gelnett	MARS Associates Inc.
Robert Gurney	Goddard Space Flight Center
Philip Hartl	University of Stuttgart
James Head	Brown University
Verne Kaupp	University of Arkansas
Thuy LeToan	Universite Paul Sabatier de Toulouse
Edward Link	USAE Waterways Experiment Station
Livio Marelli	European Space Agency
Robert Murphy	NASA Headquarters
John Neiber	Texas A&M University
Herwig Oettl	German Aerospace Research Establishment (DFVLR)
Jack Paris	Jet Propulsion Laboratory
Robert Prindle	Earth Quest
Keith Raney	Canada Centre for Remote Sensing
Floyd Sabins	Chevron Oil Field Research
Thomas Schmugge	Goddard Space Flight Center
Alois Sieber	University of Stuttgart
Leo Stroosnijder	Agricultural University
Kathryn Sullivan	Johnson Space Center
James Taranik	University of Nevada at Reno
Sid Theis	Texas Instruments
Diane Wickland	NASA Headquarters

Abbreviations

ADSP	Advanced Digital SAR Processor
AIS	Airborne Imaging Spectrometer
ARS	Agricultural Research Service
AVHRR	Advanced Very High Resolution Radiometer
AVIRIS	Airborne Visible/Infrared Imaging Spectrometer
BFPQ	Block Floating Point Quantizer
bps	bits per sample
CCT	computer-compatible tape
CIR	color infrared
CRREL	Cold Regions Research Environmental Laboratory
CZCS	coastal zone color scanner
DDHS	digital data handling system
DFQP	dual-frequency quad-polarization mode
DFVLR	German Aerospace Research Establishment
DMSP	Defense Meteorology Satellite Program
DN	digital number
EOS	Earth Observing System
ERS-1	European Remote Sensing Satellite
ESA	European Space Agency
EST	eastern standard time
GSFC	Goddard Space Flight Center
HCMM	Heat Capacity Mapping Mission
HDDT	high-density digital tape
HDDR	high-density digital recorder
HH	horizontally polarized transmission, horizontally polarized reception
HPA	high-power amplifier
HV	horizontally polarized transmission, vertically polarized reception
IOC	initial operating configuration (of EOS)
ISLCP	International Satellite Land Climatology Project
JPL	Jet Propulsion Laboratory
JSC	Johnson Space Center
LAI	Leaf Area Index

LNA	low-noise amplifier
MSS	multispectral scanner (Landsat)
NASA	National Aeronautics and Space Administration
NOAA	National Oceanic and Atmospheric Administration
NROSS	Navy Remote Ocean Satellite System
PRF	pulse repetition frequency
RBV	return beam vidicon (Landsat)
R/V	range-to-velocity ratio
RMS	root mean square
SAR	synthetic aperture radar
SASS	Seasat-A Satellite Scatterometer
SFQ	single-frequency quad-polarization mode
SIR	Shuttle Imaging Radar
SCS	Soil Conservation Service
SLAR	side-looking airborne radar
SMMR	Scanning Multichannel Microwave Radiometer
SNR	signal-to-noise ratio
SPP	special purpose processor
SSM/I	Special Sensor Microwave Imager
STALO	stable local oscillator
STS	Shuttle Transportation System
SWG	Science Working Group
TDRSS	Tracking and Data Relay Satellite System
TIMS	Thermal Infrared Multispectral Scanner
TIR	Thermal Infrared Radiometer
TM	Thematic Mapper (Landsat 4,5)
TOPEX	NASA Topographic Experiment
T/R	transmit/receive units
VH	vertically polarized transmission, horizontally polarized reception
VLSI	very large scale integration
VV	vertically polarized transmission, vertically polarized reception
WMO	World Meteorological Organization

Contents

Executive Summary v

The SIR-C Science Working Group viii

Abbreviations xi

Chapter 1 Introduction 1-1

1.1 NASA Shuttle Imaging Radar Missions 1-1

1.2 The SIR-C Mission 1-2

1.3 Science Plan Organization 1-5

Chapter 2 The Role of Spaceborne Imaging Radars in Studies of the Earth 2-1

2.1 Background 2-1

2.2 New Challenges to Remote Sensing: Global Studies 2-3

2.3 The Role of Imaging Radars 2-4

2.4 Evolution to the Space Station Era 2-4

Chapter 3 SIR-C Sensor Characteristics 3-1

3.1 SIR-C Technology 3-1

3.2 Sensor Description 3-2

3.2.1 Sensor Subsystems 3-2

3.2.2 Operational Modes 3-4

3.3 Calibration 3-8

3.3.1 Radiometric Calibration 3-8

3.3.2 Geometric Calibration 3-9

Chapter 4 SIR-C Geoscientific Experiments 4-1

4.1 Introduction 4-1

4.2 Geology 4-1

4.2.1 Background 4-1

4.2.2 Role of Spaceborne Remote Sensing in Geology 4-3

4.2.3 Role of Imaging Radar in Geology 4-4

4.2.4 Scientific Basis for SIR-C Geology Experiments 4-5

4.2.5 SIR-C Geology Experiments 4-6

4.2.6 Summary of SIR-C Mission Requirements for Geology 4-26

4.3 Hydrology 4-28
4.3.1 Background 4-28
4.3.2 Role of Spaceborne Remote Sensing in Hydrology ... 4-33
4.3.3 Role of Imaging Radar in Hydrology 4-33
4.3.4 Scientific Basis for SIR-C Hydrology Experiments ... 4-35
4.3.5 SIR-C Hydrology Experiments 4-43
4.3.6 Summary of SIR-C Mission Requirements for Hydrology 4-53

4.4 Vegetation Science 4-55
4.4.1 Background 4-55
4.4.2 Role of Spaceborne Remote Sensing in Vegetation Science 4-55
4.4.3 Role of Imaging Radar in Vegetation Science 4-56
4.4.4 Scientific Basis for SIR-C Vegetation-Science Experiments 4-56
4.4.5 SIR-C Vegetation Science Experiments 4-60
4.4.6 Summary of SIR-C Mission Requirements for Vegetation Science 4-65

4.5 Glaciology 4-66
4.5.1 Background 4-66
4.5.2 Role of Spaceborne Remote Sensing in Glaciology .. 4-67
4.5.3 Role of Imaging Radar in Glaciology 4-68
4.5.4 Scientific Basis for SIR-C Glaciology Experiments ... 4-69
4.5.5 SIR-C Glaciology Experiments 4-71
4.5.6 Summary of SIR-C Mission Requirements for Glaciology 4-80

4.6 Oceanography 4-83
4.6.1 Background 4-83
4.6.2 Role of Spaceborne Remote Sensing in Oceanography 4-84
4.6.3 Role of Imaging Radar in Oceanography 4-85
4.6.4 Scientific Basis for SIR-C Oceanography Experiments 4-85
4.6.5 SIR-C Oceanography Experiments 4-86
4.6.6 Summary of SIR-C Mission Requirements for Oceanography 4-97

Chapter 5 SIR-C Sensor Experiments 5-1

5.1 Introduction 5-1

5.2 SIR-C Calibration Experiments 5-1

5.3 Novel Sensor Experiments 5-2
5.3.1 Squinting 5-2
5.3.2 Bistatic Observations 5-2
5.3.3 SCANSAR 5-3

5.3.4 Scattering Statistics Investigations 5-3
5.3.5 Interferometric Topography 5-3
5.3.6 Observations of Rain Cells 5-6

Chapter 6 SIR-C Data Collection and Image Processing 6-1

6.1 Site Recommendations 6-1

6.2 Mission Timing Recommendations 6-1

6.3 Data Acquisition and Processing 6-2

6.4 Data Products 6-5
6.4.1 Level 0 Products 6-6
6.4.2 Level 1 (Survey) Products 6-6
6.4.3 Level 2 (Standard) Products 6-8
6.4.4 Level 3 (Special) Products 6-8

6.5 Data Distribution 6-9

Chapter 7 Summary 7-1

7.1 SIR-C Geoscientific and Sensor Experiments 7-1
7.1.1 Geology 7-1
7.1.2 Hydrology 7-2
7.1.3 Vegetation 7-3
7.1.4 Glaciology 7-4
7.1.5 Oceanography 7-4
7.1.6 SIR-C Sensor Experiments 7-5

7.2. Recommended Mission Parameters and Sensor Performance 7-6
7.2.1 Orbital Parameter and Mission Timing 7-6
7.2.2 Swath Widths and Resolutions 7-7
7.2.3 Frequencies, Polarizations, and Incidence Angles ... 7-7
7.2.4 Radiometric Calibration 7-7
7.2.5 Data Products 7-7

Appendix A: Introduction to Radar Scattering A-1

A.1 Introduction A-1

A.2 The Radar Backscattering Coefficient A-1

A.3 SAR Image Intensity (Tone) A-1

A.4 SAR Image Speckle (Texture) A-2

A.5 Surface and Volume Scattering A-5

A.6 Surface Scattering Mechanisms A-6

A.7 Volume Scattering Mechanisms A-8

Appendix B: Radiometric Calibration of the SIR-C System B-1

Appendix C: References C-1

Figures

1-1. Evolution of spaceborne SAR missions from Seasat to EOS 1-2

1-2. Wavelength, polarization, and angle of incidence SAR imaging parameters 1-3

1-3. Potential SIR-C coverage of the earth as compared to Seasat, SIR-A, and SIR-B 1-4

3-1. Block diagram of the SIR-C sensor 3-3

3-2. Schematic diagram of the distributed antenna 3-4

3-3. SIR-C operation in the dual-frequency quad-polarization mode 3-5

3-4. Dependence of swath width on angle of incidence, in both single- and quad-polarization modes 3-6

3-5. Dependence of swath width on angle of incidence, number of channels, and number of bits in the a) low-resolution mode, and b) high-resolution mode . 3-7

3-6. Maximum incidence angle achievable by SIR-C 3-8

4-1. Distribution of different types of permafrost terrain in the Northern Hemisphere 4-9

4-2. Examples of dendritic stream networks, viewed by SIR-A from above South America 4-10

4-3. SIR-B image of the Ganges floodplain in Bangladesh 4-12

4-4. SIR-A image and Landsat view of the hyperarid region of the Libyan Desert 4-13

4-5. Comparison of Landsat Thematic and aircraft L-band multiple-polarization radar images of the Wind River Basin in Wyoming 4-14

4-6. Two lava flows from the Snake River Plain, Idaho 4-16

4-7. Backscatter from volcanic materials, illustrating the differences in radar characteristics of the two Snake River flows shown in Fig. 4-6. 4-17

4-8. Recognition of variations in the surface texture of different geologic materials, using multipolarization radar images 4-18

4-9. Part of the San Andreas fault system in California, as detected by the Seasat SAR on the basis of surface-material roughness 4-19

4-10. Diagram of a possible method by which fault displacements could be measured by SIR-C 4-20

4-11. SIR-B image of the Grenville front in Canada 4-21

4-12. A floodplain in the Amazon forest, Amazonas, Brazil 4-23

4-13. The role of vegetation coverage in affecting radar returns from the Savannah River Plant, South Carolina 4-24

4-14. Examples of radar-derived topography obtained from SIR-A and SIR-B 4-25

4-15. Characteristics of hydrologic regimes 4-29

4-16. Global distribution of arid and wetland environments. 4-31

4-17. a) A comparison of soil-moisture data showing an agricultural area about 60 km southwest of Fresno, California, as imaged by SIR-B, b) σ^0 vs. soil moisture in the top 5 cm as derived from this image 4-32

4-18. Average dependence of radar backscattering on soil moisture in the top 5 cm measured as percent of field capacity 4-37

4-19. Surface reflectivity 4-39

4-20. The re-reflection effect 4-40

4-21. Spectral response of σ^0 for wet and dry snow 4-42

4-22. Calculated variation of σ^0_{HH} with depth for a dry snow layer containing ice particles 1 mm in radius 4-43

4-23. Penetration into dry sand covering ancient river beds 4-45

4-24. SIR-B image of flooded forest in coastal Ecuador ... 4-48

4-25. SIR-B image of Florida wetlands 4-50

4-26. Microwave response to leaf area index (LAI) 4-56

4-27. Radar response to various wavelengths according to the size distribution of canopy scatterers 4-57

4-28. The role of frequency in canopy backscatter 4-58

4-29. Loss factor of wheat canopy 4-59

4-30. Role of polarization in canopy penetration 4-59

4-31. Illustration of how multipolarization images may be combined to enhance discrimination among different target categories in a forest environment 4-61

4-32. Radar temporal signature of winter wheat 4-62

4-33. Interactions between radar and different ice types ... 4-70

4-34. Seasat SAR image of pack ice in the Beaufort Sea .. 4-73

4-35. Seasat SAR image of the ice island T-3 4-74

4-36. SAR image showing the breakup of fast ice in the vicinity of Banks Island and Prince of Wales Strait .. 4-75

4-37. Seasat SAR images that reveal an eddy in the ice near the ice edge in the Beaufort Sea 4-75

4-38. X/L-band comparison of pack ice 4-76

4-39. Variations in SAR imagery of sea ice, with changes in polarization 4-77

4-40. Seasat SAR image of the Alaska Range 4-81

4-41. Spatial evolution of a SAR-measured wavenumber over a 900-km Seasat pass 4-88

4-42. Seasat azimuth wavenumber falloff in a high sea state 4-89

4-43. SIR-B image of the New York Bight 4-90

4-44. SAR image of an area 100 km long, taken during a pass over the western half of a large warm-water ring less than a month before the ring began to merge again with the Gulf Stream 4-92

4-45. This Seasat SAR image of an area 100 km long, taken from above Nantucket Shoals, provides a dramatic example of bathymetric expressions occasionally evident over large areas 4-93

4-46. Seasat SAR image of an area 100 km long, located just outside the entrance to Chesapeake Bay 4-95

4-47. Comparison of SAR- and scatterometer-derived wind magnitudes 4-96

4-48. Comparison of wind-direction estimates from both the scatterometer and the SAR 4-97

5-1. Geometry for SAR interferometry 5-4

5-2. Composite made from two Seasat passes, separated by 3 days, near Baker, California 5-5

6-1. Altitude vs. orbital inclination for various orbital exact-repeat cycles 6-2

6-2. Potential ground tracks for an orbit with a 70° inclination 6-3

6-3. Potential ground tracks for an orbit with a 92° inclination 6-3

6-4. Optimum SIR-C mission times for each science investigation 6-4

6-5. SIR-C data downlink path 6-4

6-6. Block diagram of the SIR-C processing system—ADSP custom hardware is shown in dashed box 6-5

6-7. Functional block diagram of the image-formatting algorithm used by the ADSP 6-6

6-8. Expected schedule for SIR-C image products 6-7

A-1. Correspondence of the radar backscatter coefficient for the (i,j) in the scene, to the (i,j) digital number in the processed image A-1

A-2. Probability density functions for the mean of N Rayleigh-distributed variables A-1

A-3. Surface scattering from (a) rough water surfaces and (b) calm water surfaces, and volume scattering from (c) high-loss vegetation canopies and (d) low-loss vegetation canopies A-1

A-4. Penetration depth of (a) loamy soil and (b) snow as a function of liquid water content [A-1, Volume 11, Section 11-5] A-2

A-5. Two configurations of height variations: (a) random height variations superimposed on a periodic surface, and (b) random height variations superimposed on a flat surface A-6

A-6. Surface scattering by (a) tangential facets and (b) Bragg-resonant sinusoidal ocean waves, where path length ΔR is an integral number of half wavelengths A-7

A-7. Typical angular variations of the polarized scattering coefficient for a slightly rough surface A-8

A-8. Angular variation of σ^0 for surfaces of varying roughness A-9

A-9. An illustration of volume scattering A-9

A-10. Hypothetical size distribution of canopy scatterers .. A-10

Tables

3-1.	SIR-C sensor characteristics	**3-1**
4-1.	Examples of SIR-C research topics	**4-2**
4-2.	Some SIR-C geology experiment classes	**4-6**
4-3.	Some SIR-C hydrology experiment classes	**4-44**
4-4.	Some SIR-C vegetation science experiment classes	**4-62**
4-5.	Some SIR-C glaciology experiment classes	**4-71**
4-6.	Some SIR-C oceanography experiment classes	**4-87**
6-1.	SIR-C data products	**6-7**
B-1.	Dominant error sources for absolute calibration of SIR-C	**B-2**
B-2.	Shuttle-pointing determination error (in roll axis)	**B-2**
B-3.	Worst-case radiometric error from pointing uncertainty (evaluated at edge of 16-km swath for roll uncertainty of 0.66°)	**B-3**
B-4.	Dominant error sources for relative calibration of SIR-C	**B-4**
B-5.	Relative multichannel calibration error sources for SIR-C	**B-4**

Chapter 1
Introduction

1.1 NASA Shuttle Imaging Radar Missions

expanded global perspectives

In recent years, it has become clear that one of the most important problems confronting earth scientists is that of understanding the earth as a system, and that an integrated, multidisciplinary approach with new, more powerful observing techniques is needed. The central objective of such an approach would be to improve our understanding of those processes governing the biogeochemical, climatic, and hydrologic cycles of the earth. This would require, in turn, that we understand the atmospheric, biospheric, hydrospheric, cryospheric, and solid-earth components of the earth system, and that we develop new instrument systems and missions that could provide global data sets. The approach requires the expanded global perspective that can be obtained only through novel satellite and remote sensing systems whose performance has been much improved over current systems.

Spaceborne microwave remote sensing offers such an expanded view of the earth for geoscientific research, supplementing the information obtainable in the visible and infrared spectrum. The Shuttle Imaging Radar (SIR) missions, which provide microwave images of the earth, are a vital element of NASA's earth observations program. Besides valuable scientific information, these missions are yielding significant advances in spaceborne imaging radar technology.

an evolving sequence of experiments

The successful SIR-A and SIR-B missions have demonstrated that such scientific objectives as geologic mapping, regional hydrologic studies, and radargrammetric contouring can be accomplished using imagery collected during a one-week mission and with a single wavelength and polarization. These Shuttle missions have also shown that there is a significant advantage in flying, retrieving, modifying, and reflying synthetic aperture radar (SAR) sensors of progressively increased sophistication. In fact, the SIR missions may be viewed as an evolutionary sequence of experiments that, for relatively low cost, will greatly enhance our understanding of the role of wavelength, polarization, and angle of incidence, for a variety of geoscientific applications.

optimum radar parameters

Two additional Shuttle Imaging Radar missions, SIR-C and SIR-D, are planned for the 1990's. These missions will use an imaging radar with new, more powerful capabilities and will test multiparameter SAR technology as well as provide new scientific information. The missions will also allow geoscientists to determine which radar parameters are optimal for studying polar ice morphology, oceanic winds and waves, geomorphology, vegetation patterns and processes, and hydrologic environments. At the same time, SIR-C and SIR-D will permit new technologies to be incorporated into the design of a next-generation imaging radar with significantly enhanced flexibility and reliability. Because of these technological advances, the SIR-D radar can be reused directly on the Earth Observing System (EOS) polar orbiting platforms being planned for launch in the early 1990's.

1.2 The SIR-C Mission

The SIR-C mission, which will provide a powerful new tool for scientific studies of the earth, is a significant step forward in the evolution of an advanced spaceborne imaging radar. It will provide

(1) The first opportunity to use *simultaneous multifrequency* radar imagery from space for geoscientific studies of the earth as a planet

(2) The first spaceborne high-resolution imaging sensor with a *simultaneous multi-polarization* capability

(3) The first multiparameter *polar orbiting* imaging radar, which will supply coverage during *two different seasons*

In addition to these scientific firsts, SIR-C will also feature several significant technological innovations, a test-bed for distributed solid-state radar technology, and near real-time processing with the JPL Advanced Digital SAR Processor (ADSP).

evolution of SAR missions

SIR-C is part of a series of spaceborne imaging radar missions (Fig. 1-1) that began with the June 1978 launch of the Seasat SAR and continued with the November 1981 SIR-A and October 1984 SIR-B missions. The SIR-C and SIR-D missions will result in an instrument to be used on the EOS polar platform. The initial operating configuration (IOC) for the EOS platform is currently scheduled for a 1993 launch. SIR-C/D will be flown in the early 1990's. During this same general period, the L-band ERS-1 SAR (Japan), the C-band ERS-1 (ESA), and the C-band Radarsat SAR (Canada) would also be flown. These latter missions are primarily focused on particular applications (geologic mapping, ocean wind/wave mapping, and ice mapping, respectively) and have fixed parameters. By contrast, the NASA instruments are multiparameter SARs for use in several geoscientific applications.

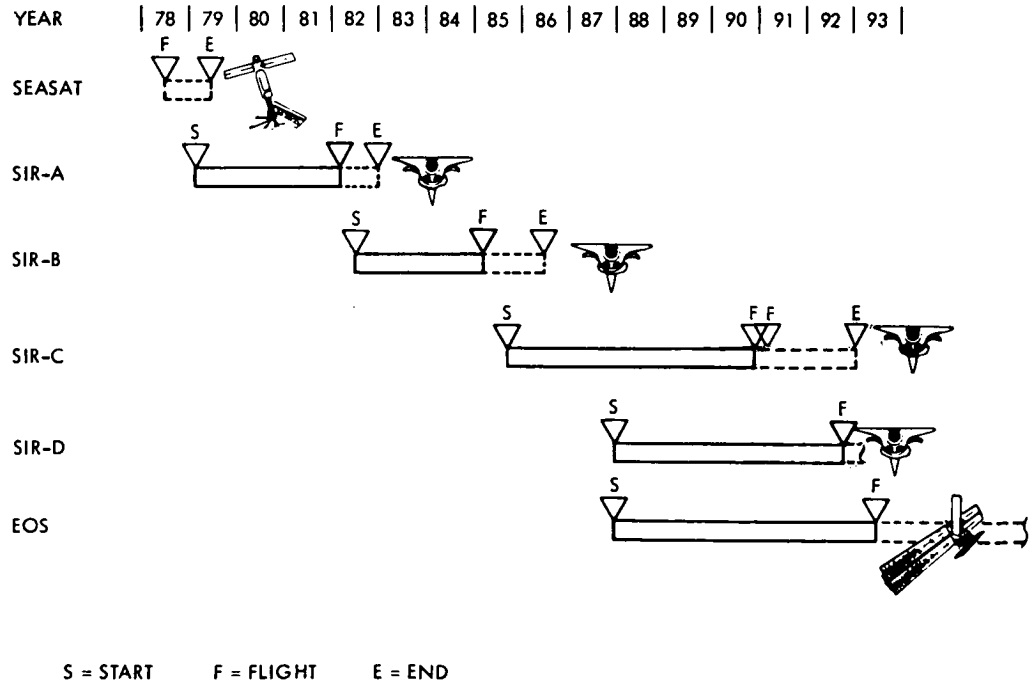

Fig. 1-1. Evolution of spaceborne SAR missions from Seasat to EOS

SIR-A and SIR-B parameters

Both the SIR-A and SIR-B sensors were derived from the Seasat SAR, and all three were operated at L-band (1.275 GHz) with HH polarization (horizontally polarized transmission, horizontally polarized reception). The Seasat SAR used a fixed 23° angle of incidence, and SIR-A used a fixed 50° angle. SIR-B provided, for the first time, the capability to mechanically tilt the antenna so that multiple angles of incidence could be obtained. Thus, SIR-B was the first spaceborne radar to provide flexibility in the incidence angle parameter. This has allowed a significant improvement in our understanding of radar backscatter models and also has permitted investigations of new radar stereo techniques for topographic applications.

SIR-C parameters

In addition to multiple angles of incidence (15°–55°), the SIR-C mission will provide multiple wavelength (L-band, C-Band, and potentially X-band through the addition of the German X-SAR instrument) and multipolarization capability (HH, VV, HV, and VH) for L-band and C-band, thereby significantly enhancing the instrument's flexibility. These three illumination parameters (wavelength, polarization, and angle of incidence) may be thought of as a three-dimensional instrument parameter space, as suggested in Fig. 1-2. As shown, Seasat, SIR-A, and SIR-B were limited to a fixed wavelength, although SIR-B allowed the angle of incidence to be varied. The range of parameters allowed by the SIR-C mission is as shown by the shaded box: 6- and 23-cm wavelengths (and possibly 3-cm), all linear polarization states (HH, VV, HV, and VH) at C- and L-bands, and 15°–55° angles of incidence. SIR-C will not only provide images of the magnitudes of HH, VV, and cross-polarized returns, it will also provide images of the phase difference between HH and VV returns.

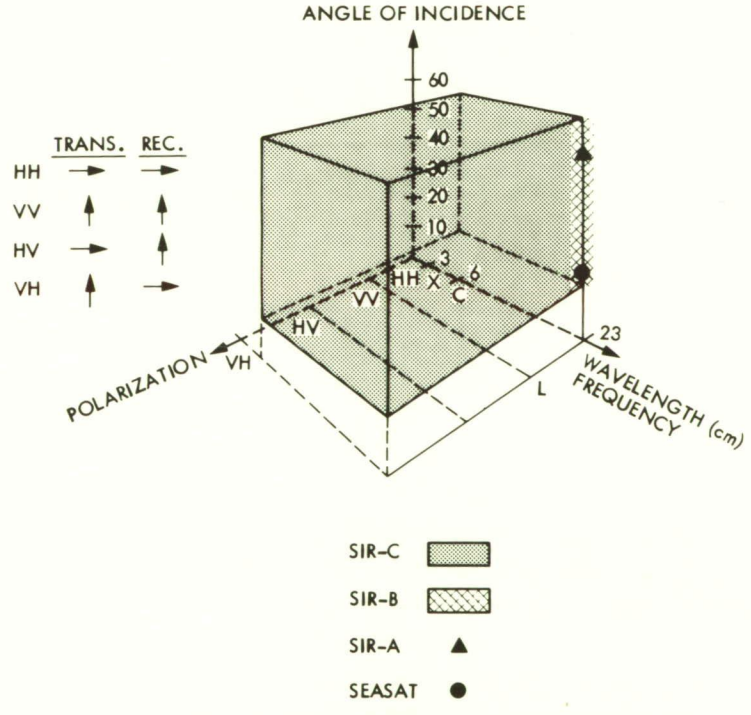

Fig. 1-2. Wavelength, polarization, and angle of incidence SAR imaging parameters, and the range of parameters covered by Seasat and SIR

Figure 1-3 illustrates the potential SIR-C mission coverage of the earth. The SIR-C mission includes two flights, thereby providing seasonal coverage of vegetation and hydrologic environments. The swath width varies from 15 to 90 km, and digital data will be stored onboard or relayed to the ground via the Tracking and Data Relay Satellite System (TDRSS) data link.

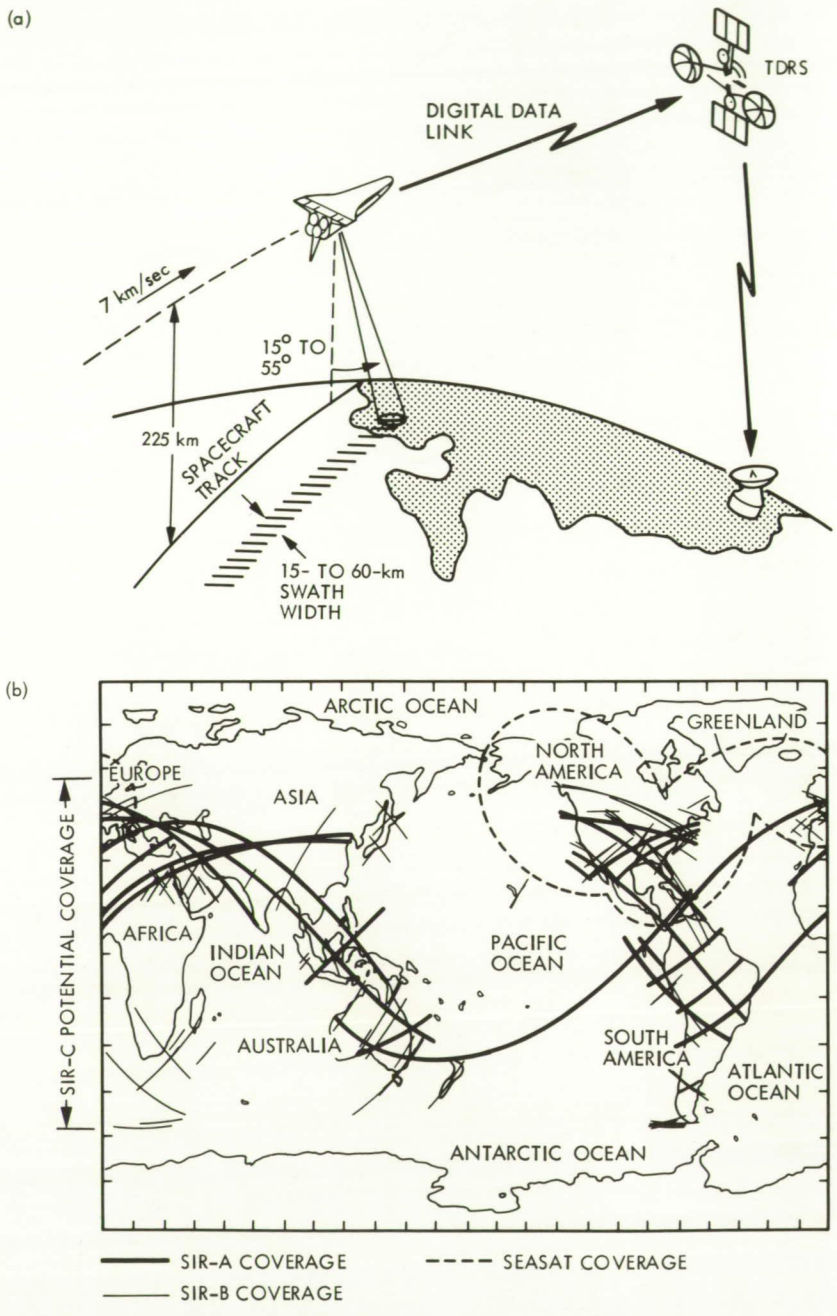

Fig. 1-3. Potential SIR-C coverage of the earth in a 57° orbit and a 90° orbit as compared to Seasat, SIR-A, and SIR-B, showing the global distribution of data coverage

In a polar orbit, SIR-C would thus have the potential to image virtually any area of the earth including the polar regions. (SIR-B was limited to $\pm 57°$ latitude, and SIR-A to $\pm 38°$.)

A more detailed discussion of SIR-C instrument characteristics is presented in Chapter 3 of this Science Plan.

1.3 Science Plan Organization

chapter descriptions

This SIR-C Science Plan provides broad guidelines for the organization of the SIR-C mission, and a general description of geoscientific experiments that are possible with SIR-C. Chapter 2 of this plan discusses the role of spaceborne imaging radars in earth observations, with particular emphasis on the evolution and scientific importance of the SIR missions. The challenges to remote sensing posed by global system models are discussed, along with a delineation of how spaceborne radar imagery will be used to gather important global data.

The third chapter provides a detailed description of the SIR-C instrument.

Chapter 4, which is the heart of this plan, presents a more detailed discussion of various geoscientific experiments that could be conducted with SIR-C, and the types of results that could be expected. This chapter is divided into separate sections on geology, hydrology, vegetation science, glaciology, and oceanography. Each of these sections seeks to answer the following questions:

(1) What are the general scientific problems for which remote sensing data are considered helpful?

(2) What is the specific role of imaging radar?

(3) What is the potential contribution of SIR-C and what kinds of experiments would be useful?

These general experiment descriptions are intended to provide guidance in the design of specific experiments. The discussions here are meant to be illustrative of the type of investigations that the science community believes will yield significant advances in our understanding of the earth as a system. *It is expected that meaningful SIR-C experiments may be conducted that are not specifically discussed in this plan.*

Chapter 5 discusses those technique-related experiments that may be conducted with SIR-C, including both sensor and data-processing investigations.

The sixth chapter outlines the general mission plan for SIR-C, with particular emphasis on data collection and image processing.

Chapter 7 provides a summary of the geoscientific and sensor experiments suggested for SIR-C and also summarizes the required mission parameters and sensor performance.

A tutorial discussion of the fundamentals of radar scattering, with particular emphasis on the roles played by wavelength and polarization in both surface and volume scattering, and a discussion of SIR-C radiometric calibration are presented as appendices.

Chapter 2
The Role of Spaceborne Imaging Radars in Studies of the Earth

2.1 Background

Seasat

Although airborne imaging radars have been used for geologic mapping for over twenty years, the era of spaceborne remote sensing with imaging radars began in June 1978 with the launch of Seasat. This unmanned spacecraft carried five sensors, including a SAR, in a circular orbit with an inclination of 108° and an altitude of 800 km. The Seasat SAR was operated at 1.275 GHz (L-band), with a single HH polarization, and a fixed look angle of 20°. After only 100 days of operation, Seasat was silenced by a power-system failure. However, during that time, a massive amount of SAR data was obtained that is still being analyzed. The SAR data were relayed from Seasat to a limited number of ground stations, which provided partial coverage of North America, Central America and the Caribbean, and Western Europe. The total surface area imaged was about 10^8 km^2. All Seasat SAR images were optically correlated, and many were digitally correlated into 100- × 100-km scenes [2-1].

Seasat results

Although Seasat was launched primarily for oceanographic studies, the SAR images have been used for both oceanic and land studies, and atlases of Seasat SAR images have been published [2-2, 2-3]. Seasat SAR images have confirmed that microwave imaging radars are very sensitive to the geometric patterns, forms, and shapes of the earth's surface, as well as to changes in dielectric properties of earth materials, particularly soil moisture properties and ice–water boundaries.

Seasat SAR images of the ocean have shown a strong correlation between SAR image brightness and the amplitude of 30-cm surface waves, which in turn are directly responsive to the local wind. Moreover, analyses have suggested that SAR ocean imagery contains information at least occasionally related to the local wind direction. Seasat has provided an extensive series of images of the Beaufort seacoast of the Arctic Ocean, and this series has been used for studies of ice dynamics and icepack features. However, it should be pointed out that there was no ground verification of the Beaufort Sea features during the Seasat mission, because of the difficulty of surface operations during the Arctic summer.

Seasat SAR images of the land surface have been used for geologic mapping, particularly for obtaining structural information, and for other surface morphology investigations. In regions of high relief, Seasat SAR images show a strong image distortion due to radar layover; in areas of gentle slope, on the other hand, there is a strong sensitivity to subtle changes in relief. The layover for mountainous regions is due to the steep (23°) angle of incidence chosen for accentuating oceanic surface features. These images have also been used for investigating soil moisture, hydrologic characteristics, urban morphology, and vegetation cover.

SIR-A mission

The NASA Shuttle Imaging Radar program has provided an opportunity to extend imaging radar observations through a series of brief missions of 7 to 10 days each. The Shuttle Imaging Radar-A (SIR-A) experiment was conducted during the 2-day flight of the Space

Shuttle Columbia in November 1981 [2-4]. The SIR-A sensor used Seasat technology and thereby used the same wavelength (23 cm) and polarization (HH). However, there were two significant instrument changes, the first being that the angle of incidence was changed to a fixed 50°, and the second that all data were optically recorded and correlated. The SIR-A mission was primarily for geologic mapping investigations, and the moderate incidence angle greatly diminished the geometric distortion of high-relief regions as encountered with Seasat.

SIR-A results

In addition to its use for geologic mapping, SIR-A provided other key results including the imaging of buried drainage channels in a hyperarid region of southern Egypt (a demonstration that many arid-region morphologic features are better depicted in radar imagery than in Landsat images), the imaging of cloud-covered tropical regions, and the repetitive observation of dynamic ocean phenomena. SIR-A images consisted of long photographically reproduced swaths about 50 km wide. Approximately 10^7 km^2 of the earth's surface was imaged with 40-m resolution for selected passes between latitudes ranging from about 41° N to 36° S.

Although SIR-A images provided new and scientifically important results, quantitative data analyses were difficult because of both the optically correlated images and the limited dynamic range imposed by the optical film. Moreover, the fixed incidence angle of 50° chosen by the team of geologists was not optimum for oceanic surface studies or for other hydrologic investigations.

SIR-B mission

The next Shuttle Imaging Radar experiment, SIR-B, took place during October 1984, with the launch on the Space Shuttle Challenger of a modified and extended version of the SIR-A sensor. SIR-B, like SIR-A, used a fixed 23-cm wavelength and a fixed HH polarization. However, SIR-B added the capability of changing the angle of incidence and also provided a means for digitally recording and processing the SAR images. The sensor's data system provided for onboard digitization of the radar echoes and for data transmission to the ground at 46 Mb/s through the TDRSS; the data system also provided a digital recording backup through a 30 Mb/s onboard tape recorder. Due to a failure of the Shuttle–TDRSS communications antenna system, almost all of the SIR-B data were recorded on the tape recorder, thereby leading to a greatly reduced swath. Swath widths of SIR-B data range typically from 10 to 50 km, depending on incidence angle.

SIR-B results

One of the key scientific objectives of the SIR-B experiment was to demonstrate the capability of stereo imaging. This was successfully achieved over a number of sites. Stereo images were used to generate a digital topographic data base of Mount Shasta. Further, computer processing allowed the generation of perspective views of the mountain from multiple look directions (see the upper right image on the front cover). This demonstrates the enormous potential of using spaceborne stereo radar data for three dimensional analyses of the surface morphology of the earth (and the planets).

Over a number of sites, multi-incidence-angle imagery was used to classify terrain units by deriving their "angular signature." This technique has been used to derive vegetation maps of the Cordon la Grasa region in western Argentina, to classify the forest cover of a test site in Baker County in northern Florida, and to classify the lava-flow types near the Kilauea Crater in Hawaii. These results are very encouraging, opening the possibility of using "imaging radar angular scatterometry" in a manner similar to visible and IR imaging spectroscopy for the classification of surface units.

2.2 New Challenges to Remote Sensing: Global Studies

discipline-specific satellites

Remote sensing as a science has developed over the years through instruments and techniques developed for specific geoscientific disciplinary problems. Most of the satellite remote sensing programs have been aimed toward one or two disciplinary objectives, i.e., Nimbus for meteorology and oceanography, Landsat for vegetation and rock type discrimination, Seasat for oceanography, GOES for meteorology, etc. The results obtained from these satellite remote sensing programs have provided a first global glimpse of the earth as a system and have been used by scientists in established disciplines in concert with data obtained by more conventional means. Certainly "single-discipline" satellites will be launched in the future, including the U.S. Upper Atmospheric Research Satellite for atmospheric studies, the Canadian Radarsat for polar ice mapping, the Japanese ERS-1 SAR for geologic mapping, and the European ERS-1 for ocean applications.

multidisciplinary approach

As mentioned in Section 1.1, one of the most important problems confronting earth scientists is that of understanding the earth as a system. This enterprise will require not only an expansion of the capabilities of current remote sensing instruments (imaging spectrometers, SARs, radiometers, etc.) but also the ability to merge images acquired from different instruments and to deliver global data sets in a timely fashion. It is clear that most of these needs are best met by observations from polar-orbiting satellites, but that there are enormous problems in downlinking, processing, delivering, archiving, and analyzing such global data sets.

We do not yet know what the optimum spectral channels are for many geoscientific problems of interest, although much progress has been made in recent years. In the microwave regime, for example, although we generally understand that L-band or C-band is best for soil moisture estimation, we do not know which frequencies or polarizations are optimum for ice type discrimination, we have not had an opportunity to test for optimum vegetation-discrimination frequencies from satellite altitudes, and we do not fully understand which wavelengths are best for the measurement of oceanic surface features. The synoptic view from space is critical to improving our understanding, since there is uniform illumination (a constant angle of incidence) across the swath, and much better long-term instrument calibration is maintained, thereby permitting quantitative studies of surface morphology.

multisensor approach

Remote sensing of the earth becomes most effective when observations are made in all portions of the electromagnetic spectrum and over long periods of time. Terrain and oceanic surface features have distinctive signatures in the visible, infrared, and microwave portions of the spectrum and usually have strong temporal characteristics that vary over periods ranging from hours to years. The history of satellite remote sensing is composed largely of missions primarily aimed at specific geoscientific problems for which sensors operating in a single portion of the spectrum were used. Broadly speaking, visible and shortwave infrared wavelengths are used when sensitivity to surface chemistry is required (e.g., the Landsat Thematic Mapper), the thermal infrared is used for sensitivity to surface temperature (e.g., the Heat Capacity Mapping Mission), and the microwave spectrum is used for sensitivity to surface morphology (e.g., Seasat).

2.3 The Role of Imaging Radars

sensitivity to surface morphology and water

Synthetic aperture radars operating at satellite altitudes provide high-resolution images that are sensitive to surface geometry or morphology and to the presence of water in its liquid or frozen states. Since the atmosphere introduces essentially no attenuation at the longer microwave frequencies (L-, C-, or X-bands), a spaceborne SAR provides an all-weather imaging capability that is independent of sun angle.

geologic mapping

Imaging radars have been shown to be very useful for geologic mapping and are especially sensitive to structural features and changes in lithology. Radar images also have been used to study very subtle geologic features related to tectonic activity and to find buried drainage systems in the Eastern Sahara.

canopy morphology

SAR imagery is also useful for vegetation studies and is sensitive particularly to canopy morphology and biomass. Moreover, when SAR imagery is combined with visible imagery (e.g., Seasat with Landsat), vegetation classification accuracy is greatly increased.

soil moisture

Because of the high dielectric constant of water (approximately 80) and low dielectric constant of dry soil (approximately 3), SAR imagery of terrain is responsive to changes in soil moisture. For this reason, SAR has enormous potential for use in various aspects of hydrology research where soil moisture is of importance. The sensitivity of SAR imagery to surface relief is also of interest to hydrologists studying watershed characteristics, runoff, percolation, etc.

ice dynamics

The Seasat SAR showed that radar imagery is very useful for studies of polar-ice dynamics, and it is expected that multiwavelength and multipolarization SAR imagery will also provide valuable information on sea-ice types as well. SAR imagery is also useful for studying freshwater ice and glaciers.

ocean surface features

SAR imagery acquired at L-band and C-band is sensitive to the short gravity waves (e.g., 30-cm wavelength) on the ocean surface, which are in turn modulated by the longer gravity waves and surface winds. SAR imagery of the ocean is in fact quite sensitive to changes in the surface geometry, which may be related to winds, waves, bathymetry, internal waves, or eddies.

2.4 Evolution to the Space Station Era

EOS

SIR-C is a logical step toward active microwave observations of the earth from the Earth Observation System (EOS), a series of satellite platforms and related information systems associated with the Space Station. As currently conceived, EOS would consist of several polar-orbiting unmanned platforms to be launched in the 1990s, each carrying various combinations of remote sensing instruments. These sensors would provide near-simultaneous observations of the earth in the visible, the shortwave infrared, the thermal infrared, and the microwave portions of the spectrum. The major scientific objective of EOS is to provide global data sets for geoscientific studies of the earth as a system.

SIR-C will provide the first opportunity to understand the optimum wavelengths, polarizations, and illumination geometries for SAR imagery of the earth and will also provide a technology test-bed leading directly to a multiparameter SAR design for use on one or more of the EOS platforms. It is expected that SIR-C will be followed by SIR-D, a Shuttle-borne multiparameter SAR that would be virtually identical to the EOS SAR.

Chapter 3
SIR-C Sensor Characteristics

3.1 SIR-C Technology

SIR-C improvements

The baseline design characteristics of the SIR-C sensor as compared to Seasat, SIR-A, and SIR-B, are described in Table 3-1. The principal improvements in the SIR-C sensor over SIR-B are: an additional wavelength band (C-band), multiple polarization capability (HH, VV, HV, VH) including the phase difference between HH and VV, dual bandwidth capability, electronic beam steering, and the capability to maximize the swath width at various look angles by exciting different segments of the antenna. In addition, an X-band VV-polarized SAR will be added to this mission by DFVLR (German Aerospace Research Establishment, Federal Republic of Germany).

Table 3-1. SIR-C sensor characteristics

Parameters	Seasat	SIR-A	SIR-B	SIR-C
Mission date	1978	1981	1984	1990
Orbital altitude	800 km	259 km	225 km	225 km[a]
Orbital inclination	108°	38°	57°	≥ 57°
Frequency	1.28 Ghz	1.28 GHz	1.28 GHz	1.25 GHz[c]
				5.3 GHz[c]
				9.6 GHz[b]
Polarization	HH	HH	HH	HH (L C)
				VV (L C X)[b]
				VH (L C)
				HV (L C)
Incidence angle	23°	50°	15°-55°	15°-55°
Swath width	100 km	50 km	20-50 km	15-90 km[c]
Azimuth resolution	25 m (4 look)	40 m (6 look)	30 m (4 look)	30 m (4 look)[c]
Range resolution	25 m	40 m	58-17 m	60-10 m[c]
Peak power	1 kW	1 kW	1 kW	3.8 kW (L)
				2.1 kW (C)
				3.3 kW (X)[b]
Bandwidth	19 MHz	6 MHz	12 MHz	10 or 20 MHz
Optical data collection	42 hours	8 hours	8 hours	N/A
Digital data collection	42 hours	N/A	8 hours	50 h/channel, 5 channels

[a]Approximate

[b]X-band VV-polarized SAR to be added by DFVLR

[c]Based on preliminary design parameters

distributed SAR

Because the SIR-C Science Working Group has recommended a cross-polarized capability at large angles of incidence (discussed later in this plan), a distributed radar approach will be implemented for SIR-C. A distributed SAR has an advantage over a conventional SAR because numerous low-power (solid-state) transmitters, distributed across the antenna aperture, are used instead of a single high-power transmitter. Since large power losses typically occur in the corporate feed of a conventional antenna, as much as an eight-fold improvement in efficiency can be obtained using a distributed SAR. In addition, a solid-state distributed system has a high inherent redundancy and potentially extended lifetime compared to a conventional single-source approach. Another advantage of a distributed antenna is that electronic scanning in both range and azimuth is more easily implemented than with a conventional antenna. The power, redundancy, and scanning requirements for SIR-C are similar to those for the proposed EOS SAR.

3.2 Sensor Description

3.2.1 Sensor Subsystems

block diagram

Figure 3-1 is a block diagram of the SIR-C instrument. The sensor will be composed of several subsystems: the antenna array, the exciter, the receivers, the data-handling network, and the ground SAR processor. The SIR-C design will allow a very flexible selection of operating modes and is further described below.

antenna

The antenna is composed of two planar arrays, one for L-band dual-polarized operation and the other for C-band dual-polarized operation. Each array is composed of a uniform grid of dual-polarized microstrip antenna radiators, each polarization port of which is fed by a separate corporate feed network. The overall size of the antenna is 12.0 × 4.0 m, with the L-band aperture being 12.0 × 2.9 m and the C-band aperture 12.0 × 0.7 m.

distributed T/R units

Amplification of the radar pulses (both transmitted and received) will be accomplished in distributed fashion, with solid-state high-power amplifiers (HPA), low-noise amplifiers (LNA), and 4-bit phase shifters distributed across the array as shown in Figure 3-2. A transmit/receive (T/R) unit is assigned to 18 microstrip elements distributed along the long dimension of the antenna. This will allow the antenna beam to be electronically steered, thereby eliminating the need for mechanical steering and providing much more flexibility during the mission for imaging at various incidence angles.

To achieve even more flexibility, SIR-C will provide a choice of partial aperture or full aperture. This choice involves either exciting a portion of the antenna's short dimension or exciting the entire aperture. The use of a portion of the aperture increases the antenna beamwidth and increases the swath width at near-nadir incidence angles.

transmitter performance

The transmitter peak power is 3.8 kW at L-band and 2.1 kW at C-band. As previously pointed out, this peak will be achieved by combining in a coherent fashion the output from 18-element subarrays of microstrip elements on the antenna surface. Each solid-state amplifier is driven through a corporate feed network by a central radar exciter, one exciter for each frequency. The exciter output is a train of chirped pulses with a 33-μs pulse width and a pulse repetition frequency (PRF) that varies from approximately 1200 to 1800 Hz.

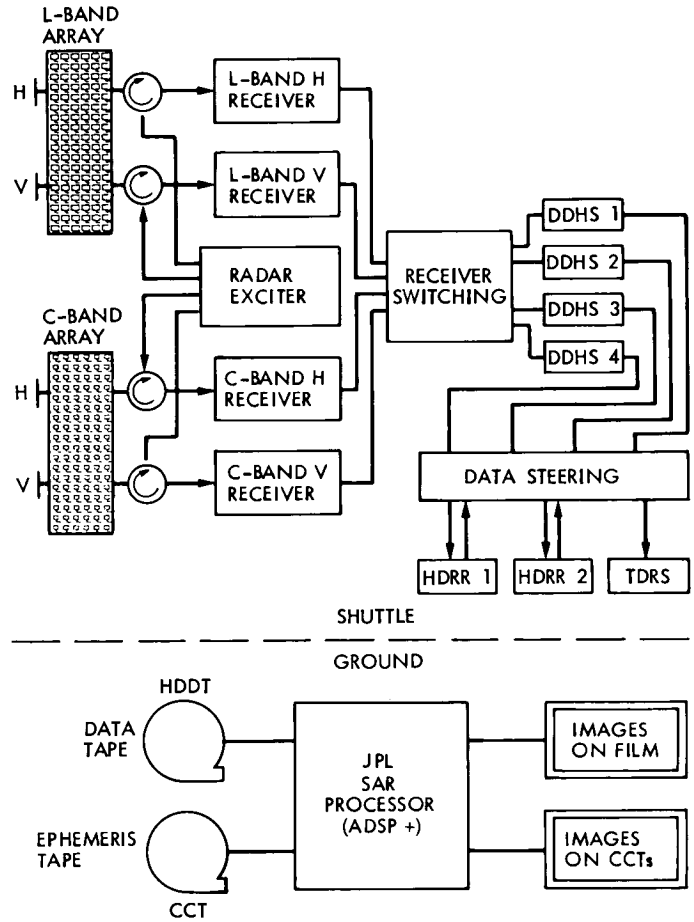

Fig. 3-1. Block diagram of the SIR-C sensor

depending on Shuttle altitude and system configuration. The bandwidths of the chirp modulator are 10 and 20 MHz at both L-band and C-band. The C-band exciter signal carrier will be derived from the L-band signal by frequency synthesis techniques.

receiver and data handling

Four solid-state receivers (back ends) are planned, two for L-band and two for C-band. The radar echoes from each receiver are routed through a receiver switching network to four digital data handling system (DDHS) networks, as shown in Figure 3-1. These will then be directed to onboard 100-Mb/s tape recorders or through the Shuttle–TDRSS Ku-band 50-Mb/s data link. This combination of real-time (TDRSS) or delayed-time (tape-recorder) data steering allows coverage of virtually any location on the earth over which the Shuttle flies.

ground processor

Data tapes either brought back with the Shuttle or recorded through TDRSS will be processed at JPL using the ADSP, leading to processed SAR images in both computer-compatible tape (CCT) and film formats.

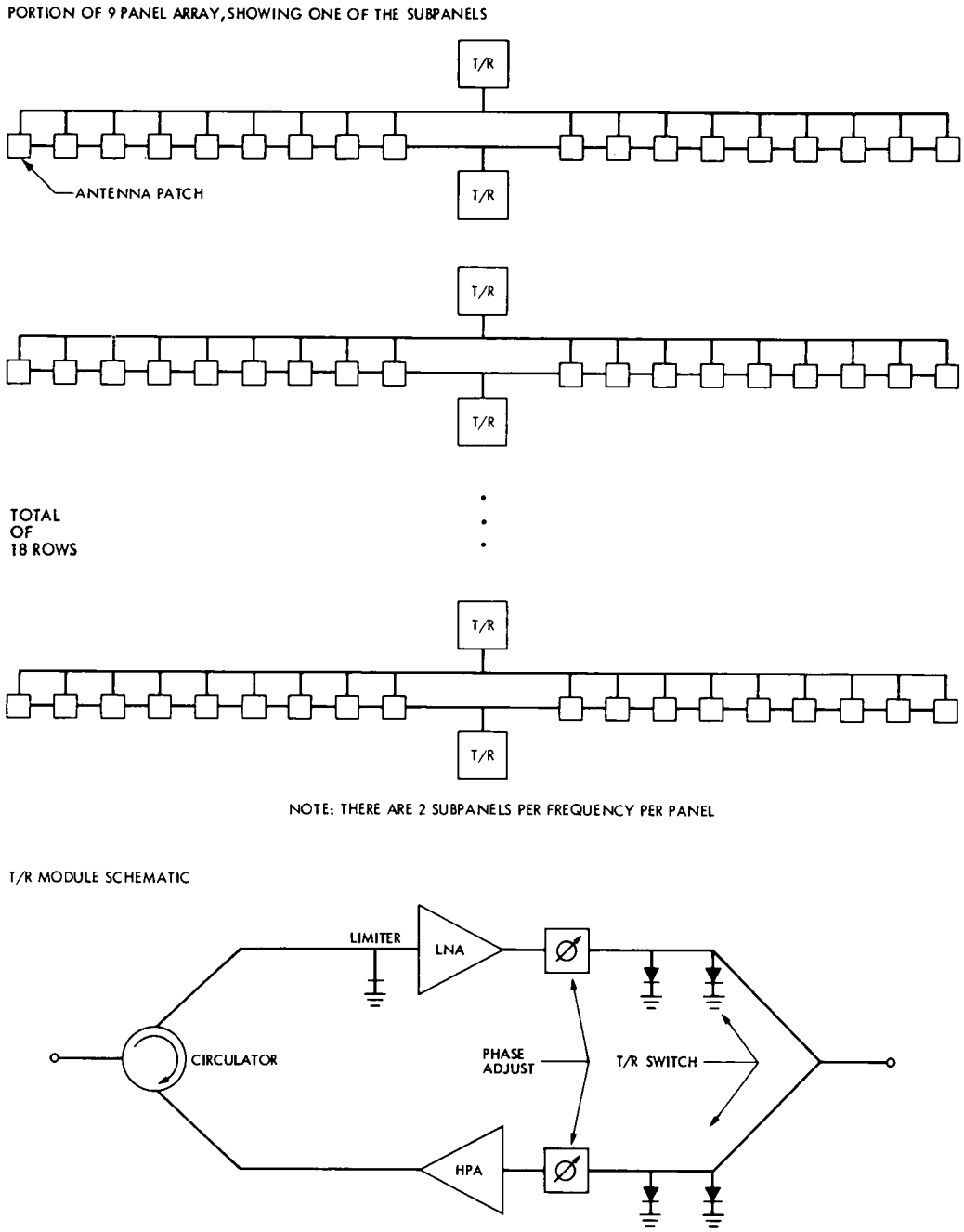

Fig. 3-2. Schematic diagram of the distributed antenna

3.2.2 Operational Modes

As mentioned above, the SIR-C sensor will be capable of operating in a number of different modes. Two of these modes are of particular interest, as they represent a novel way of acquiring simultaneous multipolarization data. These modes are the *single-frequency quad-polarization mode* (SFQP) and the *dual-frequency quad-polarization* (DFQP) mode.

SFQP mode

The single-frequency quad-polarization mode operates as follows. First, the antenna is excited so that one polarization (H for example) is transmitted. The resulting echoes are received by both receivers (H and V), resulting in HH and HV data. A second pulse excites the other polarization (V for example) so that it is transmitted, and again the echo is received by both receivers, resulting in VH and VV data. The process is then repeated one pulse repetition period (1/PRF) later. This process provides coherent and fully registered 4-polarization imagery. The disadvantage of this procedure is that the radar must operate at twice the normal PRF, thus limiting operation to lower look angles than would be indicated by the antenna-imposed range-azimuth ambiguity limit (see discussion below).

DFQP mode

The dual-frequency quad-polarization mode, which is shown schematically in Figure 3-3, is similar, with the exception that both L- and C-band H transmitters are activated simultaneously, followed by the V transmitters. The resulting data rate is, of course, twice that of the single-frequency quad-polarization data, which results in a narrower swath width (see below).

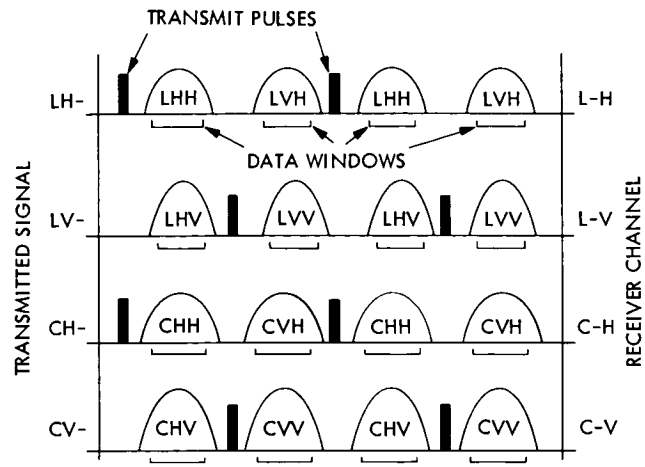

Fig. 3-3. SIR-C operation in the dual-frequency quad-polarization mode

3.2.2.1 Swath Width

The ability of SIR-C to acquire data simultaneously at multiple frequencies and polarizations will substantially increase its flexibility for conducting geoscientific research. However, as more simultaneous channels (frequencies and polarizations) and increased dynamic range are sought, the swath width decreases.

swath width limitations

At near-nadir incidence angles, the swath width is limited by the beamwidth in the cross-track plane of the antenna pattern. At large incidence angles, the swath width can be limited by the data rate that can be accommodated by the Shuttle-TDRSS digital link or the Shuttle tape recorders. The data-rate-limited swath for a given range resolution is inversely proportional to the product of the number of channels, the number of bits per sample (bps), the PRF, and the sine of the incidence angle. Figure 3-4 illustrates the dependence of the swath width on incidence angle for the SFQP and DFQP modes with varying numbers of bits per sample, and for both high and low resolutions.

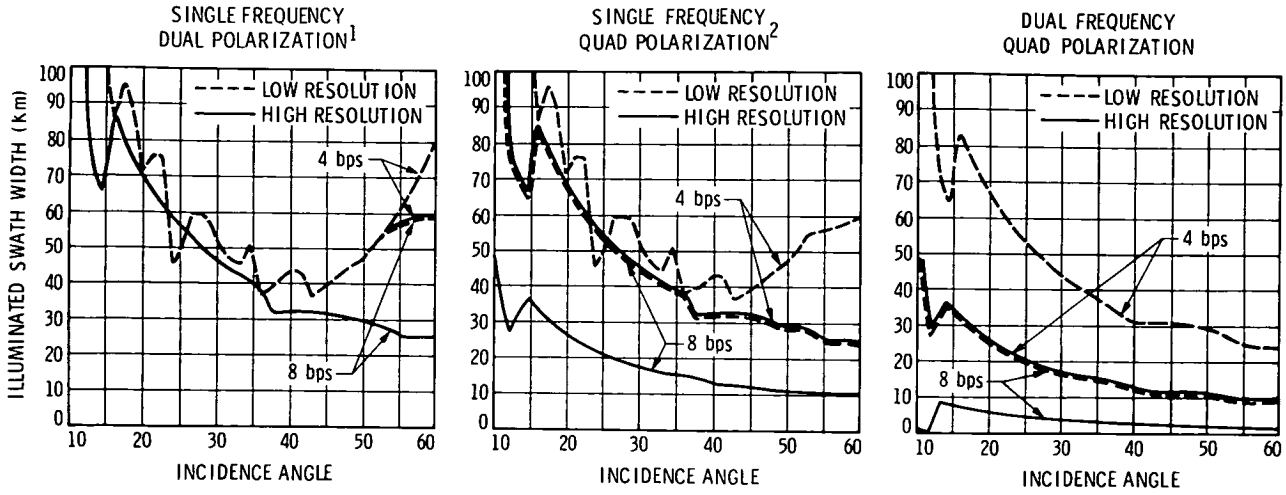

1 SAME FOR DUAL FREQUENCY, SINGLE POLARIZATION
2 SAME FOR DUAL FREQUENCY, DUAL POLARIZATION

Fig. 3-4. Dependence of swath width on angle of incidence, in both single- and quad-polarization modes. At near-nadir angles, the swath width is antenna-beamwidth limited, and at large angles of incidence the swath width is data-rate limited

Figure 3-5 is a more graphic representation of the dependence of swath width on the number of channels, the number of bits, resolution (bandwidth), and the incidence angle. The number of bits per sample determines the dynamic range of the radiometric intensity of the recorded echo. The 8-bit dynamic range of the SIR-C images is expected to be about 40 dB, with a 10 dB signal-to-noise ratio (SNR). A 4-bit quantization level would reduce the dynamic range to approximately 17 dB. Because of the data-rate limitation, increasing the dynamic range (number of bits) results in a decreased swath width at moderate to high incidence angles. For example, in the SFQP mode at a 55° incidence angle, 8-bps sampling will result in a 26-km swath width whereas 4-bps sampling will increase the swath width to about 56 km at low resolution.

BFPQ

Based on recommendations of the SIR-C Science Working Group, a Block Floating Point Quantizer (BFPQ) will be implemented on SIR-C. This technique offers a means for increasing the swath and also obtaining an effectively larger dynamic range. As the radar echoes are received, a determination is made periodically (every few milliseconds) as to which portion within the total dynamic range most needs to be sampled. This portion is then digitized with a relatively small rate (e.g., 4 bps) and recorded. For weak radar echoes from a smooth surface, for example, the 4-bps sampling window would be applied to the lower portion of the total dynamic range; for strong radar echoes from a rough surface, the 4-bps sampling window would be applied to the upper portion of the total dynamic range. In this way, an effective sampling rate of 8 bps or more is achieved, while maintaining the capability to adequately sample the entire dynamic range within the data-rate limitations. The only possible disadvantage of the BFPQ technique is for rare cases where there is an abrupt change from a weak target to a strong one, as for example with the boundary from water to land; in this case, the 4-bps sampling window may be set for low returns from the water surface, so that strong onshore returns may be saturated. Practical experience with simulated BFPQ images acquired by aircraft SAR data suggests, however, that this effect is minimal.

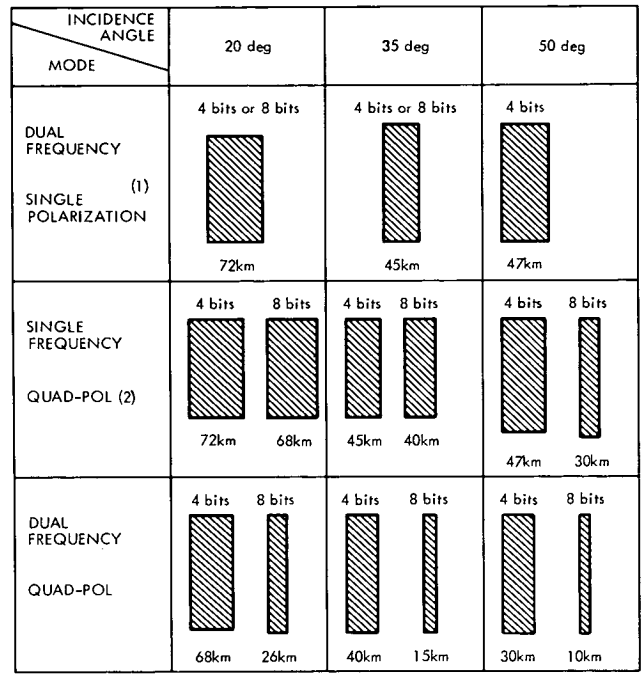

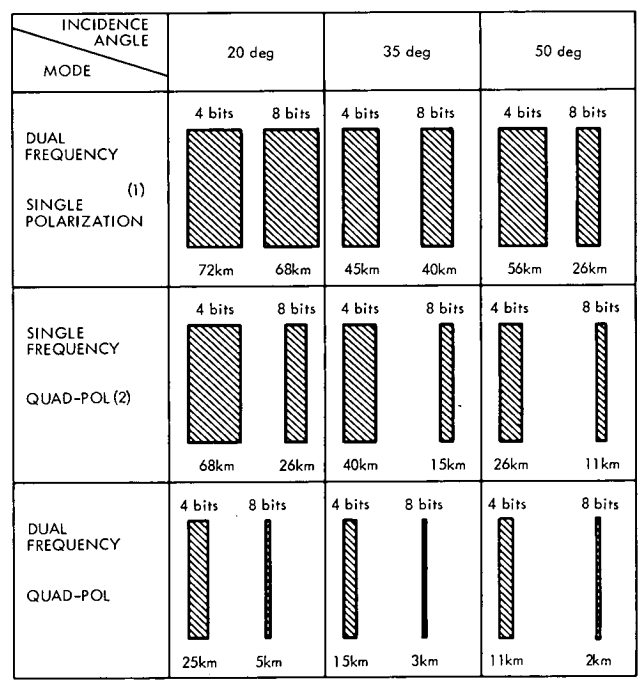

(1) SAME FOR SINGLE FREQUENCY, DUAL POLARIZATION MODE

(2) SAME FOR DUAL FREQUENCY, DUAL POLARIZATION MODE

Fig. 3-5. Dependence of swath width on angle of incidence, number of channels, and number of bits in the a) low-resolution mode, and b) high-resolution mode

3.2.2.2 Maximum Incidence Angle

backscatter assumptions

The maximum look angle achievable for single- and quad-polarization data takes for various natural targets is shown in Fig. 3-6. Most of the backscatter models used to assess SIR-C system performance were based on scatterometer data. The ocean models were based on computed maximum and minimum radar backscattering coefficients from the ocean for wind speeds of 2 m/s and 24 m/s and look directions (azimuth) of 90° and 180° relative to the wind vector [3-1]. The C-band geology models were based on maximum and minimum radar backscattering coefficients from over 50 data sets acquired for many types of bare rock surfaces [3-2]. The L-band geology models were based on maximum and minimum radar backscattering coefficients from 50 airborne scatterometer data sets acquired from many geological surfaces. The vegetation models were based on maximum and minimum radar backscatter coefficients from over 160 truck-mounted scatterometer data sets.

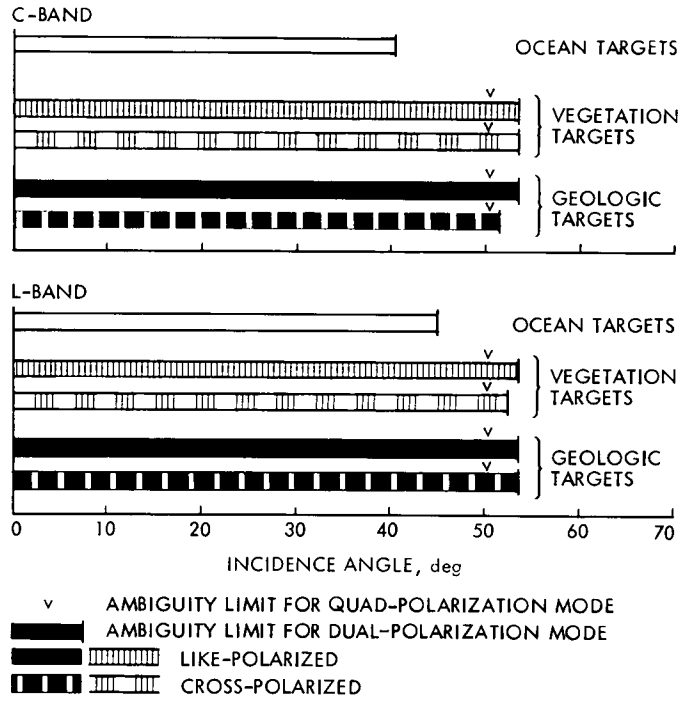

Fig. 3-6. Maximum incidence angle achievable by SIR-C

3.3 Calibration

3.3.1 Radiometric Calibration

relative vs. absolute calibration

The radiometric calibration of a SAR establishes a relationship between SAR image intensity and the radar backscattering coefficient, σ°, of the imaged surface. (For a discussion of σ°, see Appendix A, Section 2). Both relative and absolute calibration are important. The relative calibration of the SAR establishes how precisely one measurement can be related to another, while absolute calibration establishes the accuracy of the measurement of σ°. The relative calibration of a system accounts for changes or instabilities in its subsystem parameters, such as gain drifts in amplifiers. Absolute calibration takes into account biases and the absolute gain of the antenna and receiver. It establishes the constant K in the relationship $I = K\sigma^\circ$, where I is the SAR image intensity of an extended target.

Absolute calibration leading to accurate measurements is required for comparing results from different radar systems such as the Seasat SAR and the SIR-C SAR. However, for many geoscientific studies, good relative calibration of the SAR is much more important than its absolute calibration. Relative calibration allows quantitative comparative studies of the radar backscattering coefficients of vegetation, ice, geomorphic surfaces, etc., over widely dispersed geographic regions, or of the same surface on different days.

Many of the SIR-C experiments described in Chapter 4 will require good relative calibration (to 1 dB or better), and some experiments will also require good absolute calibration (to 3 dB or better). The calibration requirements for these experiments are discussed in greater detail in Chapter 4.

calibration approaches

A discussion of the contributors to errors in the accuracy of SIR-C is presented in Appendix B. Basically, achievement of good radiometric calibration will require two approaches:

(1) Calibration of individual radar components (antenna, T/R units, establishment of exact range to target, etc.)
(2) The use of corner reflectors and active calibrators at some of the test sites

Although it is likely that several test sites will have a set of corner reflectors and active calibrators, it is impractical from both a logistic and economic point of view to expect that each test site will be so instrumented. This, then, requires that the SIR-C subsystems be as accurately calibrated as possible and that the exact *in situ* antenna pattern, peak gain, and antenna pointing be accurately known. It also requires that the transfer characteristics in both the receive and the transmit modes for all T/R units be known for the cold-space environment, where large temperature excursions may be encountered as the Shuttle executes various roll maneuvers from earth-pointing to cold-space pointing.

These are difficult engineering design and test problems. However, if maximum scientific returns from SIR-C are to be achieved, the instrument must exhibit good stability over the life of the mission, images must have good radiometric fidelity across the swath, and it must be possible to relate digital number (DN) values in the image to the absolute radar backscattering coefficient, σ°.

3.3.2 Geometric Calibration

The geometric calibration of a SAR image establishes the relative geometric fidelity of surface features (e.g., agricultural fields or ice floes), and the absolute location accuracy of these features on a cartographic grid. The establishment of good relative geometric fidelity in a SAR image involves various routine image-processing steps such as correcting for image skew generated by the data-taking geometry and correcting for the variation of ground range resolution as a function of the angle of incidence. Good absolute geometric calibration requires accurate knowledge of the Shuttle position (ephemeris data) and/or the use of known ground control points found in the SAR image.

requirements

Radargrammetry experiments require knowledge of the slant range to the target, and the Shuttle position to within one resolution cell. Although other experiments do not require this degree of geometric accuracy, images acquired at multiple frequencies and polarizations must be co-registered to within one pixel. Since the pixel size will be identical for the L- and C-band systems, this should be achievable with SIR-C.

Chapter 4
SIR-C Geoscientific Experiments

4.1 Introduction

This section presents a discussion of some geoscientific experiments that could be conducted using SIR-C, and is organized by discipline: geology, hydrology, vegetation science, glaciology, and oceanography. The motivation for conducting these experiments is described in Sections 4.2–4.6. Each of these sections enumerates several geoscientific objectives and seeks to place SIR-C in context by addressing the following questions:

fundamental questions

(1) What are the scientific motivations for the research objectives, and what are the backgrounds of these objectives?
(2) What role does remote sensing in general play in conducting these research investigations?
(3) What is the specific role of imaging radar?
(4) What is the scientific basis for the use of SIR-C?
(5) What specific experiments could be conducted using SIR-C?
(6) What are the recommended parameters (orbit, mission timing, swath widths, frequencies, data products, etc.) for SIR-C?

Some of these specific research topics and experiments are summarized in Table 4-1.

4.2 Geology

4.2.1 Background

global geologic processes

The primary objective of the SIR-C geology experiments is to improve our understanding of geologic processes worldwide through time. The key experiments that can be pursued with SIR-C include investigations of cold-region geomorphology, fluvial geomorphology, rock weathering, erosional processes and geochronology, lithologic mapping and stratigraphy, regional tectonics, geobotany, and radar stereo/topography. Also, topographic data can be derived from SIR-C and used to conduct geomorphic analyses in a diverse range of study areas.

spaceborne remote sensing and the multidisciplinary approach

Many of the geologic problems for which we are seeking answers today are complex and reach beyond those that can be solved by ground-based mapping techniques. Investigations of these problems often require a multidisciplinary approach and are likely to involve related fields such as hydrology, botany, oceanography, and geophysics. Some investigations require the ability to penetrate beneath surficial cover such as vegetation, soil, or alluvium. Still others are currently not possible simply because research cannot be conducted in particular remote regions. The scale at which geologic investigations are conducted varies from tens of meters to hundreds of kilometers. Coastal-sedimentation and delta-formation studies, for example, may require information covering a few kilometers of coastline, while comparative regional tectonic studies may require data for continent-sized areas. Spaceborne imaging radars can provide valuable data for many such investigations.

Table 4-1. Examples of SIR-C research topics

Geology	Vegetation science
Cold-region geomorphology	Identification and mapping of vegetation and crop types
Fluvial geomorphology	Interpretation of landscape patterns and processes
Lithologic, rock-weathering, and geochronology studies	Assessment of biophysical properties of plant canopies
Regional tectonic studies	Determination of canopy penetration
Geobotanic studies	Modeling of vegetation structure and canopy processes
Radar stereo/topography studies	Glaciology
Hydrology	Sea-ice feature verification
Delineation of subsurface hydrologic features in hyperarid regions	Ice drift and deformation experiments
Delineation of geohydrologic characteristics	Spatial variations in pack-ice characteristics
Watershed runoff modeling	Lake-ice feature verification
Groundwater resource analysis	Bathymetry of lakes
Delineation of wetland boundaries	Ice-shelf and glacier boundaries
Estimation of snow cover and water equivalent	Snow return characteristics
Mapping of permafrost areas and determination of permafrost's distance beneath surface	Oceanography
	Ocean-wave forecasting
	Internal waves
	Currents, fronts, and eddies
	Bottom signatures
	Wind signatures

Incorporating selected test-site field measurements with SIR-C imagery would greatly enhance geologic investigations by indirectly providing quantitative results. This approach would aid the interpretation of radar data and would help develop more refined quantitative models of microwave/surface interaction characteristics. Data sets from other remote sensors could also enhance the geologic interpretation of SIR-C imagery, particularly high-resolution imagery acquired in the visible, near-infrared, and thermal infrared wavelength regions.

specific objectives

Several specific objectives have been identified as warranting a concerted investigation using spaceborne instruments such as SIR-C and advanced multispectral sensors. For these objectives, it is recommended that investigators should formulate their studies in such a manner as to extrapolate geologic/geomorphic investigations from the local scale to a scale that is either regional or global in extent, thereby taking advantage of the near-global coverage of the radar. A focus on the interpretation of geologic processes and the testing of geologic models is emphasized.

An example of such a study is the analysis of local tectonic features as a way of providing information on continental or global deformational processes associated with plate tectonics. The tectonic evolution of continent-sized areas can often be addressed by the analysis of specific structural features associated with plate boundary zones. Other investigations could concentrate on weathering processes (such as those associated with the erosion of lava flows or alluvial fans), with the primary objective of quantifying temporal changes in the morphological characteristics of Quaternary deposits. In turn, these studies could provide an insight into recent climatic change.

Testing the hypothesis that the land surface carries the record of geologically recent tectonic and climatic processes is a second key focus. In this context, the identification of the time-scale over which a landscape has evolved (from tens of years to millions of years), and the implications for life (in terms of climate, ecology, hydrology, and waste disposal) are stated goals. Specific problems that could be addressed might be the

(1) Determination of the age scales of geomorphic development
(2) Response of landforms to climatic change
(3) Response of landforms to tectonic perturbations
(4) Weathering rates of different lithologic units
(5) Connections between the lithology and ecology of a region

The investigation of ancient drainage channels in hyperarid deserts is an example of this form of analysis, wherein observed features are used to interpret geologic processes and climatic changes that have operated over the last few thousand years.

utility of Seasat, SIR-A, and SIR-B data

Spaceborne radars have proven to be very useful for geologic investigations. The Seasat SAR, SIR-A, and SIR-B all provided high-quality imagery that has been used for structural-geology studies, lithologic discrimination, topographic mapping, subsurface hydrology, etc., over angles of incidence ranging from 20° to 55°. Geologic analyses and interpretations of the image data acquired by each of these missions have demonstrated the effects of incidence angle on SAR imagery. At the low angle of incidence used with the Seasat SAR (23°), the radar backscatter is very sensitive to topography. At the higher angle of incidence used with SIR-A (50°), the backscatter is dominated by surface roughness, which in turn provides lithologic-discrimination capabilities. As mentioned in Chapter 2, the multiple look angle capability of SIR-B (15°–55°) has shown the relationship between angle of incidence and radar backscatter for different geologic surfaces and has, in addition, provided the means of stereo radar mapping.

two SIR-C flights needed

Most geologic remote sensing has the common objective of producing a map upon which subsequent interpretations can be based. In view of the great diversity of rock types, weathering environments, and vegetation cover, the selection of optimum SIR-C radar parameters for each specific target remains to be determined prior to regional mapping. This means that two SIR-C flights will be required. The first SIR-C flight would test as many radar parameters as possible in order to identify an optimum set of parameters for specific sites. The second SIR-C flight would then employ these optimum parameters in a mapping mode to acquire SAR data over larger contiguous regions. Two SIR-C flights would also allow temporal or seasonal coverage of geologic targets. The capability for viewing cold-region geomorphic features at different times of the annual freeze-thaw cycle, and river delta flooding before and during maximum river discharge, would supply data for two of several possible experiments.

4.2.2 Role of Spaceborne Remote Sensing in Geology

Landsat

Geologic applications of remote sensing data really began with the interpretation of black-and-white aerial photographs. Such photographs were of tremendous use to geologists in conducting field mapping, not only for logistical purposes, but also for focusing on

structures, outcrops, or geologic anomalies that required detailed field investigation. Geologists were among the first to use satellite multispectral images provided by ERTS (later Landsat) in 1972. These early Landsat investigations provided the first visible/near-infrared views of large or regional structural features such as faults and folds, geologic contacts expressed as vegetation contrasts or moisture differences, and areas of geochemical alteration affecting vegetation and soil. The multispectral data provided by Landsat have been augmented in recent years by imaging spectrometers such as the Airborne Imaging Spectrometer (AIS) and the Airborne Visible/Infrared Imaging Spectrometer (AVIRIS). These instruments enable scientists to identify, as well as discriminate, among rock types.

imaging spectrometers

More recent Landsats (4 and 5) have included a 100-m-resolution thermal band, and the Heat Capacity Mapping Mission (HCMM) free-flyer included a 600-m-resolution thermal band. Thermal infrared images are useful for mapping variations in surface emissivity and for the derivation of thermal inertia [4-1]. Data acquired by the thermal band of the Thematic Mapper (10.42–11.66 μm) and by the airborne Thermal-Infrared Multispectral Scanner (TIMS) [4-2] have been used for identifying certain rock mineralogies and thermal plumes associated with water discharge in coastal and lacustrine environments. Thermal measurements made by these instruments may be of value for volcanology, for the detection of ground water seeps, and for geothermal exploration. However, as with visible detectors, thermal data can only be acquired during cloud-free conditions.

TIMS

4.2.3 Role of Imaging Radar in Geology

independence from weather, sun angle

Imaging radars are used for geologic investigations mainly because of the enhanced sensitivity of such radars to topography, surface roughness, and material dielectric properties that are related to lithology, structure, geologic age, geobotanic phenomena, and geomorphology. Radar imagery's independence from weather and sun angle allows geologists to study many remote and inaccessible regions. Seasat, SIR-A, and SIR-B have already demonstrated the utility of SAR imagery for investigating previously unmapped regions or humid areas that are obscured by cloud cover. In a study of a hyperarid region of the Eastern Sahara, SIR-A demonstrated the capability of an L-band SAR to penetrate through a meter or more of dry sand and alluvium and reveal previously unmapped bedrock features as well as regionally extensive but buried fluvial topography [4-3]. The SIR-C mission offers an opportunity to further exploit for geologic mapping the penetration capability of imaging radar and to test the usefulness of various combinations of wavelength, incidence angle, and polarization for identifying rock types and structures, geomorphologic and geobotanic relationships, and the ages of geologic surfaces.

penetration

Geologic experiments will require specific combinations of swath width, resolution, polarization, wavelength, and perhaps seasonal considerations, depending upon the type and scale of work proposed. For example, a mapping project requiring large swath widths with a uniform look angle and no gaps in coverage will not be compatible with experimental objectives requiring varying combinations of wavelength, polarization, and look angle. However, with the two flights of SIR-C, it may be possible to plan experiments to fulfill both types of objectives.

4.2.4 Scientific Basis for SIR-C Geology Experiments

basis for SIR-C geology experiments

The scientific basis for the use of SIR-C data in geology experiments is founded upon several essential points:

(1) The dual-wavelength capability will allow studies of the roughness of geomorphic surfaces, as well as of the wavelength dependence of vegetation cover.
(2) The inclusion of full polarization capability will allow studies of surface and volume scatter for the discrimination of rock and ice types and for geochronology studies.
(3) The capability to image a given area with several angles permits stereo radargrammetry and therefore topographic studies.
(4) The high-latitude orbit will allow some studies of cold-region geomorphology.

models of backscatter

Because of the extreme complexity of most geomorphic surfaces, it is very difficult to construct mathematical radar backscatter models that have any real exactitude. However, a number of models of simpler geometries will offer guidance in the quantitative interpretation of SIR-C imagery. For example, we know that certain surfaces that appear to be smooth at L-band will appear to be rough at C-band, if the surface roughness falls within a certain range. Surface roughness has both a small-scale and a large-scale component.

Rayleigh criterion

A surface with small-scale random height excursions about a reference flat datum will appear to be smooth to a radar system if its root mean square (rms) height, h_{rms}, satisfies the modified Rayleigh criterion:

$$h_{\text{rms}} < \frac{\lambda}{32 \cos \theta}$$

where λ is the electromagnetic wavelength and θ is the angle of incidence. Assume that SIR-C is operating at a 50° angle of incidence. This means that at C-band (λ = 6 cm), any surfaces with an rms roughness greater than about 3 mm will appear to be rough. At L-band (λ = 23 cm), any surface with an rms roughness greater than about 1 cm will appear to be rough. If now the angle of incidence is changed to 20°, these upper limits for smooth surfaces will change to 4 mm at C-band and 1.5 cm at L-band. This would seem to imply that virtually all geomorphic surfaces are rough at L-band and C-band.

geometrical optics

However, this simple modified Rayleigh criterion does not consider the larger-scale roughness of datum undulations, tilts, bumps, and slopes that a radar images. In fact, most of the scattering accounting for texture in SAR images of geomorphic surfaces can be accounted for by geometric optic reflection and scattering from rocks, boulders, slopes, etc. The radiometric brightness of a 30- × 30-m pixel within a SAR image is the result of the coherent addition of the contributions from many individual scatterers within the pixel. Thus, the image texture or appearance of smoothness (assuming negligible speckle) over, say, a 1-km^2 area would be a measure of the spatial homogeneity of the scatterers within each of the image's pixels. At some level of large-scale surface roughness, the image will appear to be smooth at L-band and rough at C-band. One of the objectives of some of the SIR-C geology experiments might be to establish what that level of large-scale roughness is, and how it can be used to discriminate levels of rock weathering, volcanic flow blockiness, etc.

depolarization

When radar energy is incident upon terrain containing multiple scatterers, the resulting backscattered energy tends to be depolarized, i.e., it has both a like-polarized and cross-polarized component. In fact, the ratio of cross to like polarization can be used as a measure of the degree of multiple scattering, and from that a measure of the surface roughness can be obtained. This multiple scattering is more often associated with volume scattering from leaves, branches, etc., in a vegetation canopy, or with brine inclusions or air bubbles in multiyear ice, and is thus useful as an indicator of vegetation or ice morphology. However, depolarization also is associated with certain rough surfaces, although the exact relationship has not yet been determined. SIR-C will offer an opportunity to study this effect and to determine its utility for the classification of geomorphic surfaces.

4.2.5 SIR-C Geology Experiments

This section describes six different classes of geology experiments that could be conducted with SIR-C. This list, summarized in Table 4-2, is *not meant to be all-inclusive*, but is provided simply to give a general description of the nature of geology experiments and how SIR-C data might be used in these investigations. The examples build on experience gained in past or current studies performed with airborne SAR and with Seasat, SIR-A, and SIR-B. SIR-C will be more flexible than previous imaging radar systems and will offer many new opportunities to study new geologic problems that are not included in this document.

experiment classes

Table 4-2. Some SIR-C geology experiment classes

Experiment class	Scientific objectives
Cold-region geomorphology	Glacial landforms, permafrost
Fluvial geomorphology	Stream networks, hydraulic properties of stream flow, flood mapping, buried ancient drainage networks
Rock weathering, erosional processes	Weathering properties of sedimentary rocks, rates of erosion and deposition, studies of Quaternary fluvial deposits, relative age dating of Quaternary geomorphic surfaces, characterization of lava-flow types, discrimination of sedimentary lithologies
Tectonics and geologic boundaries	Structural mapping of large-scale geologic features, such as terrains, Precambrian shields, fold mountain belts, faults, and rates of fault slip
Geobotany	Discrimination of geologic units in extensive vegetated areas, using image texture and multifrequency and multipolarization radars
Radar stereo/topography experiments	Topographic mapping, studies of slope evolution, structural deformation and volcano and ice-sheet volumes

supersites

The "supersite" concept has been developed to help focus investigators' attention on a limited number of key geologic targets that could form the basis of several different studies. The exact location of these supersites will be chosen to suit the scientific objectives of the SIR-C Science Team. As a general rule, however, it is recommended that

(1) At least two of the sites include young, relatively vegetation-free areas, of which one might be for geochronological studies (e.g., the U.S. Southwest), and the other a young volcanic region (e.g., Hawaii or the Snake River Plain) for process-related investigations
(2) A polar region (most likely within Alaska) be selected for the study of periglacial features
(3) A geobotanic supersite might be selected in conjunction with other vegetation studies, but that forests within the U.S. Northeast and Europe should be suitable for investigating vegetation stress due to acid rain and effects on community composition due to rock lithology

4.2.5.1 Cold Region Geomorphology

As exploratory and exploitative activities extend further into the polar regions, there is an increasing need to understand the natural processes peculiar to these environments and to assess the impact of human activities on these processes. Polar environments are commonly cloud-covered during the time of the year when thawing occurs. Abrupt changes in geomorphic processes accompany this transition period from freeze to thaw. Some of the more notable changes are in the flow regime of rivers and glaciers, in the rate of shoreline erosion, and in solifluxion. Satellite imaging radars provide imagery that is weather-independent, unconstrained by sun angle, and has partially controllable illumination angles. Such radars are therefore ideal for observing and monitoring polar surfaces and surface processes, especially during critical periods of seasonal change. Studies are needed to

glacial landform studies needed

(1) Evaluate the use of SAR images for glacial landform mapping and interpretation
(2) Determine the optimum radar frequency, polarization, and illumination angle for glacial landform mapping
(3) Assess the advantages of variable or multiple look angles and frequencies, especially for the perception of landforms of low relief such as thermokarst, permafrost, patterned ground, etc.
(4) Evaluate the synergism of SAR (e.g., Seasat, airborne, SIR-C) and optical/IR images of comparable resolution (e.g., Landsat TM)
(5) Compare the potential uses of SAR and other forms of remotely sensed images for monitoring glacier movements, coastal erosion, floodplain development, etc.

Penetration of glacial ice by radar depends critically on the amount of liquid water in the ice and on the salinity of the ice (or the nature of the snow, in upper levels), and probably on included rock material such as medial moraines in flowing ice. It is expected that in areas of low moisture content there may be some penetration if the ice is very thin, permitting study of underlying bedrock structure.

In a polar orbit, SIR-C would be the first multiparameter radar system available with which to investigate the Antarctic. Due to the adverse climate, long periods of darkness, and the extreme physical difficulty of working on the Antarctic continent, a radar system could provide extensive baseline information on a number of geologic and glaciologic problems. For example:

Antarctic soils

(1) Some areas receive virtually no rain or snow fall, and are free from glacial ice. The very low temperatures in Antarctica have permitted a soil structure to form that is totally unlike that found in more temperate climates. Both the radar signature of

this material, and the potential for penetration by the radar signal are important to pedologists for studying cold-climate soils, and important to planetary geologists who use these areas as analogs for Mars. It is not known whether radar penetration could be achieved in these areas because as yet there have been no data acquired of these regions; however, the concept lends itself to a SIR-C experiment.

glacier dynamics

(2) Many of the structures found in ice sheets are too small to be observed on Landsat MSS or TM and yet provide important constraints on glacier dynamics and are controlled by underlying topography. Pressure ridges, fractures, and the amount of rock debris at or near the surface of the ice may all be detected by SIR-C, providing the first synoptic view of the ice sheet from its source regions to its eventual demise at its snout or as a series of icebergs at the coastline.

mapping permafrost

(3) The extent of continuous and discontinuous permafrost is of special interest to geomorphologists. The transition from one type of permafrost to another may be temperature dependent, thus permitting a radar system to provide an indirect measure of annual temperature by obtaining data at a single instant in time. Study of the process and the rate of formation of permafrost would also be of great value to the geomorphic sciences if SIR-C data were used to establish a time baseline for the distribution of permafrost features. In order to provide more complete estimates of periglacial processes, it is important to develop an understanding of permafrost relief patterns and how they relate to subsurface lithology and structure in these regions. By analyzing relief and topographic patterns evident from SIR-C data, and comparing them with ancillary geologic data compiled from mapping and drilling, it may be possible to study this geomorphic relationship.

Figure 4-1 illustrates the distribution of several permafrost environments in the Northern Hemisphere. Comparable geomorphic features exist in the Antarctic, but their distribution across the continent has not yet been fully investigated. It is not yet known what relationship there is between zones of continuous and discontinuous permafrost, and underlying geologic structure, if any. Radar coverage of an area with cold-climate landforms may allow geologists to study this relationship, and also to identify the effects of a multifrequency, multipolarization system on mapping in such regions. The basis for radar sensitivity to permafrost is discussed further in Section 4.3.5.5.

4.2.5.2 Fluvial Geomorphology

The potential for applying spaceborne radar data to the analysis of fluvial processes lies in the radar's ability to easily distinguish open bodies of water (including rivers) from surrounding terrain, to display subtle relief features associated with the boundaries of watersheds, and to allow textural analysis of landforms produced by downslope movement. Potential experiments that can be performed with SIR-C data from diverse geologic environments include the following:

watershed stream networks

(1) Dendritic streams and tributary patterns have been found to be readily identifiable on spaceborne radar images (Fig. 4-2). In the case where stream and river beds are active, the roughness of the bed (which, in youthful streams, should possess many exposed boulders) and an increase in the amount of vegetation along the banks makes the channel appear brighter than the surrounding areas. Alternatively, where the streams are ephemeral, the dry floors are topographic depressions that trap sediments and therefore tend to appear dark on radar images (due to their smoothness

ORIGINAL PAGE IS
OF POOR QUALITY

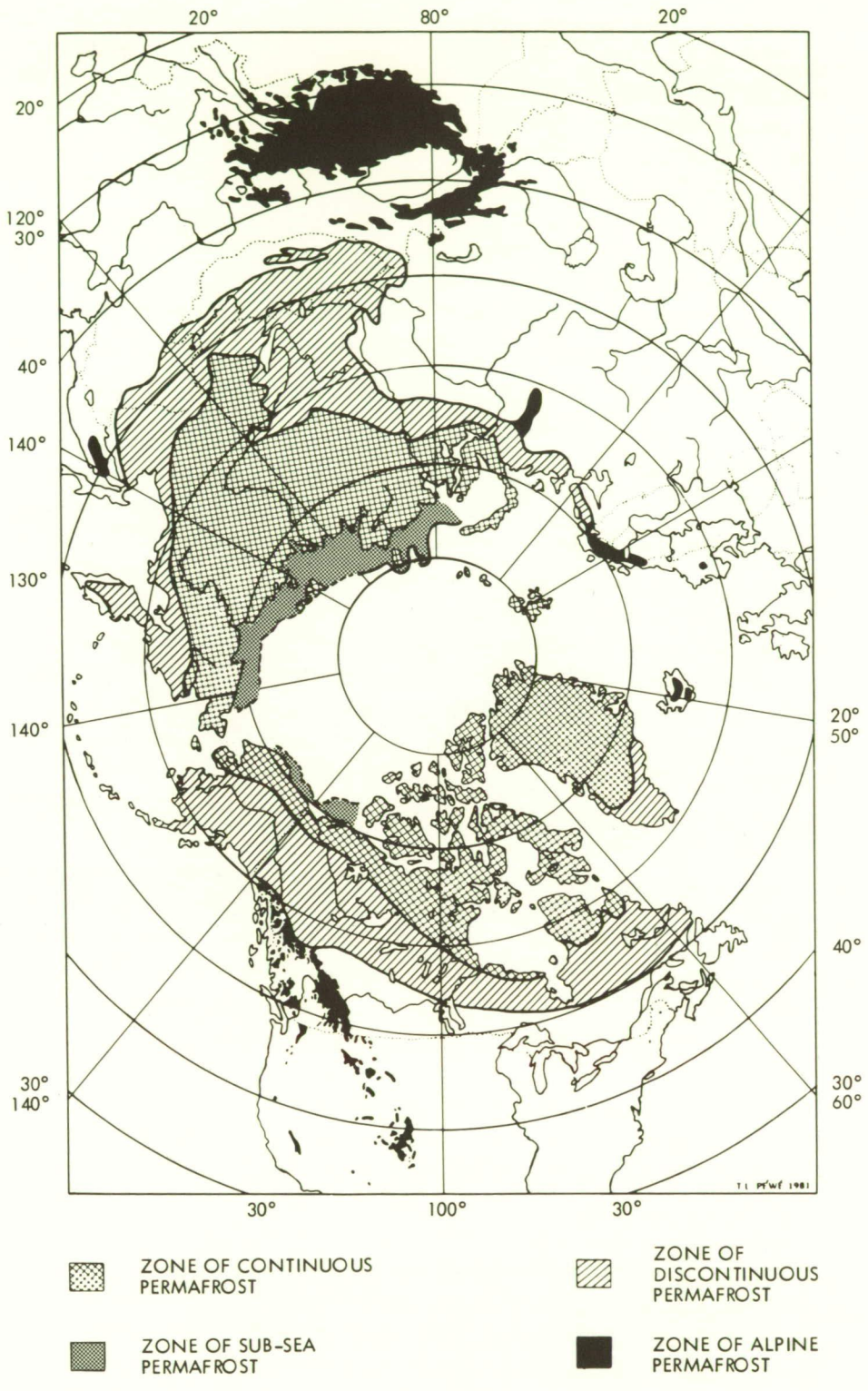

Fig. 4-1. Distribution of different types of permafrost terrain in the Northern Hemisphere [4-4]

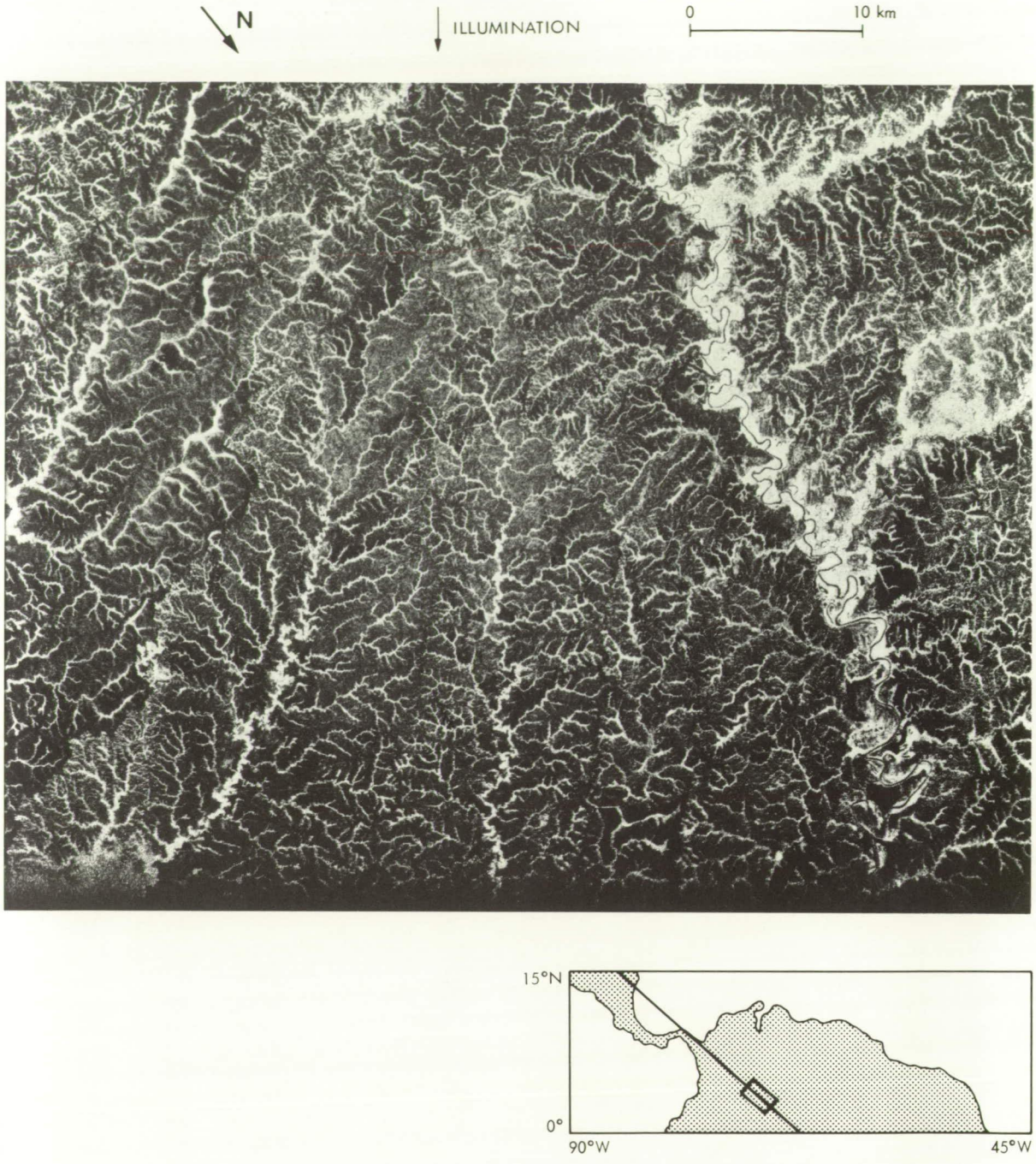

Fig. 4-2. Examples of dendritic stream networks, viewed by SIR-A from above South America. The drainage pattern is strongly enhanced in this image by the bright returns from the forested stream channels

and low dielectric properties). Recognition of areas of convergence of stream lines in valley heads, and divergence on hill spurs, permits drainage basins and watersheds to be accurately delineated. Analysis of stream order (the ranking of streams along the length of a drainage system) permits the runoff potential to be assessed. Detailed models have been developed for certain catchment areas in the U.S., incorporating channel length and width and the total area of the catchment.

Thus, some SIR-C experiments could attempt to calibrate radar-derived measures of runoff potential with actual field measurements (obtained from historical records developed over a number of years) of discharge volumes for the same river system. Furthermore, once the detailed morphological properties of a drainage system (e.g., stream order and junction angle characteristics) are known for fluvial systems on specific rock lithologies, it may be possible to extrapolate these observations to other drainage networks, thereby providing some insight into drainage basin history and/or rock lithology. Multipolarized data from SIR-C would be potentially useful for separating out specific rock lithologies.

analyzing stream-flow hydraulic properties

(2) SIR-C's multiple-look-angle capability may provide data with the potential to aid studies of slope effects on river outwash plains, and those studies may in turn permit the analysis of hydraulic properties of stream flow. A SIR-B image of a region in Bangladesh illustrates this concept (Fig. 4-3). This type of data may be particularly helpful in the description of tropical river systems. Such rivers cannot be easily mapped by conventional ground or air techniques, but the change in vegetation canopy as a function of age of channel abandonment may permit the chronology of former river channels to be identified, in addition to the current course of the river. In areas where water flow is not confined to discrete channels, the type of erosion on slopes may be determinable using the SIR-C radar operating at a steep look angle: slump features and gullying are both characteristics of sheet wash, and the low topographic features that this process creates could well be identifiable on radar images.

monitoring flood-water coverage

(3) It may be possible to monitor the distribution of flood-water coverage during the SIR-C mission. While there is no certainty that a major episode of coastal inundation or river flooding will occur during the course of the SIR-C mission, SIR-C may be able to detect sedimentary deposits left after historically recent floods on the basis of the texture of those deposits. River terraces and levees could also be mapped, to further define the extent of water inundation and sediment deposition.

detecting ancient drainage networks

(4) In addition to the use of SIR-C for defining present-day fluvial geometry, the penetration capability on the L-band signal in arid regions can be used to define the nature and extent of ancient drainage networks buried beneath a thin (up to 2 meters) cover of loose, dry, surficial debris. This capability was first recognized in SIR-A images of Egypt and Sudan (Fig. 4-4) and later tested in SIR-B images of the Sahara and other desert regions. The potential exists for using SIR-C images to provide the basis for systematic mapping of ancient drainages in areas that have undergone significant climatic change in the late Quaternary. See Section 4.3.5.1 for a further discussion.

It is anticipated that investigations of fluvial processes could be conducted in vegetated, arid, or tropical supersites.

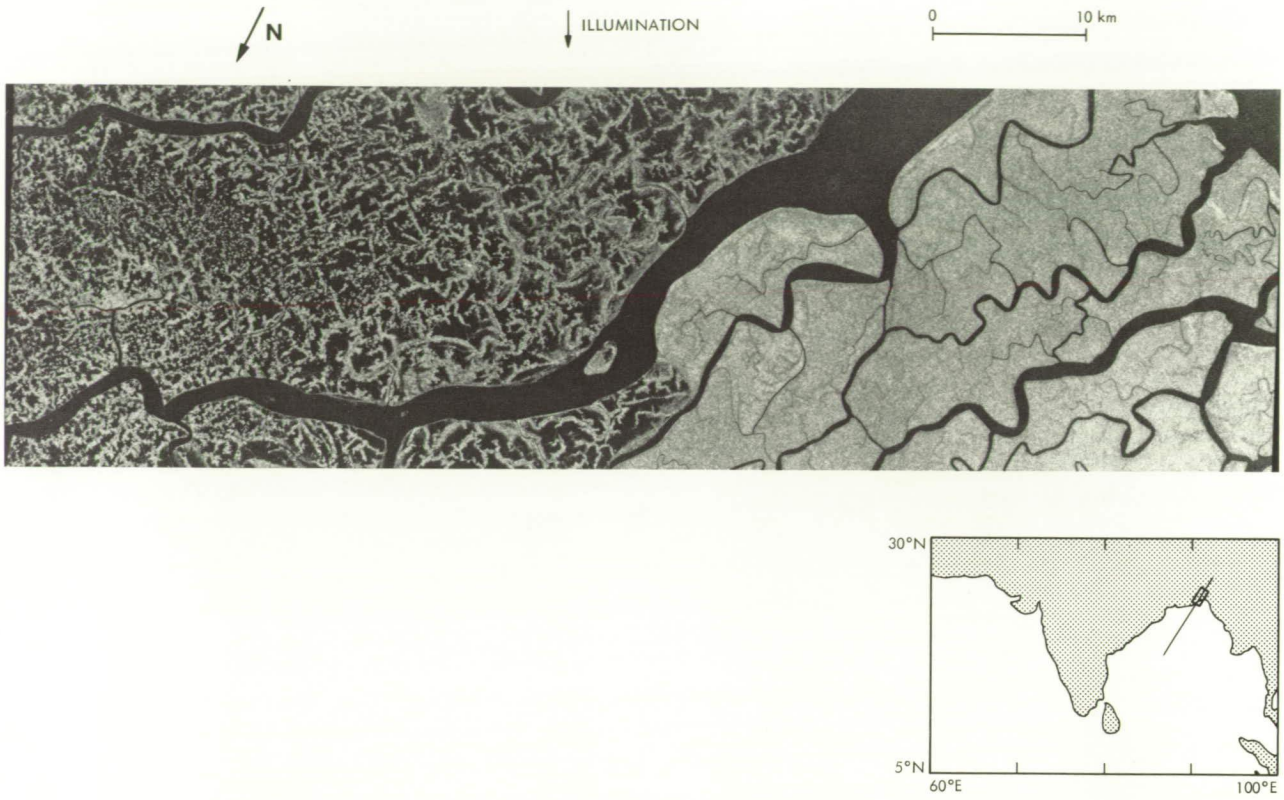

Fig. 4.3. SIR-B image of the Ganges floodplain in Bangladesh. The mottled gray and black areas are cultivated fields connected by extensive irrigation and drainage channels. The more uniform gray area is an area of the Ganges floodplain subject to flooding and major reworking during the monsoon season

4.2.5.3 Lithology, Rock Weathering, and Geochronology

discriminating sedimentary lithologies

The increased ability to discriminate sedimentary lithologies using multiple-polarization SAR in conjunction with Thematic Mapper data has been demonstrated in the Wind River Basin of Wyoming (Fig. 4-5) [4-5]. It is expected that SAR data from other sedimentary rock sequences would produce similar results. Calibrated images from SIR-C should assist in the remote characterization of lithologies by surface roughness, dielectric constant, and bulk properties, and will allow the extension of derived multiparameter radar signatures from known sedimentary basins to remote basins throughout the world. Investigations like these could be conducted in semiarid, arid, or vegetated supersites so long as some rock exposures were present.

rock weathering properties

One area in which the combination of different wavelengths and polarizations could be applied is the investigation of the weathering properties of sedimentary rocks. Different types of sandstones and limestones will erode in a manner consistent with their composition, structure, and particle size. Therefore, in the case of the multiple-polarization radar data provided by SIR-C, the structure of different weathered surfaces may enable different horizons of the same material to be distinguished from orbit. Desert sandstones and karst topography are two of many potential test targets for this kind of experiment.

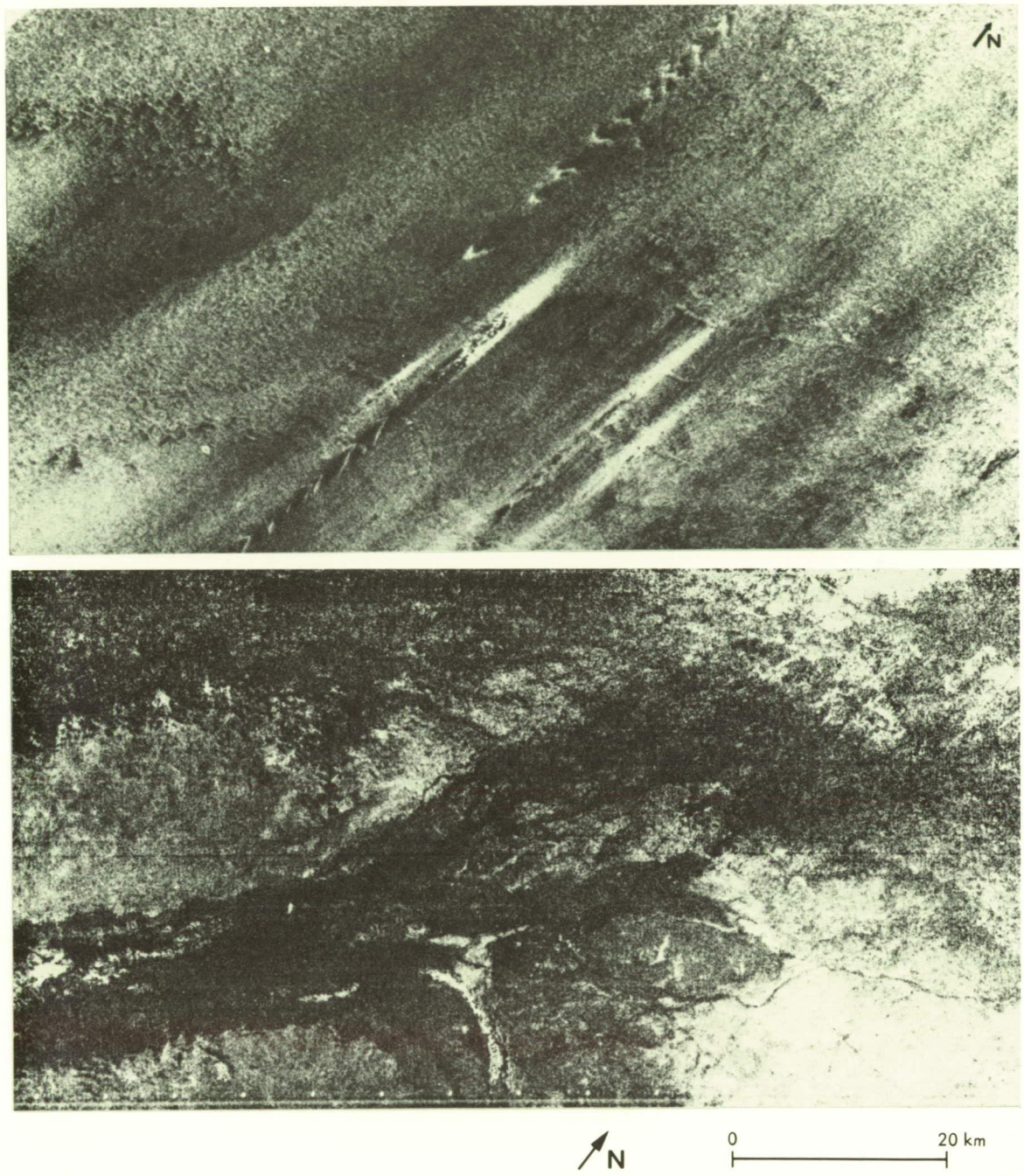

Fig. 4-4. SIR-A image and Landsat view of the hyperarid region of the Lybian Desert. Drainage features seen in the radar image are blanketed by surface deposits of windblown sand and are not readily apparent in Landsat or photographic images. Radar penetration of surface deposits in this area extends to depths of several meters

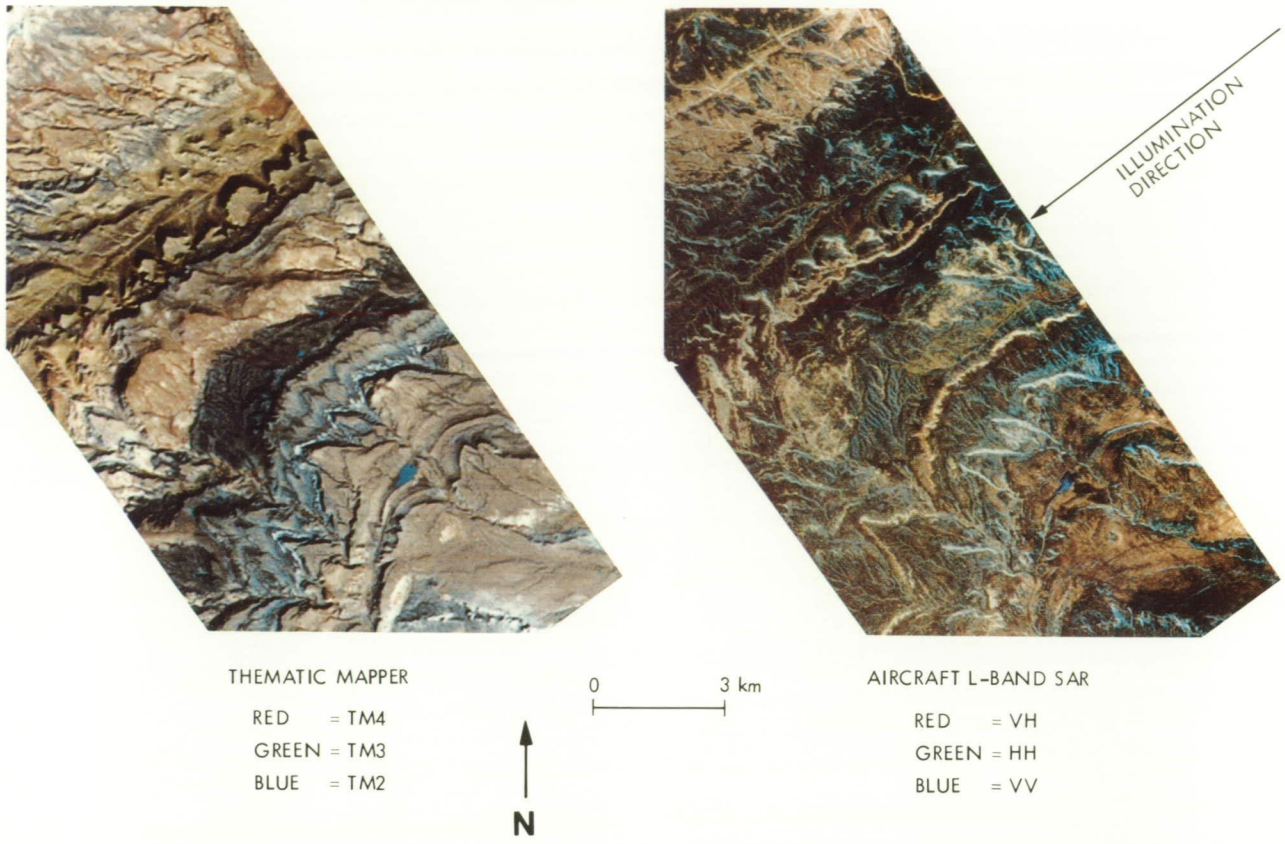

Fig. 4-5. Comparison of Landsat Thematic Mapper and aircraft L-band multiple-polarization radar images of the Wind River Basin in Wyoming

slope wash morphology

In the past, rates for slope wash have been estimated almost solely from field investigations conducted over long periods of time. A great deal of spatial and temporal variability in surface cover has been observed in imagery from the visible portions of the spectrum, but only for short-term events. As a result, the need exists to determine quantitative measures of morphology on a scale from 1 to 20 km, that can be input for available process-related models. Slope-area textural studies using SIR-C in its mapping mode, with multiple polarization and wavelength, may provide data pertinent to this problem.

penetration of hyperarid sand sheets

A major problem in geologic investigations of arid regions is determining rates of erosion and deposition by wind and running water under climatic conditions ranging from semiarid to hyperarid. One approach to this problem is to study sequences of surficial deposits such as aeolian sand sheets, dunes, and fluvial sediments in areas where measured sections can be radiometrically dated or dated from established archaeological ages of artifacts that can be used as index fossils. In the presently hyperarid Eastern Desert of Egypt, such sequences were discovered in valleys seen for the first time in SIR-A radar images, and were studied as a comprehensive field experiment after the SIR-A mission [4-3]. In these valleys, the radar allowed detection of zones of calcium carbonate accumulation in buried horizons. Such datable horizons are overlain in many areas by a sequence of alluvial and colluvial deposits, sand sheets, and sediments of mixed origin that records the interplay of geologic processes under variable climatic conditions culminating in the present hyperaridity. Many of these deposits can be correlated with known episodes of human occupation and were dated by archaeological means, yielding evidence for rates of accumulation and erosion. Potential areas of investigation include most of the great deserts of Asia, Africa, and central Australia. See Section 4.3.5.1 for a further discussion.

The ability to map Quaternary geomorphic surfaces over large areas on the basis of surface textures would be valuable for paleoclimatic, tectonic, volcanic, and arid-zone erosion studies. With age, some types of geologic surfaces in arid areas exhibit a decrease in roughness, caused by physical weathering processes that break down small-scale rock projections and fill in low areas.

backscatter dependence on flow age

A case study of the Snake River Plain of Idaho demonstrates this relationship. Figure 4-6 shows photographs of two flows that were field-mapped, and absolute age dates were determined from samples. Aircraft scatterometer measurements at two different frequencies (L-band and C-band) and at several angles of incidence were taken over both flows. The backscatter response, expressed as a ratio of polarizations for a 45° angle of incidence, is shown in Fig. 4-7. At both frequencies, the rougher, younger flow (North Crater) has a different backscatter curve than the smoother, older flow (Echo).

These curves suggest that both flows are smooth at L-band and rougher at C-band. The cross-polarized component of the radar backscatter is expected to be greater for the rougher (blockier) flows, due to multiple scatter and depolarization. This is indeed the case at C-band (6-cm wavelength) for the younger blockier North Crater flow, where the like-polarized channel (HH) is only about half the intensity of the cross-polarized channel (HV). For the older and smoother Echo flow, the cross-polarized intensity diminishes and the ratio increases to about 0.7. At L-band, the surface is smoother by a factor of about 4 (a ratio of 23-cm wavelength to 6-cm wavelength), so that depolarization due to multiple scatter from the basaltic blocks is decreased. This means that the dashed curve in Fig. 4-7 shows a slight rolloff with increasing geologic age (an increased smoothness), due to simple Lambertian like-polarized scatter behavior.

potential for relative age dating

SIR-C offers the potential for simultaneously collecting such multiparameter data for an individual site to help define the relative importance of the wavelength, angle of incidence, and polarization signatures of surfaces of varying age. In regions where the chronology of flows is known, it might also be the case that several different climatic environments exist or that different pristine lava morphologies can be identified. In these instances, the potential advantages of distinguishing surface texture by using multifrequency, multipolarization radars could be investigated as an aid to interpreting erosional processes or eruptive style. An example of this approach is shown in Fig. 4-8, which illustrates the differences among the radar signatures of lava flows in the Medicine Lake area of Northern California, as viewed by a multipolarized aircraft radar system.

4.2.5.4 Tectonics and Geologic Boundaries

Landsat hampered by forest and cloud cover

Landsat imagery has been used very successfully to map the extremely broad tectonically active zones in Africa and Eurasia and is being applied to studies of the North American–Pacific-plate boundary in California. However, in many areas, use of Landsat data is hampered by forest or cloud cover, or the difficulty of getting low-sun-elevation imagery at low latitudes. Continuing earlier airborne- and spaceborne-radar investigations, but with the additional advantage of a polar orbit, the SIR-C radar, by providing a good rendition of structure in such areas, should permit structural analysis of active faults and folds not easily recognized through Landsat or other visible/infrared sensors.

SIR-C potential for mapping fault offsets

It is possible that imaging from SIR-C could provide unique data for determining recent offsets on faults. Such offsets (from ten to hundreds of meters) are generally measured from large-scale maps, aerial photos, or ground-based field work. Attempts are then made to determine the ages of the offset features in order to estimate rates of slip. For example, a part of the San Andreas fault is detectable on the Seasat image, but not on that of Landsat

NORTH CRATER FLOW
2100–2300 years BP

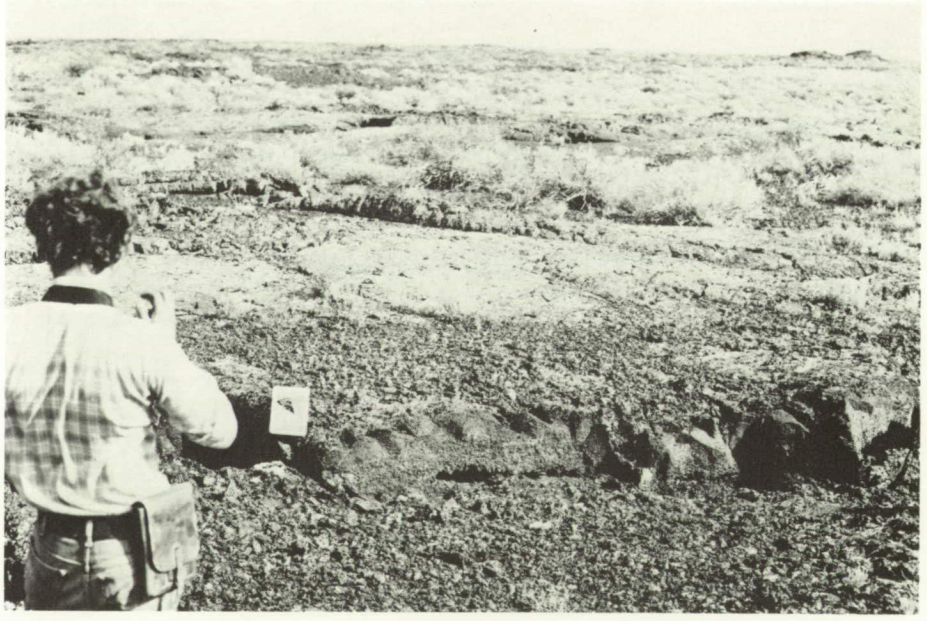

ECHO FLOW
5800–6200 years BP

Fig. 4-6. Two lava flows from the Snake River Plain, Idaho. Relative age dating of lava flows may be possible using dual-polarization, multifrequency SIR-C data. According to radiocarbon dating, these flows have ages of 2100–2300 years (top) and 5800–6200 years (bottom). These same flows can be distinguished based on their backscatter characteristics (see Fig. 4-7)

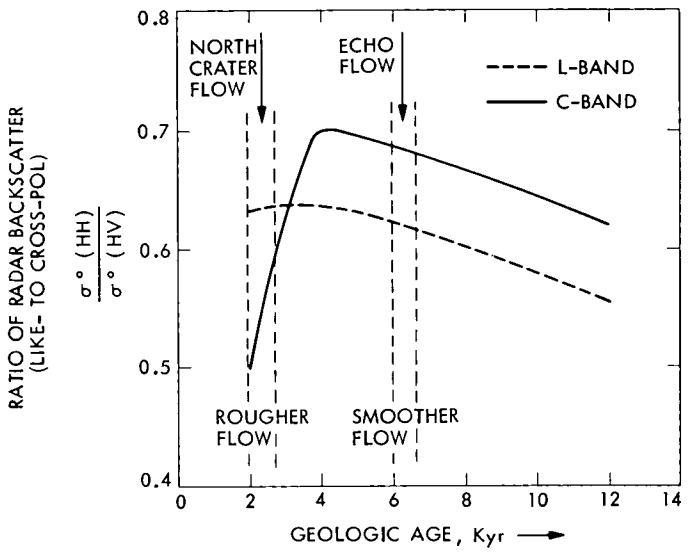

Fig. 4-7. Backscatter from volcanic materials, illustrating the differences in radar characteristics of the two Snake River flows shown in Fig. 4-6

(Fig. 4-9). This is due to the contrast in radar backscatter between units of different lithology and age, and the fault that separates them. Figure 4-10 is a hypothetical representation of an approach to measuring fault displacements. Depicted are two alluvial fans of different ages with a fault cutting the older, smoother fan but not the younger, rougher fan. Multifrequency, multipolarized data should allow detection of differing lithologies/ages because of their different polarization and frequency signatures.

Precambrian shields

All Precambrian shields for which there is sufficient information appear to be divided into natural provinces characterized by specific ages and delineated by fronts. The classic example is the Grenville front of Canada, whose origin and nature is still debated after many decades of study. Figure 4-11 shows the complexity of this tectonic region in Canada, as imaged by SIR-B. The Laxford front of Scotland is another well-known but poorly understood example. These and other fronts appear to be both metamorphic and structural in nature, but there is no agreement as to their origin. A model of their formation, when developed, will have major implications for the origin of the continental crust and the role, if any, of plate-tectonic processes in the Precambrian. SIR-C data, obtained from polar orbit and thus covering shields in all continents, will permit improved structural mapping along extensive traverses, both normal and parallel to selected fronts. It should be possible to identify the structural characteristics of the fronts themselves, and changes in tectonic style across the fronts by comparing the structures of the adjoining shield provinces.

Iceland represents one of the few areas of the world where a major spreading center (a point where new oceanic crust is created) is found on land. Thus, Iceland may be an important test area for volcanic/tectonic studies of the earth. A polar orbit of SIR-C would permit the regional geologic structure and the diverse volcanic landforms of the island to be investigated. Because many of the structural features associated with the spreading axis are frequently faults that are located in areas with high relief, a radar system with a multiple-look-angle capability such as that of SIR-C has to be employed. In addition, if multiple-look-angle/multipolarization data were acquired, many of the individual lava-flow units could also be distinguished and mapped by using data from other volcanic regions as ground truth.

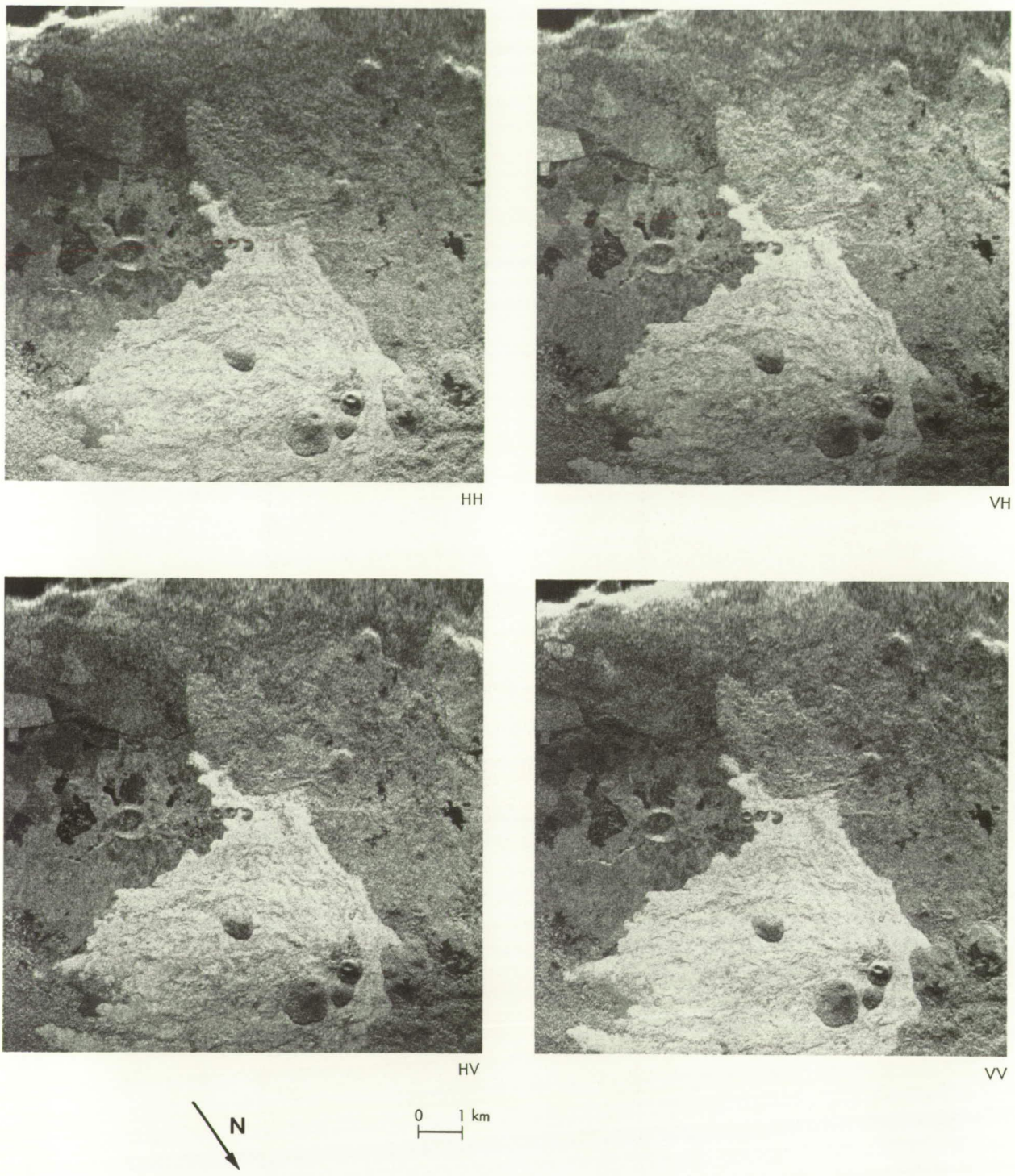

Fig. 4-8. Recognition of variations in the surface texture of different geologic materials, using multipolarization radar images, as demonstrated here for lava flows in the Medicine Lake area of Northern California. Aircraft radar images were acquired at HH (top left), HV (top right), VH (bottom left), and VV (bottom right) polarizations

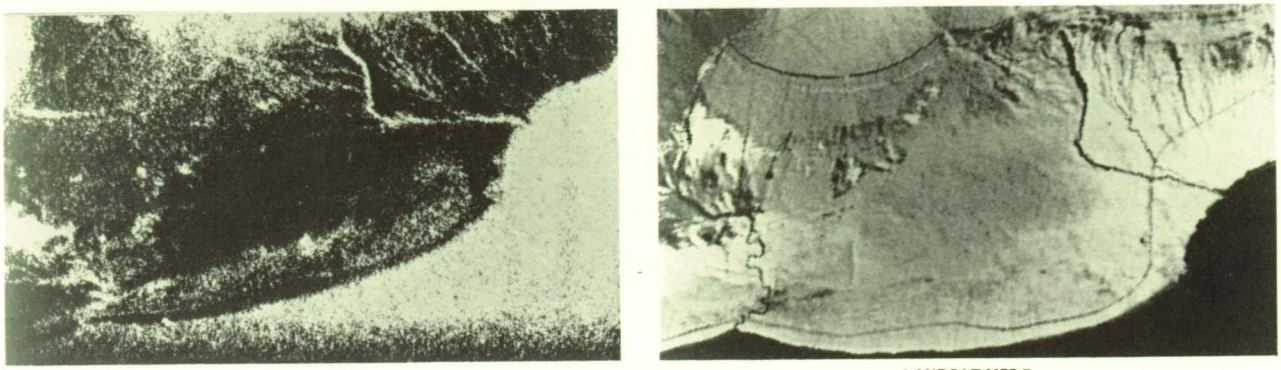

SEASAT SAR

LANDSAT MSS 5

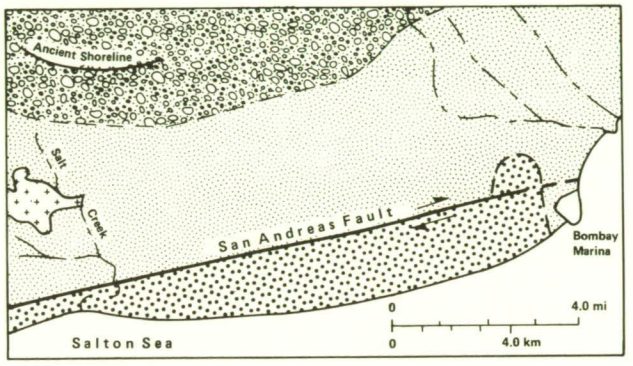

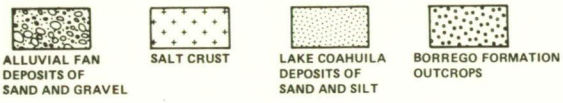

SKETCH MAP

(FROM SABINS, et al 1980)

Fig. 4-9. Part of the San Andreas fault system in California, as detected by the Seasat SAR on the basis of surface-material roughness. This same offset was undetected on Landsat MSS images, illustrating the potential of SIR-C for mapping structural features over extensive areas of the world. [4-6]

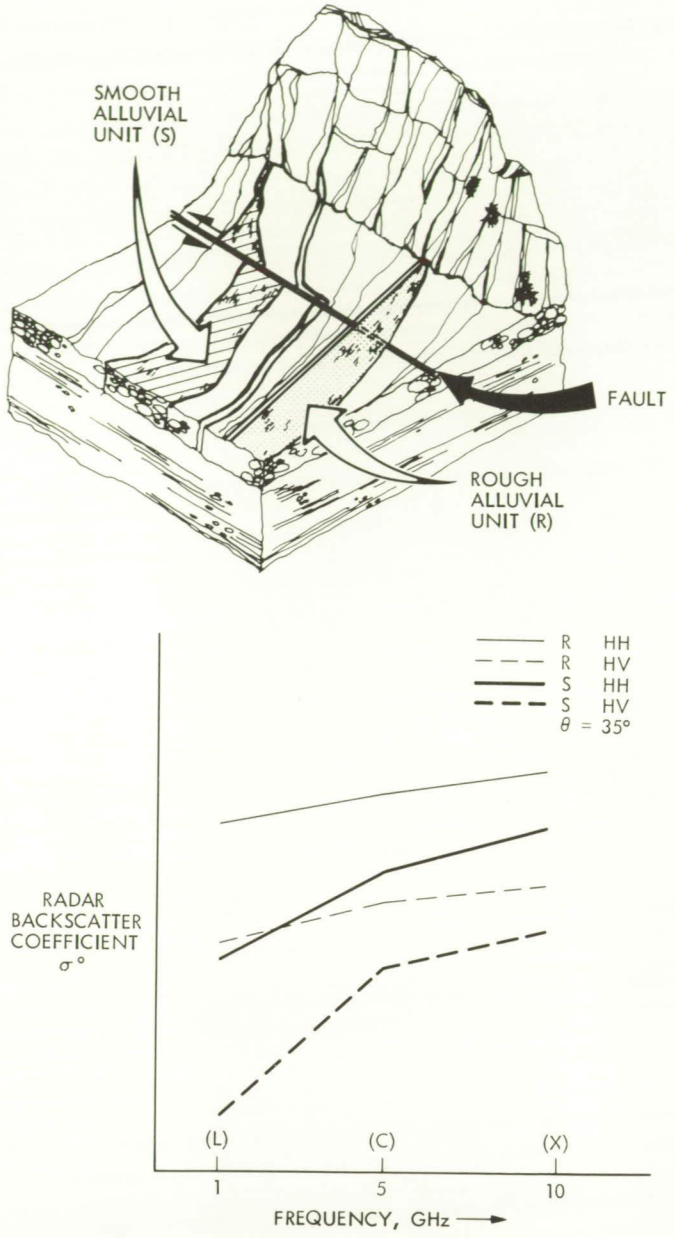

Fig. 4-10. Diagram of a possible method by which fault displacements could be measured by SIR-C, using the backscatter properties of different alluvial fans as measured at three frequencies and with two polarizations

4.2.5.5 Geobotany

Geobotany represents an evolving field in the geological sciences, but it is clear that the potential exists for conducting important vegetation studies with SIR-C, studies that will better characterize the underlying soils and bedrock. Three questions pertaining to geobotany that can be addressed by SIR-C have been identified:

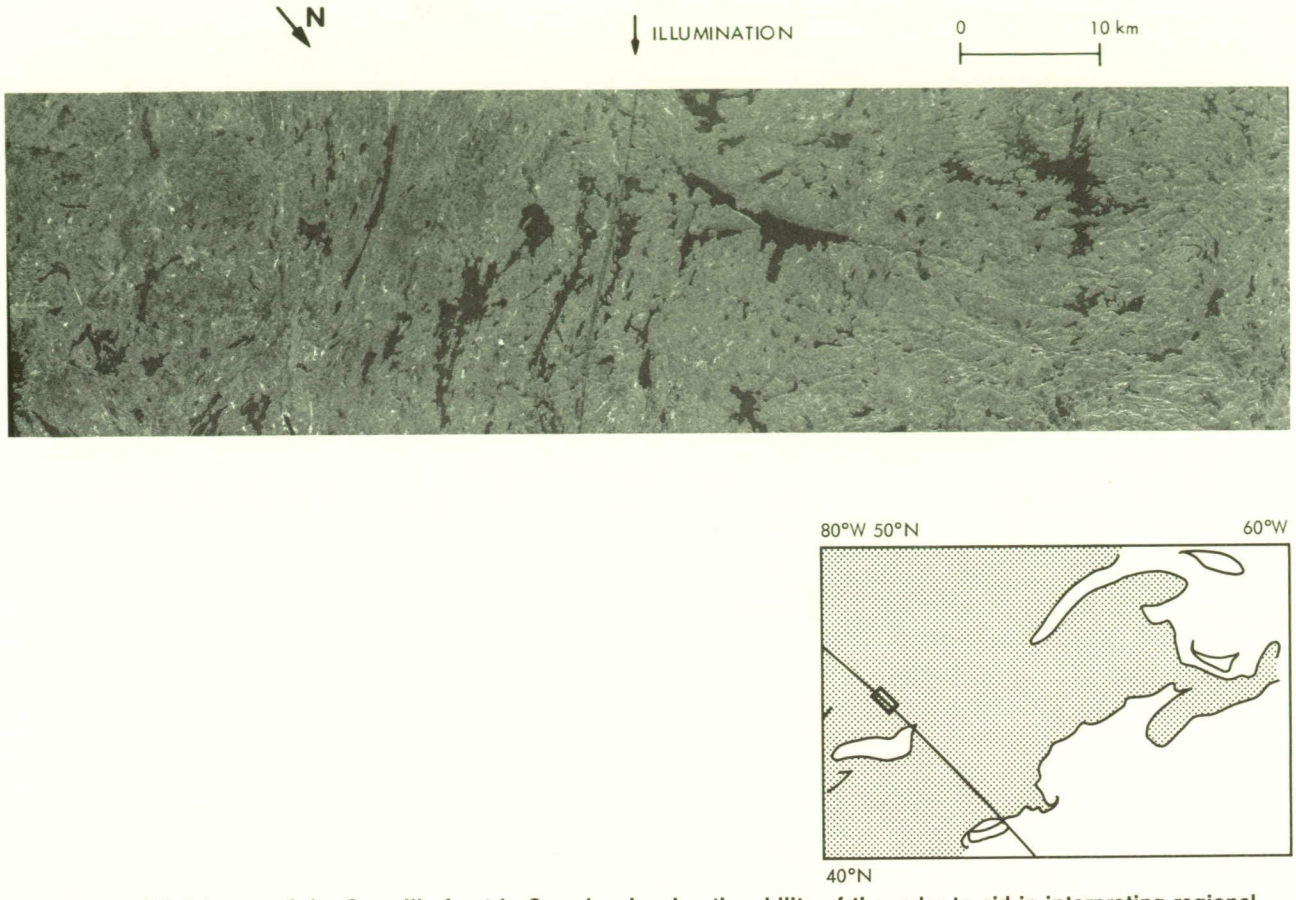

Fig. 4-11. SIR-B image of the Grenville front in Canada, showing the ability of the radar to aid in interpreting regional structural features

geobotanical issues

(1) To what extent do variations in the lithology of crustal materials govern the distribution, areal density, morphology, and condition of natural vegetation in different climatic environments? Are certain plant species direct indicators of rock lithology in specific environments?
(2) Is it possible to differentiate geologic stress conditions affecting natural vegetation canopies from other forms of stress related to variations in plant water supply, thermal conditions, and nutrient availability? (The former question serves to define the "normal" conditions within a natural vegetation canopy, which, in turn, enables us to detect departures from normality that may be stress related.)
(3) What are the interactions between vegetation and substrate physiology? Can the microwave properties of plants be combined with their spectral characteristics to help identify stress conditions?

Of key interest to geologists is the ability to recognize vegetation stress or community associations that may be produced by abnormal concentrations of metallic ions in surficial soils or the local seepage of hydrocarbon gases from a substrate oil reserve. Frequently, plant stress results in anomalous patterns in deciduous forests at the onset of budding in spring or senescence in the fall. Potential SIR-C experiments could therefore be developed to investigate these temporal variations in canopy morphology. The determination of the polarization signatures and frequency-dependent signatures of both typical and stressed vegetation may provide insight into the capabilities of radar for distinguishing characteristics of plant communities, particularly when SIR-C data from both flights are compared to identify variations in plant growth.

dependence of plant populations on bedrock type

Previous radar analyses of heavily vegetated areas have emphasized the discrimination of geologic units on the basis of their topographic and structural associations. In these analyses, the morphology of the vegetation canopy, particularly in tropical areas, has been employed to make inferences about the bedrock geology. Single-frequency, single-polarization data acquired by aircraft, by Seasat SAR, and by SIR-A have shown the capability of SAR for discriminating broad associations of vegetation types. Comparisons between airborne X-band and spaceborne L-band images of flooded alluvial forests in Brazil indicate a strong contrast between radar penetration capabilities at different frequencies (Fig. 4-12). Because radar-signal penetration in vegetated areas depends on wavelength, multifrequency SIR-C data could be employed to study the canopy structure in order to help discriminate variations in the plant population, since the population might be influenced by bedrock types.

Six different classes of SIR-C vegetation experiments are discussed in Section 4.4.5, but it is also of value for the geological community to realize that the radar signatures of different plant types might be useful indicators of the geomorphological characteristics of an area. The type and degree of vigor of vegetation cover will vary depending upon the local aspect of a vegetated slope, the stability and age of the soil cover, the ability of the soil to retain water, and the altitude of the study area. Studies of airborne multipolarization SAR images of the forest-covered coastal lowlands of South Carolina show that distinct polarization signatures can be correlated with tree size (basal area) and with the distribution and density of the vegetation cover (Fig. 4-13). In the more arid environment of central Wyoming, different lithologic units support varying vegetation densities that are identifiable on radar images (Fig. 4-5).

The capability of SIR-C to obtain simultaneous multifrequency, multipolarization data may also be useful for investigating differences in canopy morphology or the degree of vegetation cover in an area that is partially composed of exposed rock and/or soil. Thus, it may be possible to develop analytical methods by which the amount of vegetation covering pixel-sized areas could be estimated from the strength of the like- and cross-polarized returns. Synergism between the multifrequency, multipolarization radar and optical/IR data (such as from Landsat and AVIRIS) will therefore provide a greater capability not only for identifying vegetation types and levels of stress, but also for aiding in the interpretation of geologic targets that are partially covered with plants.

4.2.5.6 Radar Stereo/Topographic Experiments

topographic experiments

The potential to acquire high-spatial-resolution topographic data, derived either by interferometry or from SIR-C data takes that have at least 20° variation in angle of incidence, opens a completely new realm of investigations of the earth's geology. Figure 4-14 presents examples of this radar-derived topography from SIR-A and SIR-B, and additional investigations using digital terrain models from SIR-C are envisioned.

For much of the earth, the topography is only poorly known, so that reconstructions of continental evolution, gravity modeling, geomorphic process, and the response of the landscape to recent climatic change can at best only be estimated. Adding radar-derived topography for local- (~ 100 km^2), regional- ($\sim 10^3$–10^6 km^2) or continental-sized areas could permit many such geologic investigations, with sufficient resolution to establish quantitative

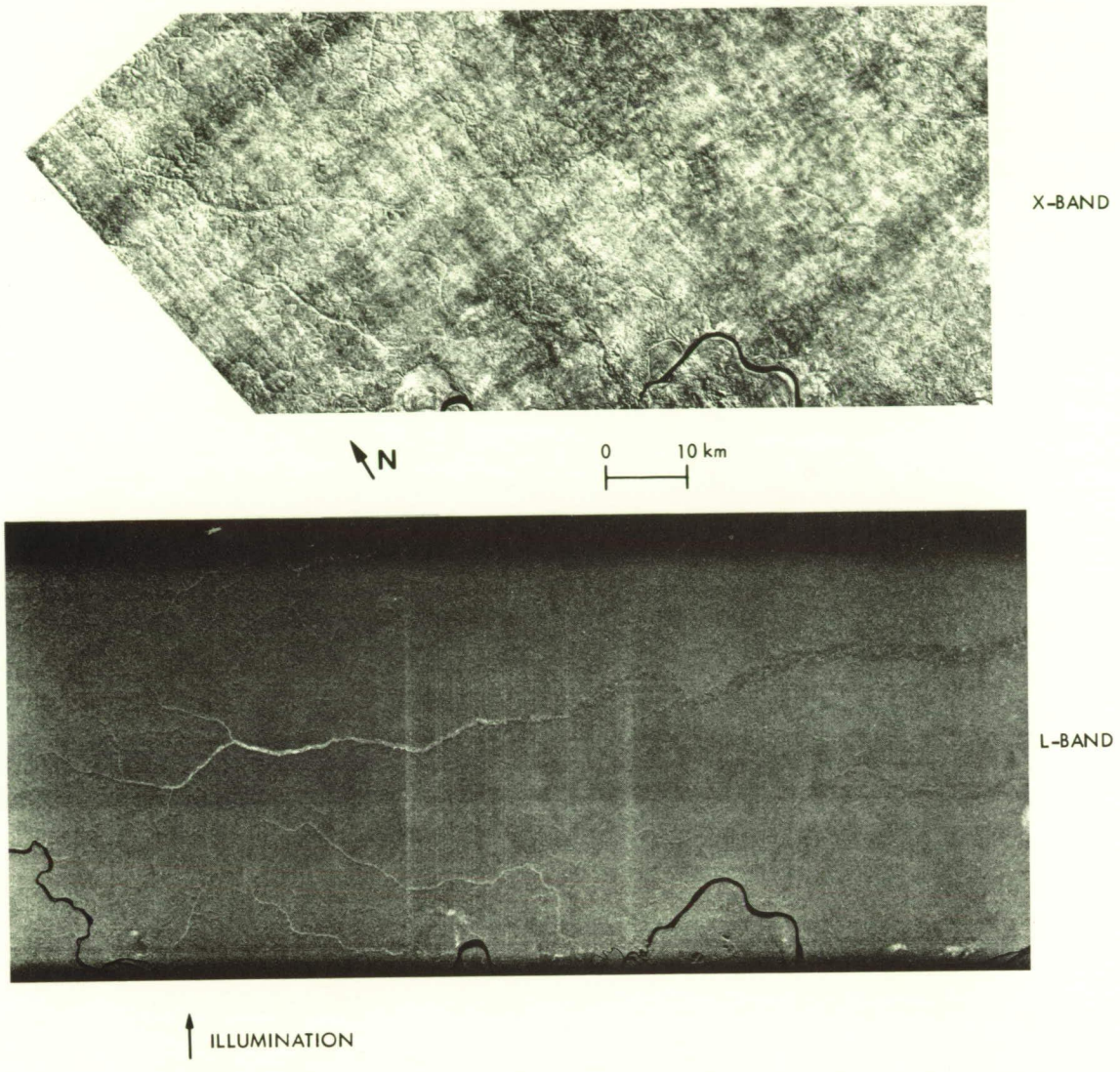

Fig. 4-12. A floodplain in the Amazon forest, Amazonas, Brazil (top image). Data were acquired at X-band by commercial airborne SAR in 1973. The bottom image, obtained by SIR-A (L-band) in 1981, shows the same area. Differences in the radar penetration of the tree canopy for the two systems is apparent. In the SIR-A image, the bright radar response in the upper reaches corresponds to points where forest cover is underlain by standing water. Such a feature is not seen at X-band, probably due to the shorter penetration length of the radar signal

models of landscape evolution. These models can potentially be inverted to infer the length of time that a particular area has been subjected to a specific set of weathering conditions, and to identify broad-scale (>1 km) low-relief landforms with greater accuracy than has previously been obtained.

The SIR-C Geology Science Working Group (SWG) has identified several potential topographic experiments, but it is clear that the following list is incomplete and is useful for illustrative purposes only:

(1) One experiment might be the determination of volcano volume and the rheological properties of the erupted magmas. In many parts of the world, but particularly the circum-Pacific "Ring of Fire," the volume of volcanic cones and their morphologic

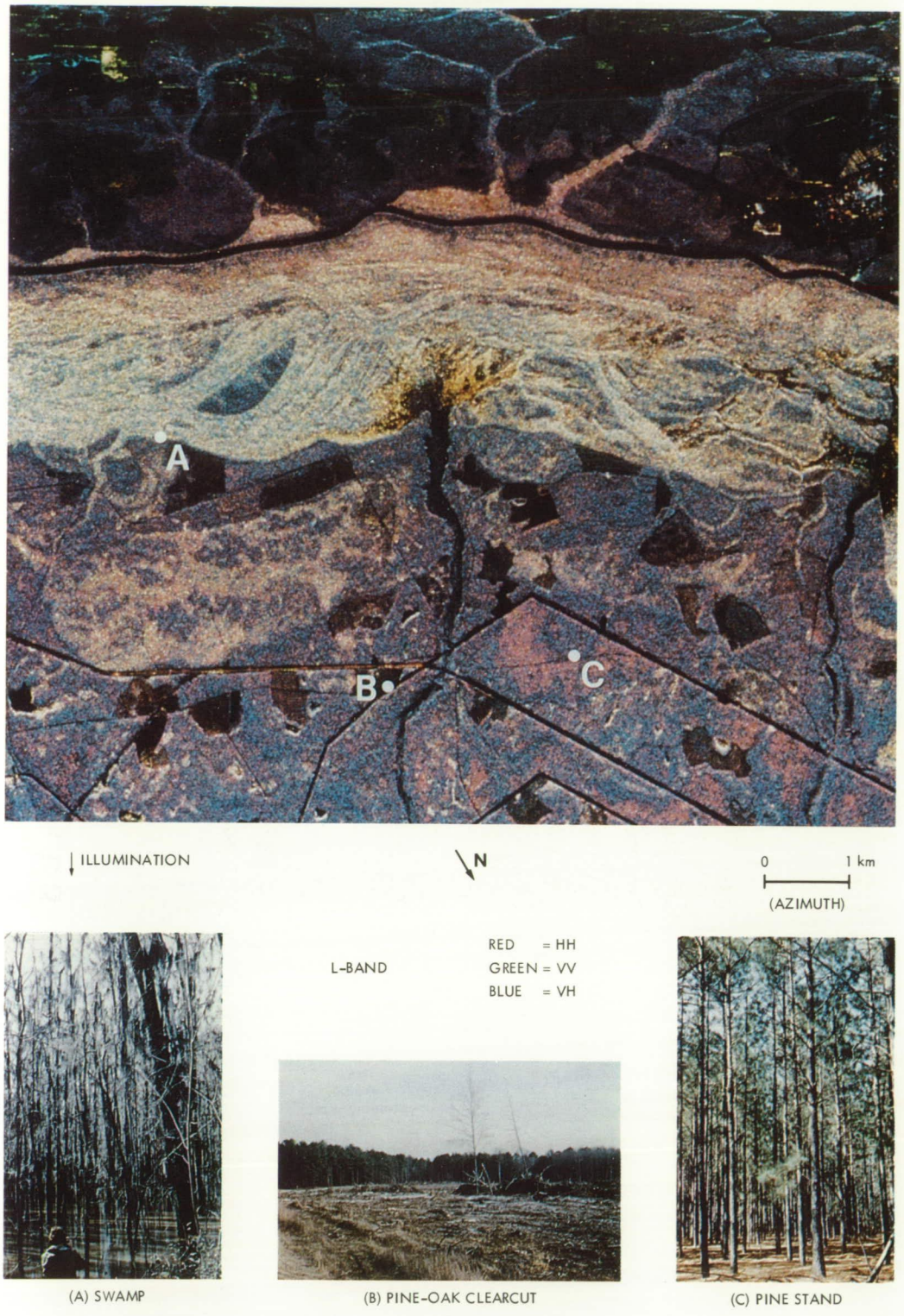

Fig. 4-13. The role of vegetation coverage in affecting radar returns from the Savannah River Plant, South Carolina. Shown is a three-color composite image obtained from an airborne multipolarization radar system, together with representative examples of vegetation types (courtesy of John Ford, JPL).

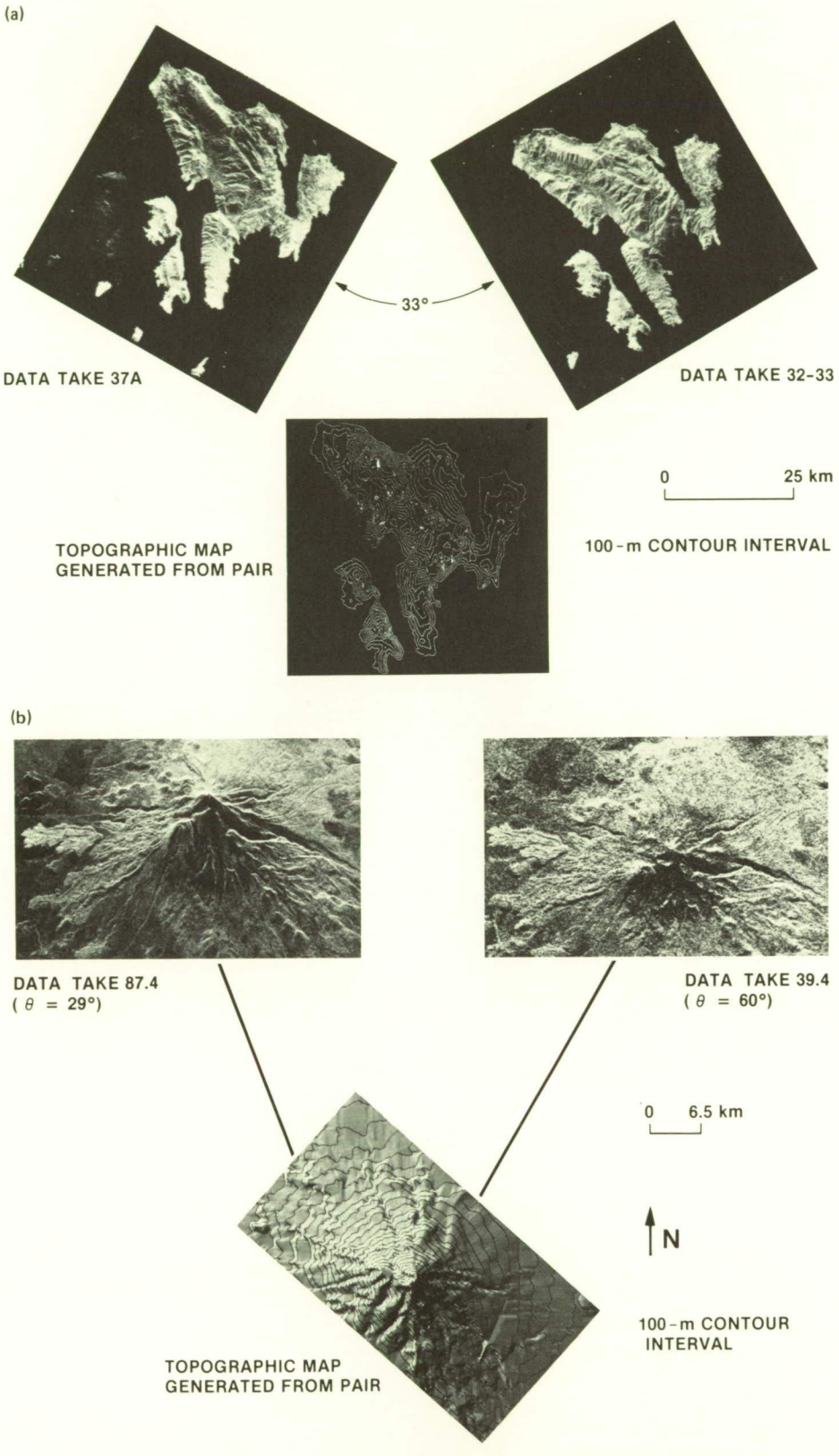

Fig. 4-14. Examples of radar-derived topography obtained from (a) SIR-A and (b) SIR-B. The difference between these two techniques lies in the orientation of the original radar data takes (courtesty of Mike Kobrick, JPL).

shape are poorly known. Using improved topographic data from SIR-C, these parameters and the eruptive style (explosive vs. effusive) of the volcano could be estimated. Furthermore, rheological models for the emplaced lava flows could then be utilized to estimate magma chemistry and diversity at given volcanic centers.

(2) Hydrologic models of river basins, and the evolution of stream networks, depend critically on the knowledge of local topography at the 100-m to 1-km scale. A comparison of drainage networks for regions of known lithology or age could be performed more completely if local stream gradients could be determined. In this manner, a topographic analysis could be correlated with the hydrology investigations outlined in Section 4.3.

(3) In geobotanic studies, the different plant communities will be affected by local slopes, both in terms of the amount of sunlight the plants receive and the drainage characteristics of the soils. Radar-derived topography could permit plant-growth differences due to the landscape to be distinguished from characteristics due to mineralization or hydrocarbon stress.

(4) Geomorphologists have long studied the slopes and regional relief of an area as potential indicators of surficial process and climatic change over geologic time. Erosion surfaces, mass-wasting products, hanging valleys, and regional slopes have all been utilized to correlate the existing land surface with present-day and former environmental conditions. Such studies have in the past been focused on North America and Western Europe due to availability of the required topographic data; in order to more fully investigate temporal changes in the erosion of the continents due to such events as ice ages and eustatic changes, these topographic investigations should be made global in extent and correlated with specific landforms and processes.

(5) While the short time interval between the two flights of SIR-C precludes any long-term investigations of the changes in ice-sheet volumes, it is recognized that a baseline data set has to be derived that will permit future spaceborne experiments to detect climate-related changes in the volume of polar and alpine glaciers.

4.2.6 Summary of SIR-C Mission Requirements for Geology

4.2.6.1 Orbital Parameters

high-latitude coverage

Several of the geology experiment classes described above require a *high-inclination orbit.* These classes include studies of glacial landforms, permafrost, and polar-region tectonics.

4.2.6.2 Mission Timing

two flights required

At least two flights are required, one in the May–June period and the other in the November–December period. This would allow seasonal vegetation and glacial-landform studies and would also allow a determination, during the first flight, of the optimum radar parameters for testing in mapping mode on the second flight.

4.2.6.3 Swaths and Resolutions

recommended modes

For the dual-frequency (L- and C- band) quad-polarization (DFQP) mode, using a 4-bps BFPQ, swath widths are expected to be about 40 km for a 35° look angle, and 30 km for a 50° angle. Even though the swaths are narrow, this mode offers the maximum potential for investigating how dependent images are on wavelength and polarization. It is recommended that this mode be used principally for studies of rock weathering rates, lithologic mapping, age dating, and geobotany. The single-frequency quad-polarization (SFQP) mode offers an increased swath (45 to 47 km at 4 bps) and is preferred for mapping experiments involving tectonics, topography, certain aspects of cold-region geomorphology, and ancient drainage systems. These swath widths assume a resolution of 30 m, which corresponds to a bandwidth of 9.5 MHz. This resolution is desirable for most of the mapping applications mentioned above since a higher resolution mode would result in a narrower swath width.

4.2.6.4 Frequencies, Polarizations, and Incidence Angles

30°–55° incidence angles preferred

Control of the angle of incidence is important for landform enhancement, for geometric fidelity, and for the discrimination of scattering units. The preferred range for angles of incidence for most geologic applications is 30° to 55°. At lower angles of incidence, distortion due to layover is objectionable for regions of high relief. Control of the illumination angle is also important for experiments in stereo radargrammetry. A pair of stereo images can be obtained by imaging a particular swath at two (or more) angles of incidence that differ by at least 20°. It is recommended that several image pair sets be acquired combining various angles of incidence, with the combinations depending on the relief of the test site—e.g., a 15°–45° pair for high-relief regions and a 30°–60° pair for moderate-relief regions.

simultaneous L-band and C-band

A number of geology experiments will require simultaneous acquisition of L-band and C-band data for like (HH and VV) polarizations; these experiments include certain cold-region geomorphology studies, surface-roughness effects in river outwash plains, and surface roughness (texture) of slopes for wash-rate estimation. Other studies will also require cross-polarized (HV or VH) data—e.g., age dating of Quaternary surfaces and geobotany investigations.

wide-swath mode

However, a number of experiments will require simply a single frequency and polarization, with as much swath as possible. These experiments include radar topographic studies, certain investigations in fluvial geomorphology, and studies of tectonic features. Those experiments seeking maximum penetration of dry soils will prefer L-band to C-band.

4.2.6.5 Data Products

BFPQ desired

Radar returns from geomorphic surfaces extend over a very wide dynamic range, at times 20 dB or so. This means that either a very large number of quantization bits must be used, or the BFPQ scheme must be used. For most geology experiments being contemplated, a 4-bps BFPQ is adequate; however, for scenes where calibrated data and absolute values are important, an 8-bps choice can be made, although the swath width will be cut by half.

calibration to ±1.5 dB

It is important that the radiometric fidelity across the swath be as uniform as possible (better than 0.2 dB), particularly for mapping-mode experiments. Calibration to ±1.5 dB or better of C-band relative to L-band is essential for geochronology and stratigraphy experiments, where the ratioing of σ° (L-band) to σ° (C-band) will be used as a measure of how dependent rock unit signatures are on wavelength.

Level 3 data products

For maximum utility in these geology experiments, SIR-C images should be specially processed to Level 3—i.e., they should be geocoded to standard map projection, radiometrically calibrated, and corrected for foreshortening. However, some experiments will also require some 4-look-survey and standard-image products that are not radiometrically calibrated.

4.3 Hydrology

4.3.1 Background

the hydrologic cycle

Hydrology is the science that studies the waters of the earth—their properties, distribution, and circulation on the surface, in the soil, and beneath the surface, and their relationship to the environment, including living things. Factors that affect the hydrologic cycle include precipitation, infiltration, percolation, surface runoff, groundwater flow, evaporation, and transpiration. Hydrologic models that assist scientists in understanding the hydrologic cycle require knowledge of, among other things, vegetation, surface features, land use, soil conditions, and meteorological information, over extended regions that have diverse physical and environmental characteristics. In addition, these data are required at frequent intervals in order to track critical parameters that control the cycle.

The flux magnitudes in the hydrologic and energy cycles provide the major constraints in the evolution of ecological systems on the earth. Surface hydrology is integrally related to climatology in that evapotranspiration is the only source of atmospheric water, and latent and sensible heat fluxes provide much of the energy to drive climate dynamics. This existing link between the earth's water cycle and its surface, the atmosphere and plant biochemical cycles, provides the primary justification for more detailed studies of the hydrologic cycle.

The energy and moisture components of the hydrologic cycle are interrelated and highly complex. Most of the earth's water (97%) is stored in areas with an extremely long residence time (> 4000 years). Some of the water storage components such as plants, soil, and the atmosphere are comparatively small, but changes in these account for the major fluxes in the hydrologic cycle and are of primary importance for energy exchanges in the atmosphere and for biological resources.

Theoretical and simulation studies have been used to study the hydrologic cycle and its response to changes in the variable storage terms. The process which drives the changes in the hydrology of the land surface can best be expressed in terms of the energy balance and the water-mass balance at the surface. These processes can be expressed as follows:

$$R_N - G = L.E + H \qquad (4\text{-}1)$$

$$P - E = Q - S$$

REGIME \ CHARACTERISTICS		VEGETATION	MOISTURE	ROUGHNESS	RELIEF	SURFACE OVERLAY
ARID	SEMIARID	SPARSE	LOW	VARIABLE	VARIABLE	NONE
	HYPERARID	NONE	VERY LOW	SMOOTH	LOW	NONE
HUMID		HEAVY WITH VARIABLE STRUCTURE	VARIABLE: MODERATE TO HIGH	HIGHLY VARIABLE	LOW TO HIGH	NONE
WETLANDS	COASTAL	SINGLE STRUCTURE	SATURATED	SMOOTH	LOW	NONE
	UPLAND	VARIABLE STRUCTURE	TEMPORALLY SATURATED	VARIABLE	VARIABLE	NONE
SNOW-COVERED WATERSHEDS		VARIABLE	VARIABLE: FROZEN/ UNFROZEN	VARIABLE	LOW TO HIGH	SNOW
HIGH-LATITUDE WATERSHEDS		VARIABLE	PERMAFROST	VARIABLE	LOW TO HIGH	SNOW, ICE, GLACIERS

Fig. 4-15. Characteristics of hydrologic regimes

where R_N is net radiation, G is the soil heat flux, L.E. is the latent heat flux, H is the sensible heat flux, P is the precipitation, E is the evaporative flux, Q is the runoff, and S is the change in storage as snow, ice, or soil moisture.

The relative magnitude of the energy fluxes input in equation (4-1) shows the importance of some of the terms which radar can help to measure. The value of G is typically a small fraction of R_N (10 to 30%), so 70 to 90% of the radiation budget gets expended as latent and sensible heat input to the atmosphere. These two inputs vary in their proportion with time of day and climate, but on the average, are about the same size. Since the latent heat flux carries about 40% of the radiation budget, it is important to be able to estimate L.E + H for its energy content and L.E alone for its water content. Modeling these, in turn, depends on surface measurements such as soil moisture, temperature, albedo, and ground cover. Several measurements which may be made using surface-viewing radars are helpful in estimating these fluxes. In order to estimate fluxes, it is necessary to have time series of several state variables, such as surface temperature and surface moisture.

As is described later, radar may be useful in making estimates of soil moisture status and snowpack properties, and certainly may be related to vegetation properties, such as stomatal water content, which are in turn related to transpiration rates. In addition, radars are useful for hydrological mapping, such as of topography, which are used then in runoff estimation. During a short Shuttle experiment, it is difficult to estimate fluxes directly by getting a time series of measurements. It is anticipated more that the SIR-C experiment will show the feasibility of making state measurements such as those related to surface soil moisture and snowpack and vegetation properties. The results can be used later, together with those using other sensors, to design algorithms that estimate hydrological fluxes globally and routinely using synoptic radar data that should be available in the next decade. This ties closely with the objectives of other parts of NASA's program, and to the aims of such related programs as the International Satellite Land Surface Climatology Project.

Radar data can make different scientific contributions in different hydrologic regimes. Five categories of hydrologic regimes can be identified based on their unique distinguishing characteristics and the contributions radar data can make in them:

(1) Arid regions
(2) Humid regions
(3) Wetlands
(4) Snow-covered watersheds
(5) High-latitude regions

Each hydrologic regime has distinguishing physical characteristics, as summarized in Fig. 4-15. Not only are these physical characteristics distinctive for each hydrologic regime, they also have a strong influence on the formation of a radar image. With each hydrologic regime, there are associated specific research objectives.

arid regions

Arid regions, the global distribution of which is shown in Fig. 4-16, have little soil moisture and receive average precipitation amounts ranging from about 20 cm per year (semiarid) to only a few mm in several years (hyperarid). As a result, vegetation is sparse or nonexistent and human population densities are low, except for irrigated regions. The surfaces of hyperarid regions are generally smooth with small slopes.

Research issues for these hyperarid regions include the mapping of subsurface relict riverbeds and channels that provide indications of the hydrologic development of the region. Specific research issues for semi-arid areas include monitoring the spatial distribution and amount of rainfall, soil moisture status, evaporation, and vegetation.

humid regimes

The humid regime is the most complex regime in terms of application of radar data to scientific problems. It is highly vegetated, containing a wide variety of vegetation geometries and sizes. The soils are mostly moist, and there is a wide range of surface roughness and topographic relief. The high-priority research objectives for this regime include

(1) Direct measurement of watershed characteristics and runoff model parameters and mapping areas of high soil moisture within watersheds to calibrate these models
(2) Measurement of the areal extent of precipitation over land
(3) Delineation of surface water, especially under vegetation canopies
(4) Measurement of vegetation characteristics which relate to transpiration

wetland regimes

Wetlands are important because they are the main chemical-reducing environments and, thus, key controls on global chemistry. They are also ecologically unique. The two basic wetland regimes are estuarine and nonestuarine. Figure 4-16 indicates tropical rainforest regimes, where a preponderance of the earth's wetlands exist. The existing wetland global maps are inadequate, which indicates the necessity of improved information about these areas. The soil moisture of the lower-lying estuarine wetlands tends to be constant with time because the surface of the freshwater table remains essentially at the same elevation in low coastal areas of normal groundwater recharge. Compared to nonestuarine wetlands, estuarine vegetation systems have relatively dense associations of lower-growing, finer-structured species. The soils of estuarine wetlands tend toward constant saturation. Riverine, palustrine, and lacustrine wetlands, on the other hand, are subject to the vagaries of rainfall or to seasonal variability in the depth of the water table. Such wetlands are also characterized by a wider variation in the size, type, and density of vegetation classes.

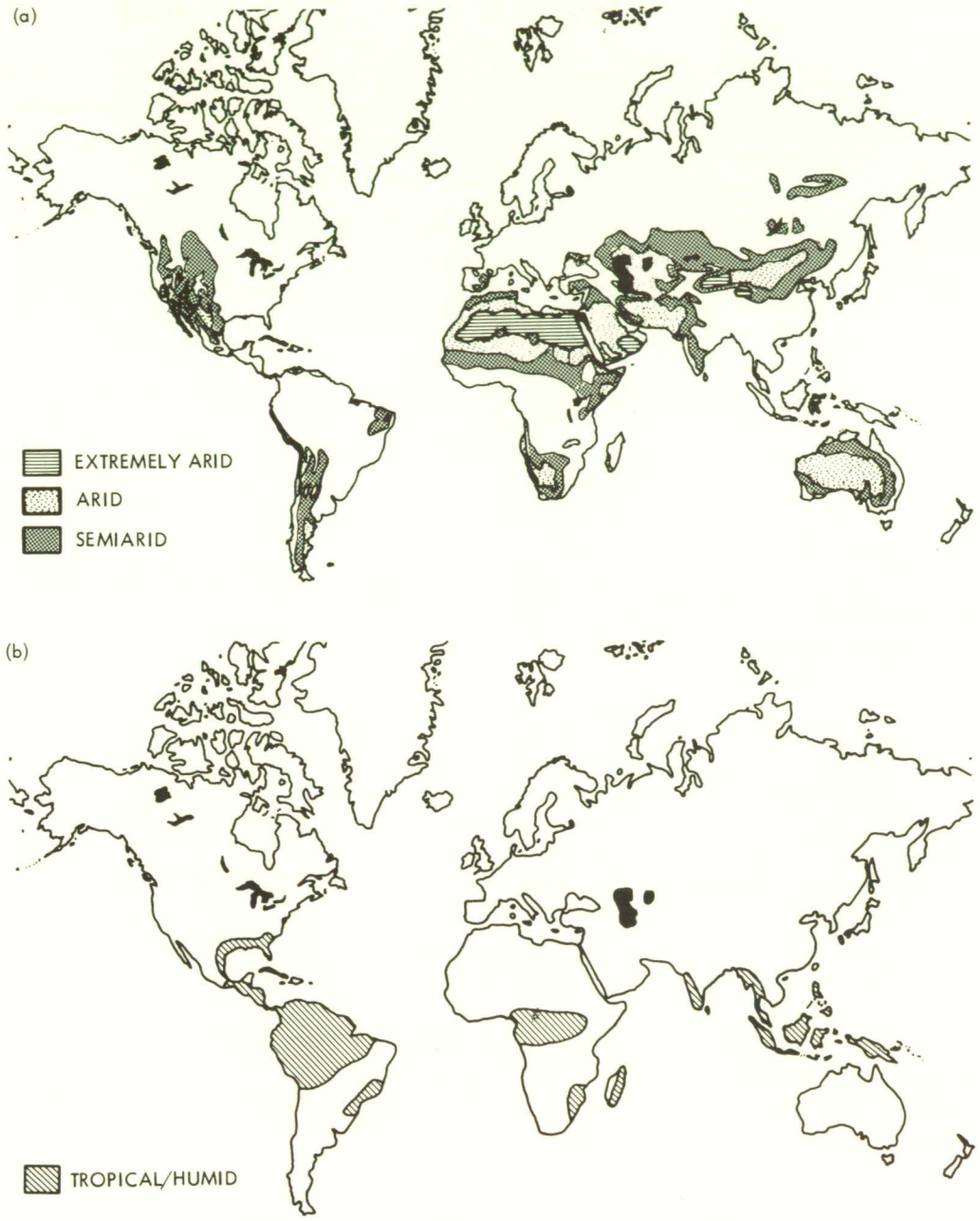

Fig. 4-16. Global distribution of (a) arid and (b) tropical/humid environments

Two important research objectives for wetland hydrology are wetland boundary delineation (the discrimination of the land–water boundary, especially when it is vegetation-covered) and the discrimination of vegetation classes as an indicator of wetland characteristics, classification, and chemistry.

snow-covered watersheds

Watersheds at mid-to-high latitudes are distinguished particularly by the seasonal presence of snow and ice. These regions are typically vegetated, but the vegetation varies widely, ranging from rangeland to forest. Also, such snow-covered watersheds occur often

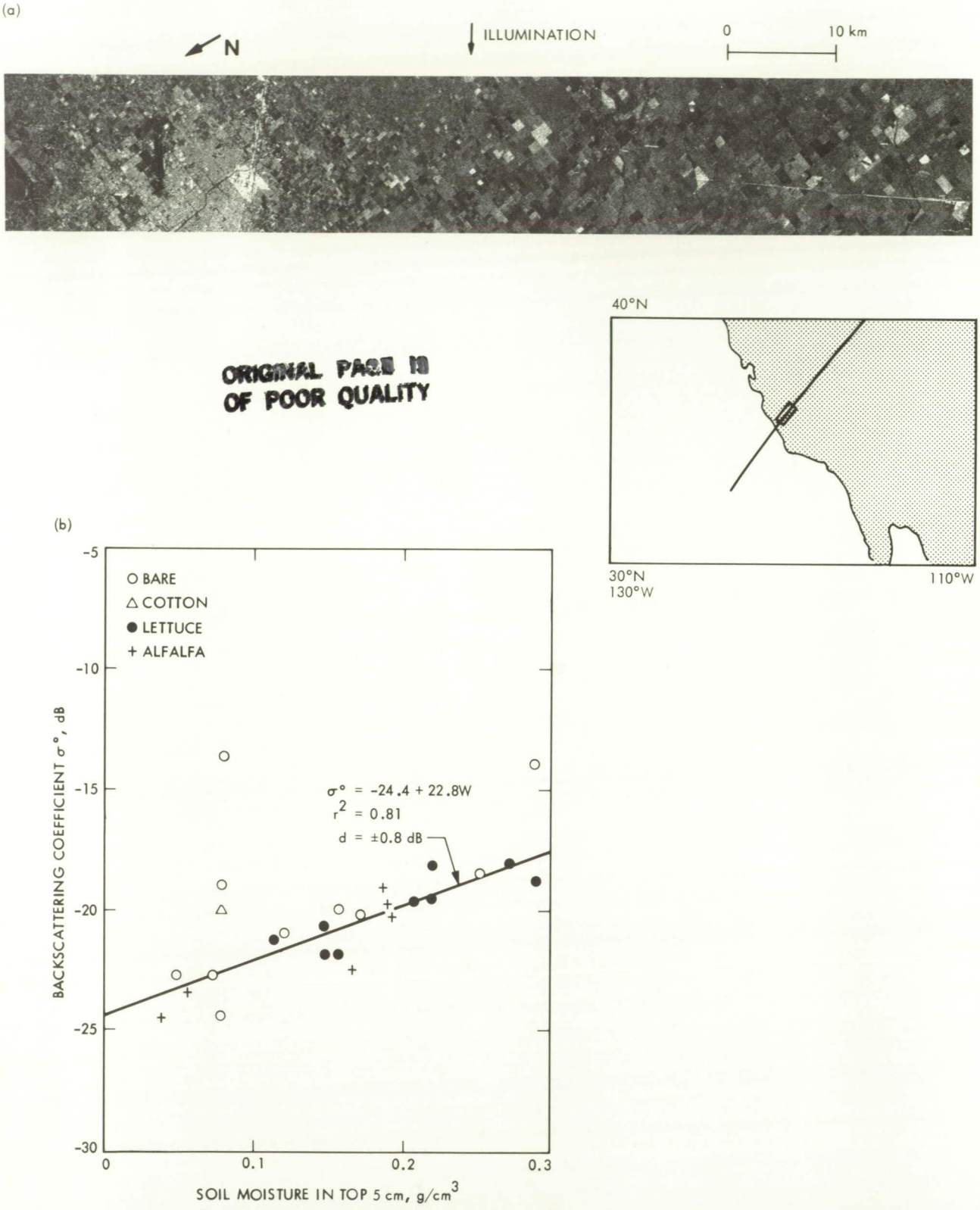

Fig. 4-17. A comparison of soil-moisture data showing (a) an agricultural area about 60 km southwest of Fresno, California, as imaged by SIR-B, and (b) σ^0 vs. soil moisture in the top 5 cm as derived (solid line) from this image and compared to scatterometer and Seasat data

in mountainous regions with considerable topographic relief. Key hydrologic research objectives for these watersheds include the measurement of snow-pack extent, the snow-cover water equivalent, and the ripeness (wetness) of the snow pack.

high-latitude regions

Characteristics of high-latitude regions are essentially the same as for snow-covered watersheds except that additional problems related to permanent, rather than ephemeral ice and snow, related to ice sheets, glaciers, and permafrost are included. From a hydrological point of view, glacier parameters such as glacier slope and contours and the volume of meltwater are important for estimating glacier dynamics. Also, the areal extent of permafrost, the depth of permafrost, and the conditions of overlying soil are of considerable interest for runoff modeling.

4.3.2 The Role of Spaceborne Remote Sensing in Hydrology

from point data to area-extensive data

Historically, hydrologic information has been obtained utilizing point data sources (e.g., rain gauges) from which area-extensive information is estimated through mathematical and statistical techniques. Typically, the area density of point data sources is too low for statistical validity. By contrast, satellite-borne imaging sensors inherently provide continuous area-extensive information on a synoptic scale. Optical, infrared, and microwave imaging and nonimaging sensors all provide useful information since vegetation, soil types, meteorological conditions, etc., all affect the hydrologic cycle. The Landsat Multispectral Scanner (MSS), the return-beam vidicon (RBV), the Thematic Mapper (TM), and the Advanced Very High Resolution Radiometer (AVHRR) have been used to acquire information on surface and vegetation features. Measurements from NOAA/TIROS-N (atmospheric water vapor and temperature profiles), NIMBUS-7 (surface temperature), and HCMM (albedo) have provided thermal IR and passive microwave data that have been used for evapotranspiration estimates. Microwave sensors operating at wavelengths from L-band to X-band have also been used to provide information, such as soil moisture, more directly. In addition, these longer wavelengths have proved to be extremely beneficial in very dry regions for probing subsurface features. SIR-C will provide a sensor capability beyond that of Seasat, SIR-A, and SIR-B. In addition, passive microwave systems operating at these frequencies can provide unique information, although at reduced spatial resolution. This section of the science plan identifies hydrologic issues that can be addressed utilizing the SIR-C system either alone or with complementary passive microwave systems or visible/near-IR sensors.

4.3.3 Role of Imaging Radar in Hydrology

radars vs. radiometers

The principal role of imaging radar in hydrology is to provide information on soil moisture, vegetation cover, glacier, and snowpack characteristics. A secondary benefit of radar relates to its ability to penetrate hyperarid sand sheets to a meter or more, thus providing valuable data on subsurface relict riverbed channels in the Sahara and similar very dry regions.

Both imaging radars and passive microwave radiometers operating at L-band and C-band have been shown to be useful for estimating soil moisture in the top few centimeters of the soil. From a space platform, an L-band radiometer would have a spatial resolution of several kilometers, while an L-band SAR would provide much finer resolution, typically

on the order of 30 meters. The microwave brightness temperature can be converted to an emissivity value by normalizing with the physical surface temperature, and subsequently related to soil moisture through a series of physically based models. The active radar backscattering coefficient, σ°, also can be related to soil moisture through physically based models, although surface roughness, slope, and vegetation can also strongly modulate the radar return. The radar backscattering coefficient is closely related to vegetation characteristics such as biomass, geometry, and plant moisture, which in turn are closely coupled to the hydrologic cycle. Ultimately, an operational system for hydrology is likely to be composed of both active and passive microwave systems giving complementary information. It is necessary first to understand, test, and refine radiative transfer models that relate radar backscatter to hydrological state variables, such as soil moisture, before we can use time series of data from both active and passive sensors, and then to look at changes in these state variables and estimate hydrologic fluxes.

Nonetheless, it is evident from phenomenological studies that there is a strong relationship between radar backscatter and various hydrologic variables. Figure 4-17(a) shows an image taken by SIR-B from above an agricultural area in the San Joaquin Valley, about 60 km southwest of Fresno, California. Individual agricultural fields are clearly separated. Figure 4-17(b) shows σ° vs. soil moisture for the top 5 cm, as derived (solid line) from this image and compared to results on similar fields, obtained earlier by aircraft scatterometer data and Seasat data.

other imaging radar capabilities

Radar data may also be used for hydrologic mapping of less dynamic hydrologic variables. For instance, the capability of an imaging radar to map topographic relief in detail can help determine parameters related to watershed runoff hydrology. Other examples of using an imaging radar for hydrologic studies are flood and coastal-area mappings, especially under cloudy conditions.

The SIR-C data requirements for scientific investigations in hydrology will call for differing sensor parameters, depending on the objective. For example, maximum swath widths and longer wavelengths are generally significant for the study of sand-mantled, buried riverine channels and alluvial deposits, such as those discovered by SIR-A in the Eastern Sahara and postulated to exist in virtually all of the earth's major desert regions. Horizontal-horizontal (HH) polarization has been shown on theoretical grounds to maximize the penetration of radar signals in such regions [4-7], but the extent to which vertical-vertical (VV) or cross polarization is important should be determined during the SIR-C mission. On the other hand, multifrequency and multipolarization options are of equal importance for other studies dealing with backscattering response to variation in soil moisture, surface roughness, and vegetation cover. An imaging radar with a single frequency and polarization (e.g., SIR-A or SIR-B) does not supply enough information to study many land surface variables in detail. This is because the radar backscattering coefficient is related to several variables, so that several measurements are needed to invert the radiative transfer equation in order to estimate these variables.

Many hydrologic studies will require two SIR-C flights separated by six to eight months at times of near-saturated and dry conditions. These flights will include mapping of seasonal changes of water storage in the form of soil moisture, wetlands, snow, and ice. Observations over two different seasons are also needed of the effect of vegetation on imaging radar remote sensing of hydrologic parameters.

4.3.4 Scientific Basis for SIR-C Hydrology Experiments

microwave sensitivity to water

A principal reason why the microwave region is useful for hydrologic investigations is its sensitivity to changes in the dielectric constant of the surface, especially changes caused by soil moisture or water boundaries. As pointed out previously, the dielectric constant of water is about 80 while that of dry soil is about 3. The dielectric constant of very wet soils may approximate 30. This is responsible for the strong dependence of both the emissivity and the radar backscattering coefficient on soil moisture. The effects of soil moisture are clearly seen in Seasat SAR images and more recently in SIR-B images (cf. Fig. 4-17). Another important reason why the imaging radar is useful to hydrologists is its sensitivity to surface roughness and slope. The intensity of radar backscatter depends strongly on local slope and is also affected by smaller-scale surface roughness.

attenuation and scattering by vegetation

Still another factor affecting radar backscatter is the presence of vegetation, whose canopy acts as an attenuator and scatterer of incident radar waves. In the hydrologic context, this aspect can be both an advantage and a disadvantage. To the extent that backscatter from vegetation is an indicator of stand vigor, it may be related to underlying soil moisture conditions and therefore be useful. However, in other situations, vegetation may act as a confusion factor that partially or completely masks underlying soil moisture conditions or soil–water boundaries. The presence of snow or ice can also affect radar backscatter, particularly at the shorter wavelengths.

the two-layer model

From a radar perspective, two layers of the earth's surface affect hydrology, and both are important for quantifying the dynamic water balance. Typically these two layers are a vegetation canopy and a soil layer, or a snow pack and a soil layer. The problem facing hydrologists using remotely sensed data is one of measuring the properties of each layer without interference or confusion from the other layer. Multifrequency SAR data will help to keep the layers distinct.

The two-layer system typical of most surfaces of hydrologic interest can be considered an inhomogeneous layer overlying a homogeneous layer. The vegetation canopy or snow pack is considered inhomogeneous because it is a mixture of materials of different dielectric properties. In this case, the transmitted radar wave is subjected to volume scattering within the inhomogeneous layer. The soil layer is considered homogeneous because its dielectric properties are relatively constant within the layer. A transmitted radar wave is subjected to surface scattering in this case. The ideal remote sensing system for hydrologic applications would consist of several frequencies and polarizations. In general, the system characteristics for hydrologic applications are as follows: for measuring upper-layer (crop or snow) properties with minimal contribution from the lower (soil) layer, the system would use shorter wavelengths (K, X, or C), larger angles of incidence, and multipolarization; for measuring lower-layer (soil) properties with minimal contribution from the upper (crop or snow) layer, i.e., for maximum depth of penetration, the system would use longer wavelengths (C, L, or P), smaller angles of incidence, and like polarization.

extracting hydrologic information from terrain-surface images

The problem of extracting useful hydrologic information from multiparameter radar images of terrain surfaces may be posed in the following quasi-mathematical way:

$$I_{nmp} = f(SM, VEG, SR, SL, CV; \lambda, p, \theta, CX) \qquad (4\text{-}2)$$

where I is the image intensity. The integers n, m, and p refer respectively to the n^{th} wavelength, the m^{th} incidence angle, and the p^{th} polarization. This equation states that the image intensity is a function of soil moisture (*SM*), vegetation cover (*VEG*), surface roughness (*SR*), slope (*SL*), and temporal cover, e.g., snow (*CV*). It also explicitly recognizes the effect of wavelength (λ), polarization (p), angle of incidence (θ), and image context (*CX*). Of course, no explicit mathematical relationships of the above type actually exist for most scenes of practical interest, because of their complexity. A typical problem confronting a hydrologist might be to estimate the soil moisture *SM* at some point in a SAR image, in the presence of the confusing factors of vegetation, surface roughness, slope, and cover. Mathematically, the problem is to invert the equation and "solve" for soil moisture. Even though no explicit relationship exists, the above formalism is useful, since it hints that even though we may have as many as five unknowns, we also have quite a number of equations provided by SAR imagery taken at various frequencies, polarizations, and angles of incidence. We also obtain additional information through context, which in the past has been virtually the only tool available to the photointerpreter.

Can we really invert this set of equations and solve for soil moisture (or for some other parameter)? The answer is "yes" for some situations, "no" for others, and "we don't know yet" for quite a number of cases. We do know, for example, that SAR response to surface roughness is relative as to wavelength, so that by perhaps ratioing SAR images taken at one or more frequencies, incidence angles, or polarizations, we may be able to estimate roughness, at least for bare soils. In general, we need a better understanding of the interaction of electromagnetic waves with hydrologic surface features and conditions. Even though a great deal of information available in the literature is based upon theoretical models and experimental measurements, these usually refer to idealized circumstances such as bare soils, uniformly vegetated surfaces, or gentle slopes.

ground-based measurements

An exhaustive series of ground-based radar measurements of the dependence of the radar backscattering coefficient on soil moisture, vegetation, and snow were made by F. T. Ulaby and his colleagues [4-8] over the period 1974–83. Most of these measurements were made using an FM-CW radar whose frequency was selectable between 1 and 18 GHz, and whose polarization and angle of incidence were likewise selectable. The soil moisture and vegetation measurements were primarily for agricultural fields. A strong dependence of σ° on soil moisture was found at both L-band and C-band; however, surface-roughness effects for agricultural fields were found to be minimized at C-band.

Figure 4-18 illustrates the truck-scatterometer-measured dependence of σ°, at C-band, on soil moisture expressed as percent of field capacity for both bare fields and fields with mature corn, soybeans, milo, and wheat. These curves are the average for 181 independent samples for the bare-soil case and 143 independent samples for the vegetated case. It should be emphasized that measured data points are scattered about these curves due to the effects of surface roughness, row direction, etc. However, several conclusions can be drawn from these curves:

(1) The total expected dynamic range of σ° as the soil goes from dry (0%) to wet (100%) is about 15 dB for the bare-soil fields and 10 dB for the vegetated fields.
(2) The vegetated fields are brighter (by about 4 dB) than the background soil when the soil is very dry (10%); however, as the soil moisture increases, the difference quickly becomes negligible because the surface scatter from the background high-reflectivity soil is much greater than the volume scatter from the vegetation canopy.

We can conclude from this that a SIR-C channel using C-band, HH polarization, and a 20° angle of incidence should see a similar strong dependence on soil moisture for both bare fields and fields planted with agricultural crops. It can also be seen that in order to use SIR-C C-band imagery for soil moisture discrimination, good radiometric fidelity must be achieved both across the swath and from pass to pass. This is because soil moisture experiments will be performed to determine both spatial variability and temporal variability:

1-dB radiometric fidelity required across swath

(1) For these experiments, it will be necessary to determine the variability of soil moisture over the entire area covered by a single pass. For example, if we wish to discriminate soil moisture over 5 discrete levels from wet to saturation (i.e., 20% soil moisture variation in each level), then for vegetated fields this would correspond to about 2 dB per level (see Fig. 4-18). This means that the radiometric fidelity over the image should be at least ± 1 dB rms.

1-dB relative calibration required

(2) For these experiments, we will want to image the same area, say, once per day to determine dry-down rates or other temporal variables. Using the above example of vegetated fields, this would mean that the relative radiometric calibration should be at least ± 1 dB, so that image intensity from day to day can be compared and used with an algorithm, such as that in Fig. 4-18, to determine temporal variation of soil moisture.

The fairly simple cause–effect relationship depicted in Fig. 4-18 makes it appear that we can use SIR-C images to determine an intensity (or $\sigma°$), and from that determine soil moisture, even in the presence of agricultural vegetation. Unfortunately, the situation in Fig. 4-18 does not consider more realistic situations where the radar backscattering coefficient is strongly modulated by local topography or surface roughness. In addition, this curve is limited to the case of agricultural vegetation and does not consider the case of a forest canopy or other vegetation. In order to achieve a more quantitative understanding of these other variables, we need additional data sets.

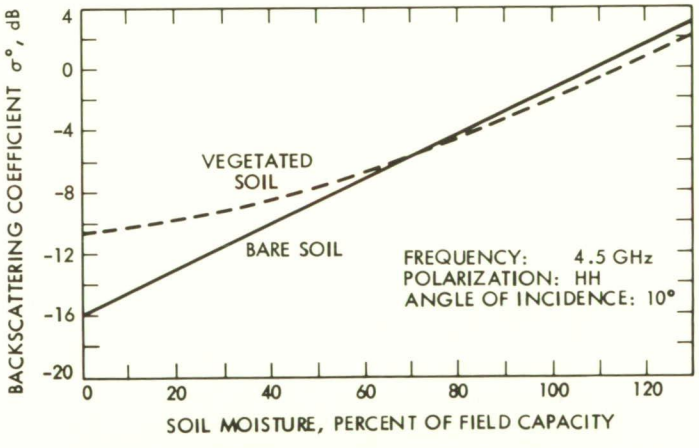

Fig. 4-18. Average dependence of radar backscattering on soil moisture in the top 5 cm measured as percent of field capacity, for both bare soil and soil covered with an agricultural vegetation mix of corn, soybeans, milo, and wheat. These curves are based on data obtained by Ulaby et al. [4-8, Volume II, p. 864] with a C-band HH-polarized radar scatterometer using a 10° angle of incidence; the curves are the means based upon 181 independent samples for the bare soil case, and 143 independent samples for the vegetation case

SIR-C will provide a unique opportunity to understand better the interaction of electromagnetic energy with hydrologic surface features and conditions through multiparameter SAR imagery. This interaction has been difficult to effectively study using the single frequency and polarization of Seasat, SIR-A, and SIR-B, in the sense that there were more unknowns than equations. We need to understand better how radar backscatter depends on the hydrologic scenes in order to make effective quantitative use of these radar images. Therefore, it is important to identify the specific classes of electromagnetic scattering and attenuation geometries for which models are needed. When idealized, these classes of geometries can be mathematically modeled to some degree, as in equation (4-2), and are very useful as guidelines in the interpretation of more complex situations. For these classes, we seek to understand the role of wavelength, polarization, and angle of incidence on the relationship of the radar backscattering coefficient (SAR image intensity) to soil moisture, vegetation cover, surface roughness, slope, and surface cover.

In this sense, there appear to be four broad areas where SIR-C could contribute to a better understanding of electromagnetic interaction:

(1) The effects of overlying vegetation
(2) The effects of surface roughness, slope, and penetration
(3) The effects of soil dielectric constant
(4) The effects of overlying snow packs and ice sheets

4.3.4.1 Overlying Vegetation

SIR-C will allow investigations of

(1) The degree of attenuation introduced by vegetation cover, leading to the masking of the underlying surface
(2) The mechanisms of scattering and re-reflection when vegetation grows in standing water
(3) The density of vegetation as a hydrologic indicator

vegetation as mask of underlying surface

Vegetation cover is a confusion factor when we attempt to measure underlying surface or soil properties. Moreover, there is a wide range of vegetation morphology apparent in scenes of interest to hydrologists. Radars are sensitive to vegetation structure, so that SIR-C will provide an opportunity to investigate the attenuation introduced by vegetation cover, as a function of wavelength, polarization, and angle of incidence.

When there is standing water or saturated soils underlying a plant canopy cover, there can be an enhancement of SAR image intensity due to the re-reflection of volume-scattered radiation from the canopy, as illustrated in Fig. 4-19. Figure 4-20 illustrates this effect as observed in a black-and-white Seasat image of a wetland region near Trinity River, Texas. The bright area surrounding the water body is due to re-reflection from understory water. This is not seen in the color image, which is an infrared aerial photograph taken at the same time. We need to use SIR-C to better understand the influence of vegetation morphology on the polarization-dependence of radar returns at long (L-band), medium (C-band), and, potentially, short (X-band) wavelengths, in these wetland regions.

vegetation as hydrologic indicator

The occurrence and type of vegetation, and its location is used as an important hydrologic indicator, especially in wetland areas. SIR-C will permit studies of the extent to which vegetation density and species can be distinguished for wetland classification purposes.

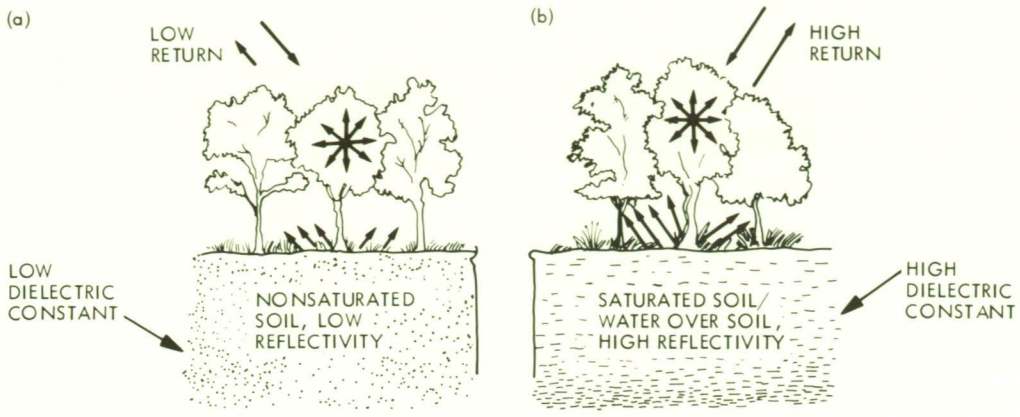

Fig. 4-19. Surface reflectivity. With dry soil (a) the surface reflectivity is low, there is little surface re-reflection of volume-scattered radiation from the canopy, and returns are low. When (b) there is standing water or saturated soil under the canopy, there is considerable re-reflection and net returns are high

4.3.4.2 Surface Roughness, Slope, and Penetration

possible surface effects

At SIR-C wavelengths, measurements of surface backscatter will be sensitive to a wide range of roughness scales from a few centimeters (small-scale roughness) to tens of meters (large-scale relief). This presents an opportunity to study the dependence of SAR imagery on

(1) Small-scale roughness
(2) Large-scale topographic relief
(3) Surface penetration

The identification and separability of small-scale surface roughness in radar images is important to the classification of runoff potential for watersheds. In addition, surface roughness can be a serious confusion factor when attempting to extract soil moisture information from radar measurements. SIR-C presents an opportunity to improve our understanding of how well radar imagery can be used to discriminate categories of surface roughness that are relevant to hydrologic classification, as well as our understanding of the relationship between surface roughness and cross-polarized backscatter.

Many watersheds lie in regions of large-scale topographic relief. Mountainous features with large-scale topographic relief strongly modulate the intensity of the radar image and may also introduce a geometric distortion known as layover, especially at near-nadir angles of incidence. This complicates the task of extracting local surface features (e.g., soil moisture) on mountainous slopes. An important problem is how to remove or minimize topographic effects from radar imagery in order to measure surface soil moisture features in mountainous regions.

It is well known that microwave wavelengths penetrate very dry soil to some degree. However, direct evidence in image form of this penetration and subsurface interaction was not demonstrated until the SIR-A pass over the Eastern Sahara. Those images demonstrated penetration of 1–3 m into the sand as well as evidence of volume scattering from subsurface calcium carbonate (caliche) nodules and other scatterers. SIR-C will provide an opportunity to replicate this experiment at a wavelength of 23 cm and at 6 cm as well. This

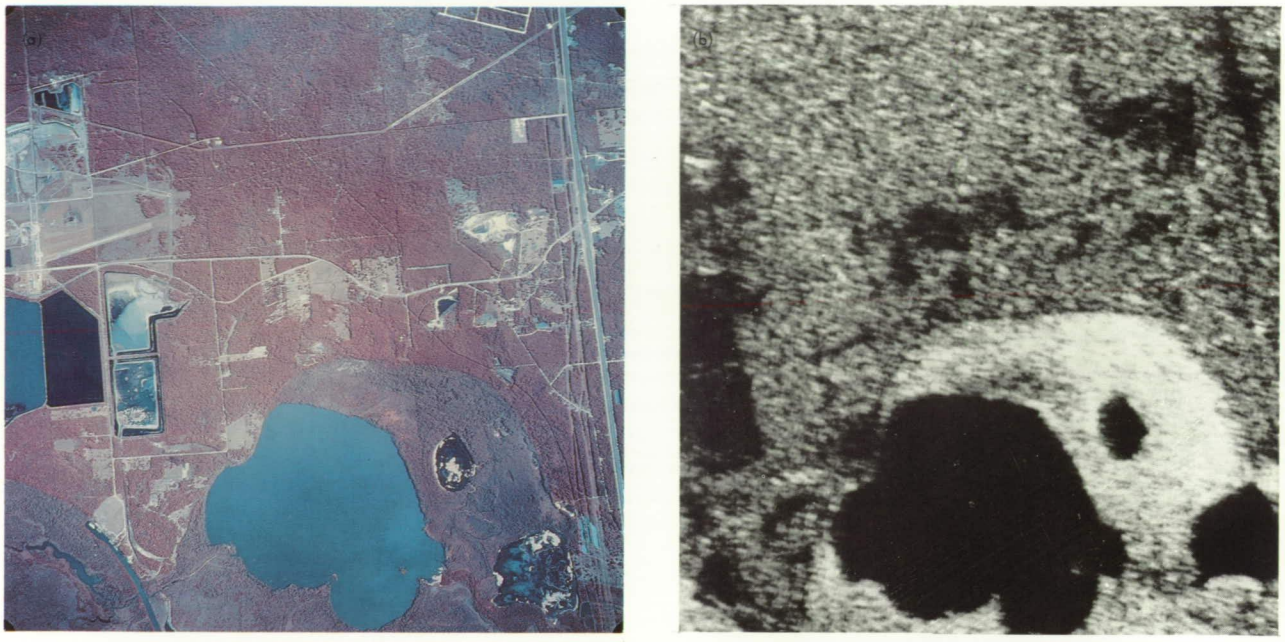

Fig. 4-20. The re-reflection effect. The Seasat image (a) of a wetlands region near Trinity River, Texas, shows a bright area surrounding the body of water. This area is due to re-reflection from understory water. The bright area is not visible in the infrared aerial photograph (b), which was taken at the same time.

should allow an estimate of the attenuation constant, thereby providing the ability to predict the depth of penetration at even lower frequencies, e.g., P-band (70 cm).

4.3.4.3 Soil Dielectric Constant

soil conditions of interest

SIR-C will permit detailed studies of the dependence of the radar backscattering coefficient on the soil dielectric constant in the presence of confusion factors such as slope, surface roughness, and vegetation. There are four soil conditions of particular interest:

(1) The low dielectric constant (approximately 2 to 3), such as obtained in arid or hyperarid regions
(2) Medium-to-high dielectric constant soils
(3) Snow or ice overlying soil
(4) Permafrost

The low soil dielectric constant associated with very dry soils leads to enhanced penetration at longer wavelengths. SIR-C will permit studies of not only the attenuation constant (see discussion above), but also the effect of subsurface random volume scatterers on the polarization characteristics of the return. This may allow some discrimination of subsurface scattering types.

Soils in humid-region watersheds have moderate-to-high dielectric constants because of the elevated soil moisture levels. SIR-C will provide the opportunity to study the response of radar backscatter to a range of soil moisture conditions for different wavelengths and polarizations. For example, SIR-C will provide the opportunity to study the relative sensitivity of cross-polarized backscatter compared to like-polarized backscatter for different surface roughnesses, as well as the water-holding capacity of soils. This capacity depends on soil texture, soil density, organic matter content, and other parameters, all of which can be expected to modulate partially the radar image intensity.

permafrost characteristics

There is little information available on the dependence of the radar backscattering coefficient on permafrost, which is composed of soil or other surficial deposits that have been at a temperature below freezing continuously over a long period of time (from two years to tens of thousands of years). Permafrost depths range from more than 3000 feet in the Arctic to as little as 1 foot over 20% of the earth's land area outside the Arctic. SIR-C may allow the establishment of radar signatures for permafrost as a function of frequency, polarization, and angle of incidence. Moreover, it may be possible to determine the effects of overlying soil conditions on permafrost signature where the permafrost does not extend to the surface.

4.3.4.4 Snow

snow parameters

Snow packs and ice sheets overlying soil are of considerable interest to hydrologists. Of particular value are three parameters:

(1) Snow pack extent
(2) Snow wetness
(3) Snow–water equivalent

In the microwave spectrum, a snow layer causes both attenuation and scattering of signals, especially at millimeter wavelengths. The microwave response to snow increases dramatically as the frequency is increased above about 10 GHz, and this is the case for both the active and the passive response.

By using ground-based scatterometers mounted on a truck boom, Ulaby and Stiles [4-9] have been able to quantify the radar response to snow. Figure 4-21 shows that the measured radar scattering coefficient of a 48-cm-deep snow layer as a function of frequency for both dry snow (0% moisture by volume) and wet snow (1.26% moisture by volume) is less than 1 dB at L-band but increases to about 4 dB at C-band and X-band. Moreover, the radar backscattering coefficient σ° increases with frequency and as the snowpack becomes dryer. This indicates that at C-band and X-band, a diurnal variation in snow wetness of only about 1% should be clearly visible in SAR imagery for snowpacks of about 40 cm depth or greater.

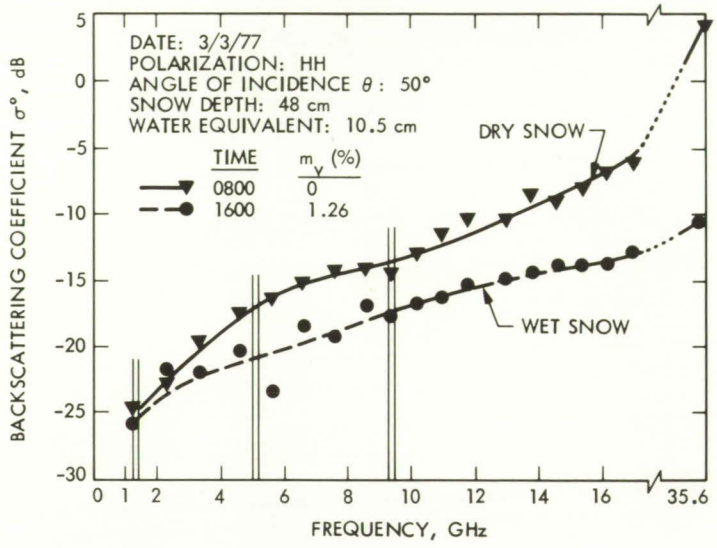

Fig. 4-21. Spectral response of σ^0 for wet and dry snow (from Ulaby and Stiles, 1980 [4-9])

frequencies C-band or higher needed for snow

The calculated dependence of σ°, at various frequencies, on the depth of a dry snow layer containing 2-mm-diameter ice particles is shown in Fig. 4-22. This is again for an HH-polarized radar using a 50° angle of incidence. It is apparent that there is no sensitivity to snow depth at L-band (1.2 GHz) and that even at C-band (5.0 GHz) a 1-m-deep snow layer produces only a 2-dB increase in σ° over the background soil (assumed here to have a dielectric constant of 5 and an rms surface roughness of about 1 cm). However, at X-band, a 1-m-deep snow layer produces an 8-dB increase of σ° over the background soil.

These measurements and calculations suggest that in SIR-C imagery, snowpacks will be essentially invisible at L-band, marginally visible at C-band, and quite visible at X-band.

	ICE LOSS FACTOR	SOIL SURFACE PARAMETERS				SNOW PARAMETERS	
f (GHz)	ϵ_i''	$k\ell$	kL	$k\sigma$	m	ALBEDO a	K_e ($Np\ m^{-3}$)
1.2	0.001	0.1	3	0.3	-	0.01	0.003
5.0	0.002	0.7	13	13.0	-	0.33	0.035
10.0	0.005	1.4	20	20.0	-	0.68	0.270
17.0	0.008	-	-	-	0.27	0.85	1.790
35.0	0.020	-	-	-	0.27	0.95	28.800

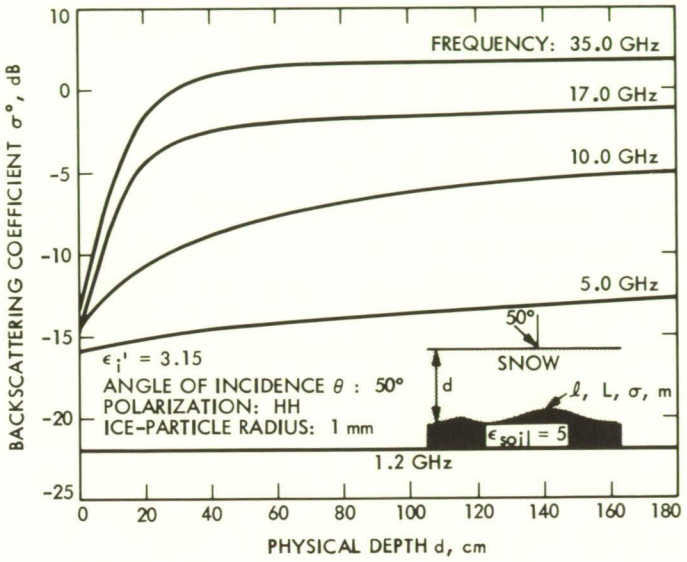

Fig. 4-22. Calculated variation of σ^0_{HH} with depth for a dry snow layer containing ice particles 1 mm in radius. Note the important role of frequency. (After Ulaby et al. [4-5, Volume II])

4.3.5 SIR-C Hydrology Experiments

hydrologic experiment objectives

SIR-C presents the opportunity to conduct hydrology experiments at two levels: the first level concerns traditional hydrologic research objectives in the various regimes, and the second an improvement of electromagnetic models applicable to hydrologic research using microwave sensors. The latter experiments and their scientific basis were discussed in the previous section. The primary hydrologic research objective of SIR-C, however, is to determine its sensitivity to soil moisture, vegetation cover, surface roughness, slopes, and snow or ice cover. The following discussion of the SIR-C experiments is organized by hydrologic regime. These experiments, summarized in Table 4-3, are included for illustrative purposes only and are not intended to be either complete or sufficient.

4.3.5.1 Arid Regimes

hyperarid regions

The SIR-A mission has demonstrated that, in at least one major arid region (the Eastern Sahara), 23-cm-wavelength radar signals refract into and backscatter from within a meter or so of very dry sand and alluvium. SIR-A images of this region revealed unmapped

Table 4-3. Some SIR-C hydrology experiment classes

Experiment Class	Scientific Objectives
Surface penetration in hyperarid regions	Delineation of subsurface hydrologic features in buried pluvials
Semiarid-region soil moisture	Temporal and spatial variation in semiarid soil moisture
Spatial variability and scale in hydrologic systems	Spatial variability of hydrologic parameters; scale of hydrologic units; development of criteria for hydrologic uniformity
SAR image sensitivity to precipitation	Direct measurement of precipitation
SAR image sensitivity to hydrologic characteristics	Area information for characterizing watershed hydrology: temporal changes in soil moisture
SAR image sensitivity to flooding	Flood extent and duration
Groundwater resource analysis	Identification of groundwater recharge and discharge areas
Wetland boundary delineation	Definition of understory landwater boundaries
Wetland vegetation discrimination	Identification of broad classes of vegetation in wetland settings
Snow extent and characteristics	Snowpack extent, snow water equivalent, and snowpack ripeness; snow runoff potential
Glacier discrimination	Distribution of morainal material, crevasse patterns, and ice surface roughness
Permafrost	Permafrost boundaries

bedrock features as well as sand-buried networks of previously unknown stream deposits dating from the Middle Tertiary to the Late Pleistocene. Subsequent evidence for radar-signal penetration up to a meter in the semiarid and arid Mohave Desert in California was described by Blom et al. [4-10], from an analysis of Seasat images of alluvium-buried igneous dikes. Elachi, Roth, and Schaber [4-7], using a simple backscatter model, have recently shown that the presence of a low-loss completely dry sand layer refracts the incident wave and actually enhances the capability of the radar to image the subsurface, particularly at moderate angles of incidence (e.g., the 50° of SIR-A) and with HH polarization. Theoretically, HH polarization offers a factor of 2 to 3 times greater sensitivity than VV polarization for detecting a dielectric layer below about 1 m of dry sand, in such hyperarid terrains. The general behavior of wave penetration and subsurface scattering in hyperarid zones is suggested by Fig. 4-23.

Given the demonstrated successes of penetration experiments using SIR-A, Seasat, and SIR-B, the SIR-C SWG recommends that one broad category of SIR-C hydrology experiments in desert regions focus on the depth of penetration at L-band, C-band, and for all polarizations (HH, VV, and HV). This may provide geomorphologic and geologic evidence indicating the possible availability of groundwater at economically recoverable depths, and will certainly add to our understanding of the attenuation and scattering introduced by these eolian and alluvial materials. However, given the widespread publicity of the successful SIR-A results from the Eastern Sahara, the SWG also wishes to emphasize strongly that the physical, chemical, and climatic conditions required for maximum signal penetration are stringent and that such conditions are likely to exist only within arid regions. The Eastern Sahara is perfectly suited to optimum radar signal penetration, being extremely dry, unconsolidated, and containing very small amounts of clay minerals that are known to severely limit signal penetration [4-11]. To help to set reasonable limits on regions proposed for desert penetration experiments for SIR-C, this plan provides a map of the semiarid, arid, and extremely arid regions of the world (Fig. 4-16). This map, however, does not show the nearly 5 million km^2 of polar deserts, which constitute over 3% of the earth's land area. Parts of the polar deserts may also be candidates for radar penetration. Penetration experiments restricted to the arid and extremely arid regions should have the greatest potential for success, but of course will depend on the lack of surface roughness, the degree of aridity, and physical, electrical, and chemical properties.

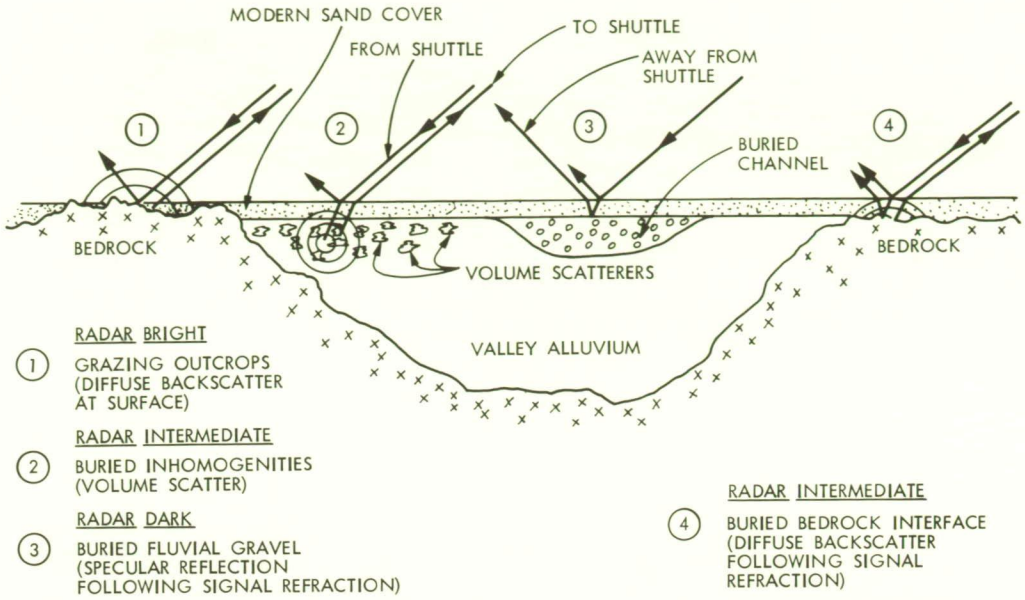

Fig. 4-23. Penetration into dry sand covering ancient river beds. Subsurface scattering is introduced by hard-pan and volume scattering by calcium carbonate nodules

semiarid regions

A second important category of SIR-C desert hydrology experiments would take full advantage of the "mapping mode." In this mapping mode, effective swath widths in excess of 150 km could be obtained from multiple passes. This would be particularly useful for studies of not only hyperarid regions, but also semiarid regions (see Fig. 4-16). Maximum areal coverage would require the lowest possible angle of incidence and would emphasize the like-polarization (HH and VV) and possibly degraded resolution in favor of more swath. Such mapping-mode experiments would provide synoptic overviews from which regional assessments of hydrologic potential could be made. These SIR-C mosaics could be more easily compared to Landsat TM and similar data.

possible rain events in semiarid regions

SIR-C experiments in the semiarid environment may be difficult to plan and conduct because of their dependency on climatic events, which are usually infrequent. However, the pointing ability of SIR-C instruments will make it possible to conduct some studies if the Shuttle crew can respond to short-notice (24-hour) data-collection requests. The most important of these studies would involve the spatial distribution of rainfall. The location of this experiment could not be planned in precise detail. Rather, the Shuttle and ground data crews would have to respond to synoptic weather observations, to approximately locate the convective rain cells. Rapid turnaround of SAR imagery would increase the chances of success because the ground data crews could be guided to areas where rain had fallen by the apparent soil moisture differences from the imagery.

Range-condition experiments could be conducted within a Shuttle mission time frame. Sites of good and poor range condition could be identified before the flight and detailed ground data-collection programs could be conducted. The questions of interest for the SAR would be related to soil moisture, soil cover, and erosion. Poor-condition rangeland typically would have lower soil moisture, less-dense canopy of more woody vegetation, and an erosion-induced rougher surface. Good rangeland features would be the opposite. Multifrequency–multipolarization studies would be possible from successive orbital passes because we could generally expect little temporal change over the duration of the Shuttle mission.

Various semi-arid regions throughout the world have recently been selected as test sites in the International Satellite Land Climatology Project (ISLSCP). Objectives of the ISLSCP include the development of methodologies for obtaining quantitative land–surface climatological data from satellite observations. A SIR–C radar system would contribute significantly to a better understanding of the hydrologic processes by aiding in quantifying some of the physical surface parameters required in modeling the moisture and energy fluxes. Active radar measurements may complement existing satellite microwave radiometer data, which are currently being evaluated in surface wetness investigations under the ISLSCP Retrospective Analysis Program (IRAP).

4.3.5.2 Humid Regimes

Humid-area hydrology presents scientists with a set of problems that, although not necessarily unique to humid areas, are intensified there. Perhaps the most important of these is the spatial variability of most factors that affect a basin's hydrology and water balance. These factors include topographic features, both micro and macro, as well as soil properties and soil moisture, drainage patterns, land use, and subsurface features.

A second major factor that affects humid-basin hydrology and that has been difficult to represent scientifically is the temporal effect of climate, both short-term (minutes and hours) and long-term (seasons). This temporal factor is complicated by the spatial variability of inputs, such as precipitation or potential evapotranspiration, and, in turn, their results, such as soil moisture or snow packs.

Although much of the current research effort in hydrology is focused on these spatial and temporal questions, no dramatic breakthroughs have occurred. The characteristics of the multifrequency, multipolarization SIR-C instrumentation could provide some of the information needed to advance our understanding in these areas. The following experiment descriptions provide examples of important hydrologic issues relevant to SIR-C radar measurements.

spatial variability and scale in hydrologic systems

There is a need to develop ways to measure the spatial variability of hydrologic parameters and variables, to determine the scale (size) of important hydrologic units, and to develop criteria for delineating areas that can be treated as hydrologically uniform. Partial-area hydrology is a hydrologic concept that has been formulated to account for spatial variability in watersheds. This concept is based on a dynamic watershed approach in which the sizes of subareas in a basin that produces runoff have dimensions that vary in time and space, subject to soil infiltration capacity as well as to storm duration and intensity. The source-area concept, on the other hand, is an attempt to account for the heterogeneous nature of natural watershed systems.

The research questions dealing with spatial variability and scale can best be studied with a series of coordinated ground, truck, aircraft, and Shuttle experiments involving selected test sites. Detailed ground measurements at these sites will define the spatial variability of the hydrologic characteristics selected for study. The characteristics selected will be those that depict decreasing (degraded) resolution, but that at the same time average or integrate the point measurements into a single response for sequentially larger areas. One or more distributed hydrologic simulation models will be used to take these data as inputs, and the simulated results will be compared to each other and to measured watershed responses. These comparisons will be the basis for evaluating the hydrologic significance of spatial variability, and the scale of the important hydrologic parameters and variables.

The SIR-C experiments should concentrate on the two layers of the earth's surface described in 4.3.4. The problems of scientific interest involve measuring spatial changes in the dielectric constant and measuring the nature (geometry) and biomass of the crop canopy. A single Shuttle flight is too short to ensure observing significant temporal changes in the target. However, two SIR-C flights scheduled approximately 6 months apart could be ideal for observing temporal changes resulting from seasonal effects. These studies should help determine the spatial distribution of the two surface layers and aid in studying the effects of topography (effectively incidence angle) on radar response. To account for topography and other unknowns, relative differences between SIR-C images acquired within one mission must be examined. Moreover, this should be done during both SIR-C missions, with one timed for wet-season coverage and the other for dry-season coverage.

Runoff prediction is generally the single most important factor affecting water-resource decisions (e.g., flow controls, drainage design, water supply, hydropower, etc). Almost without exception, precipitation data are not adequate for accurate runoff predictions because the available rain gauges do not depict the spatial distribution of rainfall over large basins. Therefore, more accurate and timely precipitation measurements, especially in areas with few gauges, could prove highly beneficial. Radar has the potential for making real-time estimates of both precipitation distribution and intensity.

radar sensitivity to soil moisture after rain events

The unpredictability of where and when rainfall will occur makes research in this area difficult to plan and conduct within the Shuttle flight duration of 7 to 10 days. However, this difficulty could be overcome if Shuttle data-collection activities were sufficiently flexible for measurements to be directed by ground observers. Depending on the dates of the Shuttle flights, some windows on the earth could be identified where there would be a good probability of significant (greater than 2-cm) rainfall at some point during the flight. Such experiments would require good weather forecasts and precise coordination between ground observers and the Shuttle crew. It would then be possible to examine time series of the drying of near-surface soil after saturation, which may be related to bulk soil hydraulic properties.

correlation of SIR-C images with rain-gauge data

A coordinated series of aircraft SAR and SIR-C tests should be designed to observe the radar response from rainfall as it is occurring and to measure the spatial distribution and amounts of rainfall after the rain has ceased. These tests should be designed to demonstrate that SIR-C images can be correlated with rain-gauge data and to determine whether imagery can be effectively used to interpolate between rain gauges for improved precipitation estimation. See the section on semiarid hydrology for additional possibilities.

direct measurement of hydrologic characteristics

The ability of remote sensing to take measurements over an entire area rather than at a single point and to average the measurements' information for that area may lead to entirely new and powerful ways to characterize a watershed's hydrology.

The ability of microwave energy to penetrate vegetation (the degree of penetration depending on frequency, polarization, and angle) and to respond to soil structure, surface roughness, and soil moisture are perhaps the most important features for hydrologic applications. These are the four watershed features that affect rainfall runoff and historically have been used as input parameters for runoff models. However, in the existing hydrologic procedures, these features are seldom measured directly, but are estimated according to arbitrary relative scales. The ability to measure the features directly could be a significant breakthrough for improving hydrologic techniques. If successful, this procedure could provide an objective and cost-effective method for obtaining input data for operational hydrologic models.

Experiments of this nature could be conducted over a site where extensive ground data collection is feasible. Concurrent ground and Shuttle data collection would not be critical, and temporal changes would not be of major importance. Multiple angle, polarization, and frequency observations of the same site would be necessary. A one- to two-day revisit schedule would be necessary.

flood mapping

Radar imagery is useful for monitoring the extent of floods and their duration, even under forested conditions, as can be seen in the SIR-B image of the coast of Equador shown in Fig. 4-24. Experiments can be designed to study SAR response to land–water boundaries and to flooding where total inundation has not occurred (i.e., islands), and SIR-C experiments can define the optimum frequencies, angles of incidence, and polarizations needed for delineating land–water boundaries through crop canopies of various densities and geometries. These objectives are similar to the research needs for studying wetlands, and well-designed experiments should satisfy both needs.

groundwater resource analysis

It may be possible to conduct groundwater resource experiments using SIR-C. The objectives of such an experiment would be to identify groundwater recharge and discharge areas in complex watersheds and to develop methods for conducting a resource inventory of groundwater by identifying seeps and springs and quantifying seasonal changes of groundwater elevation.

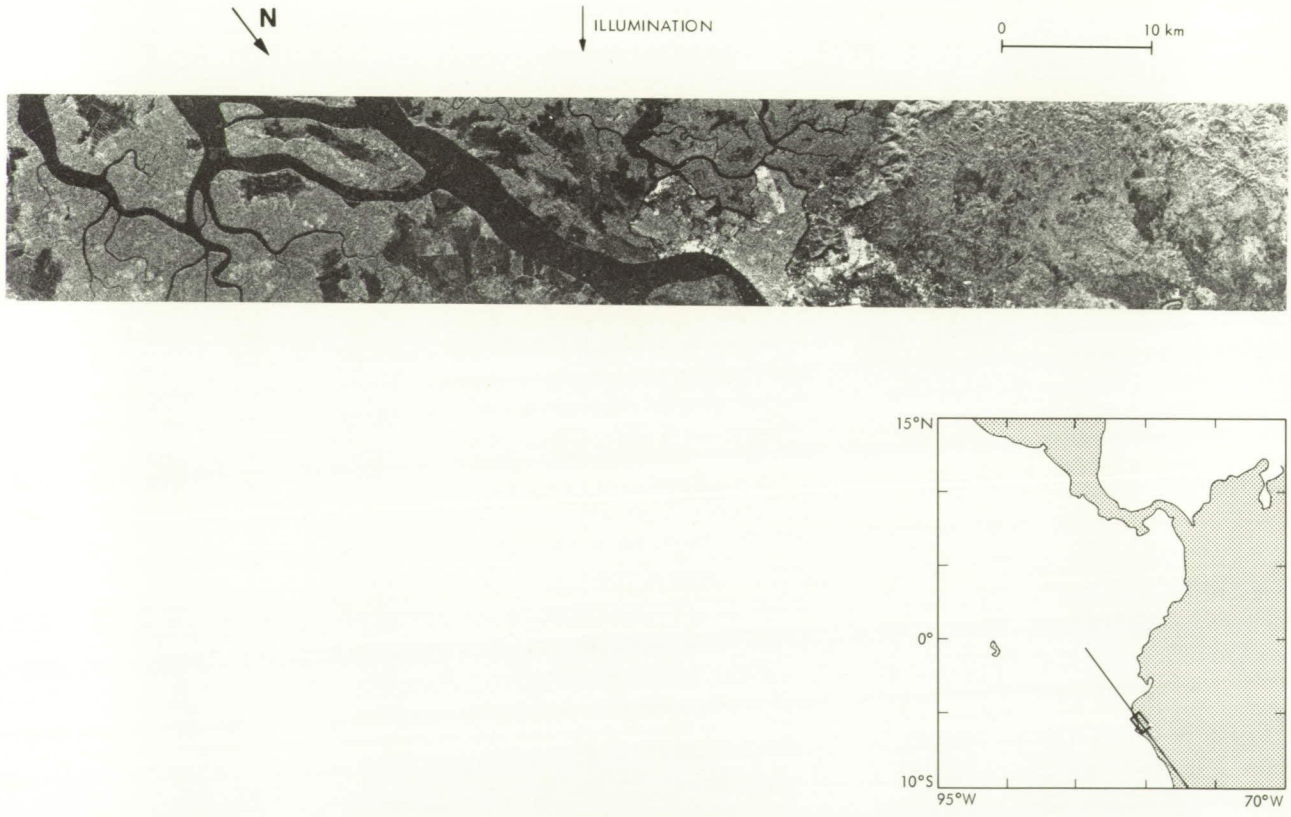

Fig. 4-24. SIR-B image of flooded forest in coastal Ecuador

Identifying groundwater recharge and discharge areas is a major aspect of any land-management program and is important to meeting certain surface-water and groundwater pollution-control objectives. Conventional methods of groundwater assessment are time consuming and costly, and any procedure that could do it more efficiently would be extremely helpful. Groundwater discharge areas often respond to seasonal differences in precipitation and evapotranspiration, and the two-flight SIR-C should provide a basis for observing spatial changes in groundwater discharge and recharge areas resulting from seasonal differences in soil moisture and surface water.

4.3.5.3 Wetlands

Because trace-gas fluxes in wetlands form a major component of the global biogeochemical cycles, wetlands are among the most important of the world's ecosystems. The role that wetlands play as filters, or sinks, for a wide variety of pollutants is well-known; wetlands act as extremely effective buffers for nearby, less resilient ecosystems (e.g., estuaries). Although limited in area compared with the major ecosystems of the world, coastal wetlands have a high per-unit-area productivity and contribute substantially to estuarine productivity as well. Wetlands are extremely vulnerable to alteration by humans. Drainage to expand urban areas or produce useable land for agriculture or forestry can drastically affect biogeochemical cycles and estuarine productivity and pollution levels. A rise in sea level, postulated as a result of global increases in atmospheric carbon dioxide, could result in a substantial loss of coastal wetlands. Changes in rivers (e.g., channelization, increases or decreases in sediment load, or alterations in flow volume or pattern) could also substantially affect wetland extent and processes. If wetlands are to be properly used and protected, it is important that they be effectively mapped and their status monitored. An accepted approach uses color infrared (CIR) photography for analysis, which is a reasonable method for determining relative biomass and for overall species discrimination. CIR imagery cannot, however, define the land–water interface in densely vegetated shoreline areas. Nor can it reliably locate boundaries between the various wetland "water regimes," i.e., soil saturation levels. SIR-C multiparameter imagery used either alone or in conjunction with photography or multispectral scanner imagery in the visible and near-IR wavelengths should be able to overcome these significant gaps in effective wetland-mapping analysis.

wetland boundary delineation

One significant problem in mapping wetlands is simply defining where they begin and end. A wetland lying hard against a water body is easy to delineate if the vegetation stops at the water's edge, but not if the vegetation continues into the water. However, a plant-obscured boundary should be definable by longer-wavelength radar energy, which penetrates the vegetation and is either reflected off the water's surface or backscattered strongly from the usually moist substrate near the water's edge. The L-band channel of SIR-C (23-cm wavelength) will penetrate wetland grasses and shrubs, but areas of larger wetland tree species will probably show stronger returns in the images. The C-band channel should behave similarly, except that even smaller flooded trees will cause significant image brightness. It would be desirable to determine the optimum wavelength and polarization for shoreline delineation in areas of various vegetation densities and stem sizes. This shoreline delineation is dramatically illustrated in the SIR-B image of Florida wetlands in Fig. 4-25.

A problem similar to shoreline delineation is that of defining the upland boundary of a wetland. A transect across a typical estuarine wetland would pass from the water to the saturated-soil wetlands that are inundated daily, then to the wetlands inundated less than

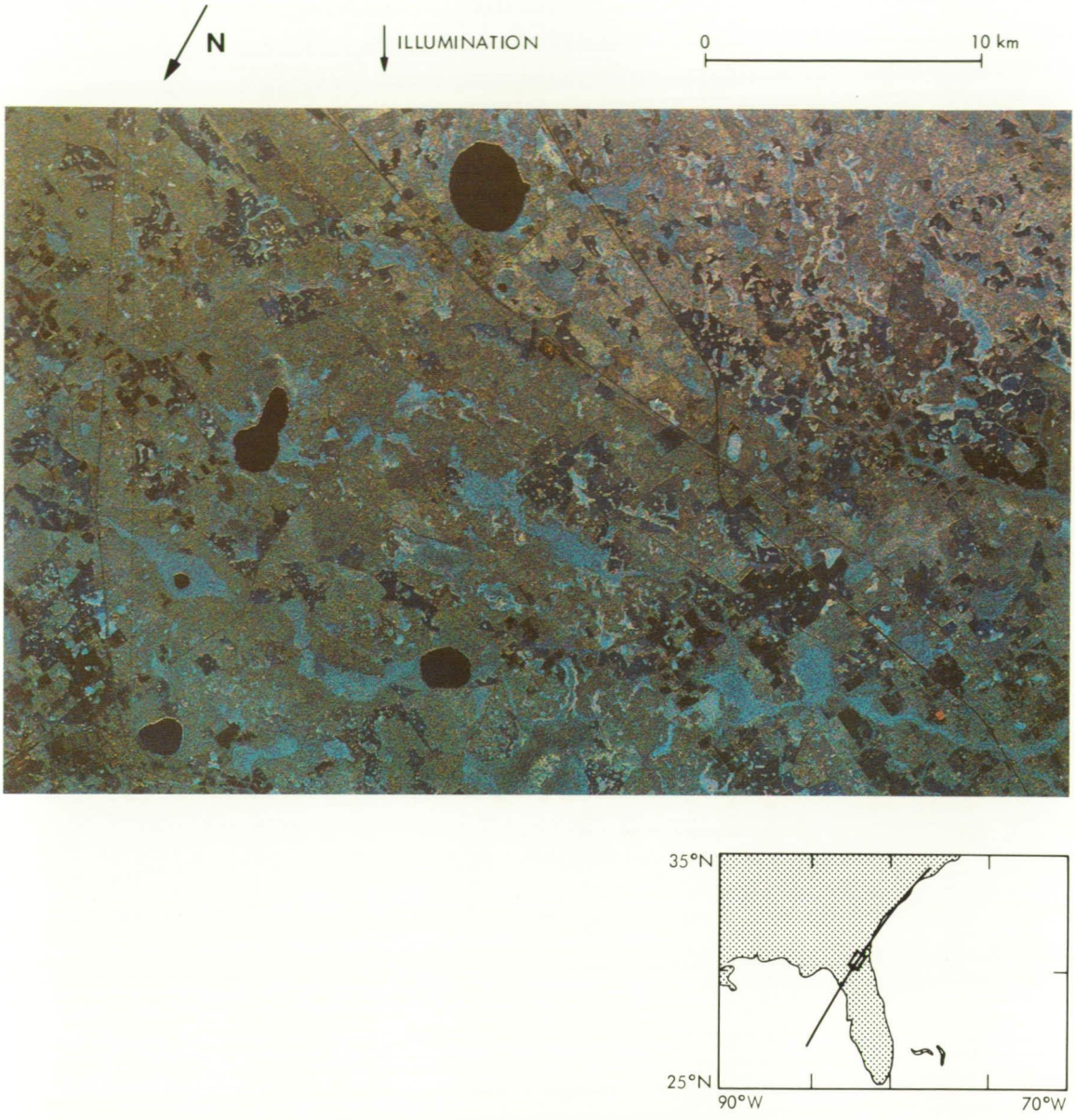

Fig. 4-25. SIR-B image of Florida wetlands

daily (which may or may not have saturated soils) then to the areas that are irregularly flooded and only seasonally have saturated soils, and finally to the uplands. These transition zones normally cannot be delimited on color infrared photography or on equivalent multispectral scanner imagery. However, it may be possible to see these transitions in SIR-C imagery, depending on how well longer-wavelength radar can portray differences in soil-moisture areas covered by vegetation. Besides determining optimum wavelengths and polarizations, we need to determine to what extent specific wetland water regimes can be defined in the imagery.

The water regime is a key factor for biogeochemical cycling in wetlands. Major fluxes of trace gases, such as methane, occur only under reducing conditions in the soil. Reducing conditions are created when soils are covered by water, which prevents oxygen from

entering the soil matrix; thus, the duration and extent of inundation controls the amount of trace-gases released into the atmosphere. Despite their small areal extent, wetlands can contribute to the atmosphere a major proportion of the terrestrial trace-gas flux. Coupling of ground measurements with remotely sensed information on the spatial extent and the temporal dynamics of flooding could yield significantly improved estimates of regional trace-gas fluxes to the atmosphere.

The water regime also influences wetland and estuarine productivity. As water flows over a vegetated surface, it brings a fresh supply of nutrients to the plants. Wetlands more frequently inundated are often more productive. Water flowing out of a wetland area removes organic detritus, which then serves as the basis for secondary productivity in riverine and estuarine ecosystems.

It may not be sufficient to determine the upper and lower boundaries of wetlands; it may also be necessary to determine the patterns of inundation within the wetlands. The spatial resolution of SIR-C should be adequate for the investigation of coarse-scale patterns of flooding. Fine-scale distributary channels may not be discriminable.

Determination of water regime is of extreme importance because of its influence on trace-gas fluxes, vegetation type, and productivity in wetlands. This information could also be useful in settling disputes over public versus private ownership of land.

vegetation discrimination

From a wetlands-analysis standpoint, it would be desirable for SIR-C to include X-band imaging radar to augment the L- and C-band imagery. Earlier investigations have shown that X-band can discriminate broad classes of vegetation in wetland settings and that when X-band is augmented by L-band, discrimination is further improved. The major advantage of L- and C-band imagery of wetlands is complete-to-partial penetration through the vegetation to the moist soil underneath. While it is desirable to know which of these two wavelengths is better for measuring relative soil saturation in wetlands of different vegetation density and species makeup, it would be even more beneficial to determine which frequency and polarization combination (among X, L, and C) would be best for discriminating vegetation types.

An example of the type of wetlands site that might be studied is the estuarine system lying near Galveston, Texas, which contains low-lying estuarine wetlands that are perennially saturated. The barrier systems contain palustrine wetlands (dune swales) as well as a variety of estuarine wetland classes. The area of the Trinity River, which empties into the Galveston estuarine system, includes riverine and lacustrine systems, and also forested wetlands standing in relict oxbows. This area encompasses many pristine and modified wetland systems: the Gulf Intercoastal Waterway cuts completely through the area and portions of the lower Trinity have been severely channelized. There is a great variety of wetland vegetation species and wetland habitat classes. This wetland system has been classified and mapped recently as a part of the U.S. Fish and Wildlife Service's National Wetlands Inventory.

4.3.5.4 Snow-Covered Watersheds

In many areas of the world, the majority of fresh water available for consumption and irrigation results from snowmelt runoff. Snowpacks providing domestic water supplies are found in varying settings; many are in rugged mountainous terrain, while others are in

higher-latitude moderate-relief plains areas. Determination of available water in the snowpack just prior to melt season is important for the proper management of river impoundments and for reservoir regulation. SARs operating at shorter wavelengths offer an all-weather capability to regularly monitor changes within the snow and provide useful information to water managers. There are three snowpack measurements of interest:

(1) Areal extent
(2) Snow–water equivalent
(3) Condition of the snowpack

Each has a specific set of parameters that affect the microwave signal and that vary during the snowmelt season. These parameters include moisture in the underlying soil, whether the soil is frozen or unfrozen, vegetation under the snowpack, whether the plains are forested, and varying topographic relief. These parameters principally affect the radar scattering coefficient, which can exhibit significant temporal changes during the melt season.

The microwave response, both active and passive, to snow–water equivalent and liquid-water content increases as the frequency is increased above 10 GHz. By using truck cherry-picker-borne radiometers and scatterometers, Ulaby and Stiles [4-9] have been able to quantify the radar and radiometer response to snow. Figure 4-21 shows the radar scattering coefficient as a function of frequency for various levels of snow–water equivalent. This indicates that we may expect some C-band sensitivity to snow, at least for thicker and wetter packs, but that for this purpose the X-band channel is even better.

For the SIR-C mission it is desirable to have a polar orbit available in late winter through spring, since otherwise the snow cover and thickness may be insufficient for observation. Changes in the snowpack would certainly be observable at X-band, and to a lesser extent at C-band. Other microwave data, however, such as from the L-band channel, or from ancillary ground or aircraft microwave radiometer data at selected test sites, would act synergistically to provide a more complete analysis of snowpack conditions. The effect of frequency and polarization dependence could also be addressed.

Snow hydrology problems suitable for study with SIR-C data would include the detailed measurement of snow-cover area (i.e., the delineation of snow–nonsnow boundaries), the measurement of changes in snow properties (wetness, water-content, grain size) with elevation and aspect, and the measurement of snow properties through vegetation (forest) canopies. These experiments could be carried out during a Shuttle mission of 7 to 10 days by selecting a study site with the kind of aspect and elevation variations that would provide differences in snowpack properties. The effects of topography on radar response (i.e., the effects of slope and aspect, both of which can cause the angle of incidence to vary) is a major research question that must be answered before operational snow-monitoring sensors can be considered.

4.3.5.5 High-Latitude Regions

glaciers

SIR-C provides an excellent opportunity to expand our limited knowledge about SAR remote sensing of glaciers. A further discussion of this potential is presented in Section 4.5.5.3.

permafrost

Figure 4-1 shows the distribution of different types of permafrost terrain in the Northern Hemisphere. Little quantitative information is available on microwave response to permafrost, so it is difficult to predict what the SIR-C response to permafrost features will be. However, there are several permafrost features of interest, including its depth; the effects of the overlying soil, whether saturated (coastal) or unsaturated (inland); and the effect of changes in terrain and vegetation.

Assessment of these features and their effects on the radar signatures will be difficult, if possible at all. Permafrost should be viewed as a target of opportunity. Data will be required at different times during the year, to separate the effects of changing surface vegetation. Variations in terrain, soils, and geomorphology will necessitate the selection of several test sites at coastal and inland regions. Previously collected Seasat SAR data will provide a basis for the formulation of the required studies, which will include consideration of the permafrost signature as related to different frequencies (L- and C-, and possibly X-band), polarizations, and viewing angles.

4.3.6 Summary of SIR-C Mission Requirements for Hydrology

It is clear that most SIR-C hydrologic research investigations will require plans that carefully coordinate SIR-C observations with *in-situ* field observations of a limited number of well-selected sites. Because of the wide diversity of hydrologic regimes, there is no common set of SIR-C mission parameters that is optimum for all hydrologic research topics. However, there are unifying themes. For example, all areas require radar parameters that maximize sensitivity to soil moisture, e.g., longer wavelengths and near-nadir angles of incidence. Vegetational investigations, e.g., in humid and wetland regions, will seek to use shorter wavelengths and diverse polarization. This section attempts to summarize the principal SIR-C mission requirements for the majority of the hydrology experiments.

4.3.6.1 Orbital Parameters

high-latitude orbit requirement

A high-inclination orbit is required for observations of high-latitude hydrologic regimes, including permafrost, glaciers, and snow-covered watersheds. A drifting orbit, which would allow wide-area coverage (mapping mode) at near-nadir angles of incidence (for soil moisture) is best for arid-region studies. However, orbits providing a revisit cycle of 1 to 2 days are preferred for humid regions and wetland studies. Many of these experiments will require a comparison of repeat-coverage images.

4.3.6.2 Mission Timing

two-flight requirement

The most desirable mission timing is that which would provide continuous observations of the earth from space, thus allowing studies of temporal variability in various hydrologic regimes. Since this is not possible with SIR-C, the next-best timing requires two Shuttle flights separated by about six months, using the same orbit inclination and launch times, so that the mission ground tracks will coincide. The scientific benefit would depend, of course, on when during the hydrologic year the flights occurred.

There are also a number of important hydrology research opportunities that are afforded by a Shuttle flight of 7 to 10 days. These studies would focus principally on optimum instrument response (wavelenghts, polarizations, and illumination geometries) for target characteristics such as soil moisture, vegetation canopy interaction, surface roughness, topography, and snow or ice cover. Carefully chosen target areas may allow these characteristics to be experimentally controlled by changing soil moisture through irrigation, by changing surface roughness through tillage, and by the removal of vegetation canopies.

4.3.6.3 Swaths, Resolutions

The swath width required depends on hydrologic regime. Wide swaths of 100 to 200 km, built up through several contiguous passes, would be required for studying hyperarid-region geohydrology, glaciers, or sites of opportunity such as flooded areas. On the other hand, a coastal wetland may require a swath of only 15 to 20 km. A resolution of approximately 30 m is adequate for wetland and humid regions, whereas a resolution of 15 to 100 m may be adequate for hyperarid-region research.

4.3.6.4 Frequencies, Polarizations, Incidence Angles

For soil moisture investigations, L-band and C-band with like polarization (HH and VV) at near-nadir angles of incidence (e.g., 20°) are preferred. Vegetation-cover studies for humid regions and wetlands will require the use of C-band and, if available, X-band. These studies will also require both like- and cross-polarization imagery acquired at higher angles of incidence. X-band and, to a lesser extent, C-band are best for investigating snow. Studies of the penetration of hyperarid regions will concentrate on the longer wavelengths, e.g., L-band, with both like- and cross-polarization.

4.3.6.5 Data Products

need for relative calibration of ±1 dB

For maximum sensitivity to soil moisture changes (especially in the presence of vegetation), it is desirable for SIR-C to achieve a relative radiometric calibration (stability) of about ±1 dB. In order to relate the absolute level of L-band response to that at C-band, it is desirable to achieve an absolute radiometric calibration of ±1 dB (relative to each other) or better.

Because ground control points can be used to establish location on a cartographic grid, absolute geometric calibration is not critical, although it is critical that the relatively narrow SIR-C swath be located in the ground-range image to within 5 km or better of the ephemeris-predicted value. Most hydrologic investigations will require SAR image products to be geometrically rectified to a standard cartographic grid, and some will require geocoded images.

4.4 Vegetation Science

4.4.1 Background

the earth's ecosystem

Vegetation is responsible for the primary production of life's essentials—from oxygen to fuel—on the earth. Energy is captured as carbon is fixed photosynthetically by green plants, and for this process to take place, solar radiation, water, and certain essential elements are required. The entire planet can be viewed as a single ecosystem, with the *biota* (plants, animals, humans, and other organisms), the *biogeochemical cycles* (such as those of carbon, nitrogen, phosphorus, sulphur, etc.), the *hydrological cycle*, and the earth's *energy balance* all inextricably linked. Thus, any change in the environment that affects photosynthesis also affects some aspect of the water, carbon, and chemical balance of the system. Moreover, the future habitability of the earth may be affected by any drastic changes in the states or fluxes of any of these components.

The goal of vegetation studies is to develop an understanding of the state of the earth's vegetated surface, the major fluxes through it, and the major exchanges between vegetation and the hydrosphere, lithosphere, and atmosphere. Past regional-scale research has focused on determining states, i.e., on vegetation mapping, documenting land cover and land use, and classifying crops and vegetation. Prior to the early 1970s, the documentation of land cover and land use relied on several types of historical data and statistics that included vegetation and land-use maps as well as agricultural and forest-production statistics. These sources of data, however, were limited to only a few regions of the world, and the accuracy of the data was often unknown. A major difficulty in studying the dynamics of the global biogeochemical and hydrological cycles has been the spatial heterogeneity inherent in the terrestrial components of these systems.

4.4.2 The Role of Spaceborne Remote Sensing in Vegetation Science

key vegetation phenomena

The vegetation phenomena that are amenable to study by remote sensing include

(1) The spatial extent and distribution of vegetation
(2) Landscape patterns
(3) The water content of plant canopies
(4) The biogeochemical composition of and fluxes through canopies (postulated)
(5) The structure and orientation of canopies
(6) Productivity (either biomass or net primary productivity)

Of these, the determination of the type, distribution, and spatial extent of vegetation, and the estimation of biomass, have received the most attention.

extension by radar of detectable range of LAI variations

Beginning with the Landsat remote sensing program in 1972, land-cover summaries have been updated frequently and with increasing reliability. Optical scanners have proved quite useful for crop biomass estimation and forest and rangeland inventorying and mapping. However, to achieve high rates of identification accuracy, it has been necessary to use multidate observations (which are often difficult to accomplish in a single season because of the presence of cloud cover). The biomass per unit area, of which the green leaf area index (LAI) is one estimate, was identified as being a key to the dynamics of the carbon cycle. Landsat MSS data have been used to estimate LAI. However, the technique is insensitive to LAI values greater than about 4, and in some forest environments, LAI values may

exceed 20. Recent research results (Fig. 4-26) indicate that it may be possible to measure LAI using radar over a wide dynamic range [4-12]. Recently, it has been suggested that *productivity* (a flux), rather than *biomass* (a state) may be the more important factor in understanding the carbon cycle—especially the effects of perturbation on the carbon cycle. Estimates of LAI from the beginning through the end of a growing season may provide such an estimate of productivity.

4.4.3 The Role of Imaging Radar in Vegetation Science

radar sensitivity to plant-canopy water content, LAI, and structure

Radar should provide complementary biophysical information about vegetation canopies, such as plant water content, leaf area index, and canopy structure. Optical sensors are most sensitive to plant structure at the micrometer scale, whereas radar responds to the centimeter and decimeter scales (see Fig. 4-27). Optical waves cannot penetrate deeply into thick vegetation canopies, but microwaves penetrate to varying extents, depending on frequency, polarization, and angle of incidence. Furthermore, because the target-wave interaction mechanisms are significantly different in the optical and microwave spectral regions, certain cover types that are difficult to discriminate in one spectral region are easy to discriminate in the other. These and other complementary attributes suggest that algorithms developed for monitoring vegetation resources in the future will employ data provided both by optical scanners and by imaging radars.

4.4.4 The Scientific Basis for SIR-C Vegetation Science Experiments

need for global data sets

Radars with multifrequency and multipolarization capabilities are powerful tools for probing vegetation canopies. Extensive research conducted over the past two decades using multifrequency and multipolarization radars has led to numerous results, including algo-

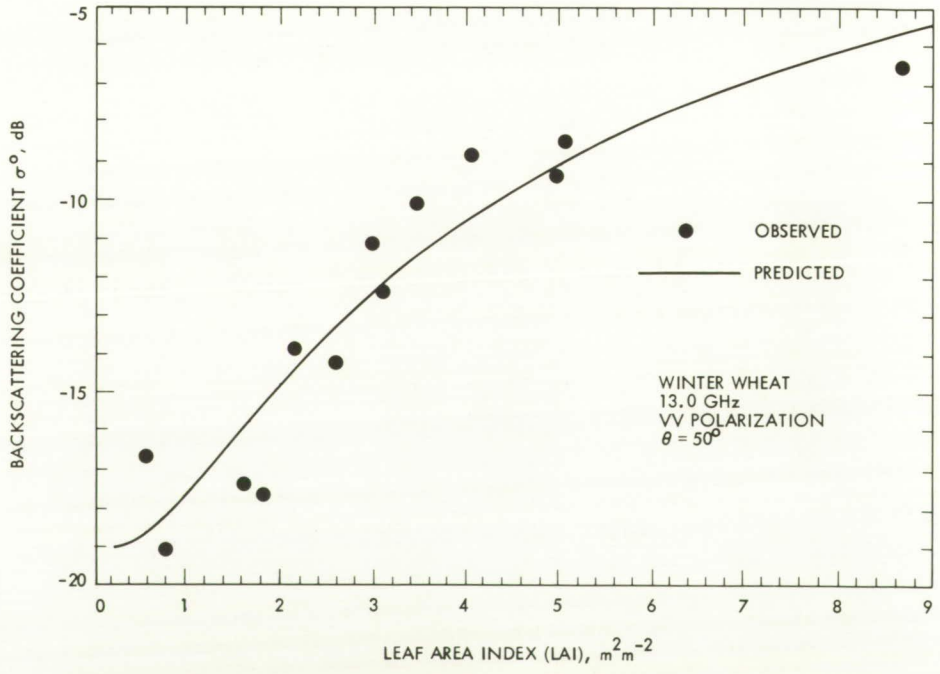

Fig. 4-26. Microwave response to leaf area index (LAI)

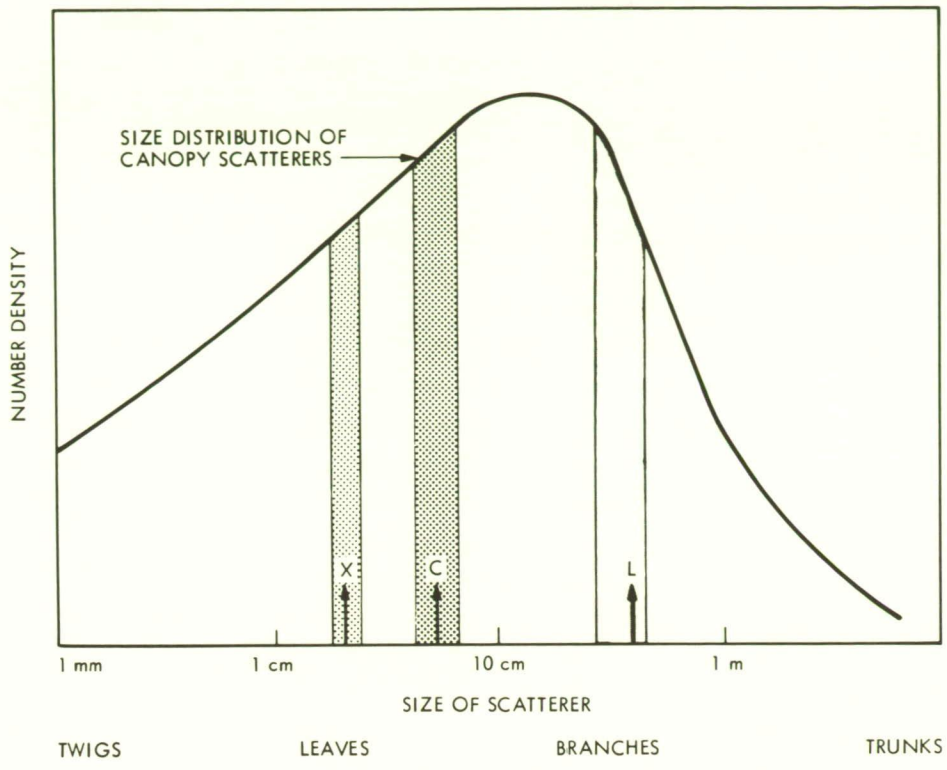

Fig. 4-27. Radar model of idealized response to various wavelengths according to the size distribution of canopy scatterers

rithms and models for separating vegetation cover types and estimating biophysical properties (most notably water content and leaf area index). The research, however, is based almost exclusively on observations of crops made from ground-based and airborne platforms. Consequently, the models and algorithms thus developed are somewhat site- and time-specific and are therefore limited in applicability. SIR-C offers the first opportunity to verify and extend the research of the past two decades by providing calibrated, multifrequency, multipolarization data for a variety of different geographic regions and conditions over the globe.

A short review of radar vegetation research is given in the SIR-B Science Plan [4-13] and more extensive reviews are available [4-14, 4-8]. Instead of providing yet another review, this section will focus on the roles of frequency and polarization as they pertain to vegetation canopies.

contributors to radar backscattering

The total signal backscattered from vegetation-covered ground consists, in the general case, of three types of contributions, as illustrated in Fig. 4-28. These include

(1) Direct backscattering from plants
(2) Direct backscattering from the underlying soil surface (allowing for two-way attenuation by the canopy layer)
(3) Plant–soil multiple scattering contributions

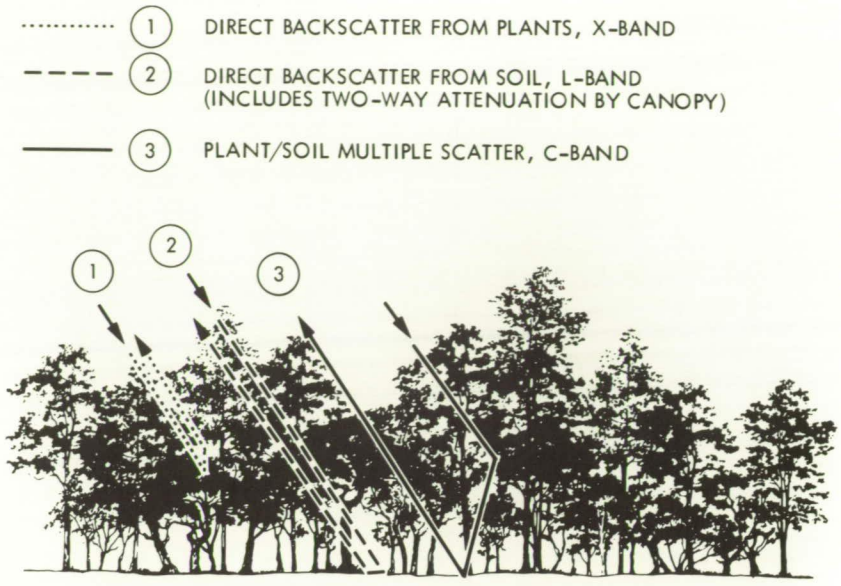

Fig. 4-28. The role of frequency in canopy backscatter

The magnitude of these contributions and their variation as a function of sensor parameters (wavelength, observation direction, and polarization configuration) depends on many factors, including the following:

(1) The dielectric constant of the vegetation material, which is strongly influenced by moisture content—because moisture content may be significantly different for different canopy constituents (such as leaves, stems, and fruit) depending on growth stage, the dielectric constants of the canopy constituents may vary as well
(2) The size distribution of the scatterers in a canopy
(3) The shape distribution of the scatterers in a canopy
(4) The orientation distribution of the scatterers in a canopy
(5) The roughness and dielectric constant of the underlying ground surface
(6) The canopy cover's geometry, including cover fraction, plant height, plant spacing, and row direction in agricultural fields

polarization-dependence of attenuation by plant canopy

Representative samples of canopy-loss measurements are shown in Figs. 4-29 and 4-30 for a canopy of winter wheat. Direct-transmission measurements were made using a transmitter placed atop a truck-mounted boom, and a receiver mounted on a rail placed on the surface of the soil. The measurements shown were made at frequencies approximately the same as those of SIR-C.

increase of canopy loss with frequency

The role of frequency is well demonstrated by the curves in Fig. 4-29, which represent two stages of growth characterized by LAI values of 4 and 8. Whereas the canopy is quasi-transparent at L-band at both stages of growth (the two-way loss is less than 4.2 dB), the canopy is effectively opaque at X-band, particularly for the higher-LAI canopy (the two-way loss is 57.6 dB).

A canopy in which a significant portion of the biomass is contained in constituents having a preferential orientation—such as vertical stems—will tend to exhibit polarization-dependent attenuation properties. The curves in Fig. 4-30 show that, as a result of the strong coupling between a vertically polarized incident wave and the vertical stems, the canopy at-

C-2

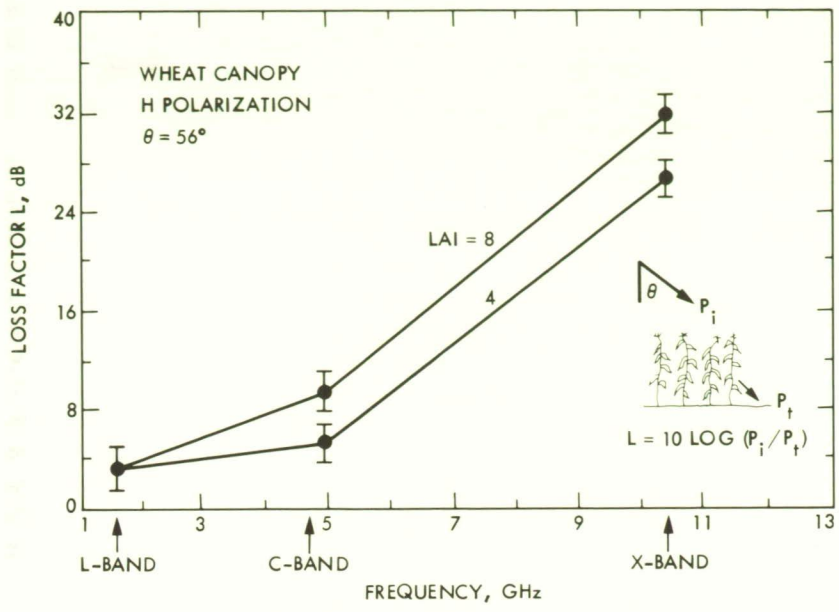

Fig. 4-29. Loss factor of wheat canopy

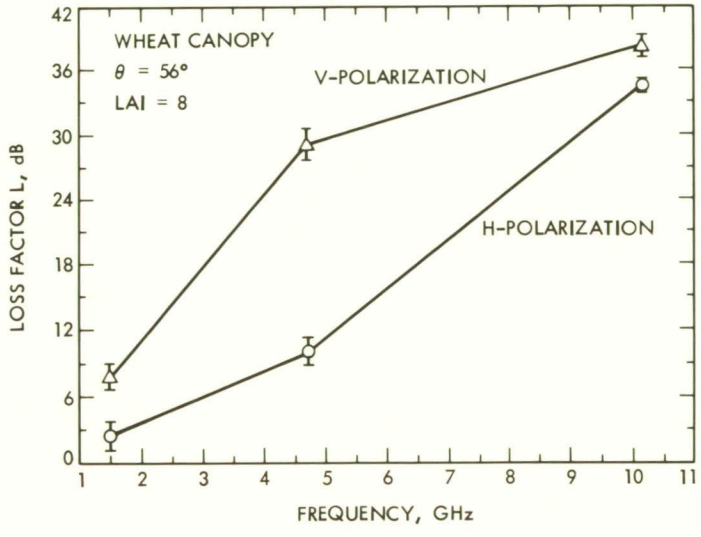

Fig. 4-30. Role of polarization in canopy penetration

tenuation is significantly higher for V polarization than for H polarization. It is hypothesized that the majority of the loss experienced at L-band and C-band is attributed to the stems in the canopy, whereas the randomly oriented leaves become the dominant attenuators at X-band, thereby resulting in a smaller difference between the two curves than at lower frequencies.

role of polarization in backscatter

The orientation of the polarization vector of the incident wave affects not only the absorption by the canopy constituents but also the scattering, including the backscattering, direction. Thus, the polarization of the wave determines the effective depth of the volume responsible for the observed backscattered energy, as well as the intensity of the backscat-

tered signal. As one might expect, the effective depth of penetration for HV is intermediate between that for VV and HH, and the signal is caused by second-order or higher scattering. Figure 4-31 illustrates how multipolarization images may be combined to enhance the discrimination among different target categories in a forest environment.

Temporal frequency is an important asset in any remote sensor used to observe a dynamic phenomenon such as vegetation. According to a study conducted by Hoogeboom [4-15], when single-date X-band radar images of a test site in The Netherlands were used for crop-identification purposes, only 30% of the fields (consisting of 182 fields comprising seven crop types) were correctly identified. When data from three dates were used together, the identification accuracy improved to 88%. Once a vegetation cover type has been correctly identified with a high degree of estimation accuracy, the next step is to estimate its biophysical properties. This may be accomplished through multifrequency, multipolarization, multiangle, and/or multidate observations. An example illustrating the temporal variation of the scattering coefficient is shown in Fig. 4-32 for a field planted in winter wheat. If multidate, calibrated radar observations are available, it should be possible to estimate stage of growth as well as LAI. Algorithms to provide this type of information from single-date, multifrequency, or multipolarization data are not available at present.

4.4.5 SIR-C Vegetation Science Experiments

experiment objectives

The primary objective of the SIR-C vegetation science experiments is to address the scientific questions related to the information needs stated above. It is desirable, although not required, that experimental designs take into account the role of the SIR-C mission as a major step in the evolution of the spaceborne imaging radar project towards an operational free-flyer on EOS. Another desirable, but not required, possibility for the SIR-C vegetation experiments would be to concentrate the majority of the experiments on a select set of six to eight supersites. The supersite approach allows several investigators to use a common set of ground observations and aircraft support data. In terms of exact location, the supersites will be chosen to suit the scientific objectives of the SIR-C Science Team. As a general guideline, however, it is recommended that

vegetation supersites

(1) At least one of the supersites encompass a major agricultural area so that the algorithms and models developed from ground-based studies of crops may be tested
(2) The remaining test sites encompass areas that are good representatives of the earth's major ecosystems, such as grasslands, deciduous forests, mixed forests, rain forests, and tundra

The second category includes representative vegetation types and will serve to provide concrete data to researchers, thus allowing them to develop models and algorithms to relate the radar scattering response to the biophysical properties of these vegetation canopies.

It is understood that information derived from the SIR-C experiments will be used either to serve as input to or to build biophysically based models of canopy structure and function. Modeling must be an essential component of any overall effort to understand regional and global processes; it should therefore be a part of the SIR-C vegetation-science investigations.

The following material discusses several classes of vegetation science experiments that could be conducted using SIR-C. However, the list (summarized in Table 4-4) should not be regarded as all-inclusive or complete.

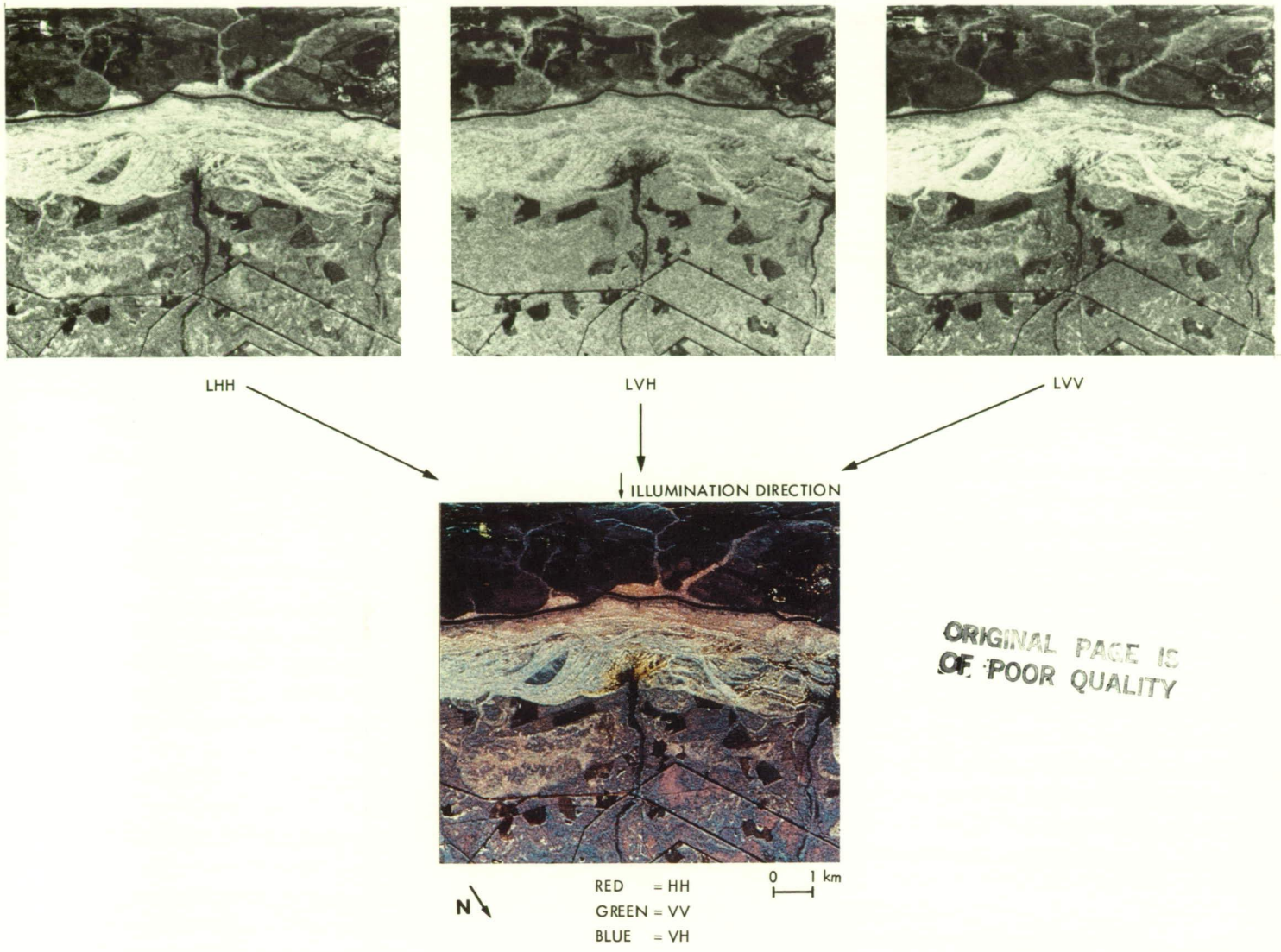

Fig. 4-31. Illustration of how multipolarization images may be combined to enhance discrimination among different target categories in a forest environment

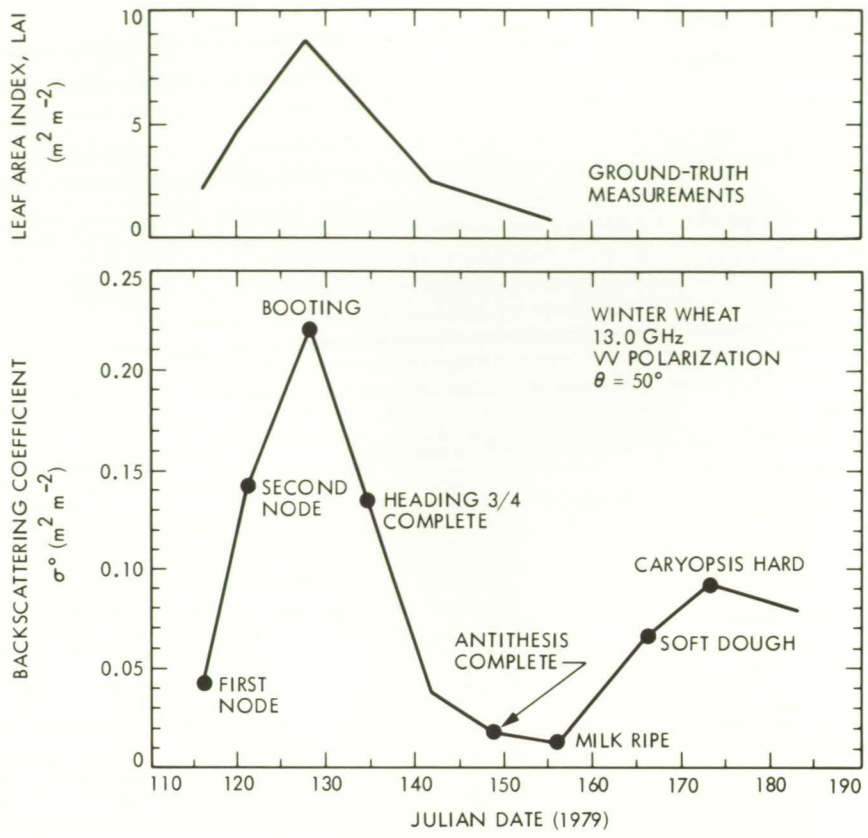

Fig. 4-32. Radar temporal signature of winter wheat

Table 4-4. Some SIR-C vegetation science experiment classes

Experiment Class	Scientific Objectives
Identification and mapping of vegetation types	Identification of forest, rangeland, crops, etc. and determination of their distribution and spatial extent (single and multidate, radar only, radar plus optical)
Interpretation of landscape patterns and processes	To understand the major factors influencing the spatial extent and distribution of vegetation and how changes in these factors affect regional processes
Assessment of the biophysical properties of plant canopies	To determine canopy structure, species geometry, foliage characteristics, and seasonal variations, and to estimate stand volume, canopy water content, soil moisture, LAI, and biomass
Determination of the radar penetration of canopies	To assess penetration of various radar frequencies and polarizations in different canopy types

4.4.5.1 Vegetation Type Identification

single-date experiments

The SIR-C mission will allow experiments to evaluate the information content from single date SAR data for vegetation type identification as a function of frequency (L, C, and X), polarization (HH, HV, VV), and angle of incidence (15° to 60°). These evaluations could be made by:

(1) Crop groups (e.g., small grains, irrigated crops, etc.)
(2) Forest types (e.g., by dominant species or by evergreen versus deciduous habits)
(3) Physioagronomic regions (i.e., soil type, climate, cultural practices, etc.)
(4) Weather conditions
(5) Time of day
(6) Topography
(7) Phenology

multidate experiments

If the SIR-C flight schedule is such that it is possible to make two observations corresponding to two different stages of growth, it would be useful to evaluate the improvement in crop-, grassland-, or forest-identification accuracy provided by the temporal dimension. Therefore it is recommended that the SIR-C mission consist of two flights, and that the flight dates be in the May–June and August–September periods of the same calendar year.

radar/optical combination

It is also desirable to evaluate the complementary and redundant aspects of radar and optical (e.g., Thematic Mapper) data for vegetation identification. For forest types, this should also include multi-temporal studies (seasonal variations and/or changes since 1978 [Seasat SAR], 1981 [SIR-A], or 1984 [SIR-B], as well as the optical data [TM]).

4.4.5.2 Interpretation of Landscape Patterns and Processes

The measurement of the areal extent and distribution of terrestrial biomes and the changes in them has been one of the basic objectives of all land remote sensing activities. Surface-texture information (e.g., gradual or abrupt changes in canopy height; the frequency and distribution of canopy gaps) from SIR-C (multifrequency, multipolarization, and multiangle) should be extremely useful in the interpretation of regional landscape patterns. Inferences about landscape dynamics may also result from the investigation of radar penetration of canopies.

4.4.5.3 Biophysical Properties of Canopies

Studies are needed to assess the dependence of the radar backscattering coefficient on the biophysical properties and conditions of plant canopies and on the underlying soil or overlying snow cover (if any), including:

(1) Productivity and phytomass (LAI)
(2) Canopy structure
(3) Stress
(4) Soil moisture
(5) Snow–water equivalent

The study should incorporate an evaluation of the roles of frequency, angle of incidence, polarization configuration, and optical data.

The identification of crops and assessment of their biophysical properties using imaging radar is often complicated by the presence of confusion factors. The radar coefficient depends not only on the type of crop under study (and its biophysical properties), but on soil roughness, row direction, row structure, the action of wind and rain, and the presence of dew. Even though some ground-based experiments have been conducted to estimate these effects, no definitive studies have been carried out using satellite radar data. It is recommended that experiments designed to estimate these disparate effects be conducted with SIR-C, using all combinations of wavelength, polarization, and angle of incidence.

forests

We need to assess radar response to the biophysical properties of forest structure and to foliage variables such as:

(1) Stand volume
(2) Productivity or phytomass (LAI)
(3) Seasonal variations (leaves on or off, snow cover, etc.)
(4) Stress (moisture, insect infestation, etc.)
(5) Tree-species geometry
(6) Clear-cut areas
(7) Foliage characteristics (broad leaves, needles)
(8) Stand structure (multiple-layer, tropical, understory vegetation)

sparsity of data on rangeland response

Very little information is available about the radar response to rangeland. SIR-C will provide an opportunity to evaluate the LAI, phytomass, plant morphology, and snow–water equivalent of the various types of grasslands and shrublands. Such an evaluation should use the full multiparameter capability of SIR-C to determine the effects on radar response of species composition, soil type, topography, cultural practices, and weather conditions.

4.4.5.4 Radar Penetration of Canopies

frequency and polarization roles in canopy attenuation

From a practical point of view, we need to develop a better understanding of both how much a plant canopy attenuates radar waves (as a function of wavelength, polarization, and angle of incidence) and how radar image texture can be used for the identification and assessment of the biophysical properties of vegetation. In the former case, SIR-C will provide an excellent opportunity to conduct experiments on canopy attenuation at L-, C-, and X-band, for HH, VV, and HV polarizations, and for angles of incidence ranging from 15° to 60°. In the latter case, we know that radar image texture is the spatial spectrum of image tone and is a consequence of natural variations in the imaged scene (over and above signal-fading fluctuations). SIR-C will thus provide an opportunity to use textural information (in addition to tonal information) for the identification of vegetation and the assessment of its biophysical properties.

Thus, it is desirable to evaluate the variation of canopy with

(1) Frequency
(2) Polarization
(3) Angle of incidence for various types and conditions of vegetation canopies, including cultural vegetation, trees, and grasses

4.4.6 Summary of the SIR-C Mission Requirements for Vegetation Science

4.4.6.1 Orbital Parameters

In order to include coverage of tundra vegetation (e.g., sedges, lichens, mosses), a high orbital inclination is required.

4.4.6.2 Mission Timing

need for May–June and August–September flights

Ideally, repeat coverage every 10 to 15 days during the growing season is needed to study the phenologic development of vegetation. However, very useful information could be obtained from two SIR-C flights, one in the May–June time period and the other in the August–September period.

4.4.6.3 Swaths and Resolutions

criticality of narrow swaths crossing supersite

A resolution of 30 m with at least four looks is adequate for many vegetation studies. Although 50- to 100-km swaths would be desirable, most experiments can use narrower swaths (20 to 30 km), when more simultaneous channels (frequencies, polarizations) are acquired. However, since supersites will be extensively used, it is critical that narrow-swath passes cover these sites.

4.4.6.4 Frequencies, Polarizations, and Incidence Angles

need for higher angles of incidence

For most of the experiments, it will be advisable to acquire as many simultaneous channels (frequencies, polarizations) as possible, because this will permit valuable studies of canopy penetration, canopy volume scattering, etc. Although it is desirable to acquire data at all angles of incidence (15° to 60°), it is expected that the higher angles of incidence (40° to 60°) will minimize the confusing effects of subcanopy surface scattering, particularly at C- and X-band.

4.4.6.5 Data Products

need for relative calibration of ±1 dB and absolute calibration of ±3 dB

In general, SIR-C imagery having pass-to-pass coregistration to within half a pixel is desirable. Images of vegetation supersites should be rectified (with respect to the ground) to within half a pixel. SIR-C images should maintain at least ±1 dB of relative calibration or stability both within a frame and over the duration of the mission. Absolute accuracy of ±3 dB is desirable. Because of the importance of using ground-truth teams to collect data from the experiment sites, it is critical that the swath be located within ±20% of the swath width.

The relative calibration requirement is important for several of the vegetation experiments listed in the previous section. For most vegetation scenes, the dynamic range of the backscattering coefficient seldom exceeds 10 dB (for a given frequency, polarization, and narrow angular range), and often is less than 6 dB. Hence, it is important that system-related variations both within a frame and between frames be confined to less than 1 dB.

4.5 Glaciology

4.5.1 Background

value of remote sensing to glaciology

Glaciology, which is the scientific study of ice in all its forms, is a field of investigation to which remote sensing has much to offer. The reasons for this are several. The areas where large snow and ice masses occur are extensive. They are also typically remote, being primarily beyond the range of human activity and hence of conventional surface observations. In addition, they are regions where it is commonly difficult and dangerous, as well as expensive, to carry out conventional surface observations. Finally, the polar regions where the largest ice masses occur are also shrouded in clouds and in darkness for much of the year, thereby restricting the effectiveness of many types of observing systems.

The specific objectives of glaciological remote sensing vary widely, depending on the type of ice mass under study. In the following, we will discuss these different ice masses and their characteristics in the context of their different observational needs and objectives.

4.5.1.1 Sea Ice

need for sea-ice data

The polar oceans and seas are covered, at least seasonally, with a shifting and broken ice pack. For an adequate description of this ice, data are needed on ice extent, ice types, ice roughness, ice thickness, drift velocities, growth and melting rates, lead and polynya patterns and frequencies, flow size distributions, pressure ridge patterns, snow cover, and ice island and iceberg sizes and locations. This information is required both on a synoptic, timely basis for ice forecasting, as well as for a wide variety of scientific and operational problems. Similar information is needed on a seasonal or yearly basis for climatological studies. Recently, these latter types of observations have received increased emphasis, in that the largest worldwide surface temperature change, resulting from CO_2-induced warming, is expected to occur in the polar regions, and changes in the nature and extent of the sea-ice cover are believed to be sensitive indicators of these differences. Of particular interest is the response of the ice cover to mechanical and thermal forcing by the air and sea. This includes ice motion, deformation, and formation/melt. By knowing more about these processes, the climatological and operational properties of the ice cover can be predicted with increased accuracy.

4.5.1.2 Lake and River Ice

hazards in lake and river ice

The formation of ice covers on lakes and rivers can result in a variety of hazards by impairing shipping and causing severe flooding. Data required for lake- and river-ice

studies are, in many ways, similar to those required for sea-ice studies, in that the ice covers on many large lakes and rivers are mobile, at least during part of the freezing season, drifting and deforming as the result of wind and current forcing. However, as will be discussed later, ice–radar interactions for lake and river ice are quite different than for sea ice.

4.5.1.3 Ice Sheets, Ice Shelves, and Glaciers

ice-sheet boundaries

The large ice sheets of the world, located in the Antarctic and in Greenland, contain the great percentage (92%) of the world's fresh water, locked up as ice. In many locations, particularly in the Antarctic, these continental ice masses flow into vast ice shelves which ultimately calve into the sea large, tabular icebergs with typical thicknesses of 200 to 250 m. Although the flow rates of large ice sheets and shelves are small, relative to those of pack ice (meters to a few kilometers per year as compared with kilometers per day), nevertheless, the deformation rates are readily measurable using modern techniques. Data of interest include locations of the boundaries of these ice masses, measurements of their internal movements, location of crevasses, distribution of morainal material, annual accumulation and ablation rates, detection of surges, and determination of the structural characteristics of the ice. SIR-C, flown in a polar orbit, could provide coverage of both Greenland and the Antarctic.

4.5.1.4 Seasonal Snow Packs

Roughly 50% of the earth's land surface is covered by snow in any given year. This snow cover is highly variable in extent and in properties. Information of particular interest includes extent, thickness, density, water equivalent, and average grain size. Snow is of interest in its own right. It also serves as an important hydrologic resource, and covers the surface of most sea-, lake-, and glacier-ice masses.

4.5.2 Role of Spaceborne Remote Sensing in Glaciology

current data sources

The need for information on ice and snow has led to the use, with some notable successes, of data from various earth-observing satellite instruments. This use includes applying Landsat data to ice motion studies; applying NOAA Polar-Orbiter data to ice extent and motion studies, notably in the Bering Sea; and extensively using a number of microwave systems to obtain data from both polar regions. The Landsat and NOAA systems use reflected visible light and emitted infrared (IR) radiation with the consequence that clouds in summer and near ice margins, the darkness of polar winter, and the low temperature contrast in summer interfere significantly with observations. Landsat also suffers from limited coverage.

Microwave radiometer and radar systems are virtually unaffected by the factors that limit visible and IR observations, and the use of those systems has significantly changed ice and snow data availability. Radiometer systems that are sensitive to emitted radiation have been flying in space since 1973 and have produced global data sets on ice type, concentration, and extent, some data on snow cover, and some information on ice sheet accumulation at fairly coarse resolution, about 25 km. Future systems may improve this resolution to about 11 km, but such a reduction would be expensive. For global, large-scale ice and snow in-

formation, no existing technology is superior to microwave radiometry. Another coarse-resolution system is the scatterometer, a calibrated nonimaging radar that flew on Seasat and will fly again on NROSS. This system is valuable in its ability to generate backscatter data at different angles of incidence.

4.5.3 Role of Imaging Radar

radar's independence of clouds and darkness

The two shortcomings of radiometry for ice observations, its coarse scale and some uncertainty of interpretation, are successfully avoided by the use of imaging radar. The great advantage of imaging radar derives not only from its ability to observe through clouds and in darkness, but also from its fine surface resolution, 10 to 100 meters, 100 to 1000 times finer than the radiometer's. This fine scale permits identification of ice features by texture and form, as well as by signal strength, thus vastly reducing interpretive difficulties, and also permits the tracking of features to develop velocity fields based on a high density of observations. Calibrated systems can also provide improved snow observations, since some of the natural spatial variability of snow can be directly observed.

Seasat discoveries

Although there is a significant body of experience concerning the interpretation of SLAR and SAR imagery of sea ice, lake ice, and glaciers, obtained by aircraft-borne systems, the SIR-C experiment offers the first opportunity to verify the interpretation of many of these features as seen in imagery obtained by a satellite-borne system. This statement needs a bit of explaining, since it is common knowledge that the Seasat SAR system obtained excellent images of sea ice along the Beaufort Coast of the Arctic Ocean. The lack of verification was the result of several factors, the most important of which was the time period when Seasat operated (June 26–October 10, 1978). Because this is a time period when surface operations in the Arctic Ocean are both difficult and dangerous, ground-truth programs were scheduled for later during the winter and early spring, when operating conditions would be more favorable. These observations, of course, never came to fruition, as a result of the power failure on Seasat on October 10. In addition, because of its timing, its orbit, and the lack of appropriately spaced receiving stations, Seasat simply did not obtain imagery of most glaciological entities of interest, including the seasonal snow cover. This situation has continued until the present, as a result of the inability to launch Shuttle missions into polar or near-polar orbits. The only exception to this statement was the SIR-B mission, where limited imagery was obtained of the northern edge of the Antarctic ice pack. The SIR-C mission, if launched into near-polar orbit, would not suffer from these difficulties. In short, there would be extensive coverage of the Arctic Basin, of Greenland, of the Alaskan glaciers, and of the Antarctic ice pack, ice sheet, and shelves. In addition, if the mission is launched in northern winter, there should be extensive ice covers on the Great Lakes and in the Bering, Labrador, and Greenland Seas. In summation, SIR-C offers a unique potential to obtain multifrequency, multipolarization, variable-look-angle SAR imagery of the majority of the large ice masses of the world. It would also result in validated interpretations of the majority of the features seen on this imagery and make possible the selection of the appropriate combinations of frequency, polarization, and look angle that will most effectively reveal glaciological features of interest. SIR-C is clearly the logical step that should lead to an optimal utilization of the free-flying SAR systems that are planned for deployment in the 1990s on missions such as ERS-1 and Radarsat, as well as to the optimal design of the SAR system for EOS.

SIR-C potential

4.5.4 Scientific Basis for SIR-C Ice Experiments

ice-scattering mechanisms

The ways that microwaves interact with ice masses can be surprisingly different. This is the result of changes in the electromagnetic characteristics of the ice and differences in the surface geometry and roughness of the ice bodies relative to the wavelength of the electromagnetic radiation that is used. For instance, sea ice is not pure ice, in that it contains entrapped sea salt in the form of both included brine and solid salt crystals. The exact amount of salt depends on the rate at which the ice grew, its age, and particularly its thermal history. Of particular interest is whether the ice has survived one or more summers, in that during the summer melt period much of the salt is flushed out of the upper portions of the ice. If the ice contains an appreciable amount of salt (first-year ice), it is a very-high-loss dielectric, and the electromagnetic radiation only penetrates, at the most, a few millimeters. In this case, the strength of the radar return is strongly influenced by the roughness of the upper ice surface. If the surface is flat, as in the case of undeformed first-year ice, the return will be low, as most electromagnetic energy is reflected away from the radar receiver. If the surface is rough, as in the case of new pressure ridges and most multiyear ice, a strong return will occur. This is a somewhat similar situation to the return from an ice-free ocean, in that a calm sea gives a low return while a rough sea gives a strong return. Fortunately, it is usually possible to distinguish between ice and open water, in that the patterns and textures of their returns are commonly different. For instance, as the result of Bragg scattering, open water usually gives a strong return at HH and a weaker return at VV. As was mentioned, the upper portion of multiyear ice is characteristically of low salinity, as the result of brine drainage. Therefore, the electromagnetic energy penetrates into the ice where it undergoes volume scattering; that is, it is scattered by the inhomogeneities (air bubbles, cracks, brine drainage tubes) within the ice mass. Accordingly, for a given surface roughness, multiyear ice commonly gives a stronger return than does first-year ice. This distinction is of interest because multiyear ice is invariably thicker and stronger than first-year ice and is, therefore, a better insulator and a more imposing operational hazard. A schematic drawing indicating the nature of radar returns from sea ice is given as Fig. 4-33(a).

ice dielectric constants

Although sea ice is a high-loss dielectric, lake and river ice are low-loss dielectrics. This is the result of the fact that lake and river ice are essentially pure ice without the impurities characteristically found in sea ice. Therefore, radiation penetrates deeply into them, and the strength of the return can be a complex function of the roughness of *both* the upper and the lower surfaces of the ice, as well as of the volume scattering within the ice. In fact, in shallow lakes, such as occur on the North Slope of Alaska, radar returns clearly indicate the portions of these lakes where the ice is frozen completely to the bottom.

Glaciers, ice sheets, and ice shelves are similar to lake ice, in that the ice masses are essentially pure ice. The electromagnetic radiation penetrates well into the ice mass where volume scattering occurs, primarily associated with the presence of air bubbles and rock and dust layers.

However, these ice masses are sufficiently thick (hundreds to several thousand meters), that at typical radar frequencies there is no return from the bottom of the ice mass (from the ice–rock or ice–ocean interface). Therefore, the strength of the return is a function of the roughness of the upper ice surface, of the volume scattering within the ice mass, and of the geometry of large discontinuities within the ice such as crevasses or major changes in ice type. The general nature of the radar return from glaciers and ice sheets, as well as from lake ice, is also indicated in Fig. 4-33(b).

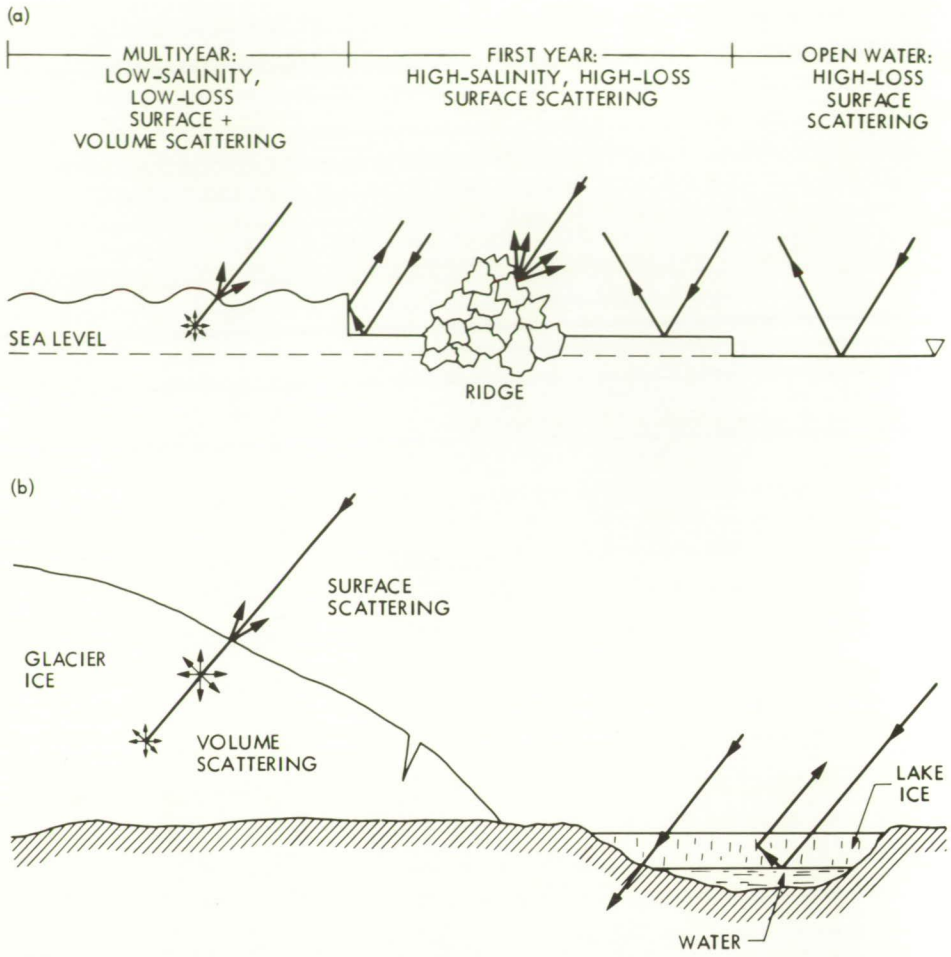

Fig. 4-33. Interactions between radar and different ice types: (a) sea ice and (b) glaciers, ice sheets, and lake ice

snow-layer effects

Seasonal snow layers are invariably thin (< 5 m), chemically pure, and of a low density. Therefore, they commonly give a very low return and, as a result, are nearly invisible at longer wavelengths (e.g., at L-band). However, if the snow is thick or wet or has densified as the result of freeze–thaw processes and, particularly if the included air bubbles are of the appropriate size to serve as effective volume scatterers, moderate returns can result. Also, the upper surface of the snow can change from very rough (sastrugi and irregular ablation features) to perfectly smooth in the matter of a few hours. Therefore, the radar return from snow is sometimes strong and sometimes very weak. One result of the SIR-C experiment should be a better understanding of these variations in radar return and their associated causes.

value of SIR-C multifrequency and multipolarization data

Mention should be made here of the unique opportunities offered by the fact that the SIR-C mission will provide both multipolarization and multifrequency data. Multipolarization data gives valuable clues relating to the scattering mechanisms, and insight into separating surface scattering from volume scattering. In the case of surface scattering, there are two well-established mechanisms: geometric optics and resonant, or Bragg, scattering. In the case of the radar return from sea ice and glacial ice, experimental data indicate that geometric optics dominate for viewing angles less than 30° to nadir and that Bragg scatter-

ing will be expected from the SIR-C radar if all the return is from the surface. Surface scattering cannot be uniquely determined without comparing polarization data. In sea ice, the absence of volume scattering implies the limited penetration of electromagnetic waves and hence the presence of younger, more saline ice types or wet multiyear ice.

A lack of polarization dependence at large viewing angles implies negligible surface scattering. In these cases the electromagnetic waves penetrate the ice and interact with subsurface scatterers. Moderate volume scattering is commonly associated with multiyear sea ice, and very strong subsurface scattering is known to occur over the ice-covered regions of Southern Greenland. In these cases, a strong HV return is to be expected, as volume scattering is invariably strongly depolarized.

SAR phase images

Recently, SAR phase images have been produced using two polarization components. Again, this is another way to use polarization data to separate surface and volume scattering in that, for reasons that are just now becoming understood, volume scattering produces a near 0° relative phase shift while surface scattering can produce a 180° phase shift.

A prime application of multifrequency data is to determine the relative size of the volume scatterers. For instance, recent airborne active and passive microwave data collected over Greenland indicate that the subsurface scatterers are large compared with the electromagnetic wavelength (C- through K-band). If this can be verified, electromagnetic theory indicates that the average radius of curvature of these objects can be determined. Observations at different azimuth angles will also reveal shape asymmetries and whether there is a preferred orientation in the alignment of the scattering objects. If the subsurface scatterers are small compared to a wavelength, Rayleigh scattering occurs and the absolute return varies as the wavelength to the fourth power. As this type of scattering is observed from sea ice, information could possibly be obtained regarding whether or not the size of the scatterers varies geographically over the Arctic.

4.5.5 SIR-C Glaciology Experiments

Some specific SIR-C experiments in the general area of glaciology are considered in the following section and are summarized in Table 4-5.

Table 4-5. Some SIR-C glaciology experiment classes

Experiment Class	Scientific Objectives
Sea ice	Sea-ice feature verification, ice drift and deformation, spatial variations in pack ice, nature of ice margin eddies, improved characterization of sea-ice type
Lake ice	Lake-ice feature verification, lake- and river-ice operations, lake-ice dynamics
Ice shelves, ice sheets, and alpine glaciers	Ice-shelf and glacier boundaries, icebergs and ice islands, ice-stream delineation, alpine glaciers
Snow	Snowpack extent, snow–water equivalent, snow wetness

4.5.5.1 Sea Ice

sea-ice imaging mechanisms

This program, which should be carried out during a polar orbiting SIR-C mission at least at two locations in the Arctic, say the Beaufort and the Greenland Seas, would be dependent upon rapid transmission of the data to ground-truth parties that have flexible logistics support. They would then have the possibility of visiting locations where unusual or interesting radar signatures are observed. For instance, the bright cigar-shaped return in Fig. 4-34 is believed to be an ice-island fragment within the ice pack, based on the fact that parts of the known ice island T-3 (see Fig. 4-35) gave a similar strong return. Whether this supposition is correct is unknown, as is the exact reason for the strong return in the first place. Similar uncertainties exist in interpreting the return patterns from the fast ice areas shown in Fig. 4-36. Simple on-site inspection and sampling should remove such interpretative uncertainties and advance our understanding of the scattering mechanisms encountered in these ice masses. The fact that SIR-C will provide multifrequency data with different polarizations and angles of incidence will significantly contribute to resolving these problems. An additional portion of a verification program would be the under-flying of selected SAR passes with high-resolution aircraft-borne SAR such as either the ERIM or the Intera systems, and aerial photography. Utilization of data obtained by other satellite systems such as the SSM/I system should also be very useful. These flights would provide instructive comparisons between SAR systems with different resolutions and also with high-resolution visual imagery. Their use would also permit the field parties to obtain the down-linked aircraft data in near real time so that *in situ* sampling can be carried out before ice drift and deformation modify the ice beyond recognition.

ice-drift and deformation experiments

Analysis of the Seasat imagery has revealed numerous eddies and complex deformation patterns within the pack ice. The SIR-C imagery should expand this data set, thereby providing modelers with an improved understanding of scales in sea-ice deformation, as well as providing valuable experience in the application of image-analysis procedures to general ice-dynamics studies. Our only reservation here is that an 8-day mission may not prove to be long enough to observe a complete deformation cycle or the growth and decay of an eddy.

spatial variations in pack ice

It is known that structural characteristics of the pack ice, such as floe sizes, ridging patterns, and lead geometry, vary with season. It is also presumed that they vary spatially at a given time, although little information is available on the subject. In that the SIR-C SAR system, flown in a polar orbit, would provide a reasonable sample of both the Arctic and the Antarctic ice packs, a detailed examination of the imagery should finally allow definitive comparisons to be made of the ''tectonic style'' of regions such as the Beaufort Gyre as contrasted with the Trans-Polar Drift Stream (in the Arctic) and the Weddell and Bellingshausen Seas, near the Antarctic Peninsula, as contrasted with other Antarctic seas not influenced by a blocking landmass.

ice-margin eddies

Summer studies of the edge of the ice pack in the Greenland Sea, made during MIZEX, have revealed the presence of well-defined eddies near the ice edge that are clearly delineated in airborne SAR imagery. These eddies have also been observed by Seasat in the Beaufort Sea (Fig. 4-37). In that large wavelike patterns appear to be present in the passive microwave images of both Arctic and Antarctic ice edges during the winter, similar and perhaps even more striking eddy generation may well occur during the winter. SIR-C, flown in a polar orbit, would provide up to an 8-day sample of the numbers and

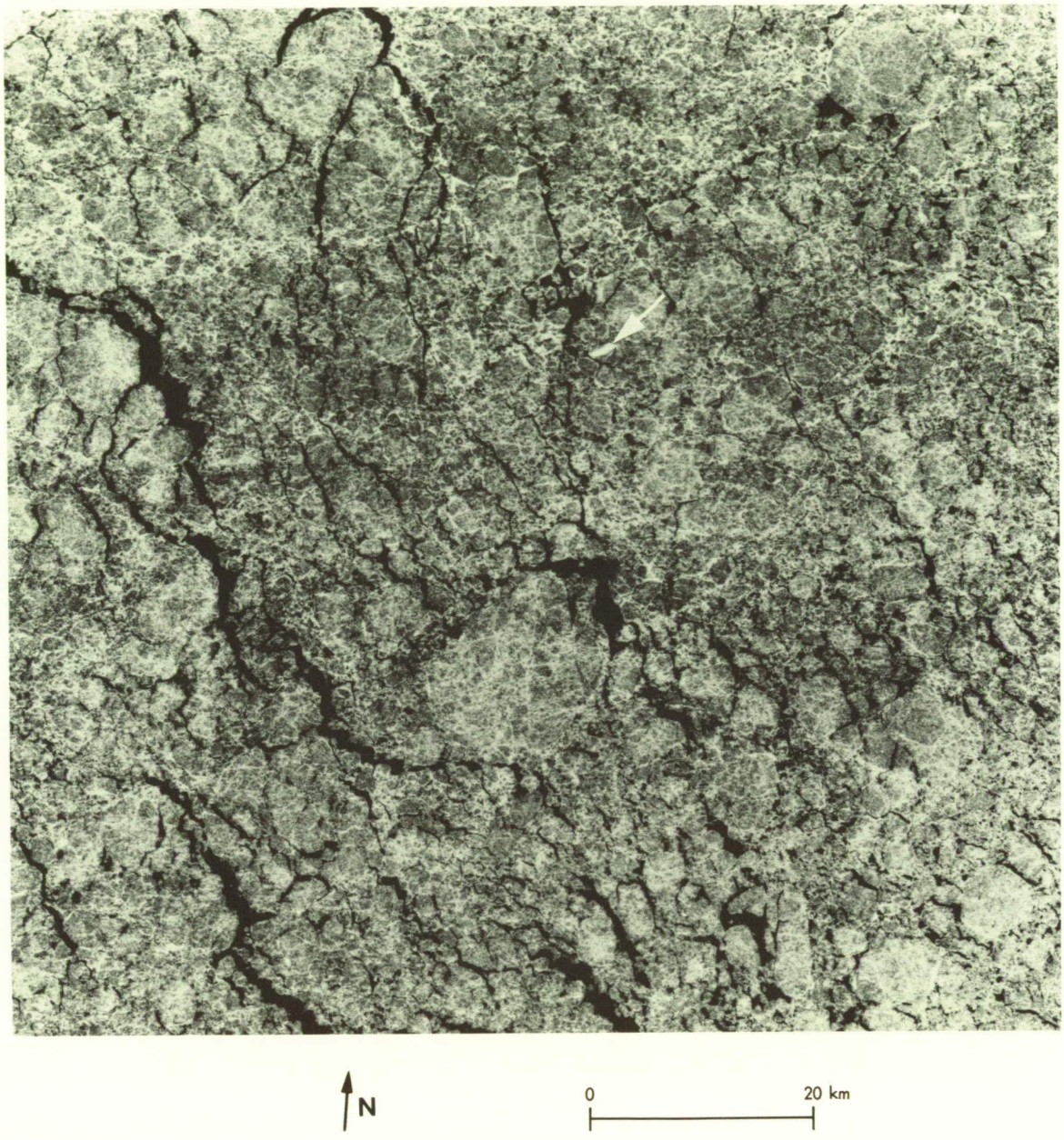

Fig. 4-34. Seasat SAR image of pack ice in the Beaufort Sea. The bright cigar-shaped object above the center of the image (arrow) is believed to be an ice-island fragment

sizes of the eddies that occur along the Arctic and the Antarctic ice margins. Admittedly, it will not provide the time series that is desired, but it will, nevertheless, result in a major improvement in our data base on this poorly understood phenomenon. Other possible experiments near the ice edge could investigate the interactions between waves and ice characteristics.

optimum radar parameters

Sea-ice radar parameters have been only partially explored up to this time. While it is known that nearly any image of the ice pack can be used with feature location and tracking for ice-velocity determination, the use of radar images to better classify ice types re-

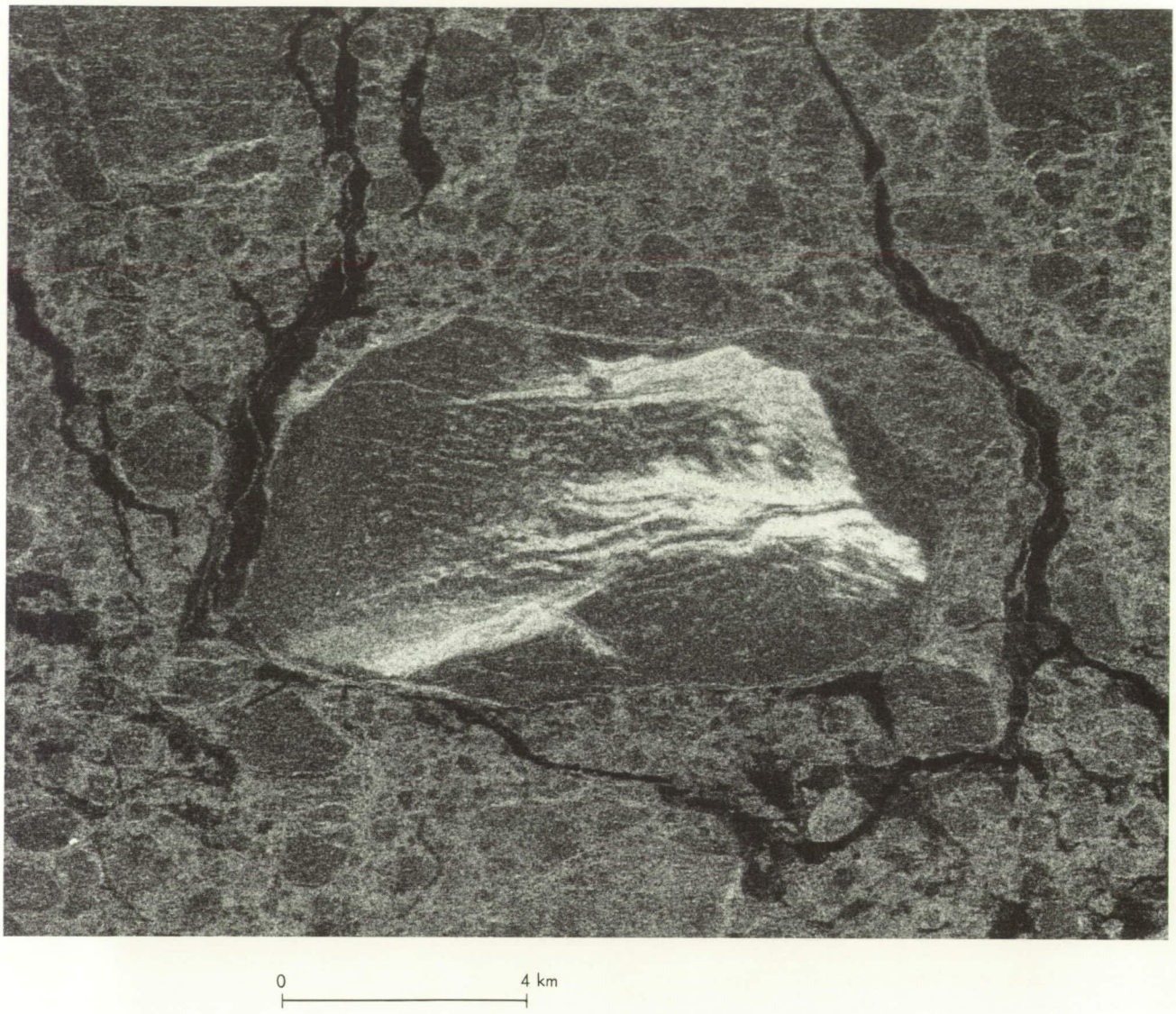

Fig. 4-35. Seasat SAR image of the ice island T-3

quires further study. The physical basis for examining backscatter-signal dependence on wavelength, polarization, and angle of incidence comes from the fact that many of the key differences in ice types are expressed in the geometry and chemical structure of the upper surface. The key differences are the density, salinity, roughness, crystal structure, and snowcover of the upper half-meter. These properties significantly affect the backscattered radiation. Since they also affect the penetration depth and the multiple scattering statistics, they should appear in the wavelength dependence and in the cross-polarization strength. A general impression of the variations in the return from sea-ice fields with changes in frequency and polarization can be obtained by examining Figs. 4-38 and 4-39. The breakdown of the ice cover by types, especially in the Arctic Ocean, is scientifically a very significant issue in that it relates to basic questions of how much ice there is and how it is formed and melted. Space-based passive microwave techniques have to date not proved able to develop this information to be the degree of accuracy desired. Imaging radar with its fine resolution and strong ice-type sensitivity is a logical candidate for the job. It now

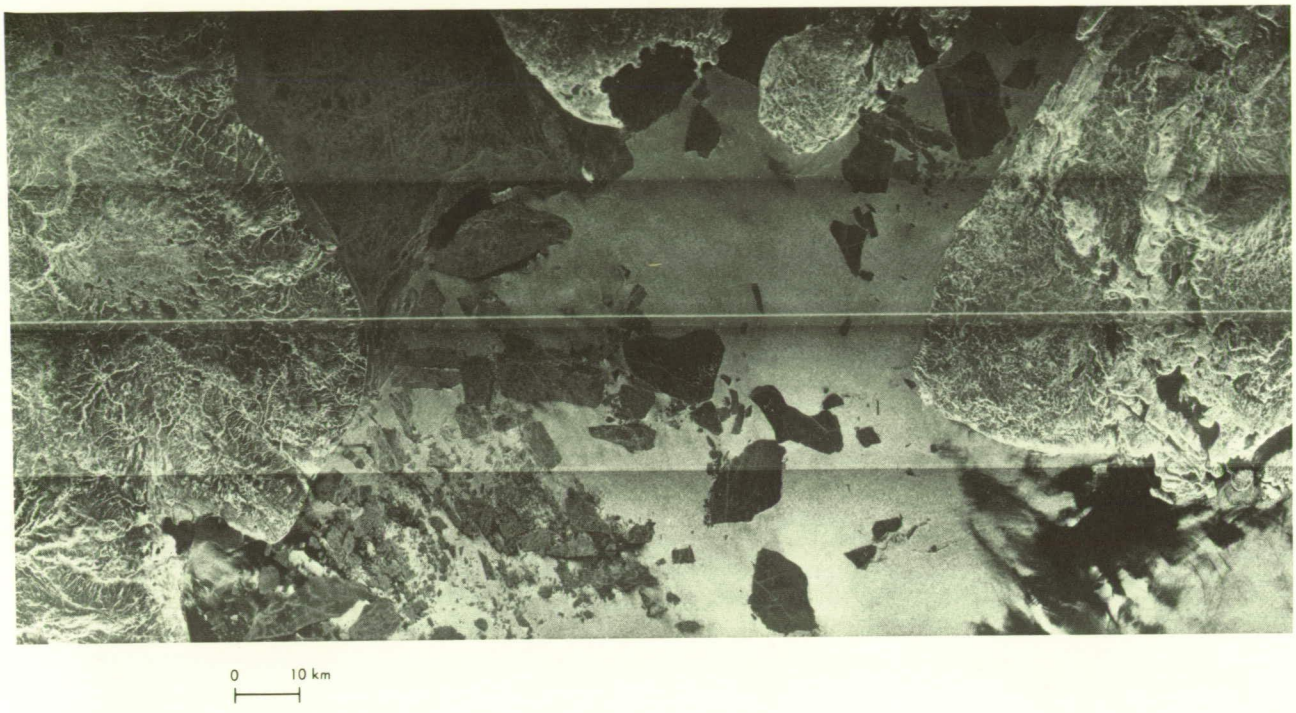

Fig. 4-36. SAR image showing the breakup of fast ice in the vicinity of Banks Island (left of image) and Prince of Wales Strait, Canadian Arctic Islands. Note the numerous features identifiable on generally low-return (undeformed) fast ice.

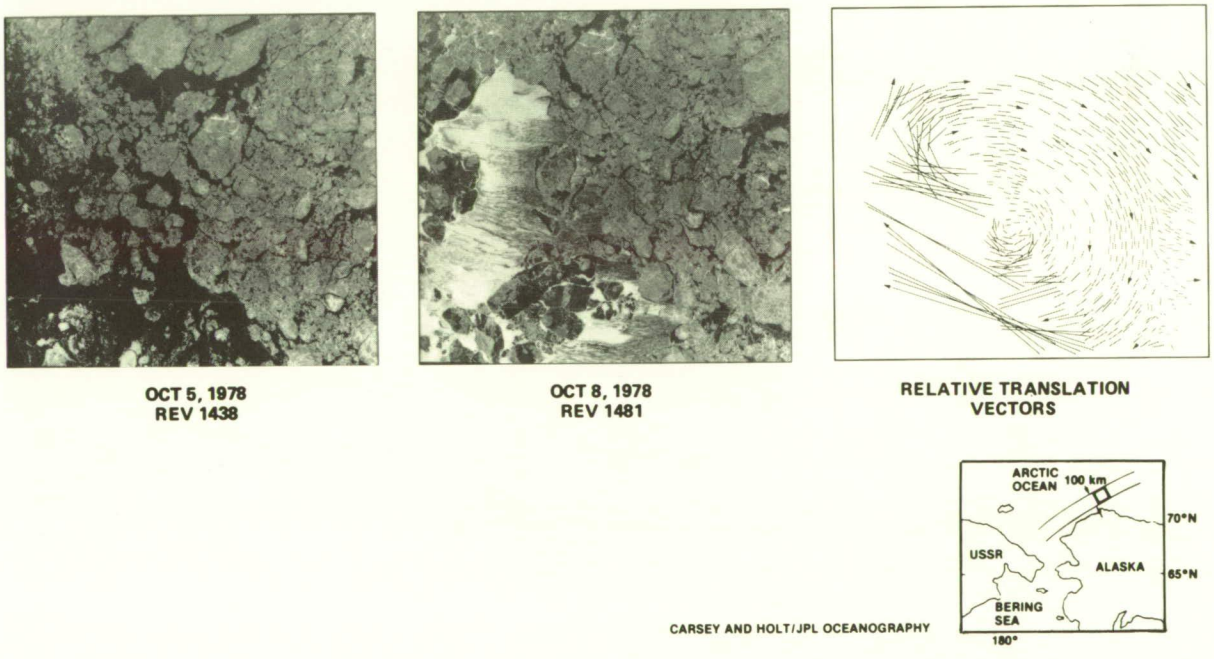

Fig. 4-37. Seasat SAR images that reveal an eddy in the ice near the ice edge in the Beaufort Sea

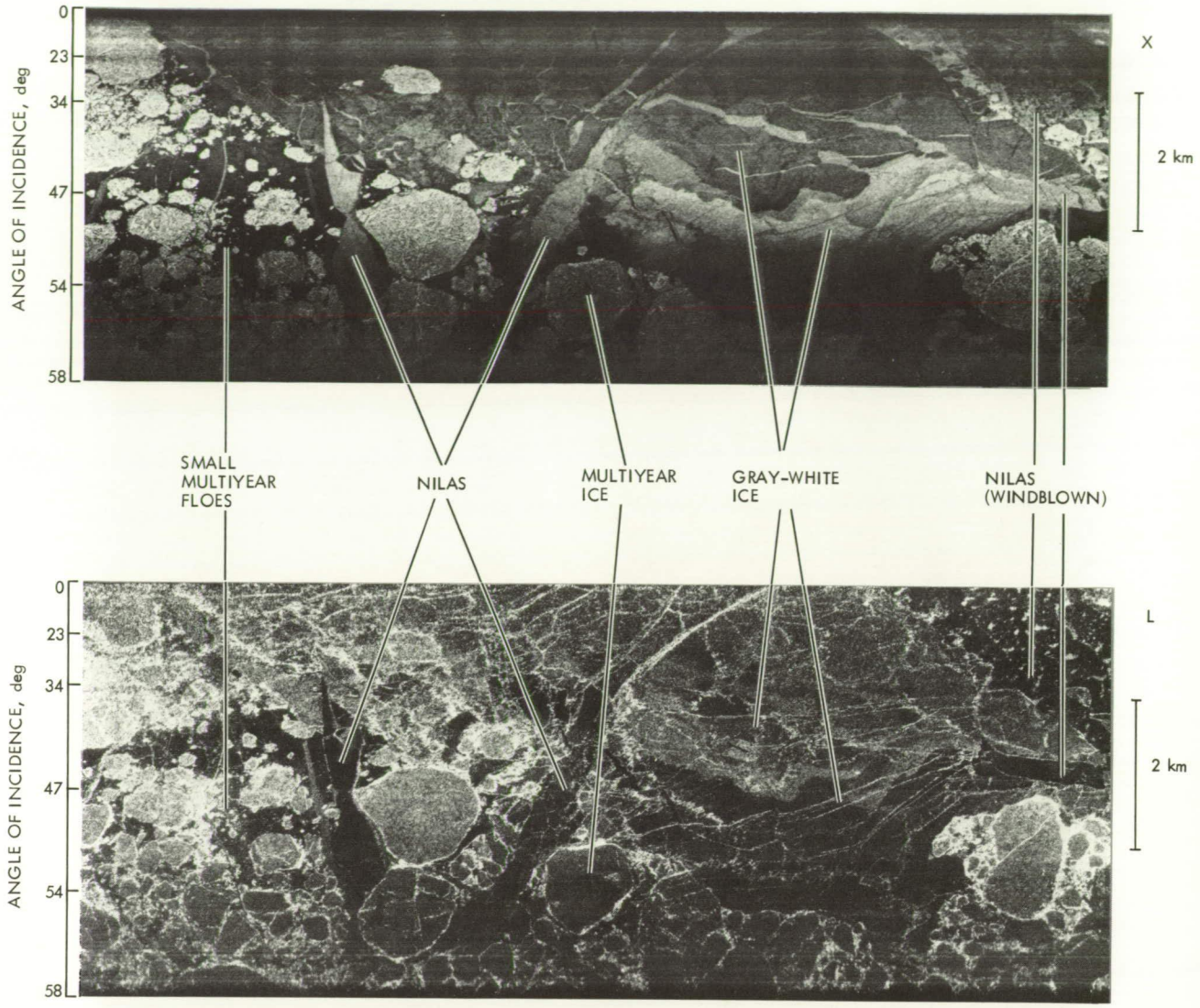

Fig. 4-38. X/L-band comparison of pack ice (data courtesy of Lawrence Gray, Canada Centre for Remote Sensing). X-band is at the top and L-band at the bottom.

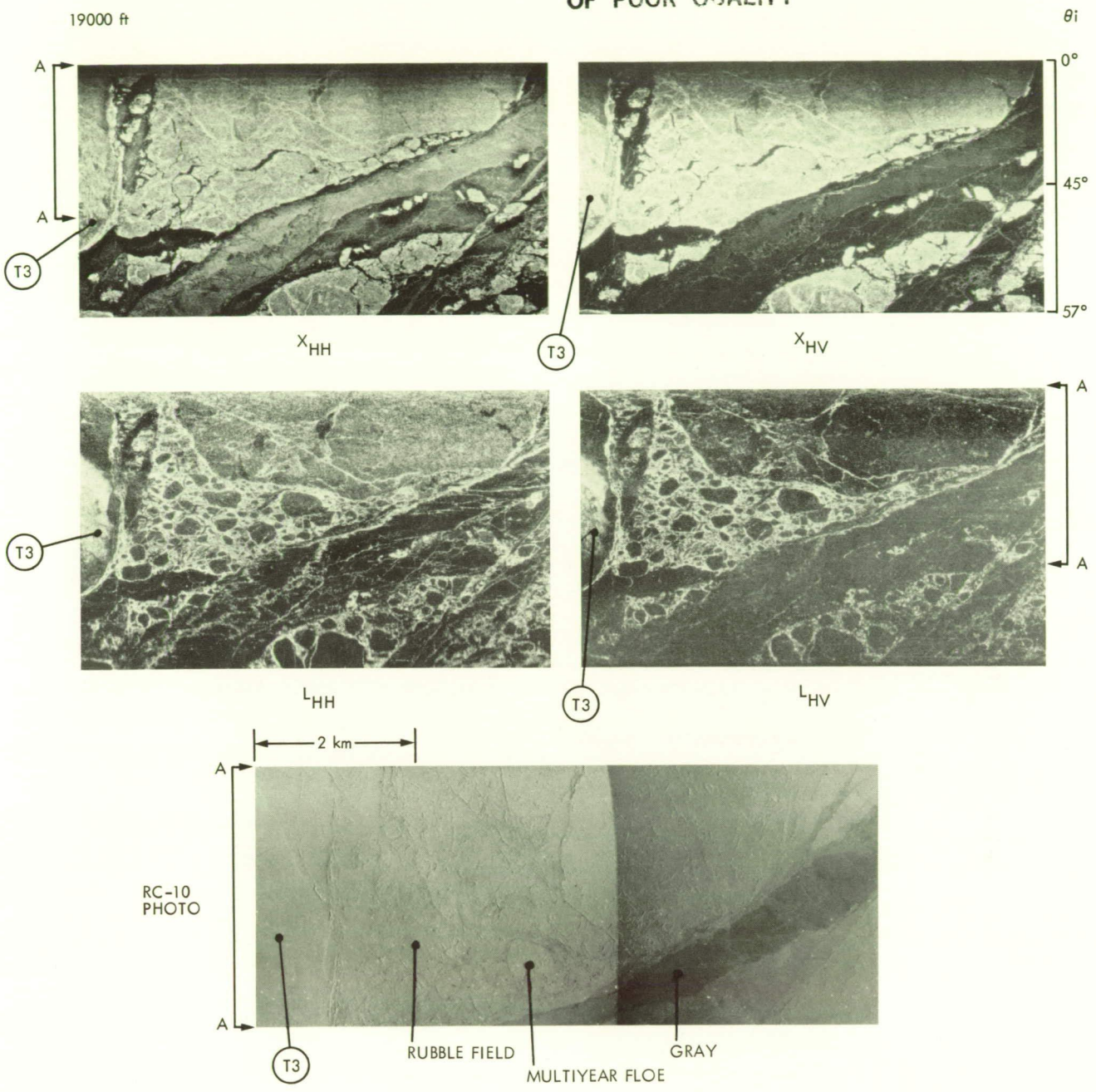

Fig. 4-39. Variations in SAR imagery of sea ice, with changes in polarization (data courtesy of Lawrence Gray, Canada Centre for Remote Sensing)

appears that frequency, angle of incidence, and polarization dependence may be key pieces of information in resolving not only this problem but also the problem of unequivocally distinguishing between thin ice and open water under all conditions and during all times of the year. SIR-C will be a most useful tool in this regard.

4.5.5.2 Lake Ice

lake-ice feature verification

The problem of providing high-quality ground-truth for the interpretation of SAR imagery from lake ice is, in a way, similar to that of providing ground-truth for sea ice. However, it is more difficult, in that in sea ice the roughness of the ice–water interface does not contribute to the strength of the return as it does in lake ice. Therefore, to adequately characterize lake ice for radar interpretation, a detailed specification of both the upper and lower ice surfaces is required, as well as information on the distribution of internal scatterers within the ice. If such observations are coupled with photographic underflights associated with SIR-C overpasses and an ice-coring program to examine internal scatterers, a major advance in the understanding of the radar returns from lake ice should result.

arctic coastal-plain lake bathymetry

Detailed studies of radar returns from shallow lakes along the Arctic coastal plain have shown that the strength of the return correlates with whether the ice is frozen to the lake bed (weak return) or is free-floating (strong return). Inasmuch as lake-ice thicknesses on the North Slope are reasonably constant, changing slowly with latitude, a few lake-ice thickness measurements coupled with SIR-C SAR imagery could provide bathymetric information on the innumerable shallow lakes on the coastal plain, in that the location of the strong-return/weak-return boundary corresponds to a water depth equal to the ice thickness. Also, if the imagery could be obtained at the time of maximum ice thickness, it would be possible to identify lakes that are suitable as year-round water supply sites.

lake- and river-ice operations

As is well known, lake and river ice development in constricted areas is the cause of a wide variety of problems associated with an extended winter navigation season on the St. Lawrence Seaway–Great Lakes and on the Ohio and Mississippi River systems. In the past, on Lake Erie, ice reconnaissance with SLAR systems proved to be extremely helpful in dealing with a variety of such operational problems. SIR-C will provide an opportunity to compare ice charts prepared from a satellite-borne system with those resulting from the analysis of aircraft imagery. Depending on the exact timing of the Shuttle mission, it may also be possible to couple ice conditions as seen by radar from space to ice conditions as seen from the bridge of a freighter transiting the lakes.

SAR and lake-ice dynamics

On many large lakes, there is an ice pack that drifts and deforms under the influence of winds and currents for at least a portion of the freezing season. Although the general physical processes are similar to those occurring in sea ice, the ''constants'' associated with the different processes are commonly quite different. The SIR-C imagery could provide a detailed data set on ice drift and deformation against which a variety of scattering model calculations could be compared and techniques for studying ice dynamics tested.

4.5.5.3 Ice Shelves, Ice Sheets, and Alpine Glaciers

ice-shelf and glacier boundaries

Although it is commonly believed that the location of the borders of such slowly varying entities as ice shelves and glaciers is well known, this is not necessarily the case. For instance, in the Antarctic much of the coast is composed either of ice shelves or of non-grounded glacier termini that discharge directly into the sea. In the past, a number of instances of large ice masses (on the order of 50 to 100 km in diameter) calving into the sea have been reported. The exact times of these calvings are commonly not known (more that within a several year interval). The same lack of knowledge applies to the drift tracks of the icebergs once they leave their region of birth. In that SIR-C, flown in a polar orbit,

would provide multiple passes over the margins of the Antarctic continent, the resulting imagery would provide a valuable delineation of the boundaries of the ice shelves as well as the numerous glacier termini that border directly upon the ocean. This "map" can then be compared with similar spotty observations acquired during the past decade by Landsat in order to assess changes in the ice boundaries with time.

A related problem in the Northern Hemisphere is the calving of tabular icebergs (the so-called ice islands) from a relict ice shelf located along the north coast of Ellesmere Island, the northernmost island in the Canadian Archipelago. The SIR-C data set should, at the least, provide an up-to-date map of the edge of this shelf.

icebergs and ice islands

As has been well known since the sinking of the Titanic, even small icebergs can pose a major hazard to the largest ships. This problem will become particularly pressing if the marine routes that have been proposed for transporting oil and gas from the Arctic are developed. Similar concerns apply to ice islands drifting hidden in the pack ice of the Arctic Seas, in that they pose a failure threat to production drilling structures that will soon be in place on the margins of the Arctic Ocean. Icebergs and ice islands are also of interest in their own right, in that their drift tracks provide us with information on the currents and winds in regions such as the Southern Ocean, where such information is generally lacking. The SIR-C data set, from a polar orbiting mission, would allow the first census of the numbers, locations, sizes, and shapes of ice islands in the Arctic Ocean and of glacier and shelf icebergs off the Antarctic continent. The former data set can be used to make reasonable estimates of encounter probabilities with offshore structures. In addition, the iceberg estimates in the North Atlantic, based on SAR, can be compared with similar estimates developed by the International Ice Patrol, using aircraft. This should be very informative in improving our understanding of the iceberg sizes and shapes (if any) that SIR-C may not see. Also, as icebergs commonly project well above the surrounding waves and sea ice, the application of shadow identification procedures and stereo-SAR should be explored. In that icebergs and ice islands are fresh ice, the radar backscatter properties are very different from sea ice. Canadian aircraft radar data indicate that L-band data may penetrate icebergs and scatter from the ice–water interface, thereby producing a bright return slightly displaced on the image. The C-band data do not show this. Available data also indicate that iceberg detection is strongly dependent on angle of incidence. Simultaneous data at different frequencies, polarizations, and angles of incidence will clearly be very helpful in studying this problem.

The use of SAR imagery in the investigation of the behavior of large ice shelves and ice sheets has been inadequately explored. The SIR-C imagery should be examined very carefully in this regard. Fortunately, because large ice sheets and shelves change slowly, most ground-truth observations could be made as long as a few months after the SIR-C mission.

ice-stream delineation

One possible observation of interest is the delineation of ice streams within the Ross Ice Shelf. Recently, it has been discovered that the Ross Ice Shelf (an Antarctic ice feature approximately the size of Texas) contains streams of rapidly moving ice within a more slowly deforming ice matrix. As these ice streams contain many large crevasses, it may prove possible to map them accurately with SAR imagery. The possibility of using movements of crevasse patterns to estimate surface flow velocities should also be explored, as should the use of both active and passive radar transponders placed on the ice surface as reference points to measure surface velocities. Such techniques could prove extremely attractive, in that the transponders would presumably still function after burial beneath the snow. Again the wavelength and polarization dependence of the scattering is expected to be strong in that the scattering occurs off the ice grains within the ice mass.

alpine glaciers

In 1978, Seasat collected data on many glaciated regions around the world. Particularly good coverage was obtained of the glaciers in the Alaskan Range (see Fig. 4-40). In addition, SIR-A observed a number of low-latitude glaciers in 1981. SIR-C now offers the possibility of examining the changes in ice extent, in crevasse patterns, in the distribution of morainal material, and in ice-surface roughness that have occurred over a 10-year (Seasat) and an 8-year (SIR-A) period. Also, as the backscattering mechanisms in alpine glaciers are still not well understood, an interesting experiment could be developed taking advantage of the multiple frequencies, multiple look angles, and variable polarization afforded by the SIR-C system. A reasonable approach to this problem would be to select a limited number of "accessible" glaciers, for which Seasat or SIR-A imagery is available, and develop an appropriate ground-truth program that would be based in part on the examination of this existing data set.

4.5.5.4 Snow

seasonal observations of snowpack

The possible timing of the SIR-C launch during midwinter in the Northern Hemisphere offers the opportunity at C-band and X-band for useful observations of the seasonal snow pack, as discussed earlier in Section 4.3.5.4. Based on a knowledge of the snowpack distribution during the SIR-C mission, the exact times of overflights, and the meteorological conditions in different areas, a snow-sampling program could be marshalled to provide a ground-truth base of direct snow observations tied in both time and space to the SIR-C data. Also useful would be comparative studies of snow properties as estimated from the passive microwave imagery that will be obtained by the Scanning Multichannel Microwave Radiometer (SMMR) system on Nimbus-7 and the Special Sensor Microwave Imager (SSM/I) system on the Defense Meterology Satellite Program (DMSP) satellite.

The SIR-C mission can provide the necessary understanding and data base required to extract the maximum amount of geophysical information on the snow and ice masses in the Northern Hemisphere from the several radar satellites that are planned for launch in the early 1990's. Its role may prove to be even more important in the Antarctic, in that, when flown in a polar orbit, it will provide the only multiparameter SAR data on this vast area until either proper receiving stations are installed in the region or improvements are made in SAR data storage and transmission capabilities, so that data obtained from the Antarctic can be retrieved with a line-of-sight communication link.

4.5.6 Summary of SIR-C Mission Requirements for Ice

need for well-planned field observations

To obtain the maximum utility from the SIR-C data for glaciology research, it will be necessary to couple it with a well-thought-out series of *in-situ* field observations. Historically such observational programs have been carried out by a multinational group of investigators supported by a variety of agencies in a manner somewhat similar to the supersites envisioned in this report. The same situation will undoubtedly hold during the SIR-C mission. Although it is impossible to exactly specify supersite locations at the present, possibilities for the polar-orbiting-mission include the Beaufort Sea north of Deadhorse or Barter Island, the Greenland Sea during the time of the WINTER-MIZEX, a U.S.-Canadian site in North Baffin, and the Weddell Sea during a cruise of the *Polar Stern* or a U.S. ice breaker. Whatever sites are selected, it is essential to have good logistic support to allow investigators to get to ice features of interest. It is also necessary to have the capability of getting SAR imagery to the investigators in the field in near real time so they can use the imagery to identify features of interest. If it proves impossible to provide the

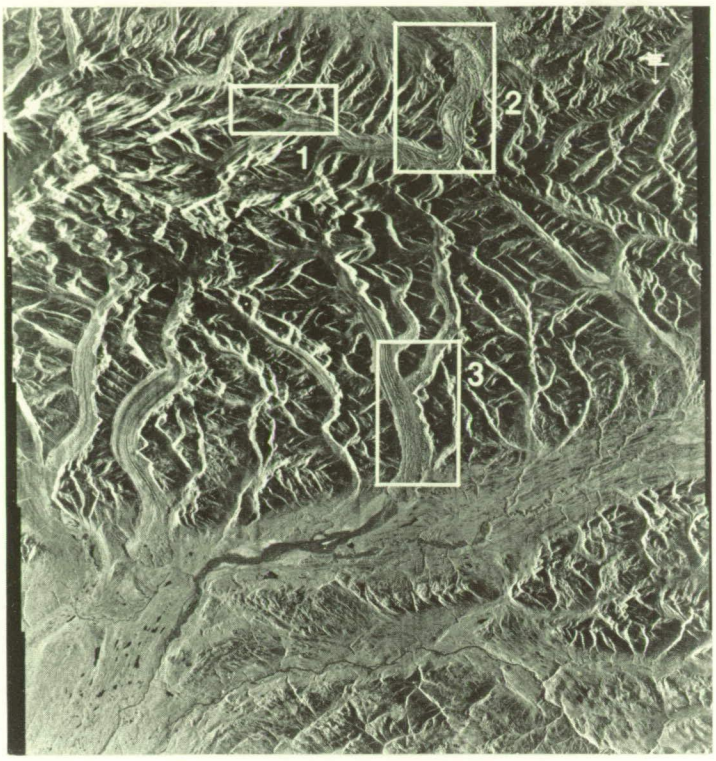

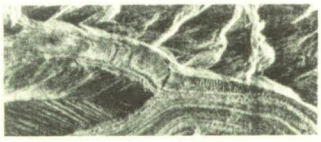

Fig. 4-40. Seasat SAR image of the Alaska Range, Alaska

field teams with SIR-C SAR within 2 days or less of the satellite pass, it will be necessary to carry out satellite under-flights with an aircraft-borne SAR system. If this proves to be necessary, it will be desirable to also obtain passive microwave and scatterometer measurements as well as high-resolution photography. Field measurements on the large continental ice sheets are not so logistically demanding, as these entities change very slowly. Therefore, field sites could possibly be visited several months after the satellite mission.

4.5.6.1 Orbital Parameters

need for near-polar orbit

Many glaciological studies of both sea ice and ice sheets require an orbit inclination between 78° and 102° (inclinations in the high 80s would allow observations of the fast-moving ice streams in the Ross Ice Shelf) and will therefore require flying SIR-C in a polar orbit. However, many of the studies described here could be undertaken using SIR-C data from a 57° inclination orbit. A nearly frozen orbit allowing variable incidence angles over the same sites would be useful. The specific inclination will influence the location of the supersites, since it would be desirable to have sea-ice motions generally parallel to the satellite ground track to maximize the length of time that a given floe could be tracked.

4.5.6.2 Mission Timing

need for two flights

Two SIR-C flights, six months apart, are optimum. The optimum periods are late February through April (Arctic winter) for the first flight and early July through mid-October (melt season through freeze-up) for the second flight. The ideal times during these periods would be late March through April for the first flight (February through early March is dark, very cold, and generally operationally difficult) and either August (maximum melting) or the first two weeks of October (freeze-up) for the second. The exact time of day is not important.

4.5.6.3 Swaths and Resolutions

Since SIR-C is both a research and a mapping mission, there is, for glaciological research, a preference for high resolution even at the expense of swath width.

4.5.6.4. Frequencies, Polarizations, and Incidence Angles

need for at least 5 bits

L-band and C-band (and, if available X-band) data will be very useful in improving our understanding of the nature of the varied scattering processes occurring within snow and ice covers. Useful polarizations include HH, VV, and cross-polarization, plus a measurement of the phase difference between the HH and VV channels. We also require the highest bandwidth that is feasible and at least 3 and preferably 4 channels of data to obtain the simultaneous use of frequency and polarization information. Five or preferably more bits of data are required to obtain dynamic range commensurate with the range of scatterers in the scenes. The use of Block Floating Point Quantization appears to be permissible. In general, the radar parameters suggested for SIR-C appear to be adequate for useful glaciological studies.

4.5.6.5 Data Products

need for relative calibration of 1 dB

The desired quality of the data obtained is determined by the range of backscatter observed on natural ice features of interest. As the range of backscatter from many ice features is within 10 dB, a relative calibration to within 1 dB would be necessary. The images should be geometrically corrected to map-correct format. Absolute data registration at sites far from distinguishing coastal features should be accurate to within 1 km for studies of ice dynamics, and relative registration to within 100 m would be useful. In coastal zones where distinguishing features are available in the imagery, registration should be at the resolution scale. It would be very desirable to have an automatic positioning system on-board the Shuttle to aid in these problems.

4.6 Oceanography

4.6.1 Background

hostile observational environment

The region near the ocean surface represents one of the most hostile environments on earth for scientific measurements. Yet it is through the ocean surface that fluxes of momentum, heat, and moisture flow between ocean and atmosphere. Systems to measure the surface signatures of these important interactions, as well as signatures of processes occurring beneath the surface, can provide vital information needed for the construction and testing of ocean and air–sea interaction models.

The geophysical phenomena of interest, however, span a wide range of spatial and temporal scales, and require frequent, high-resolution measurements covering large geographic areas for long periods of time. Such data can be acquired only from satellite-mounted instruments.

Potential applications of spaceborne SAR to oceanography and meteorology have now been amply demonstrated with both the Seasat and SIR-B data sets [2-3. 4-6]. Among the many potential oceanographic applications, SAR appears to hold great promise in the following areas.

4.6.1.1 Ocean-Wave Forecasting

inadequacy of wind-wave forecast models

Present wind–wave forecast models are generally inadequate for reliably predicting the surface-wave directional energy spectrum. Major questions exist both in properly specifying the input wind fields and in the associated growth and wave–wave interaction physics. Present theories are based primarily on directionally integrated spectral measurements. There have been few opportunities to verify and refine models with reliable measurements of directional wave spectra. Consequently, many forecast models are in gross disagreement, especially in cases of turning or growing winds, which are of the highest interest.

4.6.1.2 Internal Wave Physics

internal wave refraction at current boundaries

Although internal wave packets are fairly ubiquitous in SAR imagery along continental shelves, they are also occasionally observed in the deep ocean, presumably associated with bathymetric features, such as sea-mount chains. Internal wave patterns provide a natural test-bed with which to refine and extend SAR imaging theories. Moreover, internal waves, by virtue of their refraction at current boundaries, can provide a vehicle for the delineation of mesoscale- and submesoscale-current features. Our understanding of SAR internal wave imaging is likely to foster algorithm development in other geophysical problem areas.

4.6.1.3 Currents, Fronts, and Eddies

undetected mesoscale eddies

One of the major unsolved problems of oceanography is that of large-scale heat and mass transport. Such large-scale transport profoundly influences life on the earth and greatly ameliorates the polar-temperature extremes by carrying heat from the equator toward the poles. It is now widely recognized that the mesoscale variability can have energy levels one or more orders of magnitude greater than the mean flow. Vast regions of the ocean apparently are filled with mesoscale eddies, most as yet undetected and uncharted.

4.6.1.4 Bottom Signatures

Although Seasat was able to sense bottom signatures in a few cases, the environmental conditions for optimum surface modulation from these features is not yet understood. If reliable mapping of bottom features is possible, an inventory of sometimes rapidly changing shoals would be possible on a global basis.

4.6.1.5 Spatial Variability of the Wind Field

Conventional measurements of the surface wind field are limited to single-point temporal records, which are extremely sparse for most of the ocean. The instantaneous spatial variability of the wind field might be a key ingredient to further refinement of wind–wave generation models, which usually assume spatially homogeneous wind fields.

4.6.2 Role of Spaceborne Remote Sensing in Oceanography

understanding the behavior of short gravity waves

Previous spaceborne SARs have revealed a large variety of atmospheric and oceanic phenomena on all spatial scales from 25 m to 100 km. However, because SAR is sensitive primarily to the structure of the short gravity waves on the ocean surface, the extraction of quantitative geophysical information from oceanic SAR data is critically dependent upon understanding the behavior of the short waves—in particular, their generation and modulation by winds, long waves, and currents, and their interactions with microwave electromagnetic radiation. The relative importance of the various scattering mechanisms, and

how they act to produce or distort the final SAR image, will be one of the central future-research questions addressable using SIR-C data. Simultaneous *in-situ* measurements of short waves, long waves, winds, and currents will provide a basis for constructing and refining models relating short-wave characteristics to the larger-scale geophysical quantities of interest.

Over the past two decades, a number of spaceborne remote sensors have demonstrated their unique value for oceanography. The early Tiros and later Nimbus visible and infrared imagery has become a vital ingredient in routine weather forecasting. The geosynchronous GOES imagery provides temporal sequences of cloud cover on a global scale. Similar multi-spectral sensors, such as the Coastal Zone Color Scanner, have provided remarkable delineation of coastal fronts and eddies. In the last decade, the Seasat complement of active and passive sensors has been expanding our knowledge of global wind fields, mesoscale circulation dynamics, and the spatial evolution of wave spectra. In the coming decade, many of these prototype sensors will evolve into operational complements on missions such as NROSS, TOPEX, and ERS-1. It is clear that remote sensing will play an increasingly vital role in global-scale ocean problems, particularly in establishing surface boundary conditions with which to initialize, refine, and update global predictive models of wind, wave, and current fields.

4.6.3 Role of Imaging Radar in Oceanography

advantages of SAR

The microwave imaging radar is the only instrument with the capability to acquire all-weather measurements of ocean-surface conditions and to provide the high-resolution and wide-spatial coverage necessary for addressing the geophysical problems listed in Section 4.6.1. Because SAR is primarily sensitive to the structure of the short gravity waves on the ocean surface, the extraction of quantitative information is critically dependent upon our understanding short-wave behavior, in particular how short waves are generated and modulated by winds, long waves, and currents. If the short waves are either deterministically or statistically describable, there is a good likelihood that quantitative physical ocean parameters will ultimately emerge from SAR imagery. The scattering-mechanisms giving rise to ocean SAR images are similar to those used by scatterometers and altimeters to determine near-surface winds. Thus, increased knowledge of electromagnetic/short-wave interactions that is obtained from imaging radars with frequency and polarization diversity is directly usable for refining and optimizing other types of active microwave ocean-observing instruments.

4.6.4 Scientific Basis for SIR-C Ocean Experiments

coherent modulation of short waves by longer waves

A variety of SAR ocean-imaging theories have been advanced over the last decade, with each distinguished mainly by its assumptions regarding the spatial distribution and detailed motion of the scatterers. Most theoretical work assumes a two-scale scattering model, where the Bragg resonant short waves are simply tilted and strained by the longer waves, producing a short-wave spatial modulation which is coherently linked to the longer waves. However, the real ocean is a complicated ensemble of scatterers, some moving randomly, and others coherently linked to a variety of larger-scale phenomena, e.g., surface winds, waves, and currents. Moreover, scattering originates not only from Bragg resonance with the transmitted radiation, but also from specular reflection and wedge diffraction mechanisms. Although Bragg resonance may be dominant at angles well off nadir, specular scattering can be important at these large angles of incidence, especially for broad surface slope distributions such as are associated with high sea states or localized wave breaking.

A cogent theory for SAR imaging of the ocean is not yet available. Ocean imaging is complicated by the sometimes significant motion of the scatterers during the SAR integration time. Because it is dependent upon an accurate measurement of target radial velocity to determine azimuth position, the SAR will interpret any scatterer radial motion as a change in position. For example, a scatterer with radial velocity v_r will produce an azimuth displacement

$$x_a = (R/V) \quad v_r$$

advantage of lower altitudes for SAR imaging of ocean

where R/V is the range-to-velocity ratio of the platform. For Seasat, $R/V \approx 130$ s; for both SIR-B and SIR-C, R/V $\approx$ 35 s at the Seasat angle of incidence of 20°. Consequently, ocean motion effects in the Shuttle SARs should be nearly four times less severe than they were in Seasat, for the same angle of incidence. This improvement may be critically important in some ocean applications, particularly in the imaging of long gravity waves.

Advances in SAR ocean-imaging theory will emerge only from well-conceived and well-executed experiments. In general, such experiments will involve techniques for directly measuring or indirectly inferring the relevant scatterer velocity distribution in the presence of various oceanographic phenomena of interest. The experiments should, of course, be conducted coincidentally with the SIR-C overflights, and over a wide range of environmental conditions.

Because of the lack of well-controlled supporting experiments, Seasat SAR ocean data are largely descriptive in nature. SIR-A, with its high off-nadir angle of incidence, was not optimized for most ocean applications. However, SIR-B had much more flexibility. In spite of the reduced scope of the SIR-B mission, a number of significant ocean experiments were conducted in several regions of the world. The SIR-B experiments are still in an early stage of analysis, but it is already clear that the variable angle of incidence and the high-quality digital data will begin to resolve some of the longstanding issues in SAR oceanography. SIR-C and later SIR-D, with their ability to provide multifrequency and multipolarization data, will represent additional major steps toward the optimal definition of future SAR oceanographic missions.

4.6.5 SIR-C Ocean Experiments

Several broad categories of SIR-C ocean experiments are suggested in the following and are summarized in Table 4-6. However, this list is merely suggestive of what is possible and is not meant to be all-inclusive.

4.6.5.1 Ocean-Wave Forecasting

SAR can provide global wave directional spectra

The collection of global wave spectra is one of several rationales for flying an orbital SAR. By themselves, these spectra would be of little value, but as a supplement and periodic update to a global wind–wave forecast model, the impact of actual measurements of directional spectra could be revolutionary. For example, present wave-generation models in operation around the world are in gross disagreement with respect to the directional properties of waves generated from even the simplest wind fields. The behavior of ocean waves in the presence of turning and sometimes adverse wind fields, e.g., the active region of a hurricane, has been a particularly difficult problem, with few directional spec-

Table 4-6. Some SIR-C oceanography experiment classes

Experiment class	Scientific objective
Ocean-wave forecasting	Directional wave energy spectra, supplement to global wind–wave forecast models
Internal waves	Understanding wave–current interactions
Currents, fronts, and eddies	Detection of current-system boundaries, oceanic fronts, and mesoscale eddies; extraction of surface currents directly from Doppler spectrum
Bottom signatures	Relationship of ocean-bottom features to surface expressions, direct detection of surface gravity wave field, studies of nonlinear interactions between subsurface currents, surface gravity waves, and Bragg waves
Wind signatures	Correlation of surface-wind magnitudes to absolute backscatter

tra measurements available. There are no good data on the large-scale directional evolution of wind-driven waves, and therefore no valid criteria for the acceptance or rejection of particular wind–wave generation models.

In addition to its purely scientific value, timely knowledge of the directional wave spectrum is of practical importance to operational wave forecasting and ship routing. Over the long term, such measurements will be useful in both local and global wave climatology, with practical applications in offshore tower design and coastal erosion research. Moreover, there is some evidence that crude estimates of simultaneous directional wave spectra may be necessary to further refine scatterometer model function algorithms.

production of periodic modulation of local wind-generated short waves by long waves

Long surface waves are visible because they produce an apparent periodic spatial modulation of the local wind-generated 30-cm waves. The modulation may be much less than the noise on the scale of a single 25-m-resolution element, but the spatial spectrum of the wave field is generally well-behaved and homogeneous over tens and even hundreds of kilometers. Extensive averaging over both wavenumber and space, therefore, can reduce a very noisy background by as much as a factor of 30, revealing extremely subtle modulations of only a few percent. For example, Fig. 4-41 shows the spatial evolution of the dominant wavenumber of a swell system over a 900-km pass. The significant wave height of the swell system was under 1 m. With appropriate filtering, the spatial evolution of the dominant-vector wavenumber can be tracked with mean residuals of only a few percent. This particular spatially evolving swell system clearly shows deep-water dispersion, refraction in the Gulf Stream, and shallow-water wavelength shortening. Moreover, subtle perturbations of the wavenumber in shallow water reveal the presence of subsurface sea mounts and depressions. The spatial evolution of the wavenumber can be used to accurately locate the origin of wave-generation sources.

decreased sensitivity in azimuth direction

A number of significant advances in our understanding of SAR ocean-wave imaging are necessary prior to defining an operational system. For example, it is well-established that the Seasat SAR lacked response in the azimuth (along-track) direction, especially during high sea states. Figure 4-42, showing a Seasat SAR directional wave spectrum during a particularly high sea state ($H_S \sim 4.4$ m), vividly illustrates the azimuth falloff problem. The explanation for this falloff is presently in dispute. For example, most models predict improvement in azimuth response at lower range-to-velocity (R/V) ratios. The relative im-

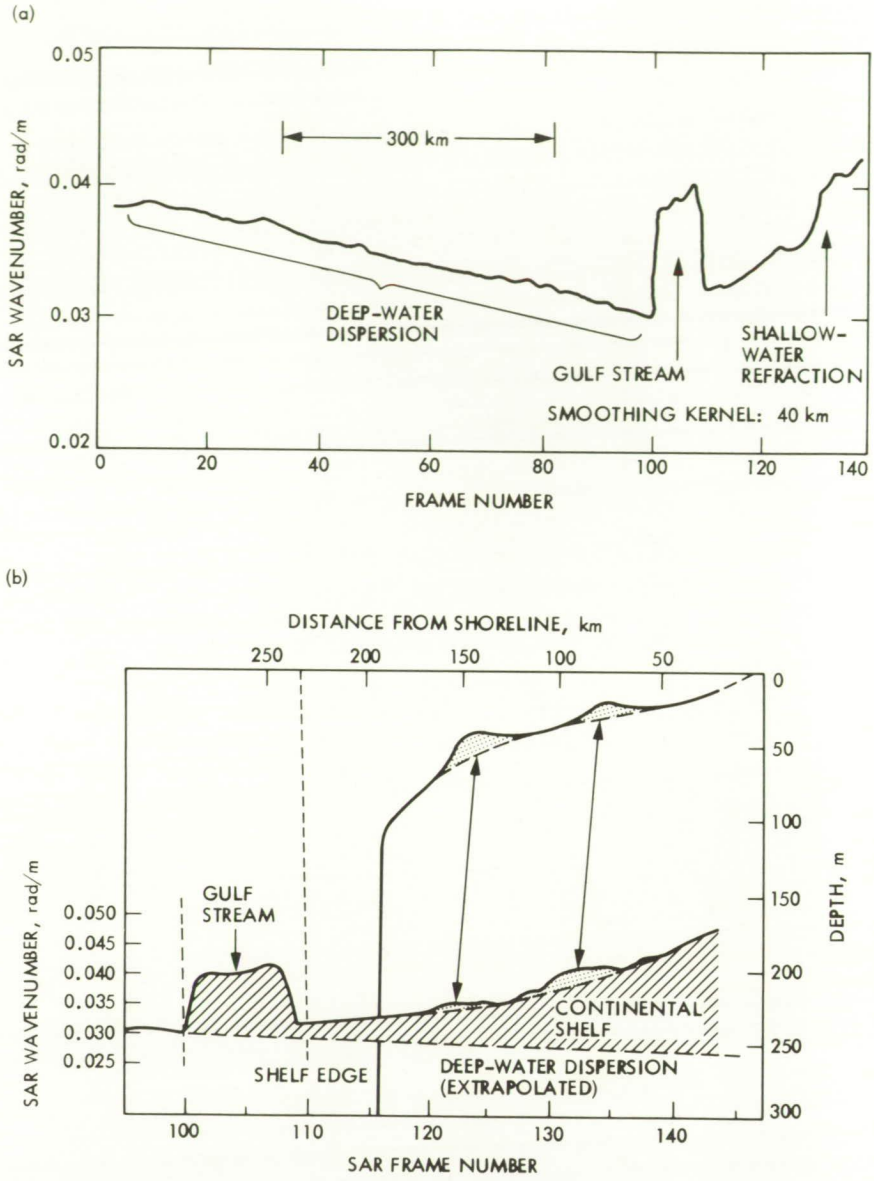

Fig. 4-41. Spatial evolution of a SAR-measured wavenumber over a 900-km Seasat pass: (a) the entire 900-km pass; (b) the northernmost 300 km

portance of instrument integration time, however, and the explicit dependence of the problem on local sea state remain controversial for lack of good experimental data. Moreover, there is no consensus yet on whether, and under what conditions, an estimate of wave energy can be extracted from SAR wave spectra. SIR-C, with its variable R/V (via angle of incidence) and multiple frequencies (therefore permitting variable integration time for comparable resolution), represents a valuable opportunity for designing experiments to distinguish among the various imaging models, and to establish the degree of uniqueness between the SAR-measured directional spectrum and the actual ocean directional spectrum.

ORIGINAL PAGE
COLOR PHOTOGRAPH

Fig. 4-42. Seasat azimuth wavenumber falloff in a high sea state; outer circle corresponds to a 50-m wavelength

4.6.5.2 Internal Waves

Numerous SAR images of surface features associated with oceanic internal waves have been obtained from Seasat, SIR-A, SIR-B, and aircraft surveys. Figure 4-43 shows tidally generated internal waves in the New York Bight, observed during the SIR-B mission. The linear features in the image are due to small-scale roughness changes induced by the internal-wave surface currents.

Dual-frequency (L- and X-band) observations of internal waves with an aircraft SAR exhibit distinct differences that have been attributed to wave–current interaction differences for short-wavelength gravity waves and capillary waves. Existing wave–current interaction theories have been found to adequately describe reported measurements of the short-gravity-wave (~30-cm) current response, but appear to underpredict the response of capillary (~3-cm) waves. These hydrodynamic results suggest that internal-wave images from an L-band SAR can be explained by known wave–current interaction phenomena, whereas

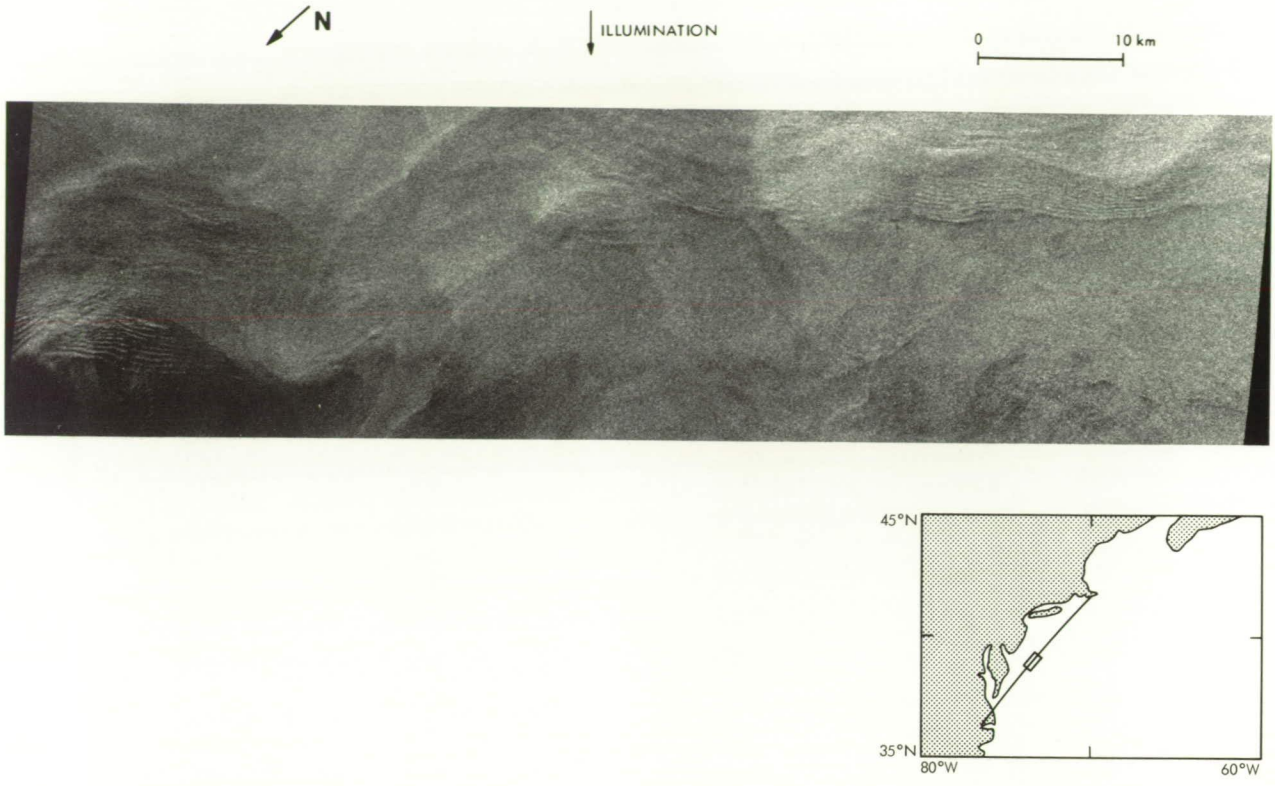

Fig. 4-43. SIR-B image of the New York Bight (Data Take 96.21)

X-band images might not agree with theoretical expectations. Research efforts using SIR-C should be directed to investigate these questions.

SIR-C sensitivity to currents, fronts, and eddies

The SIR-C experiment will be the first opportunity to obtain dual-frequency SAR imagery of internal waves from space. By varying the angle of incidence from 15° to 50°, the C-band Bragg waves will change from short gravity waves (11 cm) to near-capillary waves (4 cm). The corresponding L-band Bragg waves range from 45 to 15 cm. This large Bragg-wave variation with angle of incidence presents a unique opportunity to critically probe the hydrodynamics of wave–current interactions over a wide range of the spectrum and to elucidate the imaging processes underlying SAR signatures of internal waves.

4.6.5.3 Currents, Fronts, and Eddies

SAR sensitivity to currents, fronts, and eddies

SAR imagery from Seasat demonstrated that current-system boundaries, oceanic fronts, and mesoscale eddies can be detected via their influence on the short gravity waves responsible for L-band microwave backscatter. Figure 4-44 shows the strong expression of a Gulf Stream eddy from Seasat SAR imagery. The mechanisms by which a SAR detects these phenomena are not well understood. In at least some situations, it is likely that current gradients modify the spectrum of short waves, producing the microwave backscatter. In other instances, or perhaps concurrently, sea-state changes can also be induced by sea-surface temperature variations that alter the atmospheric boundary-layer stability, giving rise to local variations in wind drag. A third mechanism, azimuthal displacements in the SAR image plane due to Doppler frequency shifts from variable current components along the radar look direction, has also been advanced.

Seasat images of the Gulf Stream boundary and associated cold-core and warm-core rings are consistent with the first two mechanisms. Observations of mesoscale eddies provide additional evidence. Well-planned sea-truth experiments are needed in conjunction with SAR observations from space to make further progress in this area. The SIR-C mission can provide this opportunity; acquisition of dual-frequency SAR images should significantly enhance our understanding of the imaging mechanisms associated with these phenomena.

relation of surface currents to Doppler spectrum

Attempts have been made to extract surface currents directly from SAR Doppler spectrum information, with the hope of remotely measuring surface-current fields. This technique is based on the fact that the Doppler-spectrum centroid depends on the velocity of the scatterers along the line of sight of the radar. Reasonable success has been demonstrated by special processing of aircraft SAR data for currents ranging from 0.5 to 2.0 m/s. Satellite measurements present a greater challenge because the Doppler spectrum broadens due to the greater platform velocity, whereas the spectrum centroid shifts are only a few Hz for currents of interest. Research currently in progress may yield sufficiently accurate Doppler centroid estimates to warrant additional testing of this concept during the SIR-C mission. Again the dual-frequency and variable angle of incidence capabilities of the SIR-C SAR are important because the spectrum shift increases with increasing angle of incidence and decreasing radar wavelength. For example, the Doppler centroid shift at C-band and the 45° angle of incidence will be approximately 8 times larger than that observed by Seasat for a given surface current.

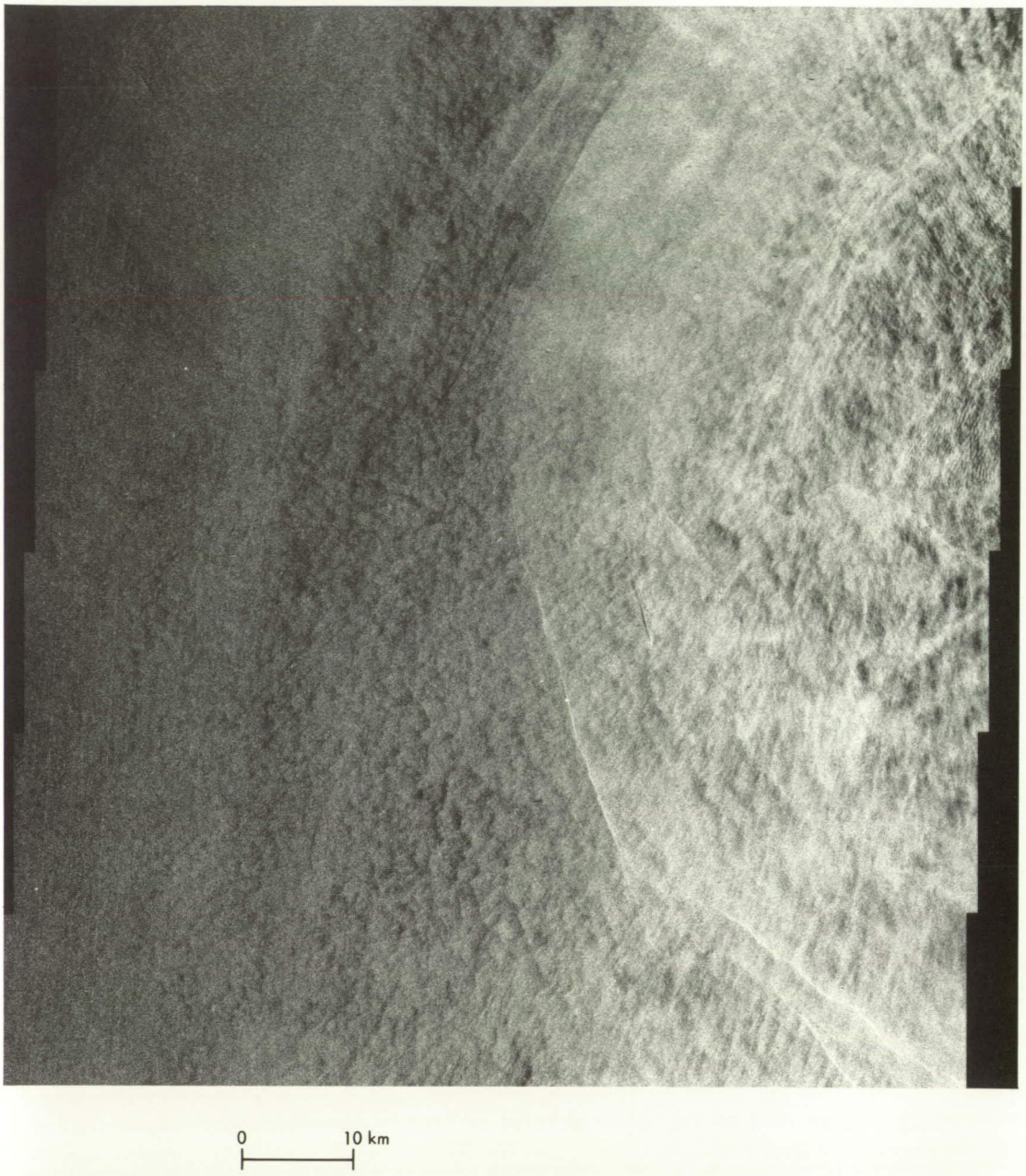

Fig. 4-44. SAR image of an area 100 km long, taken during a pass over the western half of a large warm-water ring less than a month before the ring began to merge again with the Gulf Stream. Warm ring boundaries, perhaps representing current shear zones, are particularly evident in radar imagery. The brighter radar signature inside the ring may be at least partially due to the increased surface drag at warmer temperatures

4.6.5.4 Bottom Signatures

A number of investigators have noted a variety of SAR-observed ocean-surface patterns that are closely related to submerged bottom features [4-16]. Figure 4-45 shows a striking example of a SAR signature that is clearly related to bottom topography. Even though radar wavelengths do not penetrate the ocean's surface, imaging radars (both real and syn-

Fig. 4-45. This Seasat SAR image of an area 100 km long, taken from above Nantucket Shoals, provides a dramatic example of bathymetric expressions occasionally evident over large areas. Most of the region included in this image is less than 40 m deep, a good fraction is less than 20 m deep, and portions are less than 2 m deep. The Island of Nantucket is at the upper left

thetic aperture) can detect bottom features due to interactions between physical ocean processes and the features, which result in a modulation of the small-scale ocean-surface scatterers (i.e., the Bragg waves) to which radar is sensitive. These ocean processes include surface gravity waves and currents.

two classes of surface patterns

There are two distinct classes of surface patterns caused by gravity waves. First, a SAR can often image the surface gravity-wave field itself, and from this image, estimates of dominant wavelength and direction of propagation can be extracted. The change in wavelength and direction as a wave field propagates into shallow coastal waters can be measured and used in a linear wave-refraction model to estimate water depth. This technique has been demonstrated using Seasat SAR imagery. Secondly, nonlinear interactions between the surface gravity waves and the Bragg wave sometimes result in distinct changes in radar backscatter. These nonlinear wave–wave interactions occur as the gravity-wave field propagates onto an abrupt depth discontinuity, such as a reef or shoal region surrounding an island.

Oceanic currents flowing over bottom features are the second major cause of SAR-observed bottom-related surface patterns. The precise mechanism for the appearance of these patterns depends on the water depth. Tidally driven currents flowing over shallow-water features interact directly with the Bragg waves, resulting in a distinct surface pattern. Tidally driven currents in deep water (>200 m) flowing over bottom features such as seamounts, ridges, shelves, and banks often generate internal waves and areas of upwelling.

Although the general principles and concepts responsible for SAR detection of bottom-related surface patterns are now understood, SIR-C will offer the opportunity to further study and quantify these phenomena. Research is still needed to determine the exact cause of the hydrodynamic interactions that alter the Bragg waves, and the reliability of the water-depth estimates inferred from the bottom signatures as a function of angle of incidence, radar wavelength, and surface environmental conditions.

4.6.5.5 Wind Signatures

Any geophysical process that directly or indirectly influences the short 30-cm waves on the ocean surface will produce a signature in SAR imagery. For example, surface expressions of winds, waves, currents, and bathymetry have all been observed in the imagery from Seasat. Some of these surface expressions are easily visible in the spatial domain; others are much more obvious in the spectral domain. Moreover, some signatures are instantaneous expressions of the local wind field, while others are the results of winds occurring many days previously and thousands of kilometers distant.

strong correlation of SAR image brightness with surface wind speeds

Figure 4-46 illustrates a Seasat SAR image in a region of widely varying surface winds. The overall brightness of the SAR image is generally correlated with the amplitude of the 30-cm surface waves, which in turn respond directly to the local wind. This relationship is most clearly evident at very low wind speeds, where the 30-cm waves are effectively extinguished. Although the amplitude of these waves may not continue to increase indefinitely with wind magnitude, there is good evidence that the local average brightness (or radar backscatter) of SAR imagery is strongly correlated with surface-wind magnitude at least up to 13 m/s. For example, Fig. 4-47 shows the correlation between scatterometer-deduced winds and SAR backscatter over an entire 900-km-long pass (pass 1339, September 28, 1978), in which the local wind varied from null up to 13 m/s. The deviations between scatterometer and SAR may be revealing limitations caused by excessive spatial averaging (~50 km) of the scatterometer, while the SAR accurately follows the finer-scale fluctuations in the magnitude of the wind field.

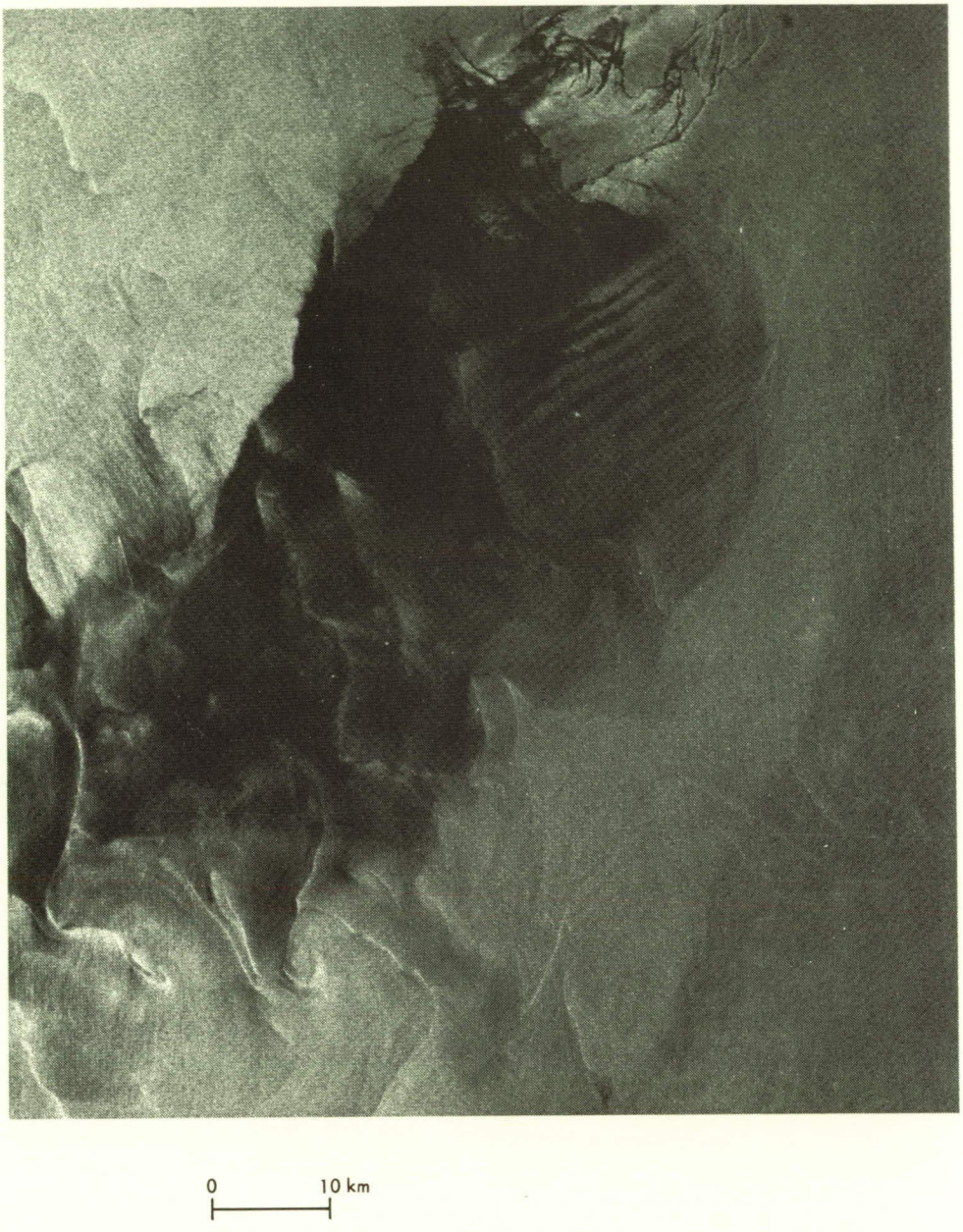

Fig. 4-46. Seasat SAR image of an area 100 km long, located just outside the entrance to Chesapeake Bay. Surface wind is essentially calm ($U_{10} \leq 1$ m/s) in the center (dark) region and gradually increases toward the edges. Surface roughness patterns on this scale reflect not only surface wind patterns but spatial changes in air-sea temperature differences, which directly affect the surface drag coefficient

wind direction information

There is also strong evidence that SAR ocean imagery, at least occasionally, contains information related to local wind direction. Under the right conditions, as the horizontal component of the wind stresses the surface, it produces large streaks in the imagery that correspond to higher backscatter and roughly align with the local wind direction. These wind streaks have spatial scales of a few hundred meters to a few km. At the higher wind speeds, and when the sea-surface temperature exceeds that of the air, elongated atmospheric convection cells can be established, with their long axes approximately aligned with the wind. These phenomena produce asymmetric directional spectra at the low wavenumbers,

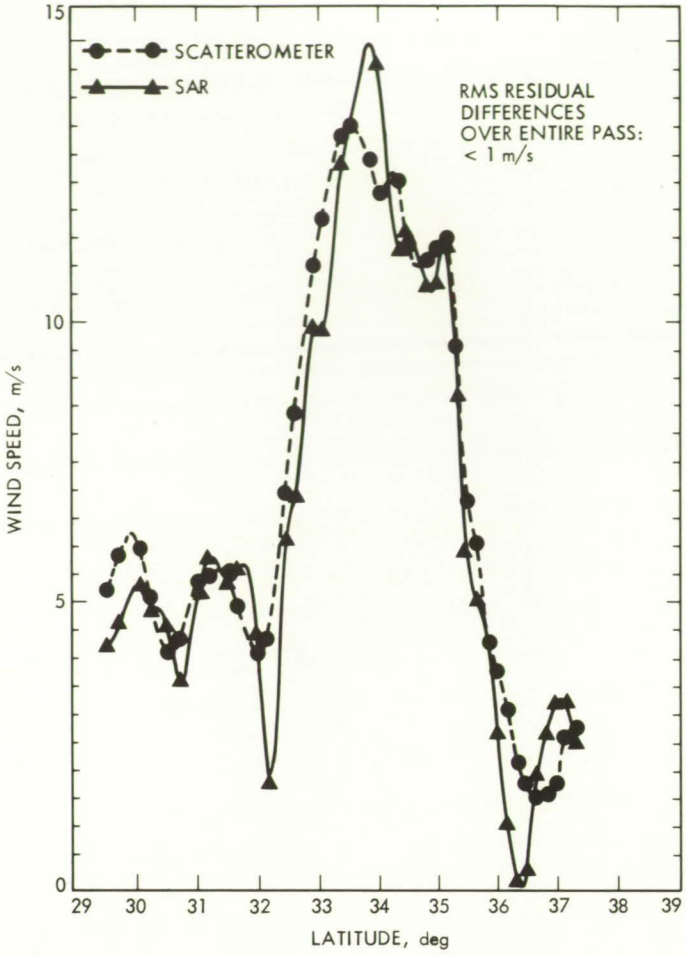

Fig. 4-47. Comparison of SAR- and scatterometer-derived wind magnitudes

which are generally aligned with the direction of the local wind. Figure 4-48 indicates the potential of the Seasat SAR for estimating wind direction with respect to the Seasat scatterometer along a single 900-km pass. On this pass, at least, the residual directional deviations from a smoothed estimate of the local wind field are approximately equal when determined with either the scatterometer or the SAR. Perhaps the SAR can provide an estimate of the fine-scale spatial spectrum of the wind field, information that would be useful in understanding the physical-error structure in future scatterometers, e.g., NROSS and ERS-1. The dependence of the SAR signature on environment, transmitter wavelength, polarization, and angle of incidence is presently unknown.

4.6.5.6 Variable Squint-Mode Experiments

The possibility of SAR operation in variable squint modes (accomplished by a Shuttle yaw maneuver of 1° to 2°/s through at least 90°) will permit a number of critically important experiments over the ocean.

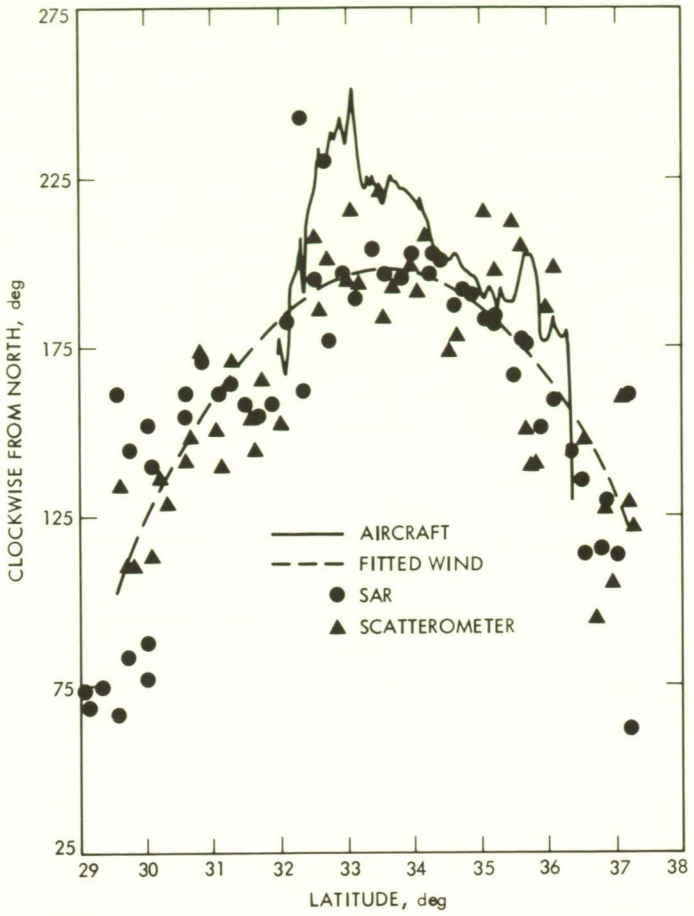

Fig. 4-48. Comparison of wind-direction estimates from both the scatterometer and the SAR

surface winds

By collecting data over a variety of look directions (squint angles)–including the wind direction (or its supplement)–the azimuth dependence of the backscatter as a function of wind speed, radar frequency, polarization, and angle of incidence can be determined.

wave spectra

Using a similar geometry, the SAR-measured wave directional spectrum can be compared with nearly coincident spectra derived with short-pulse techniques (using the same instrument, but with no azimuth processing). Such an experiment will reveal the azimuth dependence of the ocean-wave modulation transfer function.

currents

By collecting data in an area of strong currents and current gradients, raw SAR-signal phase variations can be correlated with surface-current measurements, further exploring the potential of SAR for both relative and absolute current estimates.

4.6.6 Summary of SIR-C Mission Requirements for Oceanography

The experiments discussed above implicitly impose certain requirements on the SIR-C instrument and the mission. This section briefly summarizes those system constraints.

The value of the supersite concept cannot be determined prior to the evaluation of proposals. It is unlikely that particular sites established by one discipline will be compatible with those established by the others, especially in view of the orbital constraints. Most oceanic phenomena of interest are sufficiently diffuse that they can be studied in any of several regions.

4.6.6.1 Orbit Parameters

Most oceanic experiments appear to be optimally served by a slightly drifting orbit, to allow a variety of look angles over a fixed test site.

4.6.6.2 Mission Timing

six or eighteen months separating missions

Two missions, separated by either six or eighteen months, appear optimal for gathering seasonally variable data over the oceans. For internal-wave and bathymetric experiments in the Northern Hemisphere, and extremely high storm waves in the Southern Hemisphere, the July–August period is preferred. For high waves in the Northern Hemisphere, the February–March period is optimal.

4.6.6.3 Swaths and Resolutions

desirability of dual bandwidth

The range resolution of SIR-B was significantly degraded over that of Seasat, due to a receiver bandwidth reduced from 19 MHz to 12 MHz. This resolution loss is particularly severe in monitoring ocean-wave directional spectra. An increase in the SIR-C bandwidth is desirable in order to restore the Seasat resolution while maximizing the available swath.

4.6.6.4. Frequencies, Polarization, and Incidence Angles

15°–45° incidence angles

It is desirable to obtain imagery of some oceanic test sites using all frequencies (L, C, X) simultaneously. Angles of incidence ranging from 15° to 45° are desirable, particularly to reconcile existing differences in SAR imaging theories regarding the ocean and to assist in the choice of optimum operational modes. Both HH and VV polarization are desired; obtaining cross-polarization imagery is not expected to have a high priority.

4.6.6.5 Data Products

BFPQ

A four-bit block floating-point quantizer is an excellent scheme for increasing the dynamic range while maximizing swath width. However, to prevent potential miscalibration in coastal areas, an override option should be available.

radiometric calibration stability required

Relative radiometric calibration (long-term system stability) is desirable for meaningful wind experiments. Relative stability to a small fraction of a dB is desirable over a single pass.

geometric position accuracy to 1 km

In experiments conducted over the open ocean, precise location is essential, both before and after the experiment. For many experiments involving *in situ* measurements, location accuracy to at least 1 km is necessary.

variable squint

The capability for variable squint experiments ($\sim 1°$ to $2°$/s yaw maneuver) is desirable for open-ocean experiments involving the angular dependence of the scattering.

A variety of data products, sometimes over the same test site, will be desirable to satisfy a diversity of users. In many cases, a rapid supply of raw digital data will be more useful than the refined image product. A flexible data dissemination scheme will be most efficient.

Chapter 5
SIR-C Sensor Experiments

5.1 Introduction

In this section we discuss a number of experiments that do not fall naturally into the specific geoscientific disciplines discussed earlier, either because, as calibration experiments, they fulfill the needs of all experimenters and are best carried out directly by the SIR-C Project, or because they are too novel and unproven.

5.2 SIR-C Calibration Experiments

radiometric calibration experiments

As support for the earth-surveillance experiments described in this plan, a method of calibrating the overall performance of the sensors *in situ* is very desirable. Obviously, frequent onboard measurements of transmitted and received power levels represent good engineering practice, and such measurements will be implemented to the extent possible, but the use of a distributed antenna in the SIR-C mission greatly complicates this procedure. Therefore, an overall system calibration using artificial ground targets of known scattering properties is especially important in assisting the interpretation of SIR-C radar data.

corner reflectors

There are several major roles that may be played by surface test targets. For example, radar corner reflectors placed in the vicinity of supersites and elsewhere could:

(1) Provide fiducial ground locations that can be identified in the images. In addition to improving cartographic representation of the images, observations of these identifiable reference points would allow improved accuracy in orbit determination. Both corner reflector and active calibrations (repeaters) should be used for this experiment. In addition, the method of continuously calibrating the antenna pattern in terms of angle by observing a homogeneous target should be repeated, preferably using the Amazon rain forest as in SIR-B and Seasat SASS calibration.
(2) Provide known radar cross sections simultaneously at several frequencies. Such data are essential to any attempt to verify cross-sectional changes that vary with frequency.
(3) Provide targets with "clean" polarizing properties to test the isolation of cross-polarized receiving channels. Coherent measurements of the actual scattering from such point targets can be used to improve estimates of the polarizing properties of other targets.

The SIR-B mission successfully demonstrated the practicality of emplacing artificial reflectors; the SIR-C mission, because of its distributed antenna and the several frequencies and polarizations available, is even more dependent on external calibration. In order to yield the best results, the calibrators should be viewed at the highest resolution available and at as many simultaneous wavelengths and polarization modes as possible. The penalty for such viewing complexity, of course, is a narrow swath width, and thus an enhanced dependence on accurate orbital prediction.

ground receiving stations

We also recommend that ground receiving stations be set up to directly measure signal strength in several polarizations as a means of verifying antenna patterns and the transmitting system's performance. While such observations are not a replacement for preflight and onboard calibrations, experience from earlier missions has shown the value of redundant observations to help clarify unexpected results and to verify predicted behavior.

5.3 Novel Sensor Experiments

An integral part of the SIR-C mission, in addition to applying SIR-C's multiparameter capability directly to the study of the earth sciences as described in earlier sections of this plan, is the extension of the sensor system into novel operating modes. Several examples are discussed below.

5.3.1 Squinting

By providing information on a target's scattering properties as a function of viewing aspect, the ''squint'' mode has potential applications to several disciplines. As a relatively untried technique, however, its utility must first be demonstrated. The radar system of SIR-C provides an ideal test-bed for such a demonstration, without requiring substantial modifications to the system's nominal configuration, although special maneuvers would be required during the data collection, as well as special processing of the data.

squint observations of azimuth backscatter dependence

The research areas in which the squint mode might prove especially useful include oceanographic measurements of the type detailed in Section 4.6 of this plan, as well as several terrestrial applications. For the latter, data collected at two or more squint angles would yield information on the azimuthal angle-dependence of the backscatter, which might provide a useful discriminant of surface structure. Furthermore, areas having high surface relief containing shadowed terrain could be mapped more completely by viewing them from more than one aspect angle. For both terrestrial and oceanographic applications, a variable squint or spotlight mode would allow additional radiometric resolution at no cost to surface resolution by reducing speckle caused by the incoherent averaging of an enlarged data set.

Two kinds of squint-mode experiments can be envisioned for SIR-C. The first would collect data over a given test site with two or more fixed squint angles on subsequent overpasses. The second would vary the squint angle continuously during a single overflight, so as to keep the test site within the field of view of the antenna over a range of squint angles. The latter mode (referred to as ''spotlight'') would obviously entail a more complex orbital maneuver than the former, but provides comparative data from a shorter time base, an obvious advantage in oceanographic applications.

5.3.2 Bistatic Observations

In bistatic observations involving an underflying aircraft, simultaneous data can be obtained both in the backward and in one other scattering direction. With properly chosen

angles and receiving polarizations, these measurements can distinguish diffuse from quasi-specular scattering components. If the aircraft is instrumented to receive simultaneously in several orthogonal polarizations, the data set becomes especially powerful, and contains useful redundancy. Such observations have become available for portions of Mars, and it would be useful to have terrestrial experience against which to compare the planetary data.

5.3.3 SCANSAR

For many SAR applications, frequent coverage is preferred but only modest surface resolution is required. Examples include the monitoring of sea ice, of flooding, of changes in soil moisture, and of ocean phenomena such as internal waves and eddies. In each of these cases, repetitive observation is needed at a rate that is not compatible with the finite SIR-C mission lifetime and the narrow swath widths set by the usual observing constraints. These constraints normally arise from the finite data-transmission bandwidth coupled with the need for good resolution and for multiple wavelengths and/or multiple polarizations. Even if resolution is degraded, a basic swath-width limitation remains as a result of antenna resolution in the range direction.

increasing swath width at expense of azimuth resolution

A way around these rather fundamental constraints that is particularly useful can be provided in the case where an electronically scanned antenna is available, as it is for SIR-C. By operating the radar in a burst mode, rather than continuously, the high instantaneous pulse-repetition rates necessary to prevent azimuth ambiguities can be achieved, without exceeding the data transmission-rate limitations. Furthermore, by electronically scanning the antenna up and down by a beamwidth or so between bursts, the effective swath width of the system can be doubled or tripled. The price, of course, is degraded azimuth resolution (from the finite burst duration) and a possibly reduced number of "looks" as compared to the continuous operating mode. The use of an antenna, electronically scanned in this way, has been given the acronym "SCANSAR."

5.3.4 Scattering Statistics Investigations

In some applications, the statistical variation of radar echoes from a surface that is thought to be essentially homogeneous is of interest. These variations may arise in successive observations of the same resolved surface element ("look"), or from spatially separated, but statistically homogeneous, resolution elements. By assembling data from many such elements, the statistics of the surface scattering may be determined and compared with those statistics expected purely on the basis of random scattering events. Any departure can form the basis for characterizing the surface, and may serve as a discriminant.

This type of experiment can be performed with many existing SAR data sets of course, but the multiple-wavelength capability and the uniform coverage of large areas available to SIR-C renders it a potentially more valuable resource for this application.

5.3.5 Interferometric Topography

This experiment uses a novel but powerful technique made possible by the waveform coherence intrinsic to SAR measurements. As diagrammed in Fig. 5-1, coherent echo data

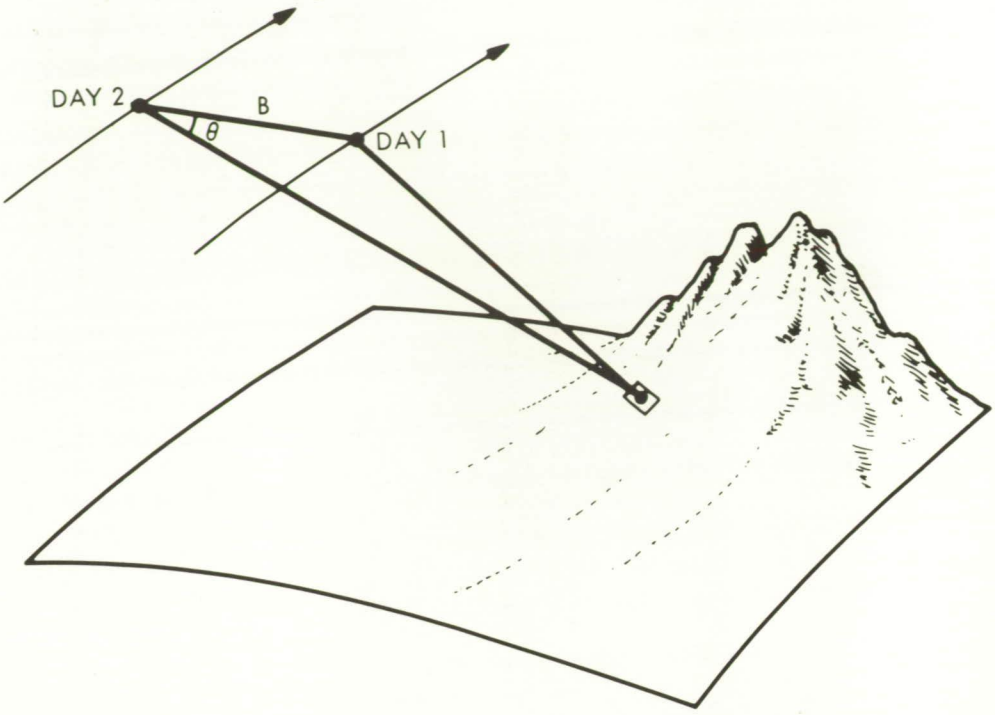

Fig. 5-1. Geometry for SAR interferometry

obtained from separate orbital passes that nearly, but not quite, reproduce each other's geometry relative to the surface are combined interferometrically. Because it measures directly the phase of the echo as received at two or more spatially separated locations, this method is very sensitive to the angle of arrival of the echo.

sensitivity to topographic variations of 5 meters or more

With a baseline having a vertical component on the order of half a kilometer, sensitivity to topographic variations of as little as five meters is possible for surface elements that have retained a fixed relationship between the observations. An example of such an interferometric reconstruction is given in Fig. 5-2. Unlike conventional stereography, it is *not* necessary to identify common feature signatures in order to determine topography from their overlap. Thus topographic measurements of featureless ''rolling plains'' are possible.

If the elements of the surface have moved by more than a few centimeters between two or more observations, the coherence is lost and the method fails. If only a portion of the surface is mobile, say the surface of a river or an ice pack, the loss of coherence calls immediate attention to this fact, and may be used to quickly identify such features.

In order to satisfy the requirements of this method, the later orbits must be suitably aligned with their earlier counterparts. Some overlap will occur near the northern and southern culminations of adjacent orbits in any case, but if this technique is to be used more extensively, it will be necessary to fine-tune the orbital periods of the SIR-C mission to ensure commensurability within the flight duration.

ORIGINAL PAGE
COLOR PHOTOGRAPH

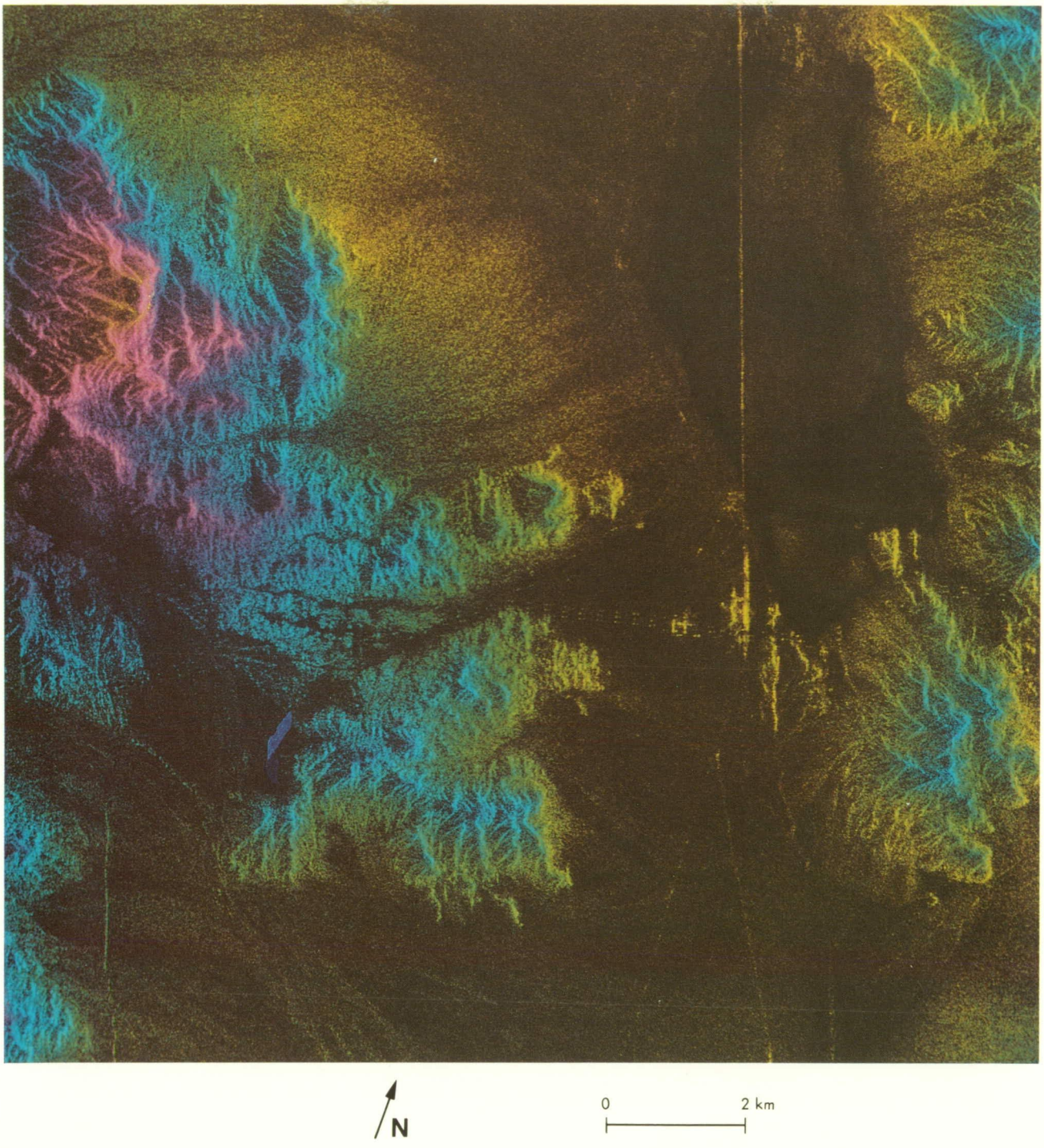

Fig. 5-2. Composite made from two Seasat passes, separated by 3 days, near Baker, California. The colors, superimposed on radar brightness, show the phase difference between corresponding pixels of the two passes. Contours of constant color are in excellent agreement with published elevation contours. The contour resolution is about 100 m. (Courtesy of R. Goldstein, JPL)

5.3.6 Observations of Rain Cells

C-band and X-band sounding of atmospheric rain cells

The C-band instrument (and X-band, if carried) can be used to sound the atmosphere for the presence of rain. Under the proper conditions, it may even be capable of mapping the location, altitude, and intensity of rain cells. To accomplish this, the Shuttle must be flown with the antenna pointing as closely to nadir as possible in one of two configurations.

In the first, the long axis of the antenna is kept parallel to the orbital velocity vector, yielding a resolution of approximately 16 km across track, and 1 km along track. In the second, the Shuttle is yawed 90° so that the short axis of the antenna coincides with the velocity. If the pulse repetition rate is increased sufficiently to suppress the associated azimuth ambiguities, an aperture can be synthesized that yields 1-km resolution along track, while the long axis of the antenna also gives a cross-track resolution of 1 km. The latter mode is particularly desirable, since rain cells are typically only a few kilometers across. Note that the echo correlation time necessary to synthesize 1-km azimuth resolution is only about 1 ms at C-band, while the observed correlation has a duration of the order of 5 ms.

Preliminary calculations suggest that rainfall rates in a cell that exceed about 1 mm/s may be detectable with the SIR-C system, provided a modulation waveform capable of distinguishing the relatively weak rain echo, occurring only a few tens of microseconds ahead of the far stronger surface echo, can be devised.

Chapter 6
SIR-C Data Collection and Image Processing

6.1 Site Recommendations

Based on experience gained during the SIR-B mission, and considering the increased complexity of SIR-C, the strategy for site selection will be to concentrate on acquiring data over a limited number of test sites. This will optimize mission operations and facilitate coordination of simultaneous ground-truth and aircraft-underflight activities. Although actual site locations will depend on investigators selected for the SIR-C Science Team, the Science Working Group recommends some general site types for each discipline:

(1) *Geology*—polar, arid, tropical forest areas (deciduous/coniferous)
(2) *Hydrology*—arid, southern coastal (Gulf of Mexico), humid, high-latitude areas
(3) *Vegetation*—northern-latitude forests, Great Plains (cultural), tropical rangeland/prairie
(4) *Glaciology*—Beaufort Sea, Antarctic (Ross Shelf), Greenland Sea
(5) *Oceanography*—Agulhas Current (South Africa), North Sea

The Science Working Group also recommends a high-inclination orbit for the SIR-C experiment. An orbital altitude of approximately 240 $\pm$ 20 km will be required for a one-day repeat cycle, as shown in Fig. 6-1. Examples of potential orbits with inclinations of 57° and 92° are shown in Figs. 6-2 and 6-3, respectively.

6.2 Mission Timing Recommendations

The SIR-C mission should comprise at least two flights. Each discipline team on the SWG has recommended optimum flight times during the year, based on maximum scientific return. These are shown in Fig. 6-4.

two flights required

For geologic investigations, one summer (May–June) flight and one winter (November–February) flight are recommended in order to enhance the seasonal differences in scenes with vegetation or snow/ice cover, and the seasonal changes in river discharge. Essentially the same rationale exists for hydrologic investigations. For vegetation studies, the first flight should be in late spring (planting time in the Northern Hemisphere), and the second in late summer (peak biomass). For glaciologic studies, the ideal time for the first flight would be late March through April (northern winter, but with enough light to permit ground-truth operations), and the second flight in either August (maximum melting) or the first two weeks of October (freeze-up). For oceanographic investigations of high waves in the Northern Hemisphere, the February–March period is optimal; for internal wave and bathymetric experiments in the Northern Hemisphere and extremely high storm waves in the Southern Hemisphere (e.g., the Agulhas Current), the July–August period is preferred.

These optimum times are obviously quite different for each discipline and there is no common set of two flight times which is best for all investigations.

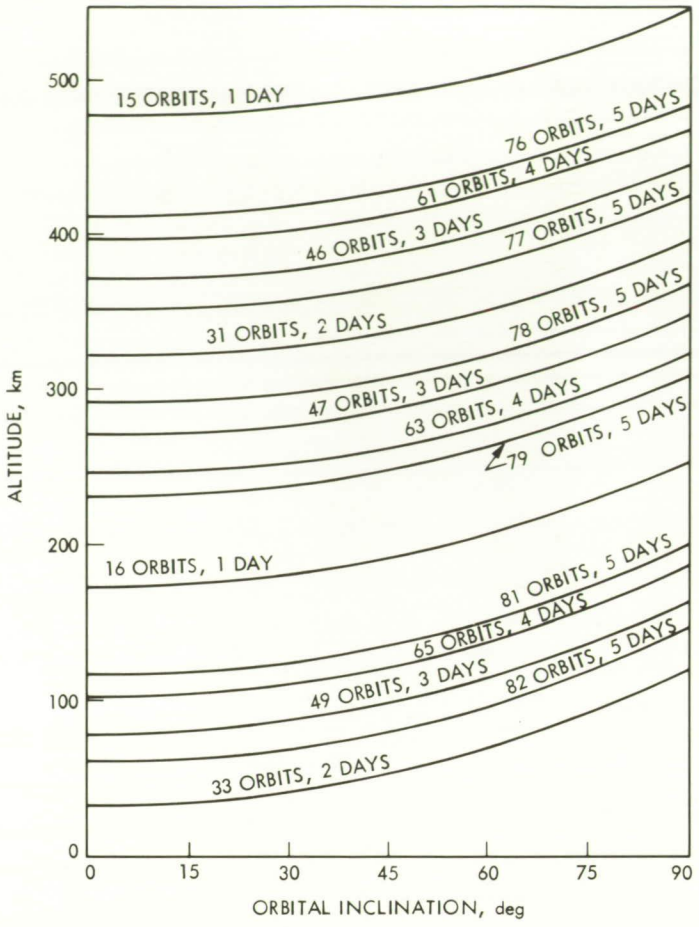

Fig. 6-1. Altitude vs. orbital inclination for various orbital exact-repeat cycles

6.3 Data Acquisition and Processing

As previously described, the SIR-C instrument will collect both C-band and L-band data with each frequency band consisting of direct (HH, VV) and cross-polarized (HV, VH) data. It will also be possible to acquire X-band VV data if the X–SAR instrument is flown along with SIR–C. Considering all possible combinations, as many as 8 to 9 different data types will be available for any given target area. These data will be digitized and formatted onboard and recorded on an onboard high-density digital recorder. In addition, some data will be downlinked directly via the Tracking and Data Relay Satellite System (TDRSS). The transmitted data will be received by the TDRSS ground station at White Sands, New Mexico, and will, in turn, be relayed via DOMSAT to the high-data-rate recording facility at GSFC (Fig. 6-5). The tapes will then be shipped to JPL for processing into imagery and eventual distribution to the SIR-C investigators.

ADSP image-processing in real time

All SIR-C raw data will be processed digitally by the Advanced Digital SAR Processor (ADSP). This processor, designed and built by JPL, can perform SAR image correlation at real-time or near-real-time throughput rates. The system configuration for SIR-C is shown in Fig. 6-6. It centers around the ADSP, which consists of 4 racks of VLSI circuit boards

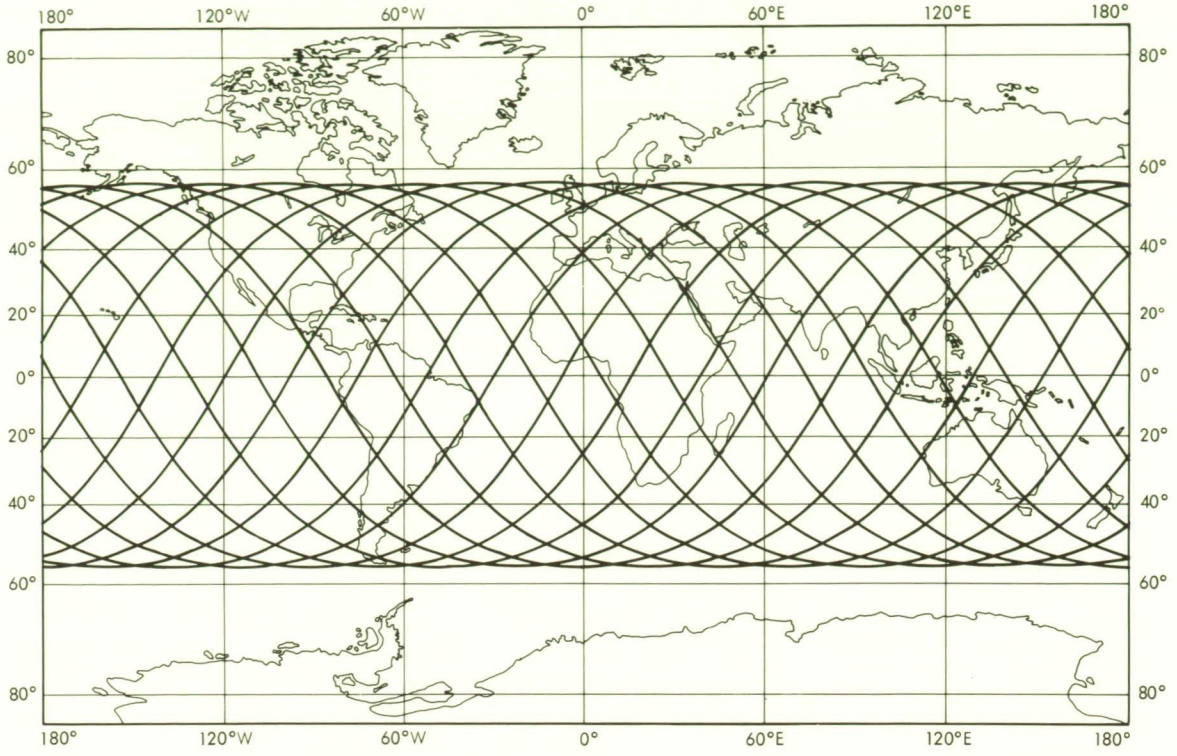

Fig. 6-2. Potential ground tracks for an orbit with a 57° inclination

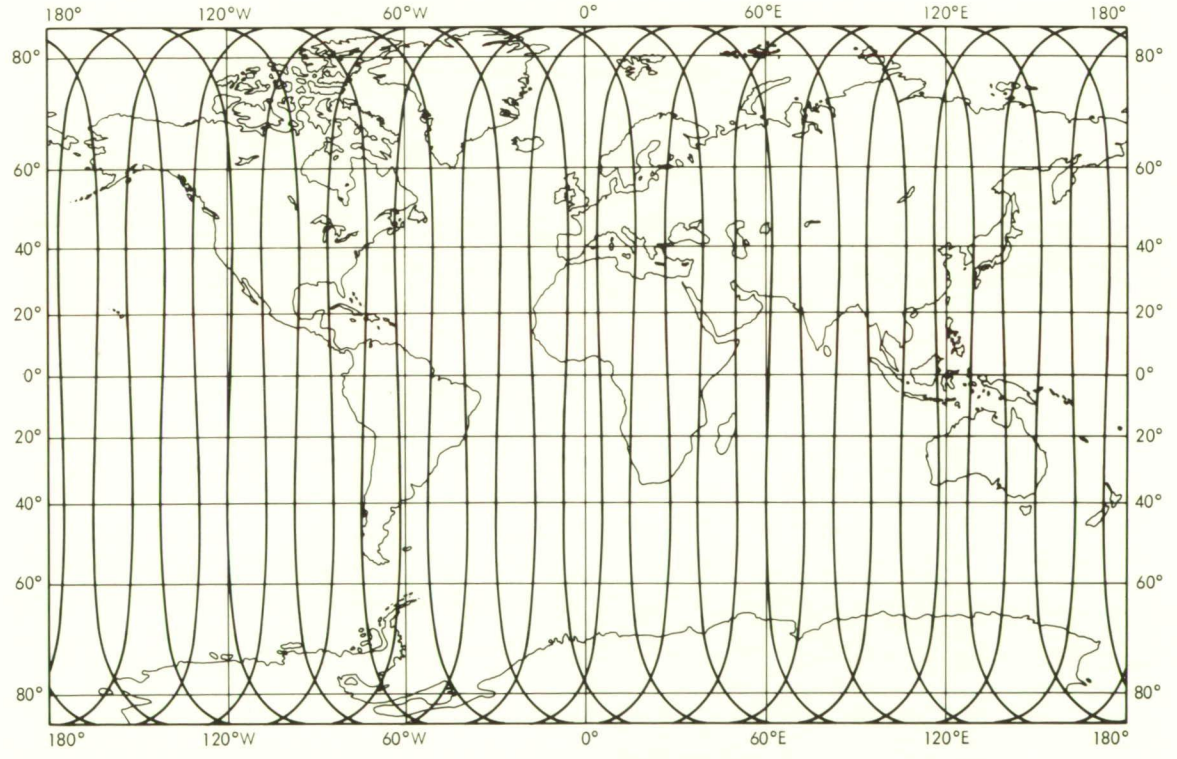

Fig. 6-3. Potential ground tracks for an orbit with a 92° inclination

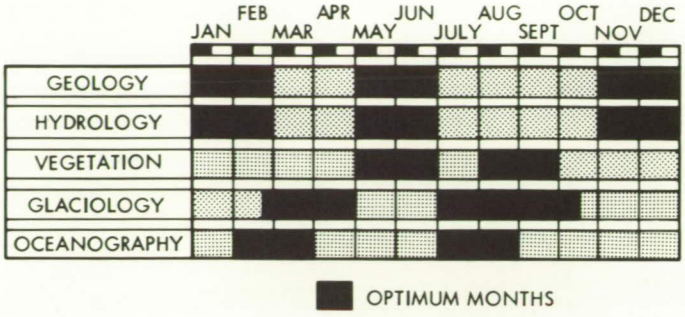

Fig. 6-4. Optimum SIR-C mission times for each science investigation

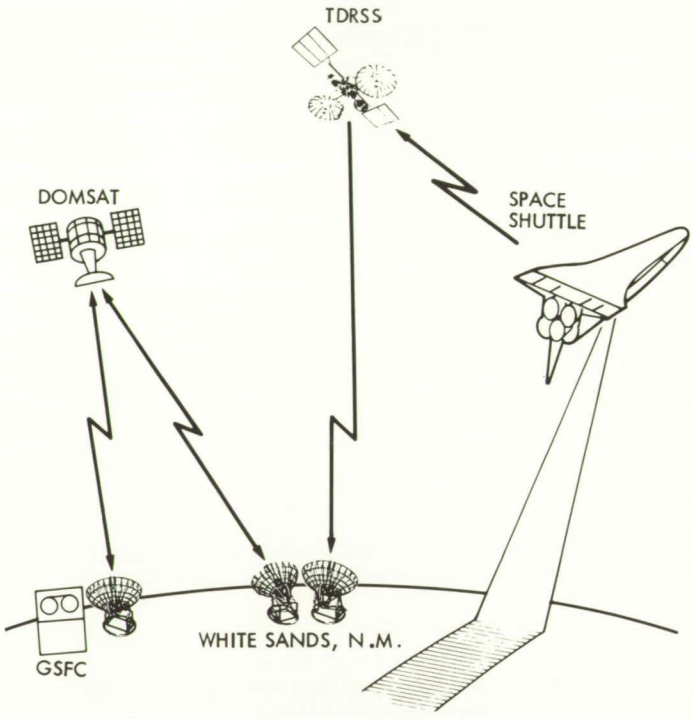

Fig. 6-5. SIR-C data downlink path

controlled by a VAX 11/730. The system also features a SIR-C specific-input interface, two high-density digital recorders (HDDRs) for the input and output data, and a scrolling display with a videocassette recorder for quick-look image products.

The input interface contains logic necessary to decode the subcommutated header data in real time and to perform data quality analyses such as bit-error-rate checks, radar-parameter change detection, or data-dropout detection. The decoded header data are transferred to the VAX controller for initialization of the autofocus and clutterlock algorithms. In addition, the data are used for determining range-line and reference-function sizes as well as for estimating the geometric and radiometric correction parameters (e.g., antenna pattern, angle of incidence, azimuth skew, slant range, etc.).

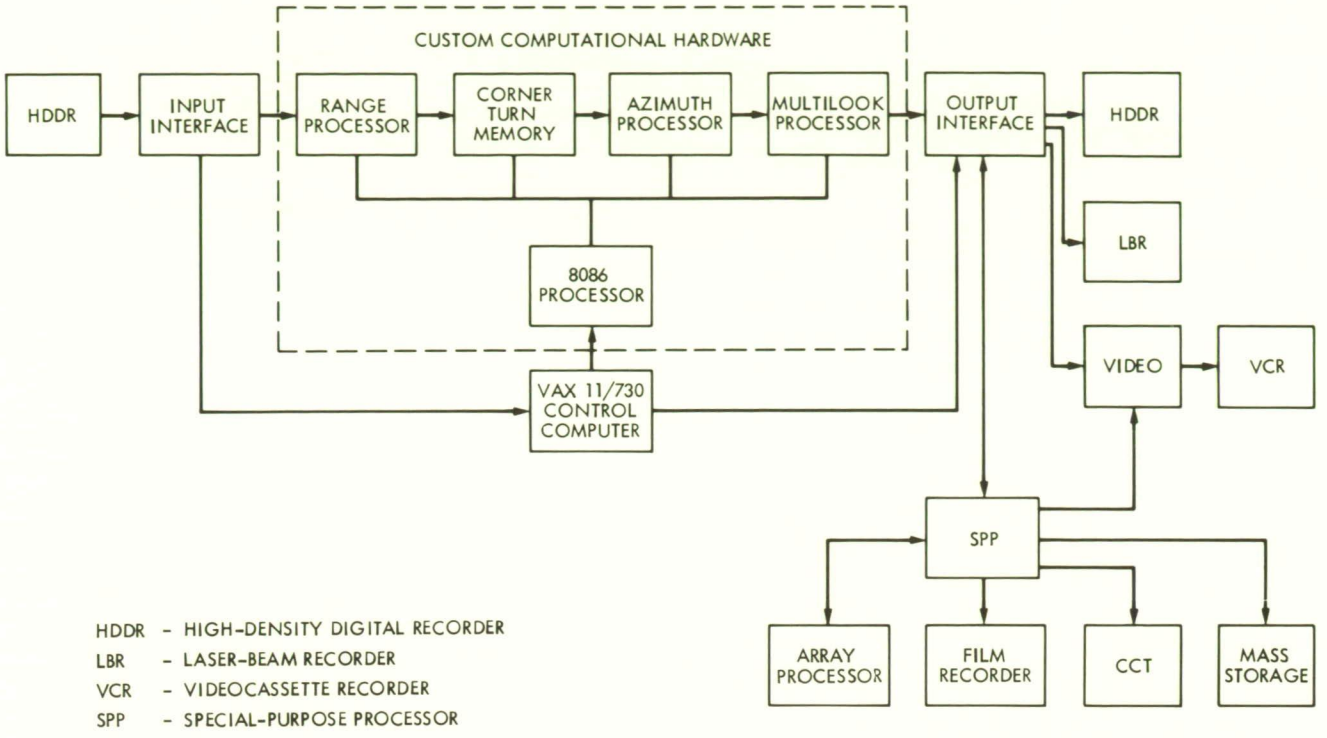

Fig. 6-6. Block diagram of the SIR-C processing system—ADSP custom hardware is shown in dashed box

The correlation algorithm is essentially two one-dimensional matched filtering operations performed in the frequency domain (Fig. 6-7). The reference functions are determined from the characteristics of the transmitted pulse for the range reference and from the Doppler characteristics of the echo data for the azimuth reference.

The ADSP can perform up to 6 x 10^9 floating point operations per second. It is designed to process raw SAR data into imagery in strips rather than on a frame-by-frame basis as in SIR-B. It also has the capability to dynamically update the azimuth reference function during the processing to compensate for variations in the earth-rotation rate or the Shuttle's attitude. However, the ADSP has a limited capability for updating the radiometric and geometric correction parameters. Depending on the stability of the Shuttle during a data take and the application of a specific data set, this may require special processing to maintain the fidelity of the output product. For this purpose a special-purpose processor (SPP) has been added to perform geometric and radiometric corrections on the image products. This system will interface with the ADSP output and will include mass storage, an array processor, a video display, and a film recorder. Its primary function is to meet the special processing requirements of the SIR-C investigators, for selected segments of image data.

6.4 Data Products

four levels of data products

SIR-C data products will be furnished at four levels, as summarized in Table 6-1. Figure 6-8 outlines the expected schedule for SIR-C image processing at each level.

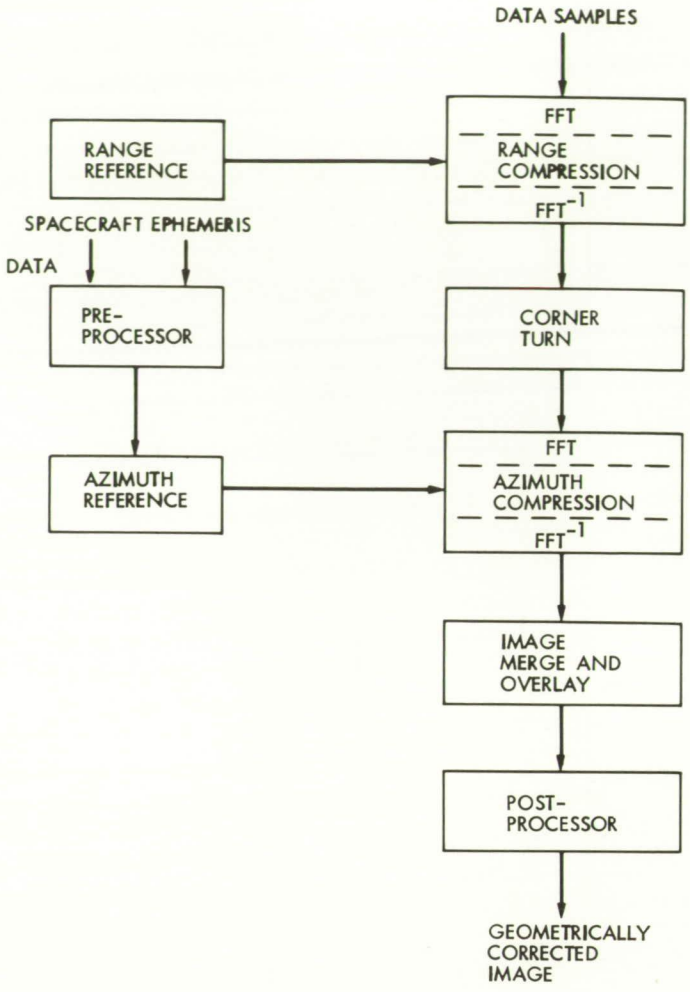

Fig. 6-7. Functional block diagram of the image-formatting algorithm used by the ADSP

6.4.1 Level 0 Products

The SIR-C raw-data set will consist of digitized echo data for two frequencies, with each frequency containing one to three different polarizations. Contained in the raw-data header are the radar parameters and Shuttle parameters required for the processing. In addition, high-precision postflight attitude and trajectory files will be available 2–3 months after the mission. Approximately 1 month will be allotted for data validation and sensor-performance evaluation. During this period copies of the high-density digital tapes (HDDTs) for other processing centers will be made and a limited number of raw data computer-compatible tapes (CCTs) will be available to individual investigators.

6.4.2 Level 1 (Survey) Products

survey products will require 2 months

Following this period, data will be processed in a Level 1 survey mode to assess the quality and specific coverage of the data set. As a minimum for this pass, all HH data will be processed, plus a subset of the VV and cross-polarized data, to ensure that some im-

Table 6-1. SIR-C data products

Data level	Description	Options
Level 0	Digitized raw echo data	HDDT in BFP CCT in BFP CCT, decoded into bytes
Level 1	Survey image data products: complex image data, 16-bit floating point	1 to 16 looks HDDT or CCT
Level 2	Standard image data products	1 to 16 looks 8 or 16 bits integer HDDT, CCT, film strip or image frame
Level 3	Special image data product	Geocoded Geophysical units Terrain corrected Phase image Phase difference

Notes: HDDT = High-density digital tapes
CCT = Computer-compatible tapes
BFP = Block floating point

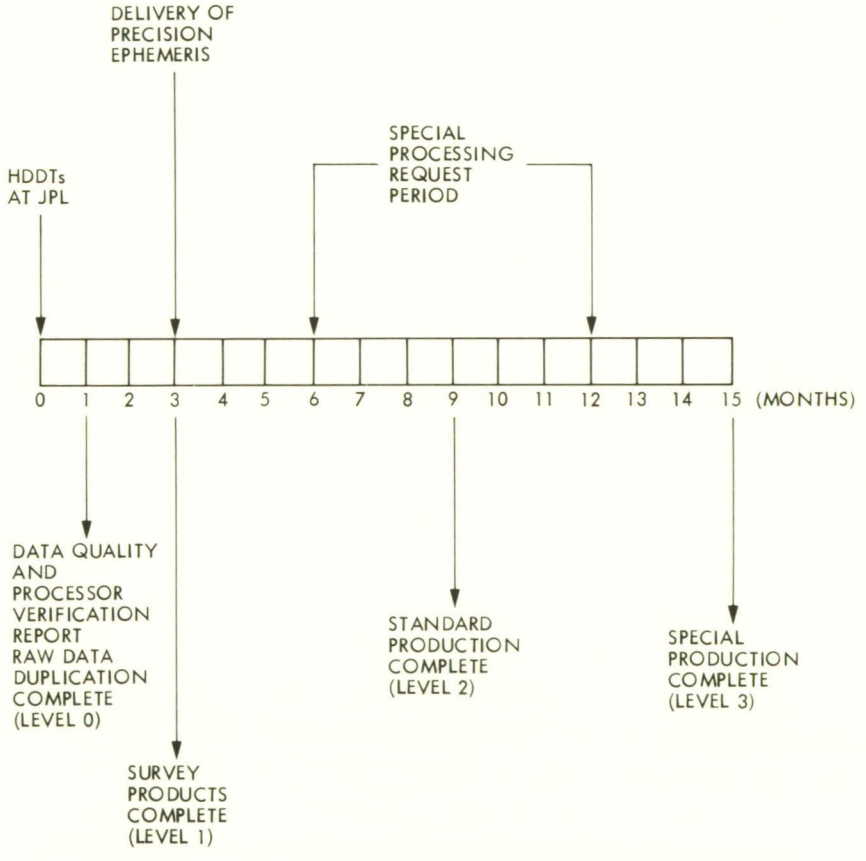

Fig. 6-8. Expected schedule for SIR-C image products. The schedule for the second flight of SIR-C is the same, beginning after month 9 on the chart

agery from each target area is available and that the processor can handle all data types. This output will be recorded on HDDT, and videocassettes or film strips of this imagery will be distributed to investigators for their test sites. This processing will not involve any special corrections for Shuttle instability, or for registration of multiple polarizations or frequencies, and will require approximately 2 months. All imagery will be detected in a 16-bit, 4-look pixel format.

6.4.3 Level 2 (Standard) Products

standard products will require 3-6 months

The third phase of the processing, requiring 3 to 6 months, will produce Level 2 standard image products as requested by the principal investigator for each data take. The proposed options are

(1) Complex image data, 16-bit floating point
(2) Single-look, double-look, or 4-look data
(3) Detected image data (byte format 8-bit or 16-bit integer)
(4) Range-compressed-only data
(5) Radiometrically uncompensated data
(6) Slant-range de-skewed data

The real-time output will be recorded on HDDT and film strips via the laser-beam recorder. These film strips will be annotated every 10 s ($\sim$70 km) with the time and location, and, for each data take, an ancillary data record will be generated containing the full set of Shuttle, processor, and radar parameters, including 10-s updates of time-varying parameters. The ancillary data record will be stored in the SPP and recorded on CCT for distribution to the investigators.

This processor will interface to both the HDDR and the ADSP and will serve an additional function as the SAR data catalog.

6.4.4 Level 3 (Special) Products

geocoded images complete within 15 months

In parallel with the generation of standard image products as described above, this processor will produce a limited amount of Level 3 special image products as required by the investigators. A proposed partial list for this category is

(1) Geocoded images (i.e., rotated to north and resampled to specified map projection)
(2) Radiometrically calibrated products in geophysical units (i.e., backscatter coefficient)
(3) Imagery corrected for foreshortening due to terrain variations
(4) Pure phase imagery, the phase difference between any two polarizations, or magnitude ratios between polarizations or frequencies

The uncertainty estimates for the radiometric and geometric calibration have been described in Section 3.3. Depending on the amount of special processing, it is expected that this phase will last from 9 to 12 months and will be completed approximately 15 months after each flight.

6.5 Data Distribution

As previously described, the special-purpose processor will also act as a data-base management system for the SIR-C, and to a limited extent, the entire terrestrial SAR catalog. The system will contain all of the fundamental and derived parameters for the SIR-C data set. The catalog will contain maps illustrating the SIR-C coverage and will also have the capability to cross-reference target location with any of the SIR-C parameters to determine the extent of a particular type of coverage. In addition, coverage maps from Seasat, SIR-A, and SIR-B will be available with algorithms for determining the extent of multisensor coverage.

The catalog will be accessible by modem to remote users, enabling them to determine processing status of a target area, or communicate to the processing team a special processing or distribution request. The plan includes providing to remote users a limited capability for on-line access to low-resolution image data. The availability of this service will depend primarily on the expected development of mass optical storage and high-data-rate modems and communication links.

The primary means of product distribution will be via air freight. Survey products (Level 1) will be in the form of a quick-look videocassette (or optical disk) or film strip of the investigator's test area. This will be provided approximately 3 months after the flight, primarily for survey purposes and, in the case of data from the first flight, providing input to data collection on the second flight. Associated with this will be a limited ancillary data set with periodic time and location updates. Note that the high-precision ephemeris and attitude data will not be available at this time; therefore, the radiometric and geometric fidelity of the survey products may not meet final product requirements.

Based on investigator evaluation of the survey products and a priority schedule determined by the science team, production and distribution of the standard and special data products (Levels 2 and 3) will begin 3 months after the flight and will last for a period of approximately 1 year. This schedule optimally will meet the special needs of the investigators by generating a variety of low-level image products. The large volume of data associated with full-resolution SAR imagery precludes electronic transfer of this imagery. However, the processor development plan will, at a minimum, include access to the SIR-C ancillary data set and, potentially, remote access to low-resolution, compressed SIR-C imagery.

Chapter 7
Summary

The purpose of this concluding chapter is to summarize the key geoscientific and sensor experiments presented in Chapters 4 and 5, and to summarize the required sensor performance for the conduct of these experiments.

7.1 SIR-C Geoscientific and Sensor Experiments

This section summarizes the various classes of SIR-C experiments that could be conducted in various geoscientific disciplines. It also summarizes various sensor experiments. It is again emphasized that this is not intended to be an all-inclusive list, and that other worthwhile experiments not included below may be conducted with SIR-C.

7.1.1 Geology

Six different classes of potential SIR-C geologic experiments have been described:

cold-region geomorphology

(1) Cold-region geomorphology experiments would concentrate on glacial and periglacial landform mapping as well as on other cold-region features, possibly including permafrost, in order to better understand how these landforms are modified by tectonic and climatic controls.

fluvial geomorphology

(2) SIR-C images would be used to display subtle relief features associated with watershed boundaries, and to analyze the texture of landforms produced by downslope movement.

lithology, rock weathering, and geochronology

(3) It is expected that the use of multifrequency, multipolarization SIR-C data will allow the detection of different lithologies/ages of stratigraphic sequences because of their distinctive backscatter curves related to surface roughness. In fault zones, this may lead to a technique to estimate the rate of slip per unit of geologic time. SIR-C multifrequency, multipolarization images would be used to study the structure of different weathered surfaces and to relate that structure to different horizons of the same material. Such a study would also attempt to use SIR-C imagery to determine quantitative measures of morphology on scales of 1 to 20 km that could be used as input into available slope-wash process models. By analyzing images of various polarizations and frequencies (which depend on surface roughness, blockiness, and age), it may be possible to derive relative age dates for lava flows and alluvial deposits.

tectonics and geologic boundaries

(4) A high-inclination orbit of SIR-C will allow the coverage of Precambrian shields on most continents, which should permit improved structural mapping along traverses that are both normal and parallel to selected fronts (e.g., the Grenville front in Canada). The multiple angles of incidence and the multipolarization capability of SIR-C may also be useful in distinguishing and mapping ophiolite complexes, lava flows, or other lithologies related to tectonism along plate margins.

geobotany

(5) The detection and evaluation of stress in vegetation is a key element in geobotanical investigations. SIR-C multifrequency, multipolarization images may help to identify the detection of distinctive signatures of stressed plant communities that are related to underlying lithologic units.

radar stereo and topography

(6) SIR-B demonstrated that images using multiple angles of incidence can be used to produce radar-derived topography. SIR-C will allow this concept to be further tested at various frequencies and polarizations. It is also envisioned that a diverse range of geomorphologic investigations could be conducted with the topographic data derived by SIR-C.

7.1.2 Hydrology

Eleven classes of hydrology experiments have been suggested, which range from arid to wetland to high-latitude regimes:

surface penetration in hyperarid regions

(1) The surface-penetration results of SIR-A could be extended by using the multiple-parameter capability of SIR-C to delineate buried ancient drainage networks and other subsurface hydrologic features.

semiarid-region soil moisture

(2) SIR-C imagery would be used to study temporal and spatial variations in the soil moisture levels in the top horizons of semiarid regions. Because of the short duration of the mission, temporal-variation studies would be based on seasonal differences or on targets of opportunity.

spatial variability and scale

(3) These experiments would emphasize the spatial variability of hydrologic parameters, especially the scale of hydrologic units. SIR-C images would be used to develop criteria for hydrologic uniformity. Because of the short duration of the mission these studies would have to be based on targets of opportunity.

SAR image sensitivity to precipitation

(4) These experiments would concentrate on relating SAR images of precipitation events (as soil moisture) to rain-gauge data and to determine if the SIR-C imagery could be effectively used to interpolate between rain gauges. The optimum frequencies, polarizations, and angles of incidence for this purpose would also be investigated.

SAR image sensitivity to hydrologic characteristics

(5) The objective of this experiment would be to determine how multiple-parameter radar measurements could be used to integrate the four characteristics that are used as input parameters to runoff models: vegetation, soil structure, surface roughness, and soil moisture.

flood mapping

(6) If a flood occurred during either mission, SIR-C imagery could be used to determine the optimum frequency, polarization, and angle of incidence for delineating flood boundaries and land–water boundaries through vegetation canopies.

groundwater resource analysis

(7) The two flights of SIR-C would be used for observing spatial changes in groundwater discharge and recharge areas resulting from seasonal differences in soil moisture and surface waters.

wetland boundary delineation

(8) This experiment would concentrate on the different vegetation-penetration capabilities of L-band versus C-band for the purpose of identifying understory wetland boundaries. It would also examine the ability to discriminate among vegetation types as an indicator of underlying soil conditions. Results from these studies would also define the system characteristics useful for flood monitoring.

snow-covered watershed investigations

(9) The shorter wavelength channels of SIR-C and, especially, the X-band will be useful for identifying snowpack areal extent, snow–water equivalent, and condition. The two-season flights and polar orbit of SIR-C should allow investigation of snow-covered watersheds over a wide range of latitudes and permit the first quantitative comparison of two radar channels (X- and C-band) for relative discrimination of snowpack properties.

glacier discrimination

(10) SIR-C offers the possibility of examining the changes in ice extent, in crevasse patterns, in the distribution of morainal material, and in ice-surface roughness that have occurred over a 10-year (Seasat) and an 8-year (SIR-A) period. Also, as the backscattering mechanisms in alpine glaciers are still not well understood, an interesting experiment could be developed taking advantage of the multiple frequencies, multiple look angles, and variable polarization afforded by the SIR-C system. (See also Section 4.5.5.3.)

permafrost discrimination

(11) Permafrost, or permanently frozen soil, is not expected to have a distinctive dielectric constant in comparison to rocks or unfrozen soil. However, it may well have a distinctive textural signature related to its surface roughness. The multifrequency, multipolarization capability of SIR-C will allow this to be studied as a target of opportunity.

7.1.3 Vegetation

Four classes of vegetation experiments have been suggested:

vegetation type identification

(1) This class of experiment involves the use of single- and multi-date radar data (at all frequencies and polarizations and at high angles of incidence) to establish the degree to which radar data alone could be used to identify vegetation types. The experi-

ments would then combine the radar data with optical data (e.g., TM) to determine the improvement in crop type identification obtained over optical data alone or radar data alone.

canopy biophysical properties

(2) SIR-C images of canopies (L-, C-, and X-band) at all polarizations and including phase images (the difference in phase between HH images and VV images) would be related to canopy leaf area index, phytomass, canopy structure, and stress.

interpretation of landscape patterns

(3) SIR-C image texture would be used for the interpretation of regional landscape patterns.

radar penetration of vegetation

(4) The multiple-parameter nature of SIR-C allows an excellent opportunity to conduct fundamental research investigations into canopy penetration as a function of wavelength, polarization, and angle of incidence. Image texture for each of these parameters would be related to canopy characteristics.

7.1.4 Glaciology

Four broad categories of ice experiments have been suggested:

sea ice

(1) The two-season coverage obtainable with SIR-C will allow valuable studies involving sea-ice feature verification, ice drift and deformation, spatial variations of ice-pack characteristics, the nature of ice margin eddies, and the improved characterization of sea-ice types. The discrimination of sea-ice types is expected to be improved by the addition of multiple wavelengths and polarizations.

lake ice

(2) SIR-C imagery would be used for lake-ice feature verification, for lake- and river-ice operations studies, and for investigations of lake-ice dynamics.

ice shelves, ice sheets, and alpine glaciers

(3) These experiments would concentrate on mapping ice-shelf and glacier boundaries, on obtaining a census of icebergs and ice islands, on delineating ice streams in ice sheets and shelves, and on studying temporal changes in alpine glaciers.

snow

(4) The shorter wavelengths of SIR-C will be used for studies of snowpack extent, snow–water equivalent, and snow wetness. X-band is preferable for these studies, but C-band could also be used, especially for thicker, wetter snowpacks.

7.1.5 Oceanography

There are five broad categories of oceanographic experiments that have been suggested for SIR-C.

directional wave spectra

(1) The purpose of these experiments is to use SIR-C imagery to estimate directional wave energy spectra as a supplement to global wind–wave forecast models.

internal waves

(2) The objective of these experiments is to improve our understanding of wave–current interactions by studies of SIR-C images of surface phenomena associated with internal waves.

currents, fronts, and eddies

(3) These experiments could utilize SIR-C imagery to detect current-system boundaries, oceanic fronts, and mesoscale eddies, and would attempt to extract surface currents directly from the Doppler spectrum.

bottom signatures

(4) SAR images of shallow-water regions occasionally provide surface expressions of ocean-bottom features. SIR-C images could be used to study the physical mechanisms responsible for bottom-feature detection, including the nonlinear-interaction mechanism between internal currents, surface gravity waves, and Bragg waves.

wind signatures

(5) SIR-C images could be used to correlate occasionally observed periodic surface signatures, on the scale of 1 km or longer, to the fine-scale properties of the surface wind field, including local wind speed and direction.

7.1.6 SIR-C Sensor Experiments

Although SIR-C is primarily a geoscientific mission, it will allow a valuable test of the performance of the sensor itself. This is important because of the new distributed SAR technology being used. The flexibility of SIR-C will also allow a number of sensor-related experiments that will improve our understanding of SAR imaging as well as the performance of the instrument.

corner reflection experiments

(1) The frequent onboard measurement of transmitted and received power levels is considered good engineering practice, although the distributed SAR technology greatly complicates this procedure. It will therefore be essential to also use system calibration techniques that employ artificial ground targets of known scattering properties. Corner reflectors could not only provide targets of known radar cross-section, but might also serve as targets having "clean" polarizing properties that could be used to establish the isolation of cross-polarized receiving channels. The use of calibrated ground receivers that could establish the antenna pattern and transmitting system performance is proposed. This calibration will be of particular assistance in the quantitative comparison of data acquired on the different flights of SIR-C.

squint mode

(2) This would include two kinds of squint operation, the first providing data over a given test site with two or more fixed squint angles on subsequent overpasses. The second would vary the squint angle continuously on a single pass so as to keep the test site within the field of view, thereby allowing a much larger number of looks.

bistatic observations

(3) This would involve coordination of SIR-C with an underflying aircraft and could provide a very useful set of bistatic imaging data at several combinations of angles, frequencies, and polarizations.

SCANSAR

(4) This experiment would utilize the electronically scanned SIR-C antenna along with a burst mode so as to achieve a high instantaneous PRF, which is necessary to prevent azimuth ambiguities. By electronically scanning the antenna beam up and down between bursts, the swath width can be effectively doubled or tripled.

scattering statistics

(5) The statistical variation of radar echoes from a nominally homogeneous surface would be examined and compared to the statistical variation expected purely on the basis of random scattering events. Departure of SIR-C radar-echo statistics from this could serve as a discriminant. The multiple-wavelength capability of SIR-C makes this an especially attractive sensor experiment.

interferometric topography

(6) Coherent echo data from two separate, parallel, and nearby SIR-C orbital passes could be combined interferometrically to reconstruct the topography of the scattering surface.

observations of rain cells

(7) The C-band (and X-band, if carried) channels of SIR-C could be used to sound the atmosphere for the presence of rain. Under the proper conditions, it may be possible to map the location, altitude, and intensity of rain cells. Special antenna orientation geometries are required for this experiment.

7.2 Recommended Mission Parameters and Sensor Performance

Based upon the geoscientific experiments discussed in Section 7.1 (and Chapter 4), recommendations of overall mission parameters and sensor performance levels can be made. Some of the sensor recommendations may be considered enhancements to the baseline SIR-C design described in Chapter 3.

7.2.1 Orbital Parameter and Mission Timing

It is strongly recommended that the SIR-C orbit have an inclination of at least 57°. Two flights, each in a different season, are required by all the geoscientific disciplines, although the optimum timing of these flights depends on the discipline. As shown in Fig. 6-4, a January–June pair would be satisfactory for geology and hydrology experiments; a March–August pair would be satisfactory for glaciology and oceanography; a May/June–August/September pair would be preferred for vegetation-science experiments.

7.2.2 Swath Widths and Resolutions

swath width of at least 15 km required

The 40-m (4-look) nominal resolution of SIR-C at a look angle of 25° in the low-resolution mode is considerably lower than that of Seasat. For estimates of directional wave spectra, it may be inadequate. While the 10-MHz bandwidth appears adequate for many other investigations; for directional wave spectra, a higher bandwidth would be better. For geologic and glaciologic mapping studies where swath widths of 150 km or more are desired, a decrease of resolution (and bandwidth) can be accommodated. The minimum acceptable swath width is 15 km.

7.2.3 Frequencies, Polarizations, and Incidence Angles

A majority of the experiments will make use of multifrequency, multipolarization images taken at various angles of incidence. Exceptions to this are oceanography, where there appears to be no interest in cross-polarization images, and mapping modes for some structural geologic experiments (e.g., studies of the Precambrian shield) where the primary interest is in maximum wide-swath imaging.

7.2.4 Radiometric Calibration

A number of crucially important SIR-C experiments will ratio images of the same test area taken at different times during the mission. These experiments will require that SIR-C demonstrate ± 1 dB relative calibration (stability) during the life of the mission, so that quantitative comparisons of temporally acquired images may be made. For studies of soil-moisture variations in vegetated regions, for example, it is required that the instrument calibration be stable to less than a dB over the life of the mission. For a comparison of images taken during the two separate missions, an absolute calibration of ± 3 dB is required.

For studies of spatial variability (across the swath), it is important that processed images show good radiometric fidelity across the swath. A good target figure is 0.2 dB in conjunction with ground calibration, or better uniformity across spatially homogeneous scenes (e.g., the undisturbed ocean or the Amazon forest).

Other experiments will ratio images acquired at L-band and C-band and use the ratio of the radar backscattering coefficients at these two frequencies to determine surface morphological parameters. These will require that both channels be calibrated to ± 1.5 dB (relative to each other) or better.

7.2.5 Data Products

Most experiments will require some quick-look (Level 0) uncorrected data delivered as soon as possible after the mission. Requirements for survey (Level 1), standard (Level 2), and special (Level 3) processing vary from experiment to experiment. Please refer to Sections 4.2.6.5, 4.3.6.5, 4.4.6.5, 4.5.6.5, and 4.6.6.5 for further details.

Appendix A
Introduction to Radar Scattering

A.1 Introduction

This section presents a brief tutorial on radar scattering as it applies to the quantitative use of SIR-C data. The relationship between the SAR image intensity and the radar backscattering coefficient is described, and a brief discussion is given of surface and volume scattering.

A.2 The Radar Backscattering Coefficient

definition of the radar backscattering coefficient

Point targets such as trucks, aircraft, buildings, corner reflectors, etc., produce a radar echo whose intensity is dependent on the target's radar cross section σ, given in units of m^2. Area-extensive distributed targets such as agricultural fields, geologic scenes, or oceanic areas produce a radar echo whose intensity is the radar cross section per square meter. The radar backscattering coefficient σ° of an area-extensive target is equal to its radar cross section (m^2) divided by its physical area (m^2) in the horizontal plane; therefore, σ° is unitless ($m^2\ m^{-2}$). For rough surfaces and/or at near-nadir angles of incidence, σ° is large. For smooth surfaces and large angles of incidence, σ° is small. The backscattering coefficient often exhibits a dynamic range extending over several orders of magnitude, particularly when angular variations are involved. To compress its range, σ° is usually expressed in decibels:

$$\sigma^\circ(\text{dB}) = 10 \log \sigma^\circ(m^2\ m^{-2}) \tag{A-1}$$

A.3 SAR Image Intensity (Tone)

After digital processing, the output product of an imaging radar is a digital image composed of a two-dimensional array of pixels, as suggested in Fig. A-1. The intensity (also called *tone* or gray level), or digital number $DN(i,j)$ of the pixel (i,j), is related to the power P_r backscattered from the corresponding ground cell by

$$DN(i,j) = a\sqrt{P_r}(i,j) + b \tag{A-2}$$

where a and b are known scaling constants. The above relationship assumes that the receiver uses linear detection, which was the case for Seasat, SIR-A, and SIR-B, and which will be the case for SIR-C. The received power $P_r(i,j)$ is directly proportional to the radar backscattering coefficient $\sigma^\circ(i,j)$ of the ground cell, i.e.,

$$P_r(i,j) = K(j)\,\sigma^\circ(i,j) \tag{A-3}$$

where $K(j)$ is a range-dependent system factor that incorporates transmitter power, range to target, area of ground cell, and antenna gain function. If $K(j)$ is known on an absolute

scale it is then possible to directly relate $DN(i,j)$ to $\sigma°(i,j)$ and therefore produce an image whose intensity can be related on an absolute scale to the backscattering coefficient. If only the relative variation of $K(j)$ is known, a relative backscattering image can be generated. Both internal and external calibration tests are planned for SIR-C; these tests will establish the radiometric calibration of SIR-C. This Science Plan calls for an absolute calibration accuracy of ± 3 dB and a relative calibration of ± 1.5 dB.

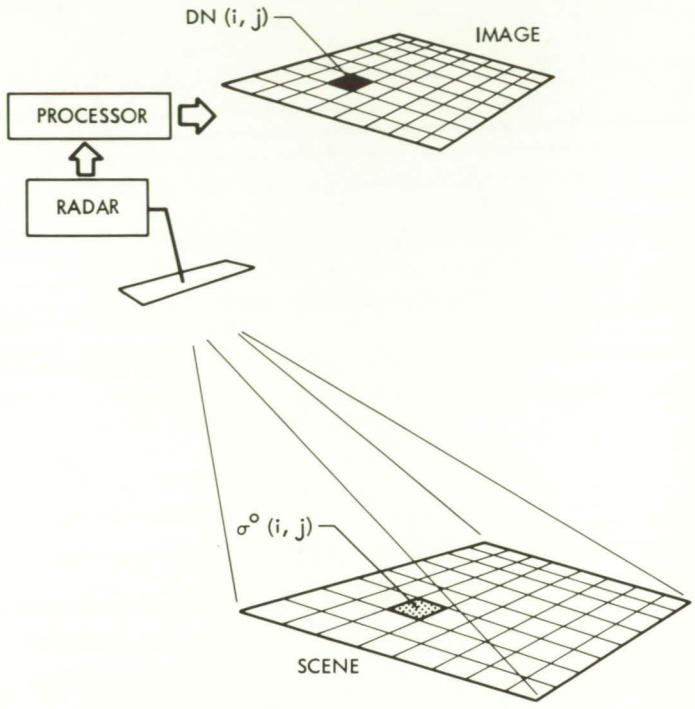

Fig. A-1. Correspondence of the radar backscatter coefficient at location (i,j) pixel in the scene, to the (i,j) digital number in the processed image

The radar backscattering coefficient, which is analogous to the bidirectional optical reflectance (BDRF) for the special case where the source and detector are at the same location, provides the link between the physical properties of the imaged scene and the radar observations. The purpose of this section is to introduce the nonspecialist to the general topic of radar scattering from area-extensive targets.

A.4 SAR Image Speckle (Texture)

SAR uses coherent illumination of the scene and coherent detection of the backscattered signal to achieve high resolution in the azimuth direction. The total signal backscattered from a ground cell is the coherent sum of the signals backscattered from all the scatterers contained in the ground cell. Terrain surfaces usually consist of a large number of randomly distributed scatterers. This randomness is responsible for *image speckle*, which takes the form of random variability of image tone among pixels corresponding to different cells of a uniform target. Thus, speckle is a consequence of the coherent imaging process

employed by SAR systems and not a result of spatial variability (natural texture) in the physical or electromagnetic properties of the surface.

statistical distribution of radar backscatter

If a radar is used to measure $\sigma^\circ(i,j)$ for a very large number of pixels (i,j) for an area-extensive target with uniform properties, the magnitude of an individual $\sigma^\circ(i,j)$ is related, in a statistical sense, to the *mean value* σ° by

$$\sigma^\circ(i,j) = \sigma^\circ F_N \tag{A-4}$$

where F_N is known as a fading random variable and has the following properties [A-1, Volume II, Section 7-2]:

Mean $\mu_F = 1$

Variance $\sigma_F{}^2 = \dfrac{0.273}{\mathrm{N}}$ for linear detection

N = number of independent samples

Probability density function ($p\,d\,f$) of F_N = N-convolved Rayleigh *pdf* (cf. Fig. A-2)

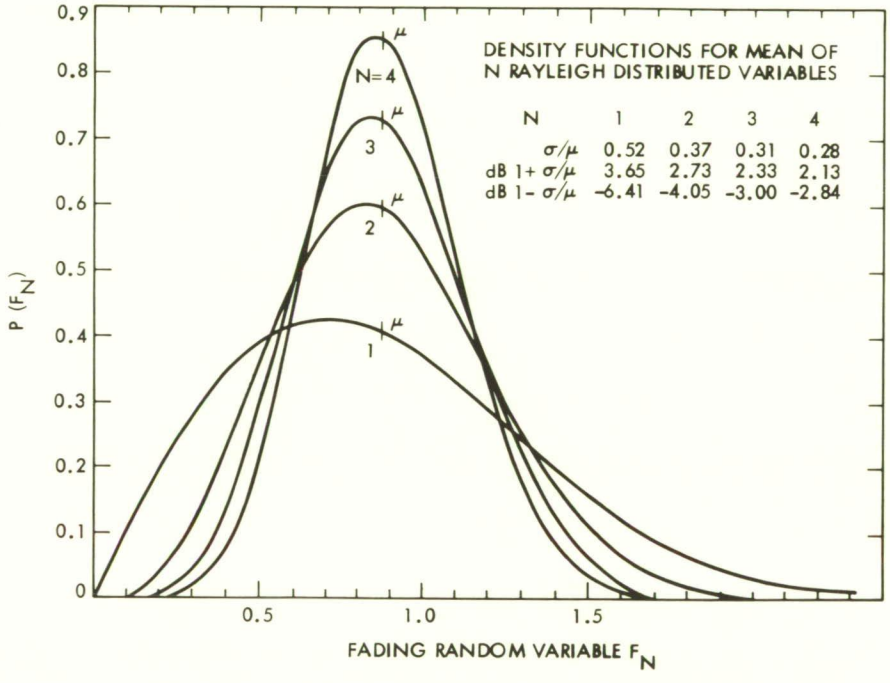

Fig. A-2. Probability density functions for mean of *N* Rayleigh-distributed variables

number of looks

The number of independent samples N, which often is referred to as the number of looks, is determined by the amount of spatial and/or frequency averaging incorporated in the processing employed in the generation of the radar image. The standard Seasat SAR, SIR-A, and SIR-B image products provided by JPL were four-look images; the azimuth resolution was degraded by a factor of four to reduce the effects of fading fluctuations. However, the capability exists to process the signal data to produce images for any integer value of N. The same capability will be available for SIR-C.

A.5 Surface and Volume Scattering

The signal backscattered from an area-extensive target may be the result of surface scattering, volume scattering, or both. The relative importance of surface and volume scattering is governed by the surface statistics of the target boundary, the inhomogeneity of the medium underneath the surface, and the penetration depth of the medium. All these factors are strong functions of the wavelength λ.

surface scattering

The penetration depth in sea water is only a few millimeters at microwave frequencies. Hence, the signal backscattered from the sea contains no scattering contributions from the subsurface water volume (cf. Fig. A-3), although it may contain volume-scattering contributions generated by inhomogeneous volumes of foam and other material riding over the water surface.

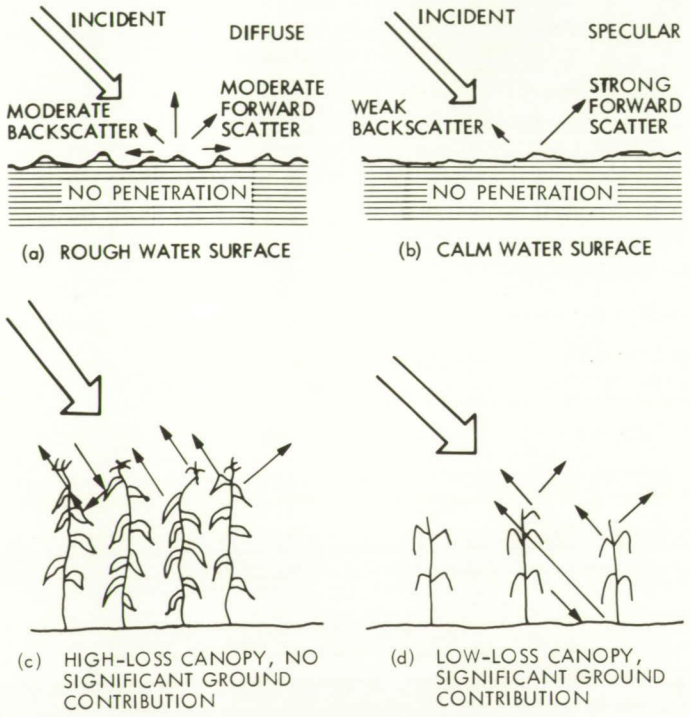

Fig. A-3. Surface scattering from (a) rough water surfaces and (b) calm water surfaces, and volume scattering from (c) high-loss vegetation canopies and (d) low-loss vegetation canopies

volume scattering

By contrast, backscattering from a vegetation canopy is dominated by volume scattering. Because a vegetation canopy is typically more than 99 percent air by volume, the average relative permittivity of the canopy is only slightly larger than unity. Consequently, the reflection coefficient of the air–canopy boundary is approximately equal to zero, which in turn leads to a negligible surface scattering contribution. The canopy interior, however, is amenable to strong volume scattering because it is very inhomogeneous at the centimeter-wavelength scale. If the penetration depth of the canopy is comparable to or smaller than the canopy slant height (along the direction of observation), contributions from the underlying ground surface may also be present in the backscattered signal.

penetration depth

The penetration depth δ_p of a medium is defined as the depth below the surface at which the magnitude of the power of the transmitted wave is 13.7 percent of its value just beneath the surface. In the majority of situations, the vertical extent (in the medium) of the region responsible for the majority of the backscattered energy received by the radar is on the order of one to three times the penetration depth δ_p.

The penetration depth is determined by both absorption and scattering losses. At centimeter and longer wavelengths, absorption losses exceed scattering losses for most natural media. If scattering losses are ignored, it is possible to calculate the penetration depth from the relative dielectric constant of the medium, $\epsilon = \epsilon' - j\epsilon''$ where ϵ' is the relative permittivity and ϵ'' is the dielectric loss factor. With the exception of liquid water, natural materials satisfy the condition $\epsilon''/\epsilon' << 1$, which allows the use of the following single expression:

$$\delta_p \cong \frac{\lambda\sqrt{\epsilon'}}{2\pi\epsilon''} \tag{A-5}$$

The curves in Fig. A-4 illustrate the variation of δ_p as a function of liquid water content m_v for both soil and snow at various microwave frequencies. It should be emphasized that these curves may not be valid in the region around $m_v = 0$ because they were computed on the basis of the assumption that scattering losses may be ignored relative to absorption losses. This assumption may not be valid when the moisture content is very small.

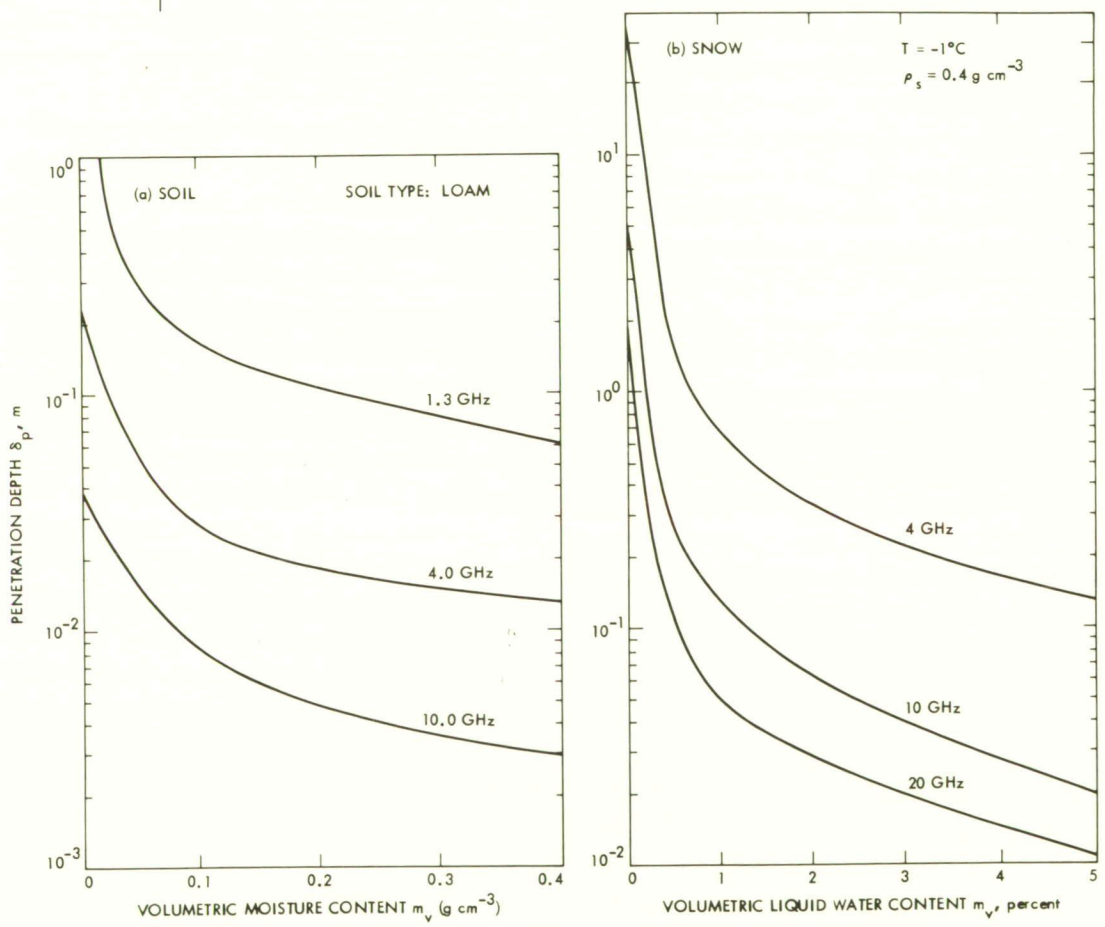

Fig. A-4. Penetration depth of (a) loamy soil and (b) snow as a function of liquid water content [A-1, Volume II, Section 11-5]

An additional caution should be mentioned as related to vegetation. The simple expression (A-5), which implies no polarization-dependence, is based on the assumption that the inhomogeneities in the medium are random in location and orientation. This is often true for inhomogeneities such as brine pockets, dust, air bubbles, etc., in polar sea ice. However, it is often not valid for vegetation. For example, stalks are oriented predominantly along the vertical direction. Consequently the penetration depth is dependent on both angle of incidence and the radar polarization configuration [A-2].

A.6 Surface Scattering Mechanisms

The roughness of a surface refers to the statistical variations of the random component of surface height relative to a reference surface. The reference surface may be the unperturbed surface of a periodic pattern (Fig. A-5(a)), as in the case of row-tilled soil surfaces or a wind-driven sea surface, or may be the mean surface if only random variations exist (Fig. A-5(b)).

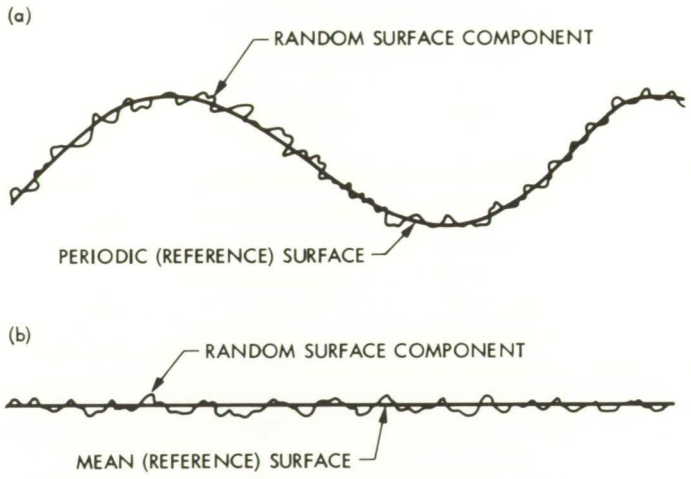

Fig. A-5. Two configurations of height variations: (a) random height variations superimposed on a periodic surface, and (b) random height variations superimposed on a flat surface

scattering models

Several theoretical surface scattering models have been proposed in the literature and have been reviewed in Chapter 12 of Ulaby et al. [A-1, Volume II]. The various models, which are applicable for different roughness scales (measured in wavelength units), relate the backscattering coefficient σ° to the surface properties through the dielectric constant ϵ and the surface-height autocorrelation function $\rho(x)$.

Figure A-6 depicts two examples of the physical mechanisms that usually underlie the mathematics of the theoretical models. In the first one, the surface is approximated as a series of small planar facets, each tangential to the actual surface. Facet models treat the scattering or, more appropriately, reflection, from the assemblage of such facets by taking into account both their reradiation patterns and the distribution of their slopes.

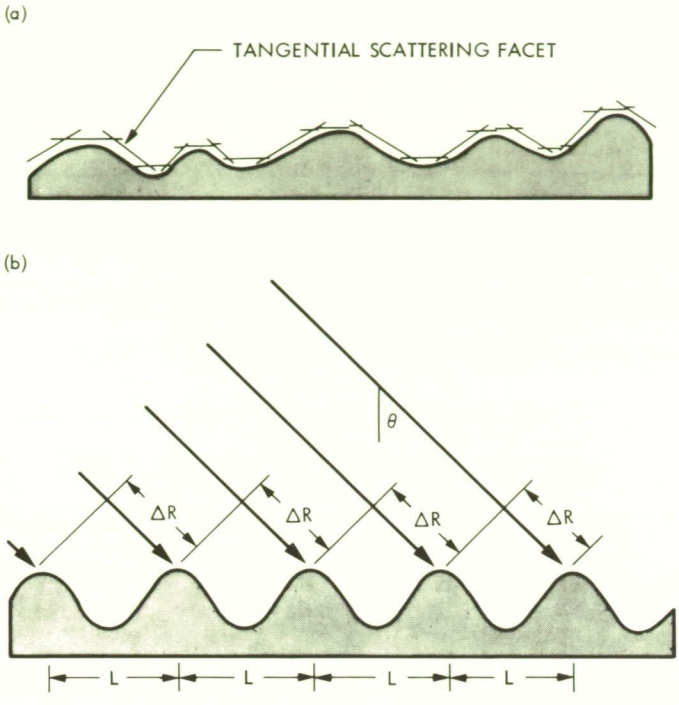

Fig. A-6. Surface scattering by (a) tangential facets and (b) Bragg-resonant sinusoidal ocean waves, where path length ΔR is an integral number of half wavelengths. The path-length difference is $\Delta R = L \sin \theta$ where L is the ocean wavelength and θ is the angle of incidence

Bragg scattering

Scattering from the ocean surface often is described in terms of Bragg resonance. The resonance takes place when the signals backscattered from the tiny capillary and short gravity waves (which ride on top of the large ocean waves) satisfy the condition

$$\frac{2L}{\lambda} \sin \theta = n, \; n = 0, 1, 2, \ldots \tag{A-6}$$

where L is the spatial wavelength of the large ocean wave. The resonance phenomenon associated with Bragg scattering can result in strong backscattering from the ocean surface, even though the scattering is contributed by a small fraction of the total illuminated area, namely those points on the surface satisfying the condition given by equation (A-6).

The variation of the scattering coefficient $\sigma_{tr}^{\circ}(\theta)$ with the angle of incidence, θ, depends on the surface roughness and the polarization configuration of the transmit (t) and receive (r) antennas. The general behavior for a slightly rough surface is shown in Fig. A-7. The HH- and VV-polarized curves are identical at normal incidence and are approximately equal for $\theta \leq 30°$. In the plateau region, σ_{VV}° may exceed σ_{HH}° by several dB.

cross-polarized backscatter

The cross-polarized scattering coefficients σ_{HV}° and σ_{VH}° (which, by reciprocity, are equal to each other) are second-order effects because they are generated by multiple scattering. Consequently, the cross-polarized backscatter is significantly lower in level than the like-polarized levels, particularly for slightly rough surfaces at angles in the neighborhood of normal incidence.

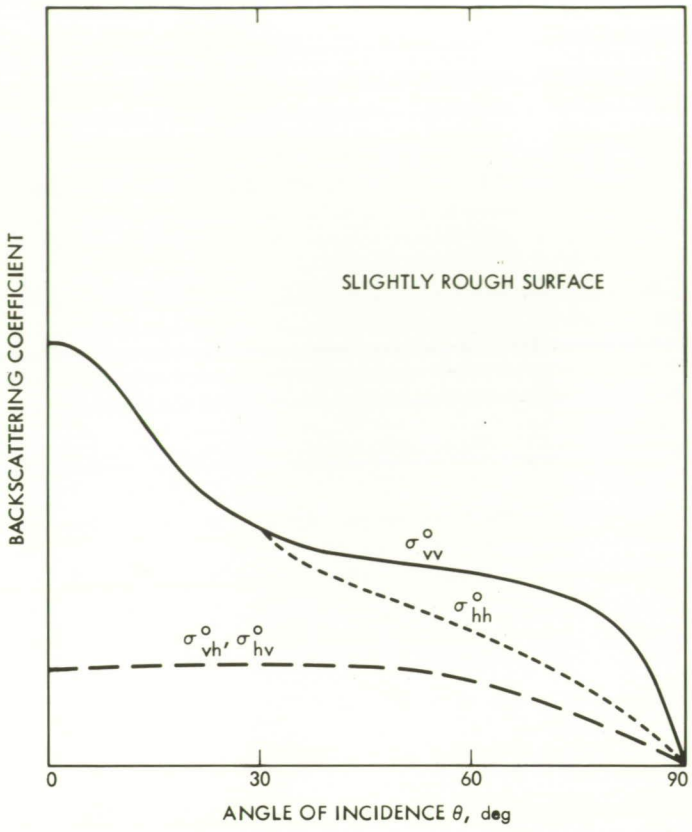

Fig. A-7. Typical angular variations of the polarized scattering coefficient for a slightly rough surface

coherent scatter superimposed on incoherent scatter

The effect of surface roughness on $\sigma^\circ(\theta)$ is illustrated in Fig. A-8. For a relatively smooth (slightly rough) surface, the backscattered signal consists of a strong coherent component that decays rapidly with increasing θ and an incoherent component that exhibits a gentle variation with θ. The coherent component exists for the like-polarization configurations (HH and VV) only. A very rough surface gives rise to incoherent scattering only, thereby exhibiting a gentle angular variation across a wide range extending from normal incidence to $\theta = 70^\circ$ or higher. Because of the over 7:1 wavelength ratio covered by the SIR-C SARs, many surfaces that may appear (electromagnetically) slightly rough at L-band will appear quite rough at X-band.

The level of $\sigma^\circ(\theta)$ is governed primarily by the dielectric constant ϵ of the scattering surface. For soils, ϵ is strongly dependent on moisture content and, to a lesser extent, on soil type [A-3].

A-7 Volume Scattering Mechanisms

dependence on inhomogeneities

Since volume scattering is caused mainly by dielectric discontinuities within a volume and, in general, the spatial locations of discontinuities are random, intuitively we expect the scattered waves (within the volume) to be in all directions (Fig. A-9). Correspondingly, the angular curve for σ° exhibits a relatively flat response with increasing θ up to about 60°, and then decreases slowly with increasing θ. The exact shape and level of the curve

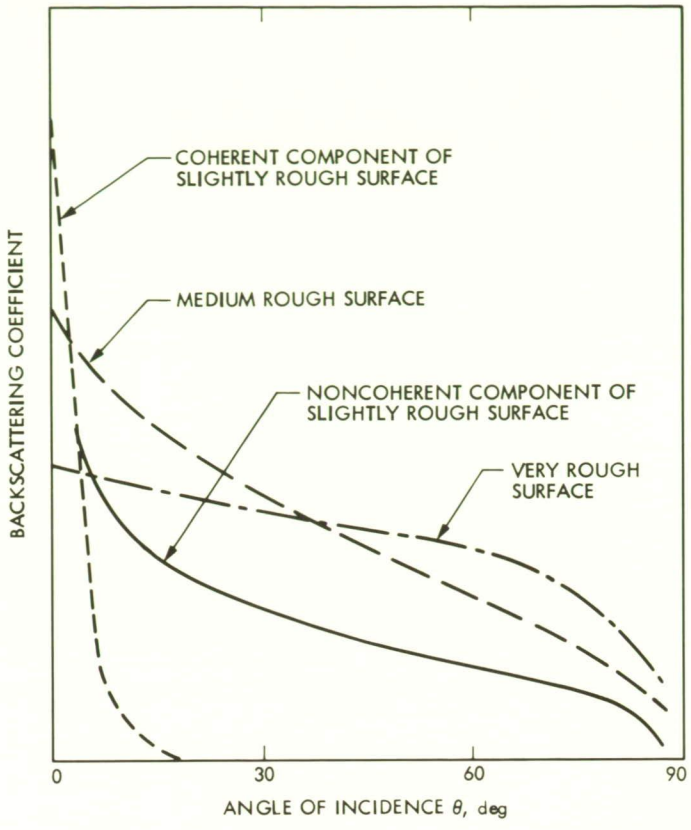

Fig. A-8. Angular variation of σ^0 for surfaces of varying roughness

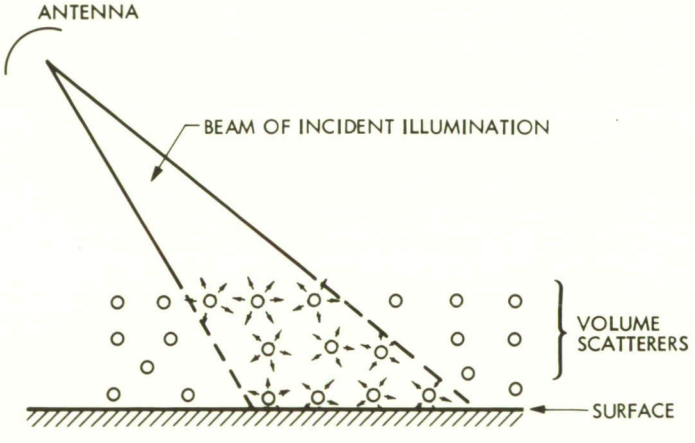

Fig. A-9. An illustration of volume scattering

depend on several factors, including the shapes, sizes, orientations, and dielectric constants of the inhomogeneities present in the medium, and the spatial density of these inhomogeneities (or the variance of the fluctuating dielectric function for a continuous random medium). In modeling volume scattering by an inhomogeneous medium, these factors are represented by electromagnetic parameters, such as the scattering albedo and the optical

thickness, which presumably form the link between the physical properties of the scattering medium and its backscattering behavior [A-1, Volume II, Section 11-5 and Volume III, Chapter 13].

strong radar response to wavelength-sized objects

The wavelength plays a very important role in volume scattering. A radar is a quasi-resonant bandpass filter that responds most strongly to objects whose dimensions are comparable to the radar wavelength λ. Most natural media include inhomogeneities that span over a wide range of sizes; a forest canopy, for example, may have a size distribution similar to the hypothetical distribution shown in Fig. A-10. The shaded vertical bars identify the locations of the SIR-C wavelengths; the L-band channel (λ = 23 cm) will probe tree branches that are tens of centimeters in length, the C-band channel (λ = 5.7 cm) will be most sensitive to interactions with leaves and/or large needles, and the X-band channel (λ = 3 cm) will respond to smaller leaves and/or needles. The wave penetration into the canopy also is influenced by the wavelength. The extinction coefficient of a canopy increases rapidly with decreasing wavelength, thereby providing a penetration depth of the order of one magnitude greater at L-band than at X-band.

The vegetation canopy example is by no means unique; similar analogies may be drawn for snow, sea ice, and other media.

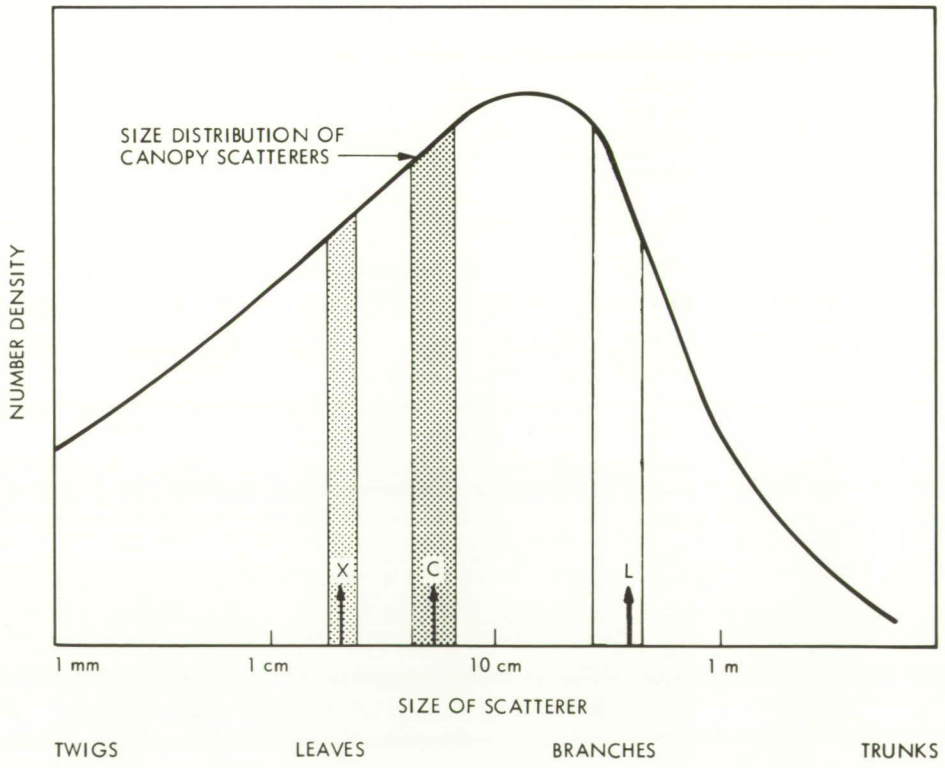

Fig. A-10. Hypothetical size distribution of canopy scatterers

Appendix B
Radiometric Calibration of the SIR-C System

The full scientific potential of an imaging radar is realized only when the processed images are in the form of radiometrically calibrated maps of the radar backscatter coefficients. The absolute and relative accuracies, as well as the repeatability of these maps, are critical factors in the utilization of these data. For the dual-frequency, quad-polarization SIR-C system, there are many possible channel combinations, each with a distinct set of contributors to calibration errors.

Within a single channel (e.g., L-band HH) there are two main radiometric calibration specifications. The first, *absolute calibration,* refers to the uncertainty in the estimation of the backscatter coefficient from the SAR image intensity as a result of system-induced errors such as antenna gain, transmit power level, and range. The second, *relative calibration*, refers to the uncertainty in the ratio of two data values in the image products (e.g., in ratioing of data values within a single scene, spatial ratio, or ratioing data values from pass to pass or mission to mission).

relative calibration

Relative calibration specifications may, therefore, be further subdivided into *short term* (data values corresponding to different points on the earth within a single scene) or *long term* (data values for a single point on the earth being compared from pass to pass or mission to mission). A SAR image with good short-term calibration will have good radiometric fidelity across the image; this means that the image intensity will be a faithful analog to the actual radar backscattering coefficients across the scene, with no artifacts introduced by the antenna pattern or processor. A SAR with a good long-term calibration characteristic (over a period of days, months, or years) will produce *repeatable* images for multiple passes over identical scenes, as a result of good stability of the system gain, antenna pointing, and image processing.

absolute calibration

The principal contributors to errors in the absolute accuracy of SIR-C are expected to be the antenna gain, the antenna-pointing direction, the transmitter and receiver gains, and Doppler errors in the image processor. Each of these error sources can be further subdivided into compensated and uncompensated errors, depending on whether systematic corrections can be applied to the data after acquisition. Table B-1 lists these primary error contributors which degrade the absolute accuracy of SIR-C by both compensated and uncompensated errors. The uncompensated error column assumes only nominal corrections for the radiometric distortions derived from preflight measurement and analysis. At the current stage of development, it is not meaningful to assign a number of standard deviations to these estimates except to say these are "best guesses" of the errors associated with each source. The antenna gain error assumes individual panel measurements and analysis to predict the full-array gain. The compensated error would utilize information from the active ground receivers and transmitters to refine the estimate during the mission. The antenna-pointing contribution derives from the pattern modulation; it is the mean absolute error across a 16-km swath evaluated for a 40° look angle with a 0.66° roll error. Table B-2 lists the factors contributing to the roll uncertainty. The compensated error value in Table B-1 assumes an echo-tracker in the ground processor to refine the look angle estimate by correlating the received pattern with the expected elevation pattern. The transmitter/receiver variation given is the estimated net system-gain change from $-20°$ to $+80°$C. The figures given in the compensated error column assume data available from temperature sensors on the antenna panels. These data would be used to derive a thermal map of

Table B-1. Dominant error sources for absolute calibration of SIR-C

Error source	Uncompensated error (dB)	Compensated error (dB)
Antenna gain (2 way)	±1.4	±1.0
Antenna pointing (2 way) (@ 40° with 0.66° roll error)	±1.0	±0.4
Transmitter/Receiver gain variations (over −20° to +80°C)	−0.6, +0.9	±0.2
Processor Doppler error (5% processor bandwidth)	−0.6, +0	±0.6
Root-Sum-Square total	−1.92, +1.94	±1.25

Table B-2. Shuttle-pointing determination error (in roll axis)

Error source	Error (deg)
Shuttle	
- Inertial pointing accuracy[1] (3σ)	±0.45
- Navigation base to trunnion misalignment[2] (3σ)	±0.36
- Zero gravity unloading (max. in roll axis)	±0.02
- Thermal bending (max. in roll axis)	±0.05
Antenna	
- Boresight misalignment (maximum)	±0.20
- Beam-steering accuracy (maximum)	±0.25
Root-Sum-Square Total	±0.661

Notes:

1. The drift error in the inertial measurement unit (IMU) system is 0.11°/hr, assuming no maneuvers since the previous alignment [B-1]. An assumption, an alignment, is made every 8 hours and the error is evaluated at the 4-hour point.

2. This factor reflects the uncertainty in alignment of the attitude sensors in the shuttle nose to the trunnion in the payload bay.

3. The calibration error resulting from an 0.66°-pointing uncertainty at each look angle is defined as the mean absolute error across a 16-km swath centered at the boresight. This is essentially a "best-case" analysis of the roll-error contribution. Table B-3 lists the peak error at the edge of a 16-km swath. This error obviously drives the overall system uncertainty. The worst-case scenario for relative calibration (pass to pass) is actually twice this peak value, assuming a positive roll on the first pass and a negative roll on the second pass, for a target area located 8 km off boresight.

the antenna that could be used to modify the estimates of transmitter and receiver gain (of the receive/transmit modules) by using curves measured before flight. The last item in Table B-1 is the error resulting from Doppler estimation errors, here assumed to be 5% of the processor bandwidth.

Table B-3. Worst-case radiometric error from pointing uncertainty (evaluated at edge of 16-km swath for roll uncertainty of 0.66°)

Look Angle	Absolute (dB)	Relative (dB)
20	±0.8	±1.6
40	±1.9	±3.8
55	±1.5	±3.0

When the radiometric accuracy of a system is specified, scene-dependent errors such as speckle, ambiguity noise, and distortion noise (i.e., quantization and saturation errors) are typically not considered. The assumption is that the backscatter estimate includes sufficient independent samples to reduce the speckle contribution and that the thermal noise determines the noise floor, which can be estimated from the out-of-band power level. This assumes that noise contributions from range and azimuth ambiguities, bit errors, quantization, and saturation are small relative to thermal noise.

In addition, the random phase and amplitude in each subsystem must be budgeted such that the integrated sidelobe energy is small (i.e., < -15 dB) relative to the main lobe energy. If this condition is not met, ground calibration utilizing point targets such as active radar calibrators (ARCs) or corner reflectors will not provide an accurate estimate of the system gain. Also inherent in the assumption that point targets can be used for calibration is that the target phase history can be precisely tracked over the synthetic aperture. Data with large Doppler shifts (i.e., squint mode imaging) will require a secondary range compression [B-2] and an autofocus to insure smaller fractional errors in the Doppler-rate estimate. This may require a special high-precision processor to be developed separate from the ADSP to process data from the calibration site.

sources of errors

The primary error sources for long-term relative calibration are the antenna-pointing direction, transmitter/receiver gain instabilities and thermal variations, and processor gain; while for short-term relative calibration it is necessary to know the antenna-pointing direction and the processor gain. These are summarized in Table B-4. Note that the antenna peak gain is not a factor in relative calibration, but antenna-pointing errors introduce errors in the antenna gain of one point (direction) in a scene relative to that of another point. The pointing error is assumed to be uncorrelated in the long-term but correlated in the short-term estimates. Also, the processor error is reduced for the short-term estimates due to the slow attitude drift of the shuttle (approximately 0.02°/sec).

Table B-5 presents a summary of the error sources for relative channel-to-channel calibration for two cases: (1) comparison of L-band HH to C-band HH; and (2) comparison of C-band HH to C-band VV. The L-band HH versus C-band HH table includes the gain uncertainty for both antennas and both transmitter/receiver networks. These errors are assumed to be independent, since the two antennas exhibit widely separated temperature profiles. The antenna-pointing contribution is small since both antennas are mechanically boresighted on the same structure, and the only pointing error derives from the phase shifters. In addition, the processor contributions are summed since the Doppler estimation error for each band is correlated.

The error summaries have assumed that the system does not fail during the mission. Until a failure analysis has been conducted for the components comprising the distributed

Table B-4. Dominant error sources for relative calibration of SIR-C

Error source	Uncompensated error (dB)	Compensated error (dB)
Long Term (pass to pass)		
Antenna-pointing direction/gain (@ 40° with 0.66° roll error)	±1.41	±0.58
Transmitter/Receiver gain variations with temperature	−0.6, +0.9	±0.28
Processor gain	−0.6, +0	−0.6, +0
Root-Sum-Square total	−1.64, +1.67	−0.88, +0.04
Short Term (within a scene)		
Antenna-pointing direction/gain (worst case, cross swath)	±2.0	±0.8
Processor gain	−0.2, +0	−0.2, +0
Root-Sum-Square total	±2.0	−0.82, +0.80

Table B-5. Relative multichannel calibration error sources for SIR-C

Error source	Uncompensated error (dB)	Compensated error (dB)
Relative errors (short term)		
L-band (HH) vs. C-band (HH)		
Antenna gain (2 way, 2 frequency)	±1.98	±1.41
Antenna pointing (@ 40°, 0.1° pointing error)	±0.1	±0.1
Transmitter/Receiver gain variations	±1.5	±0.48
Processor gain	−1.2, +0	−1.2, +0
Root-Sum-Square total	−2.76, +2.48	−1.91, +1.49
C-band (HH) vs. C-band (VV)		
Antenna pointing (0.1° error)	±0.1	±0.1
Receiver gain variations	−0.6, +0.9	±0.2
Root-Sum-Square total	−0.63, +0.92	±0.28

array, a quantitative estimate of these effects cannot be given. However, if it can be assumed that failures in the transmit/receive modules are random, that these do not cause an impedance mismatch in the feed network, and that all failures are detectable hard failures, then the resultant effect on performance can be predicted. Under this scenario, the failures are essentially analogous to array thinning [B-3] and a 10% failure of the distributed transmitter amplifiers (HPAs) would reduce the radiated power by only 0.5 dB with an additional 0.1-to-0.3-dB loss in directivity (i.e., an increase in sidelobe energy at the cost of main lobe energy [B-4]). If these failures were detectable by some type of power or current monitors in the array, then the resultant pattern could be simulated in the processor

with negligible effects on calibration. If the transmit/receive unit failures do not follow the random scenario or if an impedance mismatch results, then the directivity degradation would be more severe. In addition, errors in the beam-pointing determination could result from a nondeterministic failure mode.

Other sources that may contribute to a degradation of overall accuracy relate to transitory propagation effects. Neutral atmospheric effects and the effect of rainfall, fog, and clouds should be negligible (<0.05 dB) at these frequencies; however, ionospheric scintillation could have a significant effect on the data. This effect is limited both in the local time of day (1900 to 2400 hours) and the location (below 30° latitude); but, when it occurs, attenuations of several dB could result [B-5]. Attenuation in the propagation could also result from Faraday rotation. It has been estimated that this effect can cause variations of up to 1 dB for mid-latitudes at noon, decreasing to less than 0.1 dB at night. It may be possible to use ionoside data to compensate for significant Faraday rotation over the ground calibration sites.

Appendix C

References

2-1. Pravdo, S. H., B. Huneycutt, B. M. Holt, and D. N. Held, *Seasat Synthetic-Aperture Radar Data User's Manual*, JPL Publication 82-90, Jet Propulsion Laboratory, Pasadena, California, March 1, 1983.

2-2. Ford, J. P., R. G. Blom, M. L. Bryan, M. I. Daily, T. H. Dixon, C. Elachi, and E. C. Xenos, *Seasat Views North America, the Caribbean, and Western Europe With Imaging Radar*, JPL Publication 80-67, Jet Propulsion Laboratory, Pasadena, California, November 1, 1980.

2-3. Fu, L.-L., and B. Holt, *Seasat Views Oceans and Sea Ice With Synthetic-Aperture Radar*, JPL Publication 81-120, Jet Propulsion Laboratory, Pasadena, California, February 15, 1982.

2-4. Cimino, J. B., and C. Elachi, *Shuttle Imaging Radar-A (SIR-A) Experiment*, JPL Publication 82-77, Jet Propulsion Laboratory, Pasadena, California, December 15, 1982.

3-1. Soofi, K., *Clutter Model for Land, Forest, Snow, Sea Ice, and Ocean*, Remote Sensing Lab Report RSL RT 2923-2, 1978.

3-2. Swanson, R., *Radar Remote Sensing of Rocks: A Scatterometer Experiment*, Master's Thesis, University of Kansas, 1983.

4-1. Kahle, A. B., J. P. Schieldge, M. J. Abrams, R. E. Alley, and C. J. LeVine, *Geologic Application of Thermal Inertia Imaging Using HCMM Data,* JPL Publication 81-55, Jet Propulsion Laboratory, Pasadena, California, September 15, 1981.

4-2. Kahle, A. B., and A. F. H. Goetz, "Mineralogic Information from a New Airborne Thermal Infrared Multispectral Scanner," *Science*, Vol. 222, No. 4619, pp. 24–27, October 7, 1983.

4-3. McCauley, J. F., G. G. Schaber, C. S. Breed, M. J. Grolier, C. V. Haynes, B. Issawi, C. Elachi, and R. Blom, "Subsurface Valleys and Geoarcheology of the Eastern Sahara Revealed by Shuttle Radar," *Science*, Vol. 218, No. 4576, pp. 1004–1020, December 3, 1982.

4-4. Péwé, T.L., "Alpine Permafrost in the Contiguous United States," *Journal of Alpha and Arctic Research,* Vol. 15, pp. 145-156, Instar, Department of Geology, University of Colorado, 1983.

4-5. Evans, D.L., T.G. Farr, J.P. Ford, T.W. Thompson, and C.L. Werner, "Multipolarization Radar Images for Geologic Mapping and Vegetation Discrimination," *IEEE Transactions on Geoscience and Remote Sensing,* Vol. GE-24, No. 2, pp. 246–257, March 1986.

References

4-6. Sabins, F. F., R. Blom, and C. Elachi, "Seasat Radar Image of San Andreas Fault, California," *The American Association of Petroleum Geologists Bulletin*, Vol. 64, No. 5, pp. 619-628, May 1980.

4-7. Elachi, C., L. E. Roth, and G. G. Schaber, "Spaceborne Radar Subsurface Imaging in Hyperarid Regions," *IEEE Transactions on Geoscience and Remote Sensing*, Vol. GE-22, No. 4, pp. 383-388, July 1984.

4-8. Ulaby, F. T., R. K. Moore, and A. K. Fung, *Microwave Remote Sensing: Active and Passive*, 3 vols., Addison-Wesley, Reading, Massachusetts, and Artech House, Dedham, Massachusetts, 1981-1985.

4-9. Ulaby, F. T., and W. H. Stiles, "The Active and Passive Microwave Response to Snow Parameters, Part II: Water Equivalent of Dry Snow," *Journal of Geophysical Research*, Vol. 85, pp. 1045-1049, 1980.

4-10. Blom, R. G., R. E. Crippen, and C. Elachi, "Detection of Subsurface Features in SEASAT Radar Images of Means Valley, Mojave Desert, California," *Geology*, Vol. 12, pp. 346-349, June 1984.

4-11. Olhoeft, G. R., "Application and Limitations of Ground Penetrating Radar," *Expanded Abstracts, 54th Annual International Meeting and Exposition of the Society of Exploratory Geophysics*, Atlanta, Georgia, pp. 147-148, December 2-9, 1984.

4-12. Ulaby, F. T., C. T. Allen, G. Eger III, and E. Kanemasu, "Relating the Microwave Backscattering Coefficient to Leaf Area Index," *Remote Sensing Environments*, Vol. 14, pp. 113-133, 1984.

4-13. Jet Propulsion Laboratory, *The SIR-B Science Plan*, JPL Publication 82-78, Pasadena, California, December 1, 1982.

4-14. Ulaby, F. T., "Radar Signatures of Terrain: Useful Monitors of Renewable Resources," *Proceedings of the IEEE*, Vol. 70, pp. 1410-1428, 1982.

4-15. Hoogeboom, P., "Classification of Agricultural Crops in Radar Images," *IEEE Transactions on Geoscience and Remote Sensing*, Vol. GE-21, No. 3, pp. 329-336, July 1983.

4-16. Kasischke, E. S., G. A. Meadows, and P. L. Jackson, *Use of Synthetic Aperture Radar to Detect Hazards to Navigation*, ERIM Report No. 169200-2-F, 1984.

References

A-1. Ulaby, F. T., R. K. Moore, and A. K. Fung, *Microwave Remote Sensing: Active and Passive*, 3 vols., Addison-Wesley, Reading, Massachusetts, and Artech House, Dedham, Massachusetts, 1981–1985.

A-2. Allen, C. T., and F. T. Ulaby, "Modeling the Polarization Dependence of the Attenuation in Vegetation Canopies," *IEEE International Geoscience and Remote Sensing Symposium (IGARSS'84) Digest*, Strasbourg, France, August 27–30, 1984.

A-3. Hallikainen, M. T., F. T. Ulaby, M. C. Dobson, M. A. El-Rayes, and L.-K. Wu, "Microwave Dielectric Behavior of Wet Soil — Part I: Empirical Models and Experimental Observations," *IEEE Transactions on Geoscience and Remote Sensing*, Vol. GE-23, No. 1, pp. 25–34, January 1985.

A-4. Dobson, M. C., F. T. Ulaby, M. T. Hallikainen, and M. A. El-Rayes, "Microwave Dielectric Behavior of Wet Soil — Part II: Dielectric Mixing Models," *IEEE Transactions on Geoscience and Remote Sensing*, Vol. GE-23, No. 1, pp. 35–46, January 1985.

B-1. *Space Shuttle Systems Payload Accomodations Document*, JSC 07700, Vol. XIV, Rev. F, September 1978.

B-2. Jin, M., and C. Wu, "SAR Correlation Technique — A modified Interpolation Algorithm," *Digest 1983 IEEE International Geoscience and Remote Sensing Symposium*, pp. FA-3/1, 1983.

B-3. Hansen, R., "Communication Satellites Using Arrays," *Proceedings of the IRE*, pp. 1066–1074, June 1961.

B-4. Jedlicka, R., and B. Blevins, *Distributed SAR Architecture Study*, Physical Science Laboratory, New State University, NASA Contract NAS9-95541, February 1984.

B-5. Rino, C. L., and J. Owen, *The Effects of Ionospheric Propagation Disturbances on Satellite-Borne Synthetic Aperture Radars*, Defense Nuclear Agency, Contract DNA001-83C-0131, October 1984.

TECHNICAL REPORT STANDARD TITLE PAGE

1. Report No. JPL 86-29	2. Government Accession No.	3. Recipient's Catalog No.
4. Title and Subtitle Shuttle Imaging Radar-C Science Plan		5. Report Date September 1, 1986 6. Performing Organization Code
7. Author(s) SIR-C Science Working Group		8. Performing Organization Report No. JPL 86-29
9. Performing Organization Name and Address JET PROPULSION LABORATORY California Institute of Technology 4800 Oak Grove Drive Pasadena, California 91109		10. Work Unit No. 11. Contract or Grant No. NAS7-918 13. Type of Report and Period Covered JPL Publication
12. Sponsoring Agency Name and Address NATIONAL AERONAUTICS AND SPACE ADMINISTRATION Washington, D.C. 20546		14. Sponsoring Agency Code

15. Supplementary Notes

16. Abstract

The Shuttle Imaging Radar-C (SIR-C) mission will yield new and advanced scientific studies of the earth. SIR-C will be the first instrument to simultaneously acquire images at L-band and C-band with HH, VV, HV, or VH polarizations, as well as images of the phase difference between HH and VV polarizations. These data will be digitally encoded and recorded using onboard high-density digital tape recorders and will later be digitally processed into images using the JPL Advanced Digital SAR Processor.

There are a large number of potential SIR-C experiments. Geologic studies include cold-region geomorphology, fluvial geomorphology, rock weathering and erosional processes, tectonics and geologic boundaries, geobotany, and radar stereogrammetry. Hydrology investigations cover arid, humid, wetland, snow-covered, and high-latitude regions. Additionally, SIR-C will provide the data to identify and map vegetation types, interpret landscape patterns and processes, assess the biophysical properties of plant canopies, and determine the degree of radar penetration of plant canopies.

In the field of oceanography, SIR-C will provide the information necessary to: forecast ocean directional wave spectra; better understand internal wave-current interactions; study the relationship of ocean-bottom features to surface expressions and the correlation of wind signatures to radar backscatter; and detect current-system boundaries, oceanic fronts, and mesoscale eddies. And, as the first spaceborne SAR with multi-frequency, multipolarization imaging capabilities, whole new areas of glaciology will be opened for study when SIR-C is flown in a polar orbit.

17. Key Words (Selected by Author(s))	18. Distribution Statement
Geophysics and Oceanography (General)	Unlimited/Unclassified

19. Security Classif. (of this report)	20. Security Classif. (of this page)	21. No. of Pages	22. Price
Unclassified	Unclassified		